



**Politecnico
di Torino**

ScuDo

Scuola di Dottorato ~ Doctoral School

WHAT YOU ARE, TAKES YOU FAR

Doctoral Dissertation

Doctoral Program in Materials Science and Technology (34th Cycle)

**Development and Fabrication of
Self-Healing Hydrogels
via
Vat Photopolymerization 3D Printing
Technology**

Matteo Caprioli

Supervisor(s):

Prof. Candido Fabrizio Pirri, Department of Applied Science and Technology,
Politecnico di Torino, Torino, Italy

Dr. Ignazio Roppolo, Department of Applied Science and Technology,
Politecnico di Torino, Torino, Italy

Prof. Shlomo Magdassi, Casali Center of Applied Chemistry, The Hebrew
University of Jerusalem, Jerusalem, Israel

Doctoral Examination Committee:

Prof. Pu Xiao, Australian National University (Canberra, Australia) (Referee)

Prof. Flavia Libonati, University of Genova (Genova, Italy) (Referee)

Dr. Lucia Beccai, Italian Institute of Technology (Genova, Italy)

Prof. Paolo Colombo, University of Padova (Padova, Italy)

Politecnico di Torino

2022

Declaration

I hereby declare that the contents and organization of this dissertation constitute my own original work and does not compromise in any way the rights of third parties, including those relating to the security of personal data.

Matteo Caprioli

2022

* This dissertation is presented in partial fulfillment of the requirements for **Ph.D. degree** in the Graduate School of Politecnico di Torino (ScuDo).

*In loving memory of my grandmother Giuliana,
Tò neodo.*

Acknowledgments

Throughout the course of my PhD I have received a great deal of support and encouragement.

First and foremost, I have to thank my supervisors, Professor Candido Fabrizio Pirri and Doctor Ignazio Roppolo, for their invaluable guidance throughout my studies and for believing in my skills. The door to Dr. Roppolo's office was always open for confrontation on my incessant questions to steer me in the right direction. Without his assistance and dedicated involvement this thesis would have never been accomplished.

I would like to express my great appreciation to Prof. Shlomo Magdassi, who gave me the opportunity to spend six fantastic months in his laboratory in Jerusalem, which I would have loved to repeat if only the pandemic did not interfere. His insightful feedback and experience pushed my thinking beyond, bringing my research to a higher level.

Getting through this long experience required more than simple academic support and I have many colleagues to praise for listening to and having to tolerate me over the past years. A special thank goes to my friends Andrea, Lorenzo, Camilla, Luisa, Jacopo, Marco, Luigi, Angelo, Vittorio, Clara, Gianluca for the mutual support and happy distractions to rest my mind outside the research. A particular thanks to Dr. Annalisa Chiappone, who was always available for suggestions and discussing new thoughts, and Matteo Gastaldi, who backed my ideas with his expertise and help.

I would like to acknowledge the group in Jerusalem, in particular Ido, Efrat, Doron, Tamar, Yousef, Omri, Liraz, Michael, for welcoming me and making me feel at home, not only in a research laboratory. I would have loved to return to Israel for another year to spend more time with the group, but the pandemic kept us apart.

I am grateful to my family, for their unfailing support and continuous encouragement throughout my studies, for believing in me during this experience, and for their wise counsel.

Finally, but not less important, I wish to thank Marina, for her love, constant support, and inexhaustible patience. Every time I was ready to quit, she did not let me, and I am forever grateful, because this accomplishment would not have been possible without her understanding. Thank You.

In the end, it is needless to say that there are so many ideas, proposals, hints, and one-time tests that did not end up in this dissertation, and numerous discussions, suggestions and confrontations that are not reported here but that strongly contributed to the presented results, and to which I am grateful for.

Abstract

There is a growing attention in the scientific community towards the successful modeling and shaping of functional three-dimensional (3D) hydrogels, which could significantly and positively impact future developments in the biomedical field, but not only. Their main potential application would be as artificial substitutes for human tissues, but they must be able to replicate the natural functionalities. The two most peculiar characteristics of living tissues are the sophisticated architectures, which could be reproduced by 3D printed structures, and the ability to restore their properties after a damage, called self-healing. This property could push 3D printed hydrogels beyond their structural role, extending their lifetime performance limited by irreversible failures and expanding their application to many different fields, from soft robotics and sensors to energy harvesting and storage. Up to now, many studies in the literature have been focused on the development of self-repairing hydrogels that could be 3D printed with extrusion-based printing, which are limited in the design complexity achievable. Vat photopolymerization (VP) 3D printing can guarantee superior resolution and accuracy with a good trade off with the object size. However, there seems to be an incompatibility between the requirements for successful VP printing and efficient self-healing in the printed hydrogels. In this context, the experimental studies reported in this thesis are aimed to the development of suitable and easily adaptable approaches to combine VP printability and healability based on various different mechanisms into self-repairing hydrogels with complex three-dimensional architecture.

After a broad and comprehensive overview on self-healing fundamentals and mechanisms description (chapter 1) and a general discussion on additive manufacturing with a detailed investigation on vat photopolymerization, focused on principles, technologies, reactions and materials involved (chapter 2), the current state-of-the-art of the field of self-healing vat VP 3D-printed systems, including both dry systems and hydrogels, is reviewed (chapter 3). The experimental section is preceded by an outline of the specific goals pursued in the

following studies based on what was missing in the field at the start of the investigation and a commentary on the major critical aspects of the research to be faced (chapter 4).

In the first research presented (chapter 5) we aimed for an autonomous and rapid restoration based on dispersive forces, occurring at room temperature and without any external trigger to avoid water evaporation. The system was designed as a semi-interpenetrated network by including poly (vinyl alcohol) (PVA), exploited as a healing agent to provide repairability since it can establish extensive hydrogen bonding, within an independent covalent network fabricated during the printing process. The large volume of water embedded favors PVA chain mobility and diffusion across the rejoined interface to promote interactions beyond the surface. In our second study (chapter 6) we evaluated cooling below room temperature as trigger for self-healing and favor water retention, which is an inverse strategy with respect to the most common and easier approach to heat up the system to promote diffusion of chains across a fracture interface. Thermoreversible Pluronic block copolymer was selected as healing agent since it shows an inverse gelation behavior and forms micelles, capable of entangling and forming electrostatic interactions, that are trapped within a covalent network bearing pendant PEG chains acting as plasticizers with an influence on micelle aggregation. In the last experimental work reported (chapter 7), light, already used as polymerization stimulus during printing, was also used as a trigger for self-healing by exploiting a customized dye as healing agent embedded within the network. The dye goes from an auxiliary role of light confinement for resolution enhancement to being a major and active element responsible for restoration by acting as photoactivated switch capable of establishing dynamic boronate ester bonds with the covalent network. Light-mediated activation of labile covalent chemistries can enable controlled and localized repair of complex features or fine elements even in areas not easily accessible.

These works, achieved mainly by using commercially available compounds or molecules synthesized with simple chemistry and a commercial Digital Light Processing (DLP) printer, want to be proof of concepts taking the best of both self-healing and additive manufacturing worlds to open new possible paths.

Contents

Acknowledgments	i
Abstract	iii
1. Self-healing materials	1
1.1 Introduction and principles	1
1.2 Intrinsic self-healing mechanisms	4
1.2.1 Dynamic Covalent Chemistry	5
1.2.2 Non-Covalent Interactions	11
2. Polymeric Additive Manufacturing	21
2.1 Fundamentals and principles	21
2.2 Vat photopolymerization	23
2.2.1 Technical aspects	24
2.2.2 Vat photopolymerization disadvantages	26
2.2.3 Vat photopolymerization techniques	27
2.2.4 Photopolymerization mechanisms and materials	29
2.2.5 Photoactive species	33
3. State-of-the-art of VP 3D-printed self-healing materials	37
3.1 Extrinsic mechanisms	37
3.2 Intrinsic mechanisms	38
3.2.1 Dynamic Covalent Chemistry	38
3.2.2 Non-Covalent Interactions	45
4. Description of the presented work	55
4.1 What was missing in the field	55
4.2 Objectives of the work	57
4.2.1 Use of commercial materials or simple chemistry	57
4.2.2 Water-Based Formulations	58

4.2.3 Structural Complexity	59
4.2.4 Non-heating triggered self-healing	59
4.3 Innovation and perspectives of the work.....	60
4.4 Critical aspects of the research	62
4.4.1 Hydrogel printing via vat photopolymerization.....	62
4.4.2 Combination of printability and healability.....	63
4.4.3 Definition of a self-healing procedure	67
4.4.4 Assessment of self-healing efficiency	68
5. Hydrogen bonds-based self-healing system	71
5.1 Introduction	71
5.2 Methods	73
5.3 Discussion.....	76
5.4 Conclusions and perspectives.....	90
6. Cold-triggered self-healing system.....	93
6.1 Introduction	93
6.2 Methods	96
6.3 Discussion.....	98
6.4 Conclusions and perspectives.....	110
7. Light-mediated self-healing system.....	113
7.1 Introduction.....	113
7.2 Methods	116
7.3 Discussion.....	118
7.4 Conclusions and perspectives	128
General conclusions	131
Appendix.....	135
A1 List of abbreviations	135
A2 List of figures.....	139
References.....	147

Chapter 1

Self-healing materials

1.1 Introduction and principles

Deterioration of mechanical properties is a direct consequence of materials use and ageing, resulting in damages and eventually in failures. The most exploited response of modern society to this evidence consists in the development of disposable objects, directly replacing the components when damaged. This approach cannot be sustained in a view of materials and energy saving. As alternative, materials can be repaired exploiting different methods: temperature, soldering, material addition, etc. Repair needs to continuously monitor the mechanical properties and to intervene timely, which is not always possible and may cause undesired failures during operative life. To address this limitation and extend operational performance, materials inherently capable of autonomous repair with limited or no external human intervention must be designed, enabling the so-called self-healing. Self-healing materials are able to partially or fully restore their integrity and mechanical performance after damages, recovering from cracks at the macro or microscale (Fig. 1.1a). [1]

Among the different classes of materials, here self-healing polymers will be discussed. Those can be subdivided into two distinct groups, extrinsic self-healing and intrinsic self-healing, on the basis of the restoration mechanism (Fig. 1.1b). In extrinsic self-healing systems, the healing agents, such as unreacted monomers, solvents, or low-T_g polymers, are confined in reservoirs embedded in the polymeric matrix. The healing agents can be arranged in two different configurations: capsule-based or vascular-based. [2,3] When mechanical damage occurs, it causes chain cleavage and disentanglement, and ultimately crack formation and propagation. When those cracks reach the reservoirs, the healing agent is released and fills the cracks, to mend the fracture acting as a sealant. The restoring mechanism, based on in situ polymerization, solvent welding, or

macromolecular diffusion and entanglement with the matrix, is particularly efficient in restoring large portions of the material. On the other hand, it is evident that restoration can be achieved only once on the same site. [4]

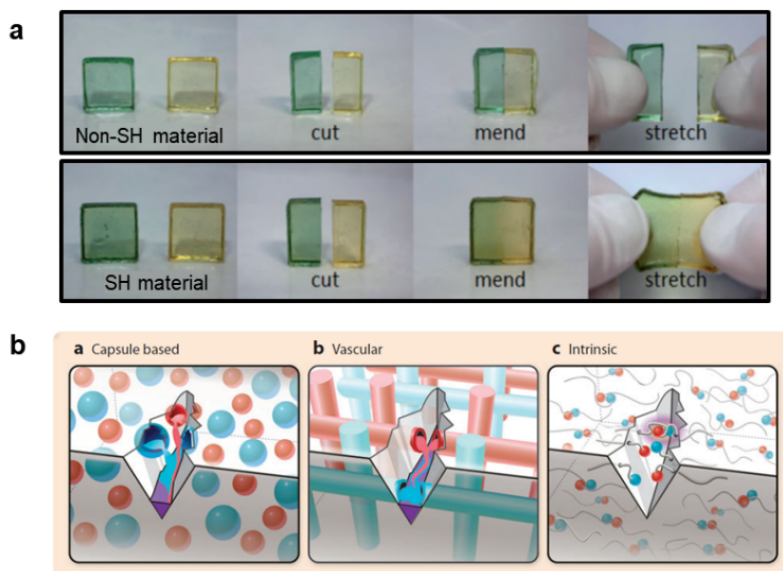


Figure 1.1 Self-healing materials and classification. a) Comparison of a visual restoration experiment between a non-self-healing material and a self-healing material. c) Schematic illustration of the self-healing materials classes. Adapted and reproduced with permission from [18,71]

Instead, intrinsic self-healing polymers are based on the restoration of reversible bonds, established by specific functionalities, which in many cases can be different from the pristine macromolecular network. The main advantage of intrinsic self-healing polymers consists in enabling multiple repair processes, usually only for small, localized damage zones but with relevant exceptions. [5] Intrinsic self-healing strategies are more versatile, being able to adapt to a lot of matrices and many external conditions. This property can be achieved following two main strategies: by chemical cross-linking through dynamic covalent chemistry or by physical cross-linking through non-covalent supramolecular interactions. However, also their combination can be exploited.

The dynamic bonds are established between latent moieties capable of selective interaction after cracks formation. This means that the presence of healing agents is no longer required, preventing problems related to inhomogeneous reservoirs distribution and compatibility with the matrix. Polymer structures can be designed to present different binding points depending on the position of the interacting groups, along or within the polymer backbone, and the

number of binding sites available, with multifunctional groups that enable the formation of a reversible network with no permanent covalent backbone. [2] Newly created surfaces expose many available functional groups that can recombine across fracture interfaces upon re-joining, whose interaction can be supported and amplified by the possibility of diffusion and rearrangement of the macromolecular segments. [6] Chain mobility, functional group availability at the surface, and their reactivity could be limiting factors to an efficient healing process, together with external chemical modifications of the useful moieties (e.g., oxidation).

Intrinsic self-healing materials can also be classified into autonomous and non-autonomous systems, depending on whether they have the ability to spontaneously reform bonds within the matrix, which otherwise would require an external stimulus to promote the restoration, such as temperature, light, and pH. [5] On the other hand, self-healing can be considered a stimuli-responsive property, since repair is always triggered by the rupture, independently of the constitutive mechanism and the autonomic or externally assisted nature of the healing process.[7,8]

Generally, independently from the specific mechanism, before the formation of the reversible bonds, intrinsic self-healing process is based on an initial macromolecular interdiffusion across the broken surfaces which occurs spontaneously for thermodynamic reasons. [9] The restoration is thus mainly governed by polymer chains motion, which depends on the chemical nature and structure of the polymer, its molecular weight, the temperature at which the healing is performed and eventually by the presence of solvents. [10] In contrast with their extrinsic counterparts, intrinsic healing materials are generally not fully autonomous, and require an external stimulus to activate local mobility. [11]

Thermoplastic polymers show molecular interdiffusion between two regions when heated above their T_g , while diffusion in thermosets is limited to free segments when heated. Soft materials, such as elastomers or hydrogels, are particularly suited to perform intrinsic self-healing since chain mobility in these systems is particularly high. [12] In hydrogels, diffusion is a rapid process even at room temperature thanks to the solvation induced by the water molecules, which enables a large free chain length and segmental motion, resulting in a deeper interpenetration and stronger interactions. This mobility at room temperature is restricted in glassy or semicrystalline self-healing polymers that require an increase in temperature to facilitate diffusion, which otherwise will reform bonds

only at the surface, resulting in a lower healing efficiency. [13] However, the reinstatement of reversible bonds is strongly time-dependent and deteriorates with time because of hydrophobic rearrangement of the hydrogel surfaces. [14,15] Only freshly cut hydrogel surfaces can undergo efficient healing because after being cut, hydrophilic moieties are initially exposed to the air, but these are rapidly replaced by hydrophobic groups to minimize surface energy at the air-hydrogel interface. This reorganization results in a barrier that prevents the interdiffusion of polymer chains when the severed surfaces are reunited, and this may affect self-healing ability after a considerable separation time. Most self-healing hydrogels do not heal if the delay between separation and rejoining of the surfaces is too long, and this result is also ascribable to solvent loss due to water evaporation. A system modification from hydrogel to organohydrogel or complete organogel via solvent displacement to replace water with an organic solvent improves drying resistance and reduces the loss of healing properties.[16]

1.2 Intrinsic self-healing mechanisms

Intrinsic self-healing in polymeric materials can be achieved by exploiting various chemistries based on many interactions among specific functional groups. A brief overview of the most common chemistries involved is presented in the following paragraphs and some of these are illustrated in Fig. 1.2. A more detailed description of these and additional approaches to autonomous restoration can be found in other reviews on self-healing mechanisms. [17–22]

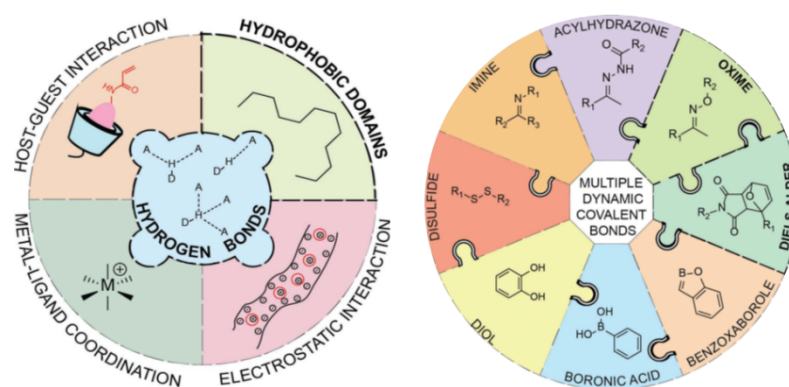


Figure 1.2 Intrinsic self-healing mechanisms. Illustration of some different non-covalent interactions (left) and dynamic covalent bonds (right) employed in self-healing materials to achieve restoration. Reproduced with permission from [25]

1.2.1 Dynamic Covalent Chemistry

The concept of dynamic covalent chemistry (DCC) includes all the covalent bonds able to break and reform under equilibrium control, providing robust materials. [23] A specific bonding energy is associated to each type of covalent bond, which defines its stability and therefore the amount of energy required to break /form the bond. These dynamic chemical bonds are usually weaker than other covalent bonds, and thus will be preferentially broken as the crack propagates upon by the mechanical stress. Dynamic covalent bonds are generally susceptible to external stimuli such as light, temperature, or pH variations that trigger the activation of the dynamic behavior at the damaged interface, which is mended by the reformation of the bonds upon trigger removal. Dynamic covalent reactions typically have slower kinetics of bond cleavage and formation, and most of them may require the assistance of catalysts to achieve rapid equilibrium. [24] Self-healing systems based on dynamic covalent chemistry can be classified according to the type of reaction: condensation, in which the small-molecule by-product is also responsible for the bond disruption and formation of the original moieties; exchange, in which functional groups recombine among them with specific controlled exchange rates; addition, in which the bond formation and rupture does not involve an additional small molecule. [25] In Fig. 1.3 the reaction pathways of various DCC are reported, those will be discussed in detail in the following sections of this chapter. Most DCC reactions do not fall into a single class, but the mechanism can be defined on the reaction kinetic and external conditions, and sometimes different types of DCC bonds are combined to enable multistimuli healing. [26]

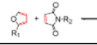
Imine Bond	Reversible formation	$R_1-NH_2 + R_2-C(=O)H \rightleftharpoons R_1-N=C(R_2) + H_2O$	Boronic-Ester Bond	Reversible formation	$R_1-B(OH)_2 + HO-R_2 \rightleftharpoons R_1-B(O-R_2)_2 + H_2O$
	Transimination	$R_1-N=C(R_2) + R_3-N=C(R_4)H \rightleftharpoons R_1-N=C(R_4) + R_3-N=C(R_2)H$		Dynamic exchange	$R_1-B(O-R_2)_2 + HO-R_3 \rightleftharpoons R_1-B(O-R_3)_2 + HO-R_2$
Oxime Bond	Reversible formation	$R_1-O-NH_2 + R_2-C(=O)H \rightleftharpoons R_1-O-N=C(R_2) + H_2O$	Disulfide Bond	Reversible formation	$R_1-SH + R_2-SH \rightleftharpoons R_1-S-S-R_2$
	Transoximization	$R_1-O-N=C(R_2)H + R_3-O-N=C(R_4)H \rightleftharpoons R_1-O-N=C(R_4)H + R_3-O-N=C(R_2)H$		Disulfide exchange	$R_2-S-S-R_1 + R_3-S-S-R_4 \rightleftharpoons R_2-S-S-R_4 + R_3-S-S-R_1$
Acylohydrazone bond	Reversible formation	$R_1-NH-C(=O)H + R_2-NH_2 \rightleftharpoons R_1-NH-C(=O)-NH-R_2 + H_2O$		Disulfide-thiol exchange	$R_1-S-S-R_2 + R_3-SH \rightleftharpoons R_3-S-S-R_2 + R_1-SH$
Urea Bond	Hydrazone exchange	$R_1-NH-C(=O)-NH-R_2 + R_3-NH-C(=O)-NH-R_4 \rightleftharpoons R_1-NH-C(=O)-NH-R_4 + R_3-NH-C(=O)-NH-R_2$	Diels-Alder Reaction	DA/rDA reaction	
	Reversible formation	$R-NH-C(=O)H + H_2N-R_1 \rightleftharpoons R-NH-C(=O)-NH-R_1 + H_2O$	Ester Bond	Reversible formation	$R_1-COOH + R_2-OH \rightleftharpoons R_1-COOR_2 + H_2O$
Dynamic exchange	$R_1-NH-C(=O)-NH-R_2 + R_3-NH-C(=O)-NH-R_4 \rightleftharpoons R_1-NH-C(=O)-NH-R_4 + R_3-NH-C(=O)-NH-R_2$	Transesterification		$R_1-COOR_2 + R_3-COOR_4 \rightleftharpoons R_1-COOR_4 + R_3-COOR_2$	

Figure 0.3 Dynamic covalent chemistries. General and dynamic reversible covalent reaction pathways. Adapted with permission from [27]

Imine bonds

Imine bonds are based on Schiff's base click chemistry, which involves the formation at both neutral and acidic pH values under mild conditions of a strong carbon-nitrogen double bond formed by nucleophilic attack of a primary amine to carbonyl groups in aldehydes or ketones. [28] Aromatic Schiff bases provide higher stability to the linkage compared to aliphatic species. Higher stability provides higher mechanical properties to the system while effectively maintaining dynamic behavior. These bonds require a long reaction time, are unstable in the presence of water, and are sensitive to many chemical and biological stimuli, such as pH variation or the presence of amino-rich species, acting as linkage competitors which can trigger the coupling/uncoupling of the imine bonds. [29] Most of the self-healing hydrogels relying on this mechanism comprise polysaccharide derivatives, such as oxidized dextran and chitosan, thanks to the richness of cross-linking sites on these biopolymers, providing greater stability and potential cell-encapsulation ability. [30]

Oxime bonds

Oxime bonds are also based on Schiff base click chemistry, comprising a condensation reaction between a hydroxylamine or alkoxyamines with an aldehyde or ketone. These linkages show higher bond strength and better stability against hydrolytic cleavage compared to those of imine bonds, resulting in a decrease in the network mobility, thus providing better mechanical properties but a lower tendency to self-healing. [31] Oxime bond formation, which takes place under mild conditions with high reaction efficiency, is orthogonal to nucleophiles in living systems and biocompatible, posing as a suitable candidate for building adaptable hydrogels for cell encapsulation. [32]

Acylhydrazone bonds

Acylhydrazone bonds are formed by a rapid condensation reaction between hydrazine or hydrazide and an aldehyde or ketone. Acylhydrazone reactions are more stable than imine bonds and have been widely used for bioconjugation due to their stimuli-responsive nature and rapid formation under physiological conditions. [33] The reversible acylhydrazone reaction can be triggered by either a thermal stimulus or by a pH variation, using glacial acetic acid as a catalyst, and the bond formation reaction rate is influenced by the temperature and pH. The bond is stable under mild acidic conditions while the regeneration of the linkage fails under neutral conditions, unless aniline is added as the catalyst to achieve an acylhydrazone exchange reaction. [34] Aromatic aldehyde-derived hydrazones

show a faster formation rate and hydrolysis compared to those of aliphatic species at neutral pH. [35] These bonds are usually combined with other dynamic covalent chemistries because of the strong influence of the pH on the bond stability, thus achieving sensitivity to multiple stimuli. [35]

Dynamic urea bonds

Dynamic urea bonds are established between an isocyanate group and a hindered amine without requiring a catalyst and can be conveniently introduced into a single network to yield cross-linked poly(urethane-urea)s. [36] These copolymers consist of hard segments, providing strong mechanical properties, and soft sections, which impart the flexibility required for efficient dynamic exchange. Replacing regular amine with bulky substituents on the nitrogen atom of the urea bond, urea linkages can reversibly dissociate into the corresponding isocyanate and hindered amine. The dynamic behavior can be easily tuned by adjusting the steric hindrance, the bulkiness of the substituents, which determines the kinetics of the exchange. The dynamic urea bond is a strong bond that can be easily broken and reformed under mild conditions, providing good mechanical strength, dimensional rigidity and chemical stability but with sensitivity to humidity. [37] These bonds are mainly exploited for welding applications, with the adhesion at the interface strengthened by a hydrogen-bonding established by urea motifs that increase the mechanical strength. Dynamic urea bonds are mainly exploited in polyurethanes synthesized through the reaction of an isocyanate and a hindered amine, both of which are widely available and inexpensive, and behave like classic thermoset at ambient conditions, but can be reprocessed and recycled by application of heat. [38]

Boronate-Ester Complexations

Boronate-ester bonds are obtained by condensation complexation reaction of boronic acid derivatives with 1,2- and 1,3-diols or carboxylic acids in aqueous solution. [35] The reversibility of the bond and thus the self-healing behavior can be triggered by various stimuli, such as changes in pH, temperature variation, or the addition of glucose. [35] The stability of borate compounds depends largely on the pH: when the pH value is higher than pKa of both boronic acid and the pKa of diol, usually under alkaline conditions, the formation of a stable borate ester bond is favored. [39] Below the pKa value, the boron atom is susceptible to being attacked by a nucleophilic reagent, for example water, leading to hydrolysis of borate ester. Therefore, the stability of this bond, and thus the resultant mechanical properties and self-healing efficiency, is highly sensitive to pH

changes. The reaction conditions are difficult to control and can be incompatible with the biological neutral environment, but the pKa values can be tuned by selecting the proper substituent of the boronic acid functional group to control the properties and develop cytocompatible hydrogels self-healable at neutral pH. [39] The kinetics of boronic ester bond formation can be tuned by many orders of magnitude by changing the neighboring groups. [40] Furthermore, phenylboronic acid derivatives have higher stability than aliphatic derivatives, due to the charge conjugation effect of the benzene ring, that provide higher hydrolytic stability than the aliphatic counterpart. [27] Various strategies have been developed based on different polyols, from natural molecules, such as catechols, inspired by mussel adhesive proteins, or glucose, to nanomaterials such as graphene oxide, to produce self-healing nanocomposites with enhanced mechanical properties. [41,42]

Disulfide bonds

These reversible covalent bonds are based on thiol/disulfide dynamic exchange reactions occurring in the presence of oxidized thiolates in a neutral or alkaline environment. The mechanism relies on the nucleophilic substitution carried out by the S atom in the thiol to cleave an S-S bond to generate a new S-S bond, forming a free thiol group. [43] However, thiols are unreactive in the reduced state, and thus reversible crosslinking given by bond dissociation into thiols by reduction and disulfide formation via oxidation instead of bond exchange can be achieved. [44] The presence of a free thiol group makes the thiol-disulfide exchange faster than the disulfide exchange, but this requires a bland oxidative environment, such as the presence of oxygen as an oxidation agent, which is sufficient to induce cross-linking. [45] Gelation occurs under mild reaction conditions, at a temperature lower than that of other DCCs without catalysts or small molecules, and the dynamic behavior can be triggered by a wide range of stimuli, including pH variation, redox potential, heat, light, or the presence of nucleophiles or external radicals. [45] Disulfide chemistry is slow at physiological pH; however, reducing the thiol pKa can promote with fast gelation kinetics while maintaining cytocompatibility in disulfide-based hydrogels, exploiting naturally existing thiol groups in peptide sequences. [46] The bonds formed among thiol side chains of cysteine groups are fundamental for folding, assembly, and stability of some proteins in biological systems. The involvement of an oxidation agent can reduce the cytocompatibility of the crosslinking process of hydrogels that relies on these linkages. Limitations to the reversibility can arise from this aspect if the system is under physiological conditions, since proteins may interfere with the dynamic mechanism and the presence of glutathione, which is a reducing agent, in some

tissue. ([46]) Nevertheless, thiolate groups are likely to be oxidized into disulfide when exposed to air, leading to the loss of the dynamic and the self-healing features with time, which must be addressed by a protection strategy by capping reactive thiolate groups with Au(I) or Ag(I) ions. [47]

Disulfide bonds are some of the most widely used reactions in dynamic covalent chemistry, because of their good simplicity and controllability, even if the healing efficiency is strongly dependent on the extension of the damaged area. [46] This self-healing mechanism exhibits obvious advantages in rubbers, such as a full recovery of appearance and mechanical properties at moderate temperatures, since these already contain disulfide links due to the vulcanization process. [45] These DCCs are also often implemented in polyurethane-based coatings, to take advantage of the intrinsic shape memory effect to achieve the closure of the crack, while healing is achieved through exchange reactions of the disulfide bonds. [48]

Diels-Alder reactions

Diels-Alder (DA) reactions are the most investigated mechanism for achieving self-healing in polymers. In DA reactions, two or more unsaturated precursors react through double bonds, forming a cyclic adduct after heat triggering. [4 + 2] cycloaddition is a fast 'click' type orthogonal reaction without side reactions and by-products that shows high selectivity and yields. It is typically performed under simple reaction conditions in an aqueous environment, without metal catalysts or coupling reagents. [49] The bond is established between an electron-rich diene and an electron-poor dienophile, and the most commonly used functional groups are, respectively, furane derivatives and alkenes or alkynes, typically maleimides, forming furan-maleimide diels-alder (fmDA) adducts. [50] The DA linkages show thermoreversibility since they can be cleaved upon heating, resulting in decrosslinking at elevated temperatures due to the occurrence of retro-DA (rDA) reactions, which leads to increased mobility. Then, upon cooling to a lower temperature, the functional units can reconnect, forming a covalent DA bond again to restore the network. [51,52] Most rDA reactions require temperatures above 100 ° C to be activated, but the reversibility of the DA reaction can be controlled by adjusting the chemical structure. To finely tune the temperature for the healing process, different substituents can be selected because of relatively simple modification techniques and numerous commercially available derivatives. [53] Selection of the proper moieties has expanded the application of DA links to biological applications in drug delivery and tissue engineering, due to the ability of the reaction to occur rapidly in an aqueous solution at room temperature and under physiologically compatible conditions. [54–56]

In addition to thermally triggered DA reactions, photochemically activated pericyclic reactions have drawn a great deal of attention as an alternative approach to build light-responsive and photoswitchable reversible systems. Bridging among specific chromophores, such as [2+2] cycloaddition for coumarin and cinnamoyl or [4+4] cycloaddition for anthracene, occurs through photodimerization and photocleavage, which occurs rapidly and at high yields also in the solid state. [57] Significant healing can be achieved in these systems by irradiating the broken surfaces with high-energy UV light to further cleave the dimers and then increase the amount of photoreactive moieties available and the polymer chain mobility, while a longer wavelength is used to reform the bonds across the joint interface. [58] Photoactivated SH is quite attractive because it can be achieved with UV light or even with sunlight, and the use of light is clean, cost-effective, highly controllable and selective, causing lower distortions in the material because it is suitable for the repair of specific injured regions without involving the overall material. [58] However, sometimes the efficiency of restoration is insufficient because of low light penetration, which results in incomplete healing of the material taking place only on the surface of the material, representing an efficient application in self-healable coatings and films. [59]

Transesterification

The typical transesterification reaction consists of an exchange between an ester group with an alcohol or a carboxylic acid, with the hydroxyl groups essential for activating the reaction, but also between epoxy and an anhydride. [60] Transesterification requires high temperature, which enables dynamic behavior and determines the time necessary for the reaction to occur, and the presence of a catalyst compatible with the polymer matrix. [61,62] The presence of the catalyst, such as zinc acetate, significantly increases the reversibility and kinetics of the reaction. [62] Thermoreversible transesterification can be exploited by a particular class of materials, called vitrimers, for topological rearrangement upon external mechanical forces based on ester exchange while maintaining a constant number of dynamic chemical bonds and preserving the integrity of the network. [63] Vitrimers behave as a typical thermosetting polymer at operating temperatures while showing a gradual decrease in viscosity with increasing temperature instead of an abrupt drop, in analogy to inorganic glass, which inspired the name of this class of SH materials. [64,65] This behavior combines deformation like thermoplastics and dimensional stability upon heating, similar to thermosets with recovery properties. Transesterification exchange reactions also enable recycling and multiple reprocessing of a covalently cross-linked network, which, along with

repairability, makes vitrimers environmentally friendly and sustainable materials, unlike conventional irreversible thermosetting. [37]

1.2.2 Non-Covalent Interactions

Under non-covalent interactions different mechanism are encompassed. Self-healing mechanisms relying on physical bonds are entropy-driven or based on molecular diffusion, and compared to dynamic covalent bond-based systems, those interactions provide soft polymers with generally lower mechanical properties. [6] On the other hand, physical interactions involve tunable viscoelastic behavior and well-defined network structures that can be rapidly remodeled, offering faster reversible recovery under ambient conditions. [66]

Supramolecular chemistry employs covalently attached moieties to the macromolecule backbone as side chains or chain ends that can establish relatively weak intermolecular and intramolecular interactions between themselves or with small monomer units or molecules. [67] Self-healing ability in these systems relies on the cooperative action of numerous non-directional dispersive forces, which are strongly dependent on the moieties' concentration and distribution. [29] In Figure 1.4 are reported some strategies to achieve self-healing mediated by non-covalent interactions.

Given their nature, most non-covalent self-healing systems can autonomously self-repair without being triggered by external stimuli. [68] The range of non-covalent bonds involves several types of interactions, which are sometimes combined with DCC bonds to enable multi-stimuli healing or with irreversible covalent networks to introduce SH into these systems.

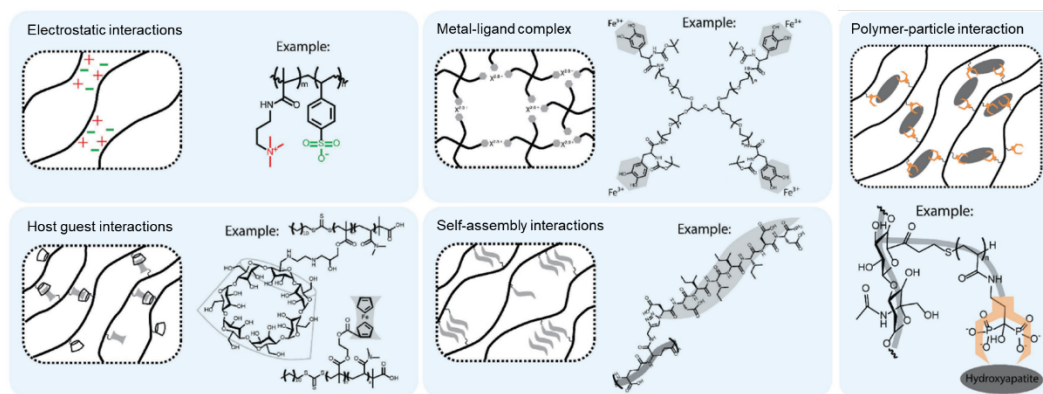


Figure 0.4 Non-covalent interactions. Examples of strategies for the synthesis of noncovalently crosslinked hydrogels with self-healing capability. Adapted with permission from [69]

Molecular Interdiffusion

Self-healing based on molecular interdiffusion relies on the flowing of a thermoplastic polymer across a severed interface to mend the surfaces by mechanically interlocking them when the system is heated above the T_g of the linear macromolecules and then cooled down. [70] The diffusing chains can entangle with the primary cross-linked network because of their free motion to form a secondary noncovalent network, thus resulting in an interpenetrated network which endows self-healability driven by the entanglement effect. The healing agent is considered an additive because it is usually made up of a material different from the matrix in which it is located. This kind of restoration, which is a bridge between extrinsic and intrinsic mechanisms depending on the topological arrangement of the healing agent in the matrix, is stored as separated phase in specific areas such as vesicles and pouches, or homogeneously distributed and mixed within the matrix without visible separation. [71] The healing agent is typically a linear polymer with structural simplicity and high chain flexibility to improve diffusivity. Common thermoplastic polymers used in these systems are poly(caprolactone) (PCL), poly(styrene) (PS), and poly(ethylene glycol) (PEG). [72,73] Furthermore, when linear poly(ϵ -caprolactone) (l-PCL) is interpenetrated in a cross-linked poly(ϵ -caprolactone) (n-PCL) network, the matrix exhibits shape recovery and gradually closes the crack when the temperature increases over the melting point of the PCL, which also activates the diffusion and chain entanglement of l-PCL. This self-healing mechanism is called shape memory assisted self-healing (SMASH). [72]

Hydrogen Bonding

Hydrogen bonding plays a critical role in many natural systems, from the pairing of nucleobases in DNA to protein folding and self-assembly in biomaterials. [74] A hydrogen atom attached to a highly electronegative atom, a donor such as oxygen or nitrogen, establishes a directional dipole–dipole interaction in proximity to another electronegative atom, called acceptor. [75] The single hydrogen bond strength varies depending on the negative charge of the acceptor atom and the pH value of the solvent in which the bonding occurs but is relatively weak when compared with that of covalent or ionic bonds. [76] However, the overall association constant increases sharply when molecules are designed to promote the formation of multiple hydrogen bonds. This extensive noncovalent secondary interaction can significantly affect bulk viscoelastic properties and establishes a rapidly reversible cross-linking useful for imparting self-healing. [76]

The hydrogen-bonding strategy requires hydrogen donors and acceptors, usually grafted as side-chain polar groups along the backbone. [14] In analogy with nucleobases, typical associative multivalent synthetic moieties are 2,6-diamino triazine (DAT) and ureidopyrimidinone (UPy), which establish triple and quadruple hydrogen bonds per group, respectively. [13,77] The complementary H-bonding donor and acceptor motifs assemble into dimers with strong binding affinity, forming clusters that result in phase segregation. Such systems show temperature-dependent dissociation and reassociation processes, leading to repeatable self-healing for both synthetic and natural polymer chains, either in dry systems or hydrogels. [78,79] The presence of water typically causes dissociation of H-bonds among the chains because it interacts with the binding sites, interfering and replacing their mutual interactions, thus deteriorating the self-healing efficiency. In dry supramolecular polymers, H-bonding competes with air moisture, while in hydrogels, multivalent motifs containing both H-bond donor and acceptor groups must be shielded within pockets by hydrophobic species from the aqueous environment to prevent the competitive effect. [80,81] Furthermore, the length of the side chain is a key factor to reduce the impact of steric hindrance: short chains hinder interactions because of the inaccessibility of the functional groups, while long pendants would lead to hydrophobic association shielding of the functional groups. [81]

Crystalline polymers also can exhibit rapid self-healing behavior through reversible and dynamic intermolecular interactions established between abundant amide or hydroxyl groups on adjacent chains, as occurs in poly(vinyl alcohol) (PVA). [82–84] The recovery efficiency in these systems is strongly related to the polymer backbone rigidity, the ratio between free and crystallized moieties, and the crosslinking density, which must be suitable to provide sufficient mobility to the chains to favor interchain diffusion and aggregation. [85,86]

Electrostatic Interactions

Electrostatic interactions are formed between two oppositely charged moieties. An ion can interact with either a polar molecule or induce a temporary dipolar character to a nonpolar molecule. [87] These non-covalent interactions show a lack of specificity and directionality, and their strength is highly dependent on experimental conditions, such as temperature, electrostatic charge density, and dielectric constant of the solvent in which the binding occurs and may also develop in electrostatic repulsion. The design of the molecules interacting via ionic bonding can vary from small molecules and ionic liquids bearing multiple charges, to polymers containing ionizable groups or side chains. This leads to a

wide range of self-healing mechanisms that rely on the strong affinity of ion pairs to reassociate. [88]

Ionomers are macromolecules containing a small percentage of monomers showing negatively charged groups, like carboxylate and phosphonate, show thermoactivated self-healing when heated after or by the damage. [89] Heat induces interdiffusion of the chains, which is favored by the temperature, elasticity of the chains, and localized interchain repulsion. [90] Polyelectrolyte complexes, on the other hand, are charge neutral because they are composed of oppositely charged macromolecules, either synthetic or natural, such as proteins and polysaccharides, which carry charges of opposite signs separately. [91] The most common ionizable moieties are carboxyl groups and amide groups, and ionic bonds are strongly sensitive to pH, temperature, solvent nature, and presence of salts. [92–94]

When an equal number of anionic and cationic are located separately in the same monomer on each chain, thus retaining overall electroneutrality, the polymer is defined zwitterionic. [95] Examples of such systems are sulfo- or carboxybetaines with a quaternary ammonium and their copolymers with neutral comonomers. [96] The self-healing at room temperature of these systems takes place regardless of the separation time because the cut surface is stabilized by a hydrated layer, and the hydrophilic moieties remain exposed and available without hydrophobic rearrangement. [15]

A specific kind of electrostatic interactions is based on π - π stacking between π orbitals in aromatic rings or by end-capped π electron-deficient species, such as imide groups or copolyimides, alternated with π electron-rich aromatic backbone molecules or units, such as pyrene. [97] The complexes arrange in a secondary structure adopting a chain-folded conformation to maximize the stacking, which can be disrupted upon heating, required to enable chain unfolding, reorientation, and mobility across the fractured surface, which is mended upon reformation of the stacking. [68] The Tg of the network can be tuned by adding a flexible spacer which would disengage the interacting moieties and facilitate the chains flow to achieve SH at a wide temperature range. [98,99]

Metal-ligand complexation

Metal-ligand coordination complexes are based on the chelation of a positive metal ion by negatively charged ligands via donation of a nonbonding electron pair to one of the empty d orbitals of the metal ion. Two or more ligands can be

ionically bridged depending on the coordination number of the ion, thus linear chains or networks can be formed. [100] The architecture of the backbone where the ligands are bound as a pendant group has a strong effect on the bond robustness, and it differs between linear, branched, and dendritic polymers. [88] Binding strength and kinetics can also be fine-tuned by choosing different metal–ligand pairs, thanks to the wide range of available ligands. [101] These coordination bonds are highly sensitive to pH, temperature, on which the equilibrium constants depend considerably, and redox potential because it influences the oxidation state of the metal ion and then the stability of the complexes.

The dynamic nature of the coordination complexes enables rapid and efficient self-healing, because of the migration of the free ions at the cut interface and the mobility of the uncross-linked portions of polymer chains. [21,102] Self-healing also depends on the size and type of counterion, which can hinder or suppress restoration if non-coordinating or too big, because of insufficient mobility of the network. [103]

one of the most common self-healing strategies relies on the introduction of ferric ions into a system containing moieties such as carboxylate or catechol groups. This approach found its basis in analogy to the self-healing mechanism of natural mussel adhesive proteins, which is triggered by multivalent cations from seawater. [104–106] Particularly interesting are hydrophilic and anionic biopolymers, such as alginate, that are ionically cross-linked in the presence of divalent calcium ions, enabling self-healing. This feature makes them very attractive for tissue engineering and drug delivery, because of their biocompatibility and low toxicity. [107]

Hydrophobic Association

In hydrogels, non-polar segment of amphiphilic polymers can aggregate among themselves and being isolated from the bulk aqueous media. Forming a hydrophobic association by physically entanglement, based on dispersive forces and not on directly interacting moieties. [97,108] Some authors refrain from calling the hydrophobic association as a type of interaction, as it has nothing to do with the forces between the hydrophobic parts. [21] When two micelles come close enough to each other, they tend to aggregate and form a larger and more stable assembly to minimize contact with water, with subsequent departure of surface-bound water molecules in between. [30,66] Hydrophobic interactions can be fine-tuned by controlling various parameters, such as the balance between

hydrophobic and hydrophilic segments, the strength of the interaction between hydrophilic units or the length of the hydrophobic chains. [22]

Self-healing dynamic hydrogels formed via supramolecular hydrophobic association are typically obtained by micellar copolymerization between macromolecular amphiphilic chains containing hydrophilic blocks with small amounts of hydrophobic units. [34] The presence of a surfactant is thus a crucial, because it determines the shape of the micelle and yields of reversible dissociation and reassociation of the hydrophobic groups into ordered nanodomains. The repair mechanism can be ascribed to this disengagement and rearrangement. [109] Self-healing behavior is lost after extraction of the surfactant from hydrogel networks because the hydrophobic interactions between pure hydrophobic units without micelles are too strong to exhibit reversibility. [110] Interestingly, the self-healing ability of the hydrogels improves increasing the length of alkyl non-polar chains until reaching a compromise between free motion and effective association. [111] As stated before, self-healing in hydrogels is typically limited in time by a hydrophobic rearrangement process of the cut surfaces. However, this rearrangement may ensure a time-independent healing of hydrogels on the basis of hydrophobic association. When the freshly cut surface is exposed to air, the micelles dissociate and orient themselves towards the air-gel interface, with the hydrophobic groups arranged in a monolayer on the cut surface. [110] This configuration enables the system to be repaired even after long separation times via micelle restoration. [30] One important drawback of the above-mentioned self-healable hydrogels is the low water-uptake caused by hydrophobic regions within the hydrogel matrix. [22]

Host-guest complexation

Host-guest inclusion complexes are based on a transient spatially targeted association driven by the affinity between a macrocyclic molecule acting as the host and a suitable molecular guest. [112] The host large internal cavity accommodates the selective physical insertion of a variety of appropriate guest molecules, from small molecules to long synthetic polymers or even large biomacromolecules. [77] The supramolecular assembly is held together by multiple reversible non-covalent interactions, and this can be exploited to achieve self-healing. [20]

Two different strategies have been used to build host-guest-based networks: a threading design and a pendant design. [30] Linear polymer chains, such as hydrophobic poly (caprolactone) (PCL), hydrophilic poly(ethylene glycol) (PEG), or amphiphilic poly(urethanes) (PUs), can be threaded within multiple host

moieties, yielding a rotaxane structure. [113–117] The formation and strength of these complexes is largely dependent on the relative dimensions of the cavity and the cross-sectional area of the polymer chain, with the possibility of multiple chains inserted in a single cavity producing multiple entanglements. In pendant systems, host and guest moieties are located along the chains as side functional groups through functionalization of polymer backbones or via copolymerization of preformed host-guest inclusion complexes (meth)acrylic or vinyl group-bearing comonomers with comonomers as building blocks, such as (meth)acrylates and (meth)acrylamides. [118–120] This configuration confers self-healing ability and shear-thinning properties thanks to the rapid bond formation and can be easily combined with stronger secondary covalent cross-linking to overcome the intrinsic weak mechanical properties.

The host-guest couple must be designed on the basis of the dynamics of the complexations and structural relationship between the moieties, which must be complementary in shape. [66,121] The selection of the proper host-guest couple as well as the backbone chains or the copolymerization monomers greatly affects the self-healing mechanics and efficiency. [112,122] The number of repeating units determines the cavity size in commonly exploited macrocyclic cavitands, including natural molecules, such as water-soluble cyclic oligosaccharides such as cyclodextrins (CDs), or synthetic molecules, such as cucurbiturils (CBs), crown ethers, calixarenes (CAs) and pillararenes. [123] Although all of the macrocycles above show potential for building self-healing gels, mainly cyclodextrins and cucurbit[n]urils have been used so far in the fabrication of self-healing hydrogels, because of their nontoxicity and biocompatibility. [30,119] Guest molecules range from polar compounds such as alcohols and amino acids to non-polar compounds such as aromatic molecules and steroidal compounds, or in the case of poly(pseudo)rotaxanes, polymeric chains as pendant groups. [117,119,124] Controllable association and dissociation of inclusion complexes is dependent on the specific nature of the guest molecule, which may be inert or stimulate responsive, such as temperature (Adamantane (Ad)), light (Azobenzene (Az)), pH (Phenolphthalein (Ph)), and redox potentials (Ferrocene (Fc)). [125–128]

Self-assembly and crystallization

The self-assembly of polymer chains can lead to their gelation arranged into regular structures that act as physical cross-links. [119] These relatively stable crystals with specific conformations are formed via multiple cooperating noncovalent interactions, such as hydrophobic association, hydrogen bonding, and electrostatic interactions, established among polymer chains. [69] The difference

with previously mentioned mechanisms is the formation of well-defined architectures to achieve self-healing via incorporation of specific moieties along the polymer chains or exploiting the intrinsic properties of the polymer chain. Such molecular assembly is typical for protein- or peptide-based systems with secondary structures but can also occur in synthetic macromolecules such as poly (caprolactone), with controllable crystallization. [72,129]

Self-healing peptide-based systems can be fabricated through the direct engineering of polypeptides or via modification of a long hydrophobic polymer backbone using hydrophilic peptides as pendant groups or copolymers, forming unique peptide sequences that are found in specific protein-binding structural motifs. [130,131] These materials have inherent biocompatibility, bioactivity, and biodegradability, and because of their amphiphilic nontoxic nature, they have been studied for controlled drug delivery of hydrophobic drugs in an aqueous environment from stimuli-responsive injectable hydrogel cell scaffolds. [132,133] The self-healing efficiency depends on the mobility of the chains to allow hierarchical assembly into specific structures responding to environmental conditions. [119] The reversible unfolding and self-assembly of these systems depend on temperature, pH, and ionic strength, enabling triggered self-healing, with conformation-dependent crystallization (α -helix, β -sheet or random coil) that provides the system stability at high temperature. [132,134] Although they exhibit many advantageous features, drawbacks in peptide-based systems are their high costs, difficult scale-up, and less controllable enzymatic degradation. The mechanical properties of self-assembled polypeptides are low, so cross-linking is usually introduced to increase stability. [135]

Polymer-nanocomposite interactions

Nanocomposites materials are composed of an inorganic component with nanometric dimensions, such as nanosheets, nanotubes, or nanoparticles, homogeneously dispersed in an organic matrix where it acts as a multifunctional cross-linker. [136] Nanomaterial incorporation allows enhancing thermal and mechanical properties thanks to its large surface-to-volume ratio, which favors strong dispersive interactions but also imparts stimuli-responsiveness, antibiofouling, or introduces electrical conductivity. [137] However, drawbacks are their inelasticity and brittleness because these nanofillers may act as stress concentration points, inducing failures in the material. [138] This problem can be partially overcome by introducing covalent crosslinking in the matrix, but the exploitation of a reversible noncovalent interaction between functional groups

along the polymer chains and the surface of the filler would provide self-healing capability. [139]

A wide range of nanomaterials, either inorganic fillers, such as clays and metal oxides, or organic nanomaterials, such as carbon nanotubes, graphene oxide, and nanocrystalline cellulose, have been used to develop self-healing nanocomposite materials. [140–143] It is fundamental to achieve a synergy between the supramolecular polymer matrix and its inorganic components to promote chain mobility and dynamic bond restoration to have efficient self-healing. Nanofillers would not provide self-healing unless all components have built-in reversibly interacting segments. Usually, polymer chains physically adsorb onto exfoliated clay surfaces via ionic interactions, while forming hydrogen bonds with organic nanospecies thanks to the presence of functional moieties like hydroxyl, epoxy, carbonyl, and carboxyl groups. [144,145]

Chapter 2

Polymeric Additive Manufacturing

2.1 Fundamentals and principles

Additive manufacturing (AM), also known as three-dimensional printing (3DP), has emerged as an advanced, versatile technology for the rapid on-demand manufacturing of solid objects created through a build-up process starting from a virtual CAD model of the geometry to be printed. It is one of the most promising fabrication technologies nowadays, currently gaining momentum in large-scale parts production, as well as opening up new perspectives to research. [146] Unlike traditional manufacturing processes, AM technologies have the advantage to allow the fabrication of arbitrarily complex shapes almost without limitations. This means to re-think the way products are designed and manufactured, gathering a controlled spatial arrangement, to achieve hierarchical and intricate architectures, with graded or multimaterial structures. [147] 3DP can be slower compared to conventional processing, but it is more versatile and agile since it relies on single-step fabrication of a near-net shape object. This reduces the number of processing and post-processing steps required to achieve the final component, leading to a significant reduction in the overall operational time. [148]

3DP enables the on-demand fabrication of customized products in a cost-effective manner, especially for limited productions, due to the ease of creating, remodeling, and personalizing CAD files to meet any requirement. These modifications can be translated with ease into parts that are manufactured close to the designer, thus saving on time and transportation costs. [149] This computer-aided manufacturing (CAM) relies on the deposition of materials in layer-by-layer fashion with a high degree of automation and reproducibility, allowing precise control over the result. These models are created by the selective and successive addition of material, layer by layer, until completion. The different layer fashions derive from converting the 3D CAD into a computer-readable format, usually an STL file, comprising processing parameters highly dependent on the printing

technique, which allows the machine to produce the object. [150] In addition to these advantages, there are environmental benefits such as lower energy consumption for small-batch productions and more efficient material use, since waste is extremely limited by the possibility of reusing almost all the feeding material. However, drawbacks related to the suitability, toxicity, and sustainability of materials still need to be fully addressed. [151]

Despite the great promises of 3D printing as an advanced form of manufacturing, the major challenge is the limited availability of materials specifically designed for AM, since their development did not keep pace with the evolution of the techniques. [152] In the last decade, novel materials have been developed to be processed via 3D printing and provide advanced properties to the final object. The combination of additive manufacturing and functional properties, such as stimuli responsiveness, is called 4D printing and is aimed at integrating specific structures and smart functionalities to enable applications in advanced fields such as medicine and aerospace. [153]

Several AM fabrication technologies are available and can be grouped according to the raw material used, and then based on how the layers are created and bonded determined by the operating principles. According to the American Society for Testing and Materials (ASTM), there are more than 50 different AM technologies that can be classified into seven different categories: material extrusion, material jetting, binder jetting, sheet lamination, vat photopolymerization, powder bed fusion, and direct energy deposition. [154] These techniques rely on different characteristics of the printer and fabrication parameters, which influence the model design and topological optimization and determine the object resolution and production times, with a different ability to control the size of the features at various scales. [155] The various techniques can also be divided into stimulus-triggered AM techniques and deposition-based AM techniques, depending on the method of manufacturing the fundamental building block, called voxel. [156] In the first class, the material is precisely located in specific positions in the space forming the desired 3D object, while in the latter the voxel is generated by solidification of a starting in response to a triggered stimulus, for example, a light irradiation, to create the designed structure. Sometimes these two approaches can be also combined.

2.2 Vat photopolymerization

Light-triggered AM techniques are based on spatially controlled light irradiation, to selectively induce the hardening of a liquid precursor contained in a reservoir, called ink or resin. The light irradiation corresponds to the sliced cross section of the final 3D product. [157] The object is fabricated layer by layer on a build platform that moves accordingly and stepwise at certain heights, equal to the thickness of one layer as defined by the layering in the 3D digital model. The process occurs in a sequential fashion where the resin is cured to a depth equal to the thickness of a single slice and then the build stage is translated along the z-direction. This enables new uncured resin to flow under or above the cured part (according to the configuration of the 3D printer) to recoat again the printing area before fabricating the next layer, and these operations repeat until the part is complete. [158]

Independently of the technology employed or of the polymerization mechanism, resins for VP must contain a photoinitiator (PI) and curable species, along with some other optional ingredients that can enhance printability or provide specific properties by design. Additional discussion on the components of a VP resin is provided in a later section. Patterned exposure to light activates the PI, which absorbs incident radiation and generates reactive species, typically radicals, promoting the conversion of the liquid resin to form a cured covalent network. [159] The photoinitiator must be compatible with the wavelength of the light source, generally UV or visible light, with the latter being much safer and compatible with cell-laden water-based inks. [160,161] Photocurable species, such as monomers or oligomers, bear single or multiple active groups as side chains or polymer chain ends, enabling their association into a cross-linked network primarily in the irradiated regions. [162] In resins for VP an accurate tuning of composition and properties is required to define curing kinetics and penetration depth, which in combination with adequate printing parameters, like light intensity and time of exposure, allow a successful VP printing in terms of layer curing speed (on the order of seconds), precision and mechanical integrity. In addition to liquid photopolymers, slurries containing organic solid additives, ceramic or metal particles can also be processed with VP, which allows easy production of polymeric and inorganic phases mixtures. [163]

The use of photoactivated reactions enables precise spatiotemporal control over localized gelation of the precursor material, which if well controlled results in high shape fidelity of the final object compared to the CAD model. The layer

thickness during a specific printing process should be selected to reach a suitable compromise between high resolution and short build times. The resin transparency strongly influences the step size, which should be sufficient for the entire layer to be cured but not too small to avoid a curing depth beyond the designed layer height. [164] The ideal depth of light penetration should be higher than the height of the layer to ensure gelation and integration at the interface between two consecutive layers, but this could cause unwanted polymerization in areas initially designed to remain uncured, such as pores, introducing artifacts in the final structure. [165] The vertical resolution depends mainly on the precision of the step-by-step screw of the printer and the accuracy of its rotation that controls the motion of the building platform. [166] However, the resolution on the Z axis can be adjusted by tuning printing parameters, such as irradiation dosage and wavelength, but also by adding suitable additives, dyes and photoabsorbers to reduce the depth of light penetration. [167]

2.2.1 Technical aspects

The printing hardware determines the minimum feature that the light pattern can resolve, defining the theoretical resolution, and the presence of light-absorbing species further confines the already patterned light along the horizontal plane. [168,169] Furthermore, the exposure dose for each unit of area, called pixel, can be theoretically adjusted separately, as each pixel of the layer is autonomous independently from the light source (Fig. 2.1a). [159] A grayscale pattern can be realized by controlling the light intensity and exposure time point by point, thus locally defining the properties of the polymerized object. Polymerization kinetics and the diffusion of reactive species also play a fundamental role in lateral resolution, which can be improved by adding radical-scavenging species capable of quenching radicals outside the irradiated area. [165] The printing resolution on the horizontal plane, perpendicular to the direction of the light, and in the vertical direction parallel to the irradiation path, outlines the minimum volume unit, or voxel, that can be resolved by the light-induced curing process. [170] The illuminated section and the curing depth accurately transfer liquid polymer resin to solidified voxels, determining the roughness profile and topography of the external surfaces of the printed object. Light-induced polymerization enables customized and complex shapes with superior resolution compared to extrusion-based 3DP techniques and freedom of fabrication of free-form structures or using topical support material. [171]

VP machines can be classified depending on the relative position of the light source with respect to the vat and the orientation of the movement of the building platform along the vertical axis, as the cross-linked part is either sunken into (top-down) or lifted from (bottom-up) the vat (Fig. 4.1b). [172] In the top-down approach, the platform and object under construction are submerged by the liquid resin during manufacturing, the light source is situated above the vat, and the reaction occurs on the free surface. [152] For each cured layer, the object descends deeper into the liquid precursor to coat another fresh uncured layer above it, and this requires deep tanks and large volumes of resin. In the bottom-up configuration, the photo-cross-linking occurs at the bottom of the vat because the light hits the resin from below through a transparent window, and therefore the printing stage moves upward. [173] This arrangement is usually preferred over the top-down one because the object is not submerged, and thus less printable material and shallow vats can be used.

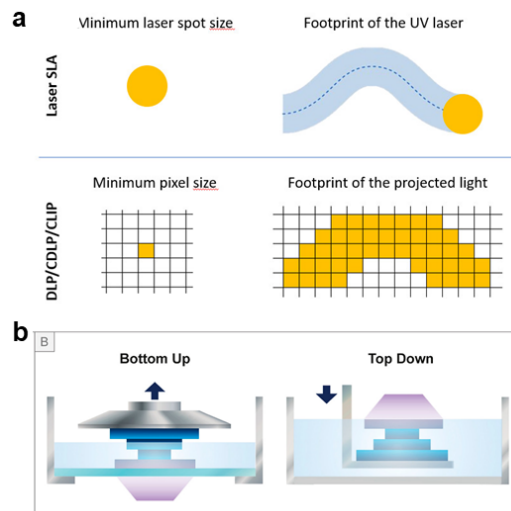


Figure 2.1 Vat photopolymerization technologies comparison. a) Planar resolution comparison between SLA and DLP. b) Different configurations of platform movement along the z axis and relative position between light source and vat. Adapted and reproduced with permission from [160,171]

In either configuration, a fresh layer of uncured liquid resin is located between the latest printed layer and the light source; hence, the viscosity of the ink plays an important role. [172] Low viscosity, often achieved by introducing additives or solvents, is beneficial because it facilitates flow above or beneath the printed part and homogeneous distribution for even layer formation. [174] Furthermore, the low viscosity is advantageous because it enables the evacuation of excess resin from pores or narrow negative features during printing and its removal when the

process is finished, allowing ink reuse. Washing the printed part, typically with ethanol, improves the resolution because it drains out resin residues to avoid polymerization in the subsequent post-process curing. [173] This further treatment, such as heating or photocuring, enables the long-term structural stability to be achieved by increasing the final cross-linking density, since the printing is performed to reach the gel point without inducing complete conversion of the reactive species. [175] This method provides a compromise between adequate printing speed, minimal cross-linking required to avoid the dissolution of the part when immersed in the liquid precursor, avoid deformations in the part during processing, and preserve some unreacted functional groups finalized to ensure correct adhesion via covalent bonding between consecutive layers. The latter aspect produces quasi-isotropic mechanical properties, unlike extrusion-based techniques, even though each layer is patterned individually, but printed parts still tend to be weaker to forces parallel to the printing direction. [173]

2.2.2 Vat photopolymerization disadvantages

The main time-consuming step in VP is the motion of the build platform, to allow the deposition of the fresh layer of resin. This takes about 10 seconds, while the irradiation itself, usually occurs in a few seconds. Platform movement is particularly slow in bottom-up configurations because there is a double motion, first upward and then downward, to allow the resin to flow correctly beneath the object, during which the light source is turned off, whereas a top-down process comprises only a descending motion and then a lower wait time. Another major disadvantage is that VP printing relies on photoinduced polymerization and thus is limited only to photoreactive species; therefore, the addition of unreactive elements, light-absorbing species, or large amounts of solvents can greatly hamper or even block the process. In top-down approaches, free radical chain growth photopolymerization takes place at the air-liquid interface, and then oxygen inhibition can occur, hindering the correct formation of the layers. [176] In the bottom-up configuration, the reacting resin is less susceptible to oxygen inhibition because it is not in direct contact with the ambient air. Contact with the optical window could be a drawback, since undesired adhesion of the cured layers to the bottom could occur, causing delamination and incomplete printing. [177]

Working at the gel point keeps the network insoluble in the resin, while avoiding deformation and delamination caused by the shrinkage induced by solidification. [178] The curing gradient caused by the monodirectional irradiation can induce internal stresses that result in curling and other deformation problems.

[179] Support structures can sometimes be introduced to contrast warpage, especially after post-printing, and enable the correct formation of overhanging features and cavities, but these additional elements must be later manually removed, with an important influence over the roughness. [180] Unlike extrusion-based technologies, support structures are usually made of the same material of the object and must be accurately designed and positioned for removal, given the inherent complication of lithographic approaches to print multiple materials. [181] Another disadvantage is represented by the health risks posed by uncured monomers and photoinitiators when in direct contact with the human body and the potential environmental harmful effects, which require their management at end of life as hazardous chemical waste. [182]

2.2.3 Vat photopolymerization techniques

Vat photopolymerization techniques can be classified into linear, planar, or volumetric buildings according to the number of dimensions involved in the solidification of the liquid precursor (Fig. 2.2a). [165] Stereolithography (SLA) is based on the first configuration, relying on serial irradiation in a line-by-line fashion performed by the light spot produced with a laser source. The second configuration, involving illumination via conventional light sources in a specific area with a bi-dimensional pattern, is typical of the projection-based VP techniques. The third approach concerns the projection of a holographic pattern into a rotating vat, and it is called volumetric 3D printing. [183] The first two modes are the main ones employed with self-healing polymer-based systems and thus will be discussed in more detail. Volumetric printing has not been used yet in the field and is beyond the scope of this work.

Stereolithography (SLA)

Stereolithography techniques are based on a coherent light source, usually lasers emitting in the UV-Vis range, which produces a beam that sequentially raster the plane on the surface of the photosensitive material following a path defined by the pre-designed CAD model geometry. [184] The selective polymerization of the liquid resins occurs at the focus point, and the time required to produce one entire layer of the structure depends on the scanning speed of the beam and on the size of the illuminated area. The light beam is moved across the surface by the controlled rotation of two galvanometric mirrors along the X and Y directions, and this precise motion provides a high spatial resolution, which is also proportional to the spot size of the focused laser beam, around 1 μm , and inversely proportional to the rastering speed. [185] Fabricating a large structure

with high spatial resolution requires long printing times due to the slow scanning of the laser across each layer, which is a time-consuming step.

Projection-Based Vat Photopolymerization

Projection-based VP, also called Digital Light Processing (DLP), closely resembles classical lithography and is often referred to as dynamic or digital mask photolithography. [152] In analogy with lithography, the entire cross section of a layer is exposed all at once to the projection of a selectively masked light source that produces a bidimensional pattern. [171] The total area is divided into pixels, which determine the smallest unit of area that can be irradiated, and only the illuminated ones will contribute to define the shape and resolution of each printed slice. [186] The pattern is transferred to the resin via a digital micromirror device (DMD), which is an array of independent micromirrors that can be individually rotated in an 'on' or 'off' position to direct light towards the bottom of the vat to generate black and white images. The light sources employed range from classical lamps, emitting broad white light, to LEDs, which provide light at a well-defined wavelength from deep UV to visible, but with a low light intensity and power. Light crystal display (LCD) screens can also be used as light sources, producing less distortion than DMDs, resulting in a cheaper alternative. [184]

The lateral resolution of these projection-based techniques depends on the technology used as light sources, the number of pixels / mirrors and the optics used to project, resulting in a range between 10-200 μm . [187] This method allows for considerably faster fabrication rate compared to SLA because a whole layer of the structure is produced in one exposure step, and the build time depends solely on the layer thickness and required exposure duration. The build time can be further reduced by using a layerless fabrication with continuous liquid interface production (CLIP) in a bottom-up configuration. [188] This approach takes advantage of the effect of oxygen inhibition on photopolymerization by using an oxygen-permeable window to generate a region where photopolymerization is inhibited between the growing part and the bottom window. This interface eliminates the need for an iterative stepwise layer-by-layer process and produces isotropic mechanical properties. However, to be applied in CLIP, resins must have a very low viscosity, and the application is limited to species reacting only via polymerization mechanisms sensitive to oxygen inhibition, such as free-radical chain growth polymerization. A schematic summary of the three major VP techniques is shown in Fig. 2.2d.

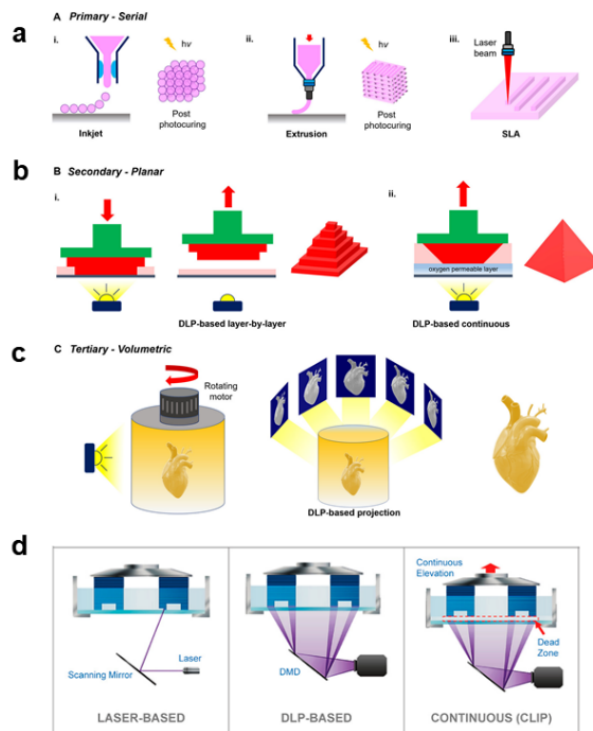


Figure 2.2 Classification of light-based 3D printing modalities. a) Primary configuration involving dot-by-dot or line-by-line deposition. b) Secondary configuration involving planar 2D patterning. c) Tertiary configuration involving volumetric 3D patterning. d) Schematic representation of the three main vat photopolymerization technologies. Reproduced with permission from [160,165]

2.2.4 Photopolymerization mechanisms and materials

Vat photopolymerization relies on reactions that can be divided according to the initiation mechanism: free-radical chain growth polymerization, thiol-ene step growth polymerization, and ionic polymerization. [189] The first two mechanisms have been extensively used in VP SH materials, as will be shown in Chapter 3, and thus will be discussed in later sections. Cationic polymerization of epoxy or vinyl ether-based resins has not yet been used in the field, and thus, it will not be discussed here.

Free-Radical Chain Growth Polymerization

Most of the materials used in VP and commercial resins undergo free radical chain growth polymerization upon light irradiation to form a cross-linked network, because of the rapid reaction rate of the functionalities involved and tolerance to impurities. [190] In the first stage of polymerization, radical species are generated under light absorption by the photoinitiator. After successful

initiation, the free radicals react with double bonds on monomers or polymer chains, forming new covalent bonds and reactive carbon radicals (Fig. 2.3a). [191] These intermediates serve as kinetic chain carriers that react with subsequent reactive groups, resulting in the propagation of radical species by attacking nearby free unreacted monomers and adding them to the polymer chain that grows in a chain-like fashion. [192] The propagation of the polymer chain continues until termination reactions occur, such as a combination of two propagating chains, transfer of the propagating radical to another molecule or disproportionation by hydrogen abstraction. The propagation of free radicals can also be quenched by interaction with inhibitors, such as oxygen molecules in open vat systems, which can be used to mitigate polymerization and improve the printing resolution by capturing radicals that diffuse quickly outside the activated area. [193]

Monomers have been developed on the basis of a wide range of functional groups, including (meth)acrylate and (meth)acrylamide, which are compatible with different types of commercially available and custom-made 3D printers (Fig. 2.3b). [170] The reactivity of these moieties toward radical polymerization decreases from acrylates and acrylamides to methacrylates and methacrylamides, which have a lower tendency to homopolymerize than the former. [194] In some cases, a system comprising both an acrylate and a methacrylate is preferable because it allows for sufficiently rapid curing while providing adequate mechanical properties required to maintain fidelity during the printing process without distortions. [195] The reactivity of the different functional groups can be easily modulated and increased by adjacent electron acceptor groups that impart stability to intermediate radical species. [196] Because not all monomers contain the desired reactive alkene for free-radical polymerization, moieties having a polymerizable double bond, such as methacryloyl groups, can be introduced onto the backbone of an unreactive species, usually by esterification with hydroxyl or amino groups, to provide photoreactivity. [197] This approach enables the functionalization of both synthetic polymers and natural molecules, such as polysaccharides and polypeptides. [198]

The reaction behavior of the resin strongly depends on the number of functionalities present in the reactive species. Multiple functionalities result in shorter reaction times because of the autoacceleration in the early phases of propagation, higher viscosity, and a dense and stiff network, leading to a considerable amount of unreacted double bonds. [160] Monomer molecular weight heavily affects the behavior of the system, with low-molecular-weight species that lower viscosity and increase flexibility and reactivity, while higher-

molecular-weight monomers can reduce the shrinkage but have restricted mobility that induces higher viscosity, requiring a reactive diluent. [199] The monomer backbone influences mobility, mechanical strength, flexibility, and shrinkage, independently of the functional groups: cycloaliphatic or aromatic cores tend to undergo less shrinkage compared to more linear aliphatic monomers. [200] The propagation of the reaction has a diffusion-controlled kinetics, with the limited mobility of the macroradical chain ends that produces a heterogeneous network containing highly and loosely cross-linked regions. [201] Rapid formation of radical concentration gradients can lead to a mismatch between bulk and local (microscale) properties. [196]

Photo-induced thiol–ene reactions

Photoinduced thiol-ene reactions follow a thiol-Michael addition-like step-growth pathway (Fig. 2.3c) that requires a free radical photoactivated initiator, whereas conventional thiol-Michael addition requires a chemical catalyst. [202] The radical generated by the PI abstracts a hydrogen atom from a thiol group, converting it into a reactive thiyl radical. This intermediate forms thioether bonds with the electron-rich double bond of an alkene, generating a carbon-centered radical, which then repeats the cycle by abstracting a hydrogen atom from another thiol group to reform the thiyl species. This reaction proceeds in a step-growth manner because of a predominant chain-transfer reaction, which would theoretically require a lower initiator concentration to proceed. [203] Thiol–ene networks are formed rapidly, achieving a higher rate of conversion under ambient conditions with reduced shrinkage and mechanical stress. [204] Furthermore, thiol-ene reactions are less susceptible to oxygen inhibition compared to traditional free radical chain growth mechanisms, as oxygen abstracts a hydrogen atom from a thiol group to form a reactive thiyl radical. (Fig. 2.3d). [205]

Photoinduced thiol-ene reactions fall into orthogonal click chemistry because each available thiol group only reacts once with one alkene double bond and vice versa, producing homogeneous polymer networks with consistent bulk and local properties. [206] The selective behavior of the reaction can be exploited by performing the reaction in an off-stoichiometric ratio to achieve full conversion but still having residual functionalities from the excess component available for post-printing functionalization. [207] The kinetics of the thiol–ene reaction is highly dependent on the reactivity of the chosen alkene, which increases as the electron density of the double bond increases, with norbornene showing the highest reactivity due to its inherent ring strain. [48] The reactivity of ene groups is also influenced by the stability of intermediate carbon-centered radicals and the

steric hindrance, with terminal ene groups typically more reactive than internal ene groups. [208]

The regular network formation can be achieved by using multifunctional thiolated cross-linkers with more than two moieties, which can also undergo reversible disulfide bond formation as a side reaction when in large excess that can provide dynamic behavior. [209] Thiol-ene bonds are flexible, resulting in less brittle polymers than (meth)acrylate networks, often leading to soft materials and low operational temperature ranges. The rigidity can be increased by exploiting hydrogen bonding between urethane chains end-capped with norbornene as -ene building block. [210] Thiol-ene systems exhibit reduced shrinkage stress compared to acrylate-based formulations given by the delay in the gel, point toward higher conversion, but are hampered by a limited number of reactive species available. [211] Similarly also thiol-yne chemistry can be exploited. [212]

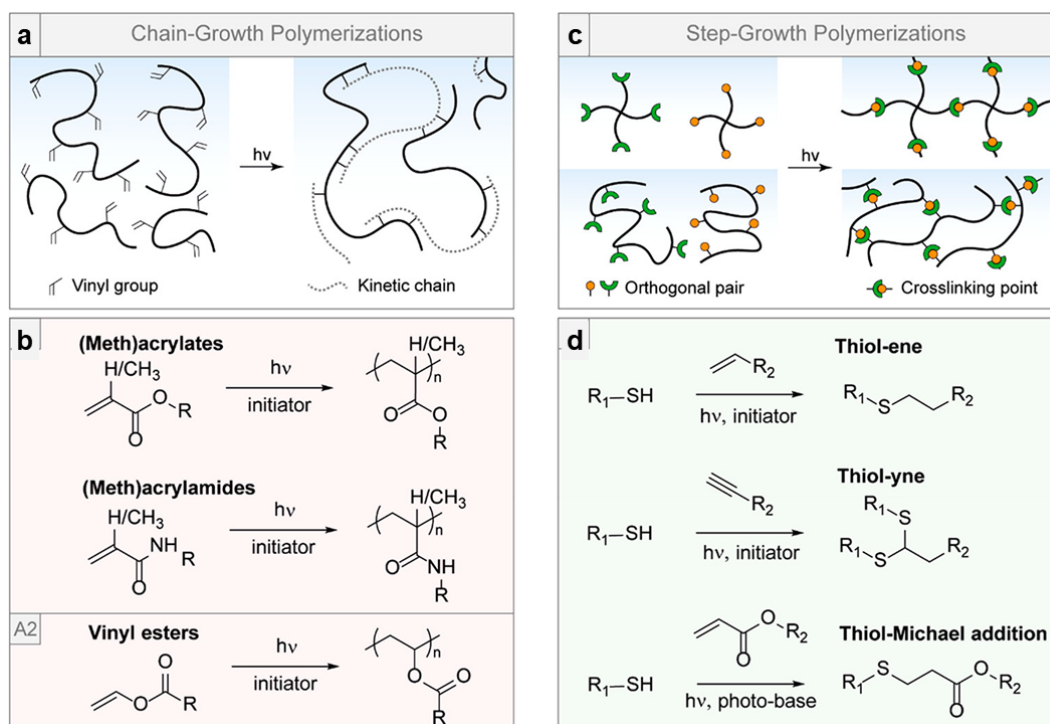


Figure 2.3 Photopolymerization mechanisms. Photopolymerization mechanisms. Schematic representation of a) chain-growth and b) example of reactions for various classes of reactive species. Schematic representation of c) step-growth polymerization mechanisms and d) example of reactions for various classes of reactive species. Reproduced with permission from [160]

2.2.5 Photoactive species

Photoinitiators

A photoinitiator or photoinitiation system converts absorbed light into the reactive species to initiate polymerization. [191] PI goes through a photoinduced rearrangement to generate the radicals that activate the polymerization process, and its chemical structure, number of effective radicals generated, and concentration determine the wavelength and intensity of incident light required. [213] The choice of the most appropriate PI is fundamental in vat photopolymerization because it must be compatible with the light source employed, and it determines the efficiency of the polymerization, which governs the printing time and the final resolution. [165] Common PIs generally absorb light in the near ultraviolet range, but photoinitiators that absorb longer wavelengths in the visible-light range have also been developed. [214] PIs working in the visible light are required to have large aromatic structures, which enhance delocalization of the molecular orbitals, leading to better light absorption properties, such as red-shifted wavelengths in the visible region and higher molar extinction coefficients. [214] Multiple radical photoinitiators are common solutions in resins intended for AM, in which a species is used as a photosensitizer that absorbs the wavelength of the light source and activates the actual PI that initiates the polymerization. [162] Visible light sources ensure reduced risk of eye damage and do not produce ozone during irradiation. Furthermore, visible light is more benign to living cells and is preferable for biomedical applications and dentistry, given the cytotoxic effects of near-UV light. [187] Another fundamental element for safety and cytocompatibility is the solvent employed in the resin, among which water is preferable. On the other hand, the 3D printing process of structures containing high contents of water can be problematic, especially in terms of geometries achievable. Furthermore, PIs are generally characterized by low or no water solubility. These aspects will be explored more in detail in chapter 4.

Radical photoinitiators can be classified into Norrish Type I, usually a single component initiator, or Type II, a double component initiator in combination with a photoinitiator. [215] In addition to these radical PIs, initiators for photomediated redox reactions have also been used. An example of the most commonly used photoinitiators and their principal absorption wavelength is presented in Fig. 2.4.

Photoinitiators undergoing the Norrish type I reaction generate two free radicals by cleavage at the α -position of carbonyl groups that results in the

homolysis of weak bonds. [216] The cleavage process starts once the molecules reach the excited singlet or triplet state after absorption of a light with the appropriate wavelength.

Benzil ketals such as 2-hydroxy-2-methyl-1-phenyl-propan-1-one (Irgacure 1173) and 2,2-dimethoxy-2-phenylacetophenone (DMPA; Irgacure 651) absorb light in the UV range and have been used in different SLA processes. [217] One of the most commonly used benzil ketals, 2-hydroxy-4'-(2-hydroxyethoxy)-2-methylpropiophenone (Irgacure 2959) possesses a hydroxyethoxy group, which gives it a hydrophilic nature with slight water solubility. [218] Its photocleavage does not produce cytotoxic benzaldehyde as a byproduct, which makes it compatible with cells, but it absorbs in the UV range below 300 nm, which is associated with phototoxicity and mutagenicity. [219] Irgacure 2959 has limited molar absorptivity at wavelength 365 nm, resulting in the need for high concentrations to achieve sufficient reaction efficiency. [220]

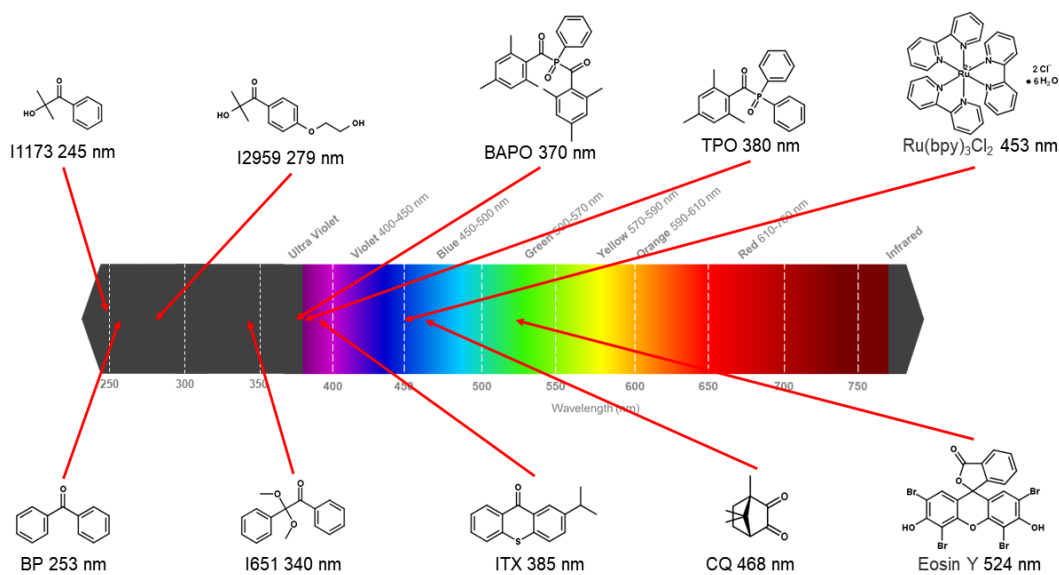


Figure 2.4 Photoinitiators absorption. Chemical structures and maximum absorption wavelength of some photoinitiators employed in 3D photopolymerization. Some of these PI have multiple absorption peaks.

Phosphine oxide-containing photoinitiators present lower energy level of the excited state due to the phosphorus atom adjacent to the carbonyl group, therefore absorb at higher wavelengths around 400 nm, which is preferable for DLP-based systems. [221,222] Acyl phosphine oxides, such as diphenyl(2,4,6-trimethylbenzoyl)phosphine oxide (MAPO or TPO) and bis(2,4,6-

trimethylbenzoyl)phenylphosphine oxide (Irgacure 819; BAPO) were originally intended as UV photoinitiators exclusively for organic formulations. [223] They provide sufficient photosensitivity in the wavelength range 380–450 nm to generate radicals under visible light irradiation. [224,225] The synthesis of BAPO-type PIs is more demanding than that for TPO, which also has the advantage of being colorless, enabling the fabrication of objects with optical transparency. [226]

Photoinitiating systems undergoing the Norrish type II bimolecular reaction are based on an uncleavable photosensitizer undergoing hydrogen absorption or electron transfer when it reaches the excited triplet states under light exposure in the presence of a coinitiator (or synergist) which produces an initiating radical. [227] The most commonly photosensitizers are camphorquinone (CQ), benzophenone (BP), and isopropylthioxanthone (ITX), while common co-initiators are tertiary amines, which produce stable radicals. [228] These photosensitizers absorb in the visible light range, and CQ is largely used in photocuring dental composites. However, these systems suffer from poor water solubility, low reactivity, and a tendency for discoloration. [161,229,230]

Another common and cytocompatible visible-light photoinitiator is Eosin Y, a xanthene dye commonly used in histological staining. It absorbs light in the visible range, between 490 and 650 nm, it requires both a tertiary amine co-initiator and a nitrogen-containing monomer, 1-vinyl-2 pyrrolidinone (NVP), to activate the polymerization reaction. [161]

Besides Norrish type II reactions, eosin-Y has also been reported to facilitate photomediated redox reactions without the need for a co-initiator. [230] The excited PI oxidizes phenolic tyramine groups into tyrosyl radicals, which are then subsequently quenched by forming dityrosine bonds with other nearby tyrosine groups, forming a cross-linked tyramine network. [231] Organometallic complexes, such as tris(2,2'-bipyridyl)-ruthenium(II) chloride hexahydrate ($[\text{Ru}(\text{II})(\text{bpy})_3]\text{Cl}_2$), can also facilitate photomediated redox reactions due to strong visible light absorption, relatively long-lived excited states, and suitable redox potentials. [232] RuII complexes are water soluble and can be used in combination with a persulfate capable of accepting electrons when Ru is photoexcited to triplet state. [233] After electron transfer that leads to RuIII formation, persulfate dissociates into sulfate radicals that can activate free-radical chain polymerization or thiol-ene chain polymerization.

Photoabsorbers or dyes

Photoresins for AM processes contain various additives besides monomers and initiators; some of these additives aimed to enhance specific properties or provide new functions; others, such as photoabsorbers or dyes, were useful for improving the fabrication resolution on all axes during printing. [234] These non-reactive molecules compete with the photoinitiators because they exhibit absorbance at the wavelength of the irradiation source, limiting both overcuring across printed layers and light scattering. [187] Dyes are fundamental for high-fidelity printing and for avoiding a loss of features and precision by attenuating light absorption and reducing the penetration depth, which is strongly dependent on the wavelength and concentration of both photoinitiator and photoabsorber. [152]

These light absorbing molecules include natural or synthetic dyes that absorb in the UV-visible light range at precise absorbance peaks, which can be used with specific photoinitiating systems, depending on their absorption wavelength. Synthetic photoabsorbers, such as Reactive Orange, and Methyl Red and Methylene Blue (Fig. 2.5a), have been used in aqueous and nonaqueous resins for vat photopolymerization, but also natural food dyes, such as Tartrazine, Curcumin, and Anthocyanin (Fig. 2.5b), have been proven to be effective with water-based prepolymer formulations. [166,235–238]

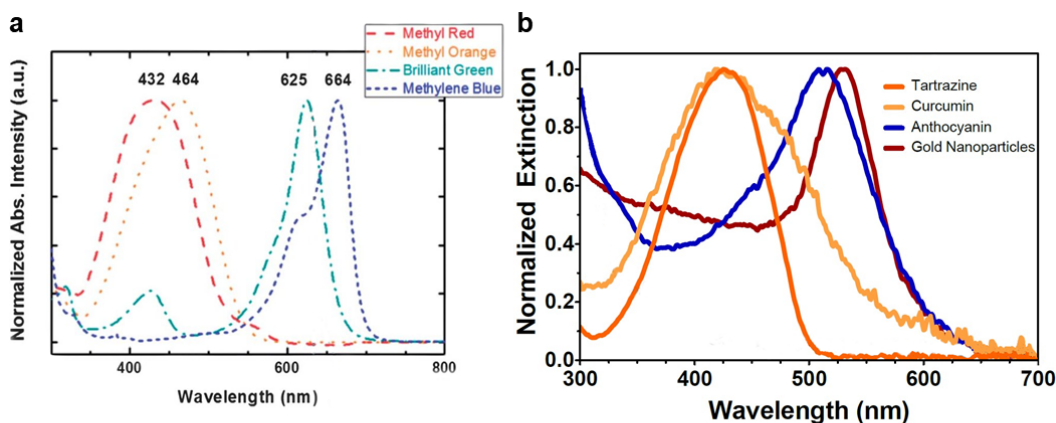


Figure 2.5 Dyes absorptions. UV-Vis absorption spectra of organic dyes and biocompatible photoabsorbers commonly used in vat photopolymerization. Adapted with permission from [166,238].

Chapter 3

State-of-the-art of VP 3D-printed self-healing materials

In this section, various self-healing systems 3D printed with Vat Photopolymerization are reported, classifying them according to the self-healing mechanism involved, mainly focusing on the printing step and the healing efficiency achieved.

3.1 Extrinsic mechanisms

Vascular systems are quite common in extrinsic self-healing systems fabricated via extrusion-based printing because they are easily manufactured, but this configuration is complex to achieve via vat photopolymerization, thus the reported studies are mainly focused on capsule-based systems. Sunlight-triggered autonomic self-healing was achieved upon puncture in silicone (polydimethylsiloxane) (PDMS)-based elastomeric membranes for soft actuators fabricated via photoactivated thiol-ene click reaction between multifunctional mercaptosiloxane (MS) and bifunctional vinylsiloxane (VS). [239] Capsules containing low viscosity unreacted prepolymer resin were retained and incorporated into the composites during printing and had the ability to rapidly release newly exposed thiol-ene fluid that could polymerize within 30 s in ambient sunlight after damage thanks to the lack of oxygen inhibition and rapid polymerization. Sunlight as a stimulus for self-healing is of interest for particular outdoor applications. A synthetic antagonistic muscle actuator, Kagome tower, and a bear were printed using a high-transparency poly-4-methylpentene (PMP) build window to achieve correct detachment of the printed parts from the bottom of the transparent vat, typically made of siloxane-based polymer.

Another feasible approach is the incorporation within the matrix of pockets containing a solvent compatible with the matrix to achieve solvent-welding-based autonomous self-healing. Sanders et al. modified a commercial photocurable resin by embedding anisole and poly (methyl methacrylate) (PMMA) filled vesicles

encapsulated using in situ polymerization of urea-formaldehyde in an oil-in-water emulsion. [240] When the damage ruptures the capsules, the solvent is released, promoting the diffusion of polymers and the formation of entanglements between cracks in the matrix. SH efficiency was investigated with mode I fracture tests, resulting in an 87% recovery of the initial critical toughness after 72 h at room temperature. The presence of microcapsules gave the resin a turbid appearance, but no noticeable effect on the print quality due to light scattering was observed; thus, it did not affect the print quality of the self-supporting holed tetrahedra, which also showed self-healing ability. This system was envisioned to improve the lifetime expectancy of bone cement due to the low toxicity, high boiling point, and immiscibility of anisole with water.

3.2 Intrinsic mechanisms

3.2.1 Dynamic Covalent Chemistry

Disulfide Bonds

Yu and colleagues proposed a photoelastomer ink based on (mercaptopropyl)methylsiloxane-dimethylsiloxane copolymer (MMDS) and vinyl-terminated poly-dimethylsiloxane (V-PDMS) containing both thiol and disulfide groups, where the former facilitates a thiol-ene photopolymerization during the additive manufacturing process, while the latter enables a disulfide metathesis reaction during the self-healing process (Fig. 3.1a). [241] dumbbell-shaped specimens were printed and cut into two parts and healed at 60 °C for 1 h, showing a total recovery of the original strength that remained above 90% efficiency even after over 10 damage-healing cycles, without requiring any solvent as a plasticizer to induce restoration. Various free-form architectures were printed (Fig. 3.1b), and the healing of fatal fractures in complex structures was proven by twisting the healed samples by 540 degrees without failing (Fig. 3.1c). Multimaterial structures composed of a non-healable stiff plastic phase and a healable soft elastomer phase with relatively strong interfacial bonding between the two phases were fabricated to be employed as soft actuators, multiphase composites, and architected electronics. In all these components, SH was proven through restoration of the initial characteristics after healing them for 2 h at 60 °C.

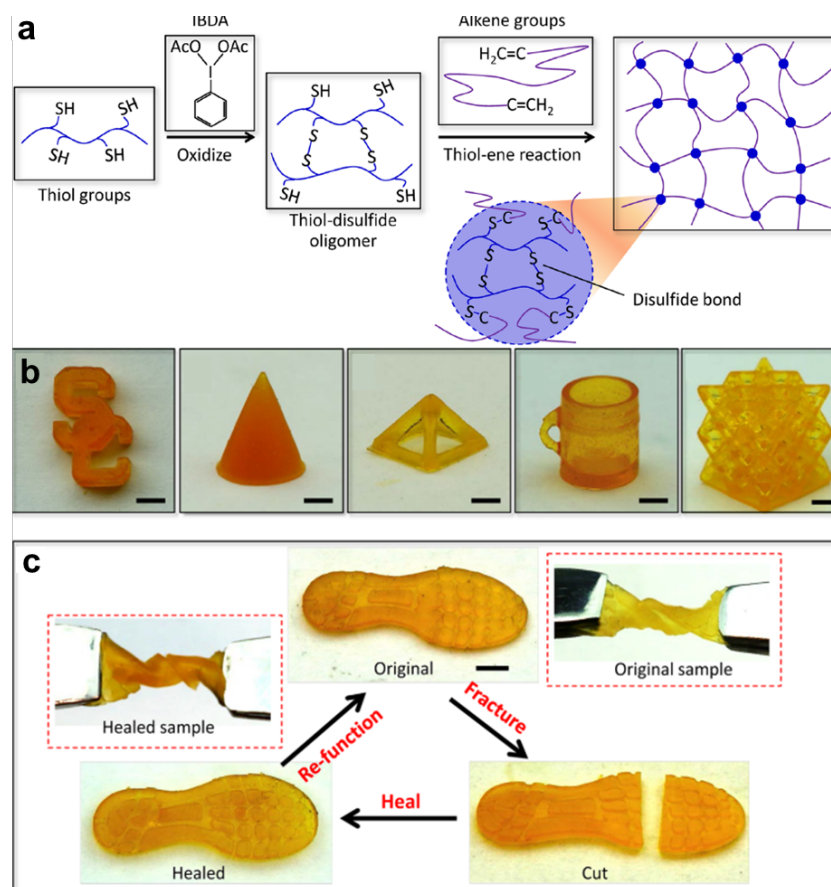


Figure 0.1 Additive manufacturing of self-healing elastomers. a) Molecular design of the self-healing elastomer based on dynamic disulfide bonds among thiol-disulfide oligomer formed by thiol-ene reaction. b) Various manufactured 3D samples: logo of the University of Southern California, a circular cone, a pyramid lattice unit, a cup, and an octet truss lattice. c) Self-healing of a shoe pad-shaped sample. (scale bars 4mm). Adapted with permission from [241]

The same group exploited disulfide-based self-healing mechanisms in transformable lattice structures enabled by fracture and shape-memory-assisted autonomous healing. [242] The polymer network was constructed by an aromatic diisocyanate (isophorone diisocyanate (IPDI)) and a diol (polytetramethylene ether glycol, PTMEG) via urethane links, onto which dynamic disulfide bonds were incorporated by linking a diol-terminated disulfide (Fig. 3.2a). Printability via photocuring was enabled by embedding hydroxyl-ended acrylate groups onto the polymer backbone, and thus, the ink was made of disulfide-linked urethane-acrylate oligomers. The healed strip sample can sustain a weight of 50 g after being brought into contact at 80 °C for 6 h, resulting in a 90% recovery in tensile strength compared to the original samples. Three-point bending tests were also performed, showing that the effective moduli and strength of the healed lattice

structures fluctuated between 85% and 105% of those of the virgin lattice without showing evident degradation trends during ten healing cycles. Very complex and intricate lattices were printed, and it was impossible to reconnect the internal parts through manual contact for healing (Fig. 3.2b). The transformable structure can recover fracture-associated distortion thanks to the shape recovery due to crystalline domain dissociation and reassociation, and enables the alignment of two inaccessible broken surfaces, permitting the recovery of structural function after damages, mode-I fractures, dent-induced crashes, and impacts. The potential application of this system is in lightweight, healable and reusable components, such as aircraft panels, automobile frames, body armor, impact mitigators, vibration dampers, and acoustic modulators.

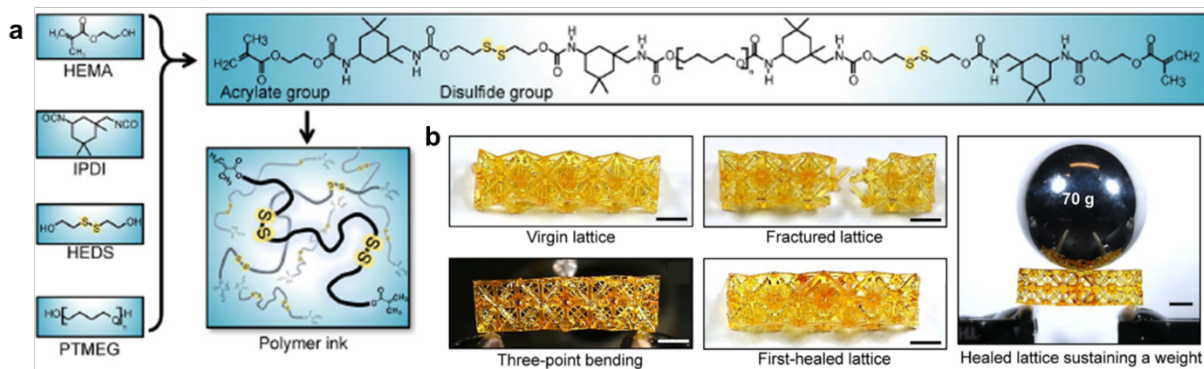


Figure 0.2 Transformable lattice structure with shape-memory-assisted healing.

a) Schematics of the system, with key monomers, the chemical formula of the urethane-acrylate oligomer with disulfide-bonds incorporated. b) Manual-contact-assisted healing process of an octet lattice structure capable of sustaining a static weight after rupture under a three-point-bending load (scale bars 4mm) Adapted with permission from [242]

Another polyurethane (PU)-based elastomer healable via the metathesis of disulfide bonds was proposed for applications in applications in flexible electronics, soft robotics, and sensors based on polyurethane chains functionalized with both acrylate and disulfide functional units compounded with hydroxyethyl acrylate as a reactive diluent (Fig. 3.3a). [243] Multiple healing cycles at 80 ° C for 12 h with an efficiency in recovery of tensile strength decreasing from 95% to 60% due to defects present in the broken surfaces were proven on dumbbell-shaped specimens cut from UV-cured sheets. Self-healing was also visually proven by cutting small cylinders of different colors, connecting and healing them to form a healed cylinder that could lift a weight of 100 g and be stretched to a large deformation. Complex structures with high shape-retention were printed (Fig 3.3b) and showed self-healing ability since they could be freely bent to a large deformation without breaking (Fig. 3.3c).

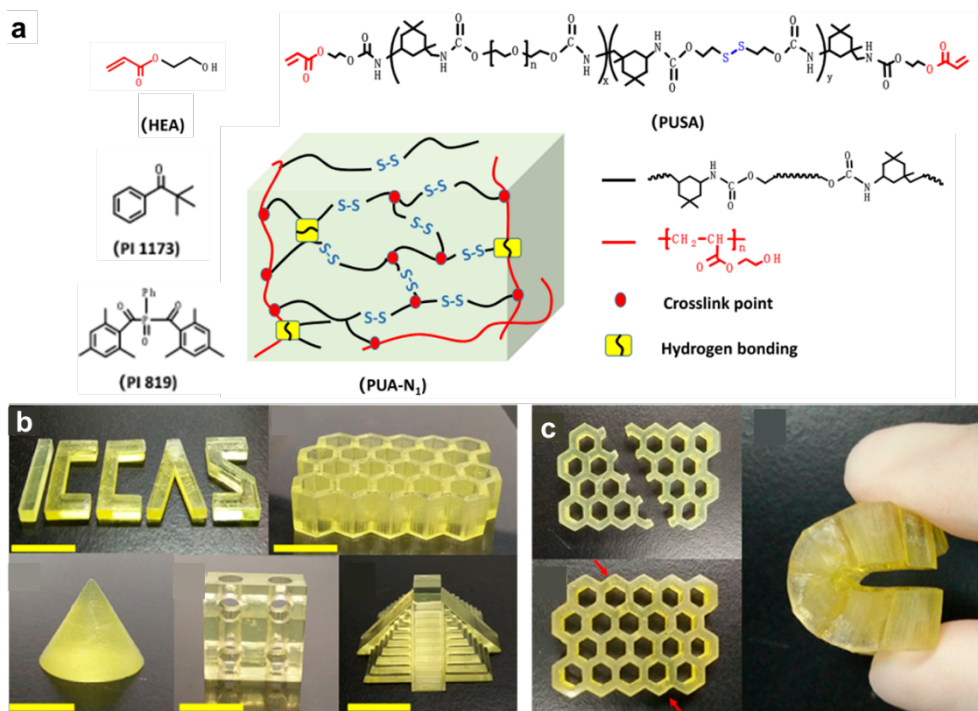


Figure 0.3 Self-healing Polyurethane-based Elastomers. a) Composition of the resin and schematic representation of the polyurethane elastomer with disulfide bonds in the network after UV irradiation. b) Various manufactured 3D samples: Letters, a honeycomb structure, a circular cone, a hollow cube, and a Maya Pyramid (scale bar 10 mm). c) Self-healing experiment of the honeycomb structure with bending deformation after healing. Adapted with permission from [243]

Transesterification

Prof. Ge's group proposed a reprocessable thermoset system made of commercially available chemicals, including 2-hydroxy-3-phenoxypropyl acrylate and bisphenol A glycerolate (1 glycerol/phenol) diacrylate, able to be reshaped, repaired, or recycled due to the presence of zinc acetylacetonate hydrate as a catalyst to accelerate transesterification reactions. [244,245] The heat-triggered bond exchange reactions (BERs) involved hydroxyl functional groups and adjacent ester functional groups capable of simultaneously breaking and reconnecting across the two damaged surfaces. Self-healing was obtained by deposition of virgin material in the damaged area, followed by healing at 180 °C for a few hours, resulting in 100% recovery of stiffness and 93% recovery of strength. The uniaxial tensile test was performed on a printed strip with a circular hole to simulate a mechanical flaw that was filled with the reprocessable thermoset solution and irradiated compared to a virgin unflawed sample. A printed rabbit with broken ears was repaired by polishing the damage site to achieve a flat surface and then performing a new 3D printing to rebuild the

missing part, after which the rabbit was heated to 180 °C for 4 h to regain mechanical performance. A Kelvin foam was thermally treated to increase its mechanical properties, while and a planar thin strip with the letters SUTD was thermoformed into 3D cubic and wavy shapes. The authors also proposed that introducing reshapeability, reparability, and recyclability into 3D printed structures will contribute to alleviating environmental challenges associated with the continuous increase in the consumption of 3D printing materials.

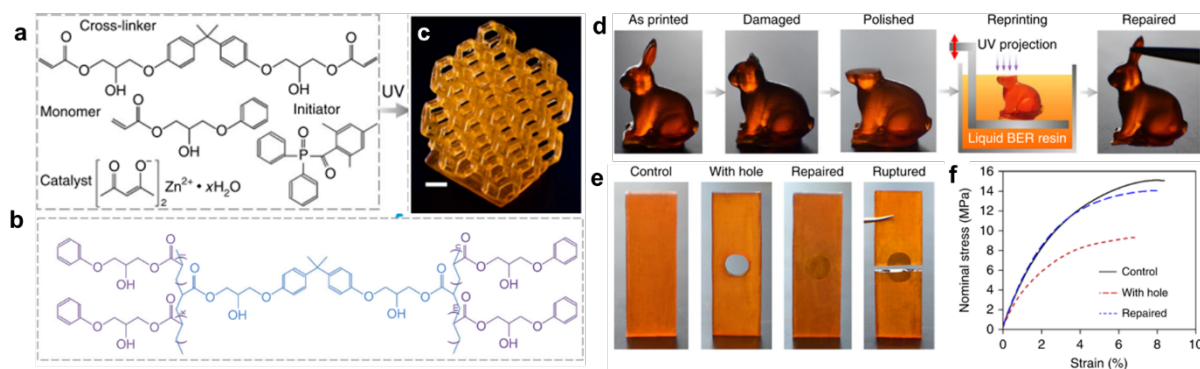


Figure 0.4 Reprocessable repairable thermosets system. a) Chemical composition of the photopolymer solution and b) resulting permanent (blue) and reversible (red) covalent bonds. c) 3D printed Kelvin foam (scale bar 1mm). d) 3D printed rabbit undergone to preparation and reprinting process for restoration. e) Uniaxial tensile test samples before and after testing and f) resulting stress-strain curves. Adapted with permission from [244]

The transesterification of exchangeable β -hydroxyl esters integrated in the oligomer can be combined with hydrogen bonds into an acrylate-based vitrimer composed of a diacrylate prepolymer synthesized by the chemical reaction between glycidyl methacrylate (GMA) and suberic acid (SA) mixed with acrylamide (AAM) and tetrahydrofurfuryl acrylate (THFA). [245] The network rearrangement proceeds upon heating, with the gradual disappearance of hydrogen bonds at increasing temperatures, imparting reprocessability into the printed structures. A tensile lap shear test at room temperature was used to check the welding of two pieces of fractured vitrimers by partial overlap followed by pressing at 180 °C for 1 h, resulting in a welding efficiency of 73%. Objects with various complex structures were printed, such as a set of gears and a honeycomb, and could be remolded again by dissolving them in ethylene glycol, allowing the material to be recycled, or reformed after being ground to fine powders and subsequently pressed at 180 °C for 1 h with a pressure of 1000 psi.

Schlögl et al. presented a new transesterification catalyst based on a soluble monofunctional methacrylate phosphate that does not compromise cure rate and

pot life and is covalently incorporated into a network obtained by click reactions of thiol-acrylate between hydroxy-2-phenoxypropyl acrylate, glycerol 1,3-diglycerolate diacrylate (DGDA) and trimethylolpropane tri(3-mercaptopropionate) (TTMP) (Fig. 3.5a). [246] The liquid catalyst is able to catalyze esterifications and transesterifications in the solid polymer network, which rapidly undergoes thermoactivated rearrangements of its topology, because of functional thiols acting as chain transfer agents in exchange reactions with hydroxyl groups present on acrylate monomers. Healing efficiency was determined by printing uniaxial tensile tests with circular-shaped holes in the center fitted by a circular-shaped counterpart and healed by thermal treatment at 180 ° C for 4 h, resulting in a total recovery of the original tensile strength compared to a defect-free bar (Fig. 3.5b-c). 3D objects with simple planar shapes and various substructures with different dimensions were printed (Fig. 3.5 d-e), demonstrating triple shape memory upon heating and programming the network above its two transition temperatures, for the fabrication of customized soft actuator and soft robotics, as shown by the example of a grabber.

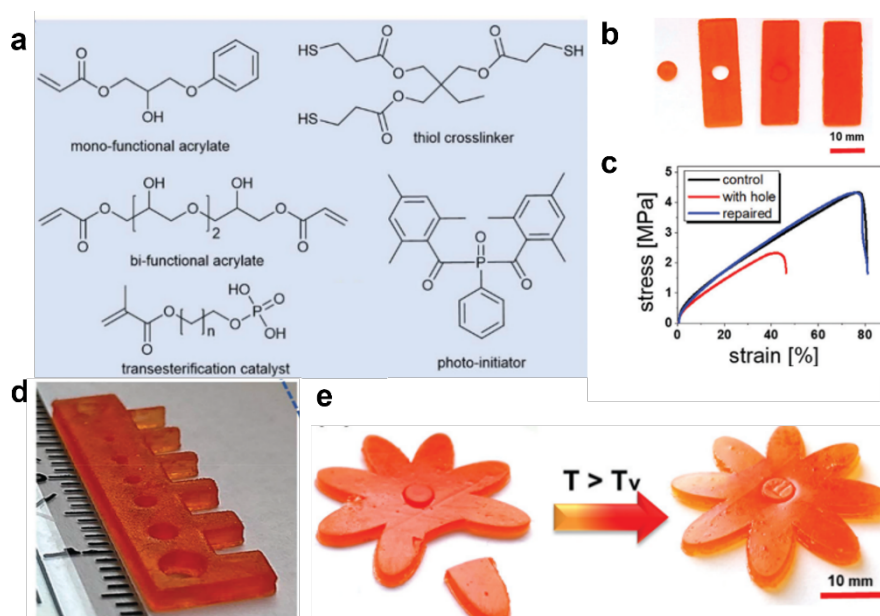


Figure 0.5 Thiol-acrylate vitrimers. a) Composition of the resin used for the preparation of covalent adaptable thiol-acrylate photopolymers. b) Uniaxial tensile test samples before and after testing and c) resulting stress-strain curves. d) 3D printed test structure with a length of 2.6 cm. e) Thermally triggered healing of a flower-shaped 3D printed specimen. Adapted with permission from [246]

Urethane Bonds

Photosynthesis-Assisted Healing was recently proposed as an innovative self-healing solution different from conventional SH mechanisms. Hybrid synthetic living materials can remodel their microstructures or recover mechanical properties by photosynthesis of embedded living chloroplasts extracted from spinach leaves to generate glucose capable of forming urethane strong linkages (-NH-CO-O-) with isocyanate distal groups (NCO) incorporated onto a poly (tetrahydrofuran)-based polymer functionalized with isophorone diisocyanate, dimethylacetamide, dibutyltin dilaurate, and hydroxyethyl methacrylate (Fig. 3.6a). [247] Samples are endowed with matrix strengthening and crack healing when exposed to white light, which induces the formation of stiff regions with 'artificial polysaccharides'. The additional cross-linking could be reversed by cleaving glucose with periodic acids. 3D printed dumbbell-shaped samples with free NCO groups and embedded chloroplasts were cut, rejoined and then subjected to 4 h illumination and 4 h darkness, resulting in a smooth healing interface with a healing strength ratio of $70 \pm 7\%$, while a control polymer without embedded chloroplasts exhibited poor healing performance with a healing strength ratio as low as 9%. Various architectures could be printed, such as treelike, Popeye-like structures and octet lattices, all of which showed tunable stiffness and healing ability that enabled mechanical properties recovery, as demonstrated by the healing of a boat propeller (Fig. 3.6b).

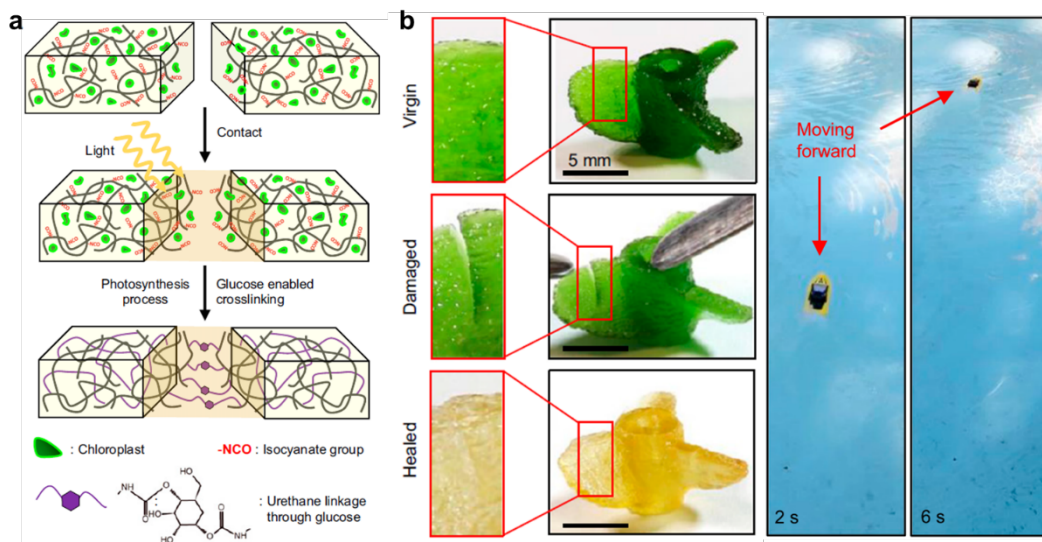


Figure 0.6 Photosynthesis-assisted Self-healing. a) Schematic of the healing mechanism based on the formation of additional cross-links between free isocyanate (NCO) side groups and photosynthesis-produced glucose around the fracture surface. b) Healing process of a 3D printed propeller and practical demonstration of the correct operability. Adapted with permission from [247]

Dynamic Urea Bonds

Modular 4D printing enables to fabricate shapes by assembling multilayered complex structures and integrating multiple materials. Building blocks can be connected through hindered urea bonds, since these do not require a catalyst, and their dynamic characteristic can be tunable by simply adjusting the steric hindrance. [248] The photocurable formulation was based on a diacrylate cross-linker containing crystallizable polycaprolactone (PCL) and dynamic hindered urea linkages, synthesized functionalizing polycaprolactone diol with ditin butyl dilaurate (DBTDL), isophorone diisocyanate (IPDI), N,N'-diisopropylethylenediamine (DPEA) and 2-isocyanatoethyl acrylate (IEMA) and mixed in toluene with two other monofunctional monomers, 2-phenoxyethyl acrylate (PEA) and isobornyl acrylate (IBOA) (Fig. 3.7a). The precursor was poured into a reaction cell and subjected to double side irradiation with a commercial projector, followed by uncured monomers and solvent removal from the cured film to develop the 2D film into 3D structures due to material heterogeneity and internal stresses. Modules were assembled in a layered fashion by interfacial bond exchange by annealing at 160 ° C for 2 h (Fig. 3.7b), and welding performance was evaluated by bringing together two halves of a cut sample, annealing them, and testing the sample by uniaxial tensile testing, showing an identical modulus and breaking strain comparable to the original one (Fig. 3.7c). Sophisticated multilayered complex structures were assembled, including a 3D Miura-patterned structure with zero Poisson ratio and a Kresling-patterned cylindrical structure, and these devices can undergo complex morphing and reconfiguration through a shape memory mechanism (Fig. 3.7d). Modules with independently controlled geometric shapes and material properties could be assembled by interfacial welding into complex 3D objects (Fig. 3.7e).

3.2.2 Non-Covalent Interactions

Hydrogen Bonding

Invernizzi and colleagues were the first to demonstrate SH in shape memory objects fabricated by vat photopolymerization using poly (caprolactone) dimethacrylate (PCLDMA) methacrylated 2-ureido-4[1H]-pyrimidinone (UPyMA) units co-cross-linked together. [249] Shape memory and self-healing functionalities are both thermally triggered, respectively, due to PCL, based on its crystallization and melting, and UPy motifs, which can establish four hydrogen bonds. The self-healing performance of both the surface and the bulk was evaluated, with a superficial scratch and a sample cut into two parts showing

restoration after 1 h at 80 ° C with a healing efficiency calculated on a tensile strength of 54% after a damage cycle. A L-shaped layered structure was printed to mimic the index finger and the thumb, which was partially cut and then repaired to prove that shape memory functionalities are still preserved after healing, making these printed actuators suitable for soft robotics (Fig, 3.8).

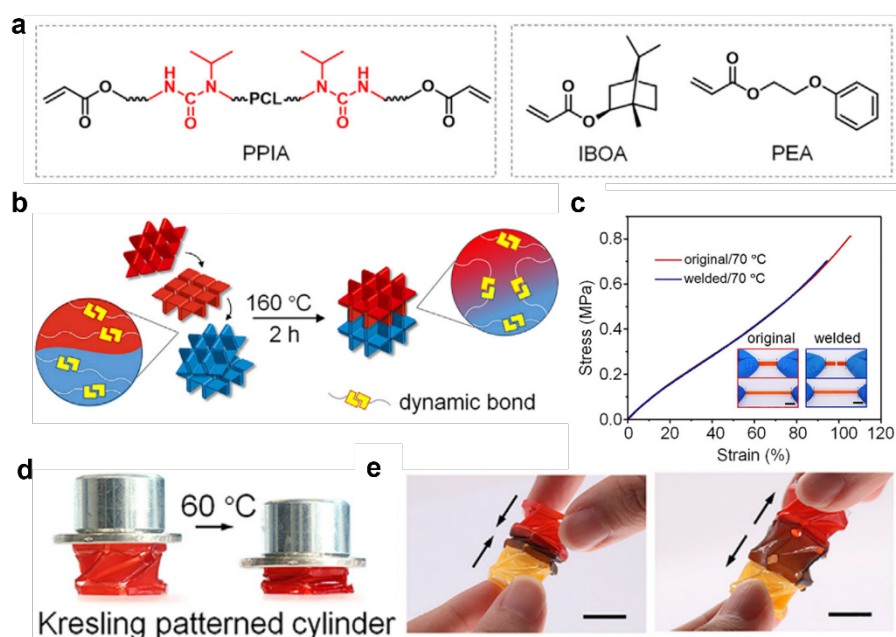


Figure 0.7 Modular 4D Printing via Interfacial Welding. a) Composition of the printing precursor with functional groups capable of establishing dynamic urea bonds highlighted. b) Schematic illustration of the module assembly and c) demonstration of the welding. d) deformation behavior of a Kresling-patterned cylinder and e) assembly of a Kresling-patterned multi-material cylinder. Adapted with permission from [248]

N-acryloylmorpholine (ACMO) is another species capable of establishing abundant intermolecular hydrogen bonds and can be used as a matrix within which carboxyl multi-walled carbon nanotubes (c-CNTs) can be dispersed as the conductive medium by using a BYK surfactant (Fig. 3.9a). [250] Self-healing can be attributed to the interactions formed between carboxyl groups of c-CNTs and carbonyl/amino groups of poly (ACMO), activated by a water-uptake process when two pieces are brought together for few hours in a humidity chamber. Mechanical self-healing efficiency was defined as the ratio of Young's modulus of self-healed and original samples, and it was around 96% after the first cut-healing cycle, but gradually decreased with increasing healing times and cycles as resistance increased because of the restricted mobility of free groups in breakages. Printability of complex structures was proven, such as a ladder pyramid, a conical gear, a bolt and a set of spikes, but no SH was shown on printed

objects(Fig. 3.9b-c), which were used as strain sensor for the detection of human activities.

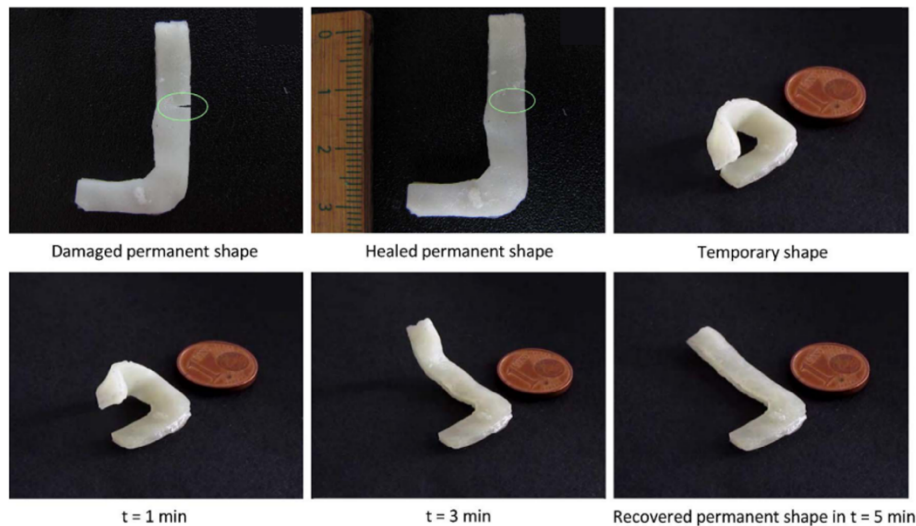


Figure 0.8 Shape memory-assisted self-healing. L-shaped 3D printed sample healed after thermal treatment shows retention of shape memory property with complete recovery of the original shape. Reproduced with permission from [249]

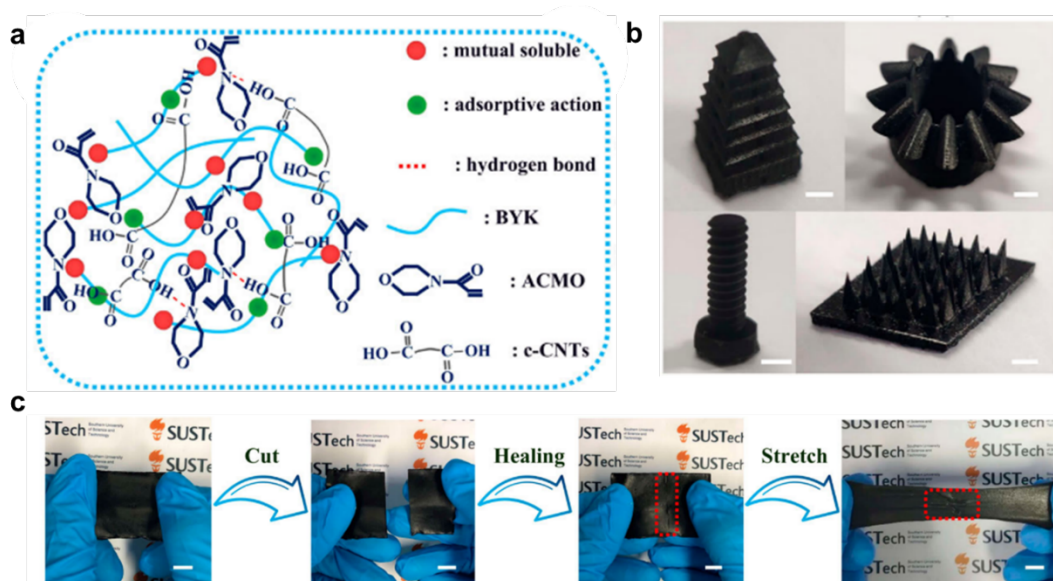


Figure 0.9 CNT-mediated self-healing. a) Schematic diagram of BYK-assisted dispersion-based system. b) Various manufactured samples: stepwise pyramid, conic gear, bolt, spiked plane (Scale bar: 2 mm). c) Demonstration of the self-healing and stretchability of a film (Scale bar: 10 mm). Adapted with permission from [250]

Hydrogen bonding can also be established between carboxyl groups and carbonyl groups of alkyl acrylate units copolymerized together. Self-healing

elastomers (SHEs) were prepared by mixing acrylic acid (AAc) with alkyl acrylates with various chain lengths to tune the Tg. [251] PAA alone exhibited a typical elastic behavior above its Tg, but no self-healing was observed, confirming that the interaction between AA units alone could not provide SH. AA was replaced by methyl methacrylate (MMA) to copolymerize with butyl acrylate (BA), and the newly obtained elastomer did not exhibit self-healing behavior, proving that the self-healing behavior can be ascribed to the interactions between the ester carbonyl group of BA units and the carboxyl group of AA units (Fig. 3.10). The self-healing efficiencies were evaluated by comparing the tensile strength and elongation at break of pristine and healed samples for 12 h at room temperature, resulting in a complete recovery of the mechanical properties, as also shown by a scratch-healing test under optical microscopy as a visual demonstration. Various specimens were printed, such as a gear, the model of an ear and of a hand, a honeycomb lattice, and a gecko, with the latter used to prove effective self-healing by replanting its tail after cutting. Given the absence of a chemical cross-linker, the copolymer elastomers were soluble in various solvents, and therefore, they were reprocessed by the solvent-casting method. The introduction of carboxylic ionic liquid led to the formation of a non-leaking and attachable ionogel by 3D printing for the detection of various human gestures.

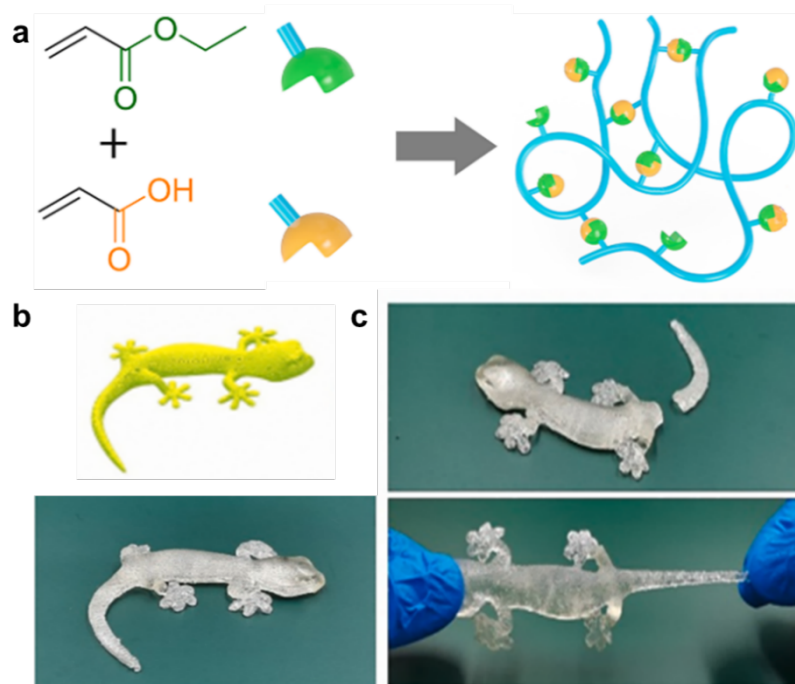


Figure 0.7 Biomimetic, Adhesive, and Self-healing Elastomers. a) Composition and schematic illustration of the copolymer elastomer formation. b) CAD file and printed gecko undergoing c) cutting and healing cycle. Adapted with permission from [251]

Intrinsic SH in vat-photopolymerized hydrogels was reported in a system designed as an interpenetrated network based on poly (acrylic acid (AAc)-N-vinyl-2-pyrrolidone (NVP)) and carboxymethylcellulose (CMC) was printed without the use of a cross-linker (Fig. 3.11a). [252] A dual physical interaction occurs between the CMC and poly (NVP-AAc) based on Zn^{2+} ligand coordination and hydrogen bonding, imparting toughness and self-healing ability to the gel. Custom objects for wearable human motion sensing were printed with high resolution and tested in real time, such as the fingertip, knuckle, and manipulator (Fig. 3.11b). Self-healing efficiency was assessed by cutting and rejoining printed dumbbell-shaped hydrogels at room temperature for 24 h, showing that the healed samples regained 81% and 91% of the original stress and strain (Fig. 3.11c).

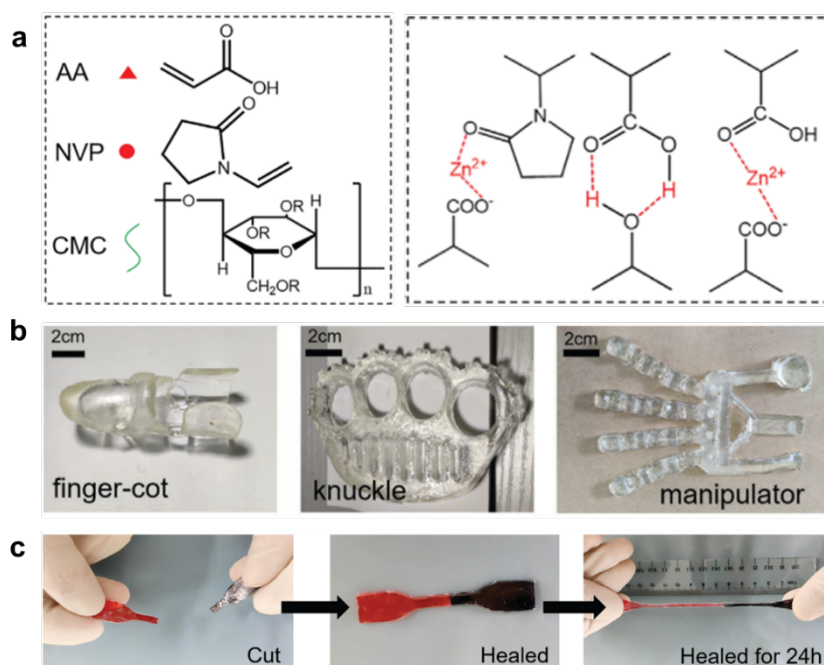


Figure 0.8 Fully physically cross-linked double network. a) Composition of the resin and schematic representation of the hydrogen bonds and metal-ligand bonds formation. b) Various manufactured wearable flexible sensors. c) Self-healing process and stretching of a dumbbell-shaped sample. Adapted with permission from [252]

Ionic Interactions

Self healing in silicone elastomer could be achieved by interpenetrating amino-modified silicone oil (PDMS-NH₂) and carboxyl-modified silicone oil (PDMS-COOH) with thiol-modified silicone oil (PDMS-SH), vinyl-terminated polysiloxane (PDMS-Vi) (Fig. 3.12a). [253] Thiol-ene photopolymerization between the thiol and vinyl functionalities enabled rapid formation of the primary covalent cross-linked network by VP, while thermoinduced ionic association

between carboxyl and amido moieties formed a secondary reversible network. Self-healing was achieved by heating the system at 120 ° C and then cooling it to room temperature, activating the dissociation and reassociation of ionic bonds that could also proceed slowly at room temperature. Repeatable healing tests were performed using uniaxial tensile tests on printed dumbbell samples, showing a recovery of 92% in mechanical strength after triple healing cycles. Thick planar-layered architectures with no complex features were printed, such as gears and a half moon, and efficient self-healing was proven by healing and deforming cut samples without immediate failure (Fig. 3.12b). The system also showed repeatable reprocessability with a recovery of 90% of virgin mechanical strengths, and the reprocessed elastomers could still repair damages with an efficiency of over 90% after thrice reprocessing (Fig. 3.12c).

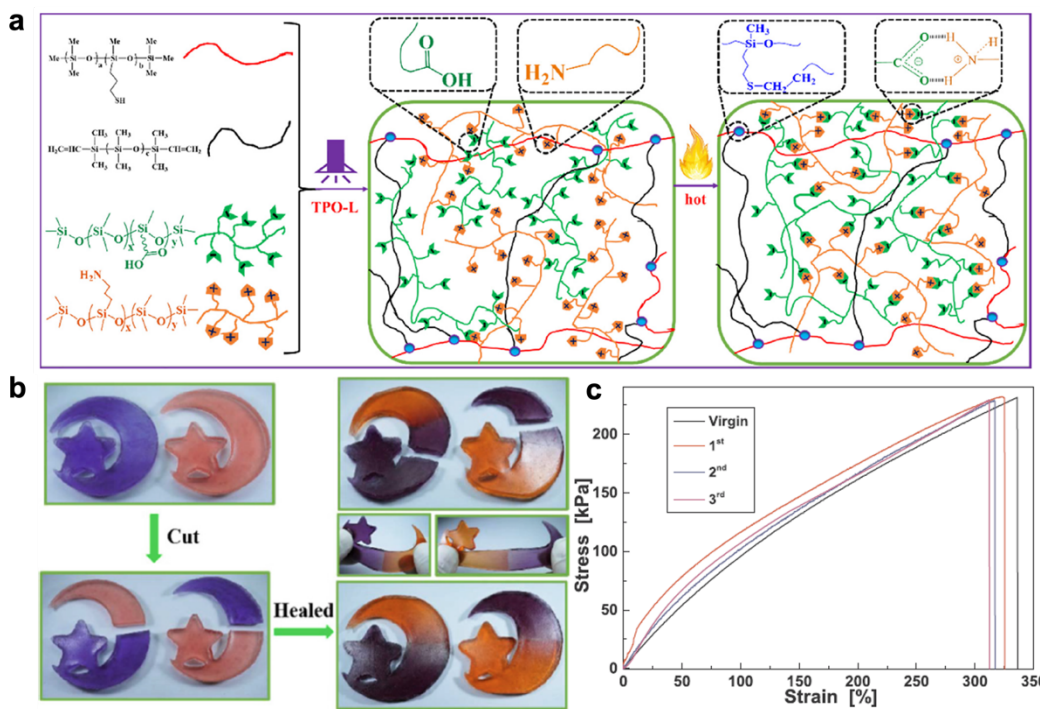


Figure 0.9 Dually-cured recyclable elastomer. a) Composition of the resin and schematic representation of photo-thermal dual-curing and interactions. b) Self-healing process of a 3d printed component. c) Stress–strain curves of repeatedly self-healed 3D printed samples. Adapted with permission from [253]

Recyclable and self-healable structures can be printed using a resin comprising urethane monoacrylate (UMA) and acrylic acid (AAc), zinc dimethacrylate (ZDMA) as the cross-linker (Fig. 3.13a). [254] Monomers are cross-linked by ionic bonding between Zn²⁺ and –COO– and hydrogen bonding between –NH or –OH and –C=O that can be dissociated when heated and while

the bonded state is restored upon cooling (Fig. 3.13b). Mechanical tests were carried out on printed dogbones, which exhibited a healing efficiency greater than 75% after healing at 90 °C for 12 h, decreased for shorter times or lower temperature. Self-healing was also proven by the recovery in conductivity after healing of a sample coated with Ag nanowires. By varying the monomer ratio, soft elastomers to rigid plastics could be selectively printed into complex architectures, such as a soft octopus or rigid bridge, showing healing ability Fig. 3.13c-d). Soft and rigid parts were assembled into more complex structures, including a thin-wall structure reshaped at high temperature into a cylindrical structure and a modular snowman model. The dynamic nature of the bonds endowed the samples with repeatable recycling with a treatment under a pressure of 10 MPa, with over 70% of the mechanical properties that could be recovered.

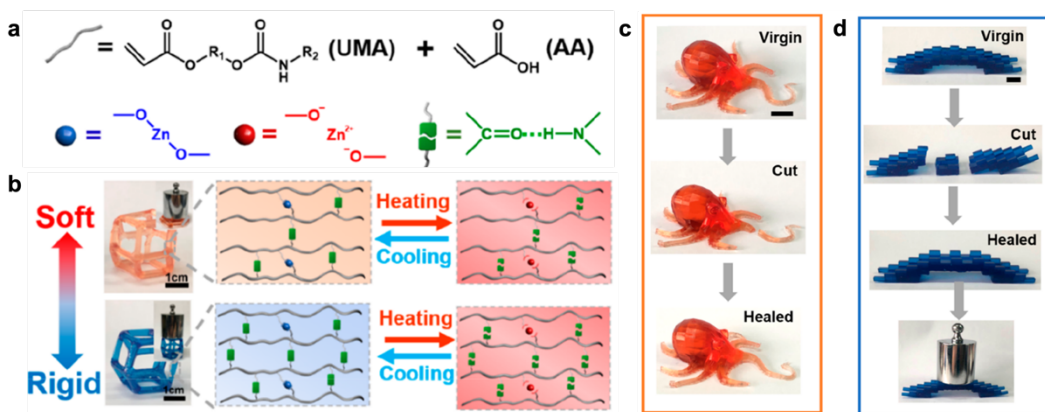


Figure 0.10 Temperature-dependent rigidity. a) Temperature-dependent behavior. b) Dynamic polymer networks cross-linked by reversible ionic bonding and hydrogen bonding. Self-healing demonstration of various manufactured samples: c) soft octopus and d) rigid bridge. Adapted with permission from [254]

Modular 4D printing can also be obtained by exploiting ions introduced later in the structure by soaking. Self-adhesive hydrogel building blocks made of covalently cross-linked poly (ethylene glycol) diacrylate (PEGDA) in the presence of dispersed anionic high-molecular-weight poly (acrylic acid) (PAAc) could be printed and connected via ion-mediated adhesion (Fig. 3.14a). [255] Trivalent ferric cations bridged between PAA polymer chains on adjacent surfaces, and this coordination bond can be reversed using EDTA to chelate ferric ions. Self-healing was assessed by cutting a cylindrical specimen in half with a scalpel, and then both halves were brought back in contact into a ferric ions solution. After 60 min, the structure was able to support itself against gravity and was tested using a three-point flexural test that showed a flexural modulus similar to ionically cross-linked uncut samples but with a lower displacement (Fig.

3.14b). Cylinders and a salamander were printed to prove effective self-adhesion (Fig. 3.14c), whereas LEGO-like hydrogel blocks with internal channels and external mechanical connectors were fabricated to be stacked into complex microfluidic devices and multilevel architectures.

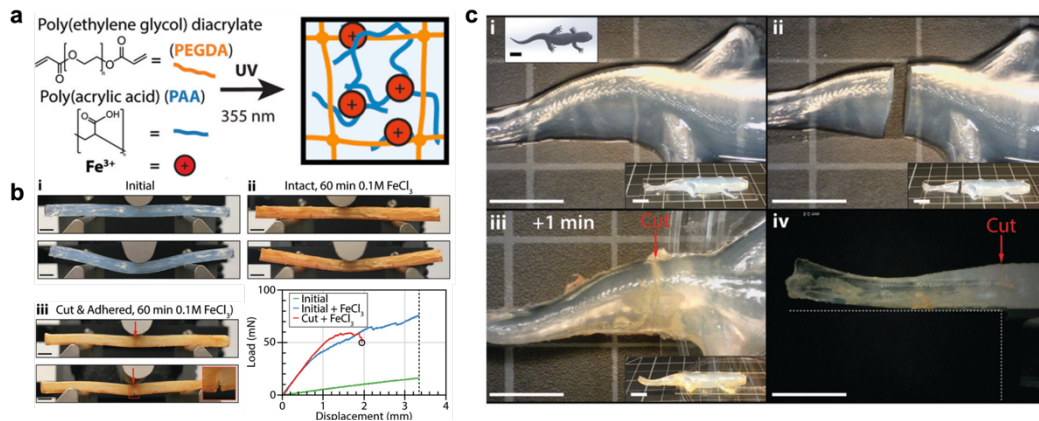


Figure 0.11 Self-adhesive hydrogels. a) Chemical composition and schematic illustration of the ionically crosslinked system. b) Comparison among different samples under 3-points bending test and resulting load-displacement curves. c) Self-adhesion of a manufactured salamander tail. Adapted with permission from [255]

Molecular Interdiffusion

PCL can be used as a mending agent for autonomous self-healing, also in VP-printed objects, by incorporating the linear polymer into a covalent network made of poly (ethylene glycol) dimethacrylate (PEGDMA) and benzyl methacrylate (BMA) (Fig. 3.15a). [256] The SH process is based on thermally triggered PCL semicrystalline domains melting, diffusion across the boundary and bonding of two damaged surfaces by entangling upon cooling (Fig. 3.15b). Mechanical properties of a damaged structure could be recovered to more than 90% when evaluated with uniaxial tensile tests on overlapped 3D printed rectangular samples severed and then healed for 20 min at 80 ° C. The printing solution was obtained by increasing the temperature above the melting temperature of the healing agent (about 60°C) to obtain a material with the ability to spread onto the platform. A chess piece, a Kelvin foam, a closed gripper, and a cardiovascular stent were fabricated, then damaged and healed at 80 ° C for 5 min to show recovery in mechanical properties and shape memory ability to restore correct functionality (Fig. 3.15c-d).

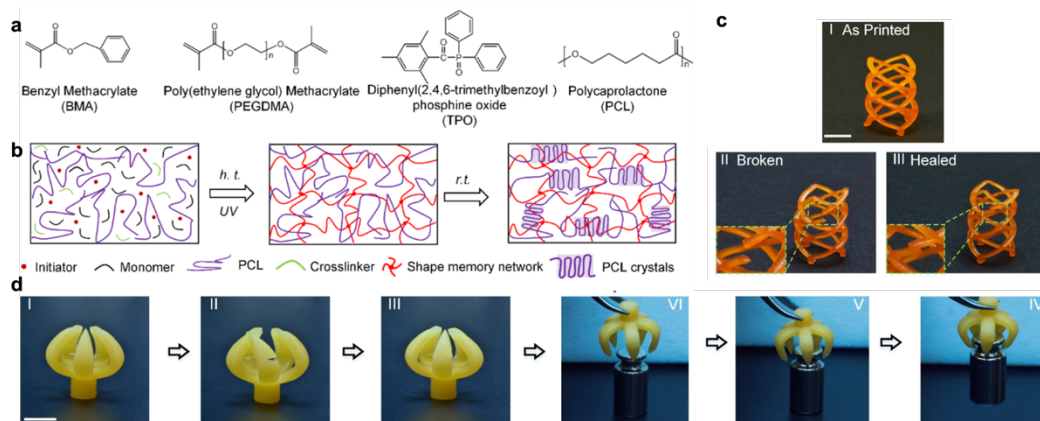


Figure 0.12 Self-healing and shape memory double system. a) Chemical composition and b) schematic representation of the double network. c) Self-healing process of a manufactured stent. d) Self-healing and application demonstration of a manufactured gripper. Adapted with permission from [256]

Chapter 4

Description of the presented work

4.1 What was missing in the field

As presented in the previous chapters, the literature review can be summarized in these few bullet points:

- DLP-printed hydrogels are nowadays well established, even if there is still a huge work on the design of new hydrogels;
- There is a wide variety of self-healing hydrogels in 3D printing, obtained through different techniques. The SH mechanics exploited are many, sometimes also combined. There are also examples of DLP-printed self-healing dry systems, both thermosetting and elastomers, but a combination of the three characteristics had not been shown so far.
- To go beyond the actual intrinsic limitations of these systems, it is necessary to identify which are the critical aspects of each combination and to define clear and achievable goals to establish which are the trade-offs to be addressed.

Approaching the experimental investigation, it must be considered that hydrogels cannot be repaired following common mending methods for standard polymeric materials, because adhesives or fasteners are not suitable options. Soft hydrogels undergo irreversible failure even though they can provide good compliance between surfaces, and rigid hydrogels cannot be restored as well in any way in case of damage. Two rigid plastic elements can be soldered, glued, or riveted, while hydrogels, either soft or rigid, cannot be mended. For these reasons, to possess SH characteristics in hydrogels is advantageous. On the other hand, there are some characteristics of hydrogels that facilitate self-mending because the presence of water facilitates the first step of the restoration mechanism, i.e., is the diffusion of the chain across the interface, which is necessary to enable the interaction due to newly established dynamic bonds.

Furthermore, hydrogel shaping is complicated and up to now the main application of SH hydrogels was limited to bidimensional systems, such as protective coating or films, electronic skin, and sensors. Introducing the printability would expand the potential applications, opening the way for new applications in a variety of fields.

Among the different 3D printing techniques, vat photopolymerization relies on irreversible covalent bonds, and this strongly limits the useful life to irreversible failures because the object must be completely replaced after damage. The ability to self-repair would largely extend the useful life of a 3D printed object because it could be repaired completely, restoring completely the initial properties and thus theoretically guaranteeing unmodified properties for several damage even at the same site. Furthermore, SH could be combined with a more accurate and tailored component design, accurately studied to prevent potential damage and ruptures, and therefore indirectly providing additional safety. As shown in the previous chapter, the field of VP printed self-healable systems is expanding rapidly, but soft hydrogels were missing. Water-based systems are getting enormous attention especially in the biomedical field, since they can act as host for cell encapsulation and proliferation, but at the same time, they can mimic the physical and mechanical properties of natural tissues. Natural self-repairing tissues are characterized by complex multiscale structures with tiny features and a high level of detail, reproducible with 3D printing and VP in particular, which enables the fabrication of large objects with a tenth of millimeter resolution and high shape fidelity. This kind of structure is not standardized, and it is hard to fabricate them serially because they are usually personalized and unique. Furthermore, intrinsic SH would facilitate restoration after simple rejoining without requiring any action on the interacting surfaces and elements, which could be not easily accessible or hard to manage, maybe because they are too small. The combination of self-healing ability and multiscale characteristics could be extended to many other fields other than tissue engineering.

Intrinsic SH is advantageous because recovery of initial bulk properties, either structural or functional, would be achieved without affecting the local properties and preserving the overall functionality/structure. On the other hand, the use of an external adhesive could affect the properties of smaller features, perhaps not affected by the damage but disturbed by the external repair, which is focused on the macrostructure and its characteristics, especially bulk mechanical properties. Macroscopic restoration could be achieved with comparable efficiency, but the use of an external healing agent could cause a loss of the advantage arising from

the use of VP in terms of accuracy, selectivity, topology, and geometrical complexity. Starting from a liquid formulation enables large variability and adaptability of the resin components, especially when using complex synthetic molecules that gather different properties, such as copolymers. However, the printing techniques largely limit and exclude several potential interactions commonly used in self-healing mechanisms and require specific characteristics, especially the presence of irreversible covalent bonds.

As a result, this thesis work has as final goal the fabrication of 3D printed objects via vat photopolymerization 3D printing technique. In this context a series of subtasks were fixed: to use of commercial resins, to obtain complex shaping and to avoid the use of heating as external triggering.

4.2 Objectives of the work

4.2.1 Use of commercial materials or simple chemistry

The use of commercial chemical species available in large quantities makes the proposed solutions as ready-made formulations easily scalable for larger batches even on an industrial level. Commercial compounds guarantee a relevant consistency in performances, repeatability and easy reproducibility of the system even under different conditions and performed by different operators. By using commercially available materials, our research would enable the fast adaptation of the approach to researchers from a variety of fields. There is a growing attention for simpler processes and friendly materials because complexity hinders the mass production and economic practicability, restricting a wider application. [64]

When we were unable to achieve the desired properties by using commercial materials, we opted for simple modification reactions of commercial materials that did not involve stringent reaction conditions, complex synthesis, and purification procedures, and we limited the use of toxic chemicals. This was mainly driven by the will to keep the processes as simple as possible, with easily tunable and modifiable species combined with our difficulties to perform complex synthetic reactions.

The main drawback of this approach is the limitation given by the availability of useful water-soluble species compatible with the healing mechanism and the selected printing technique. Commercial materials have well-defined characteristics that cannot be excessively modified to meet the necessary requirements, and therefore the system has to be adapted according to several

trade-offs between the desired goal and the available properties. An additional drawback is that sometimes chemical species with the desired properties are commercially available but are very expensive or sold in extremely low quantities, usually incompatible with the volumes required to set up and test a resin for vat photopolymerization.

4.2.2 Water-Based Formulations

The use of water as the main solvent or only solvent is advantageous because it enables the avoidance of organic solvents in the formulation, more compatible with common photocurable species but that must be removed and replaced with water by swelling the sample after printing. [257,258] Water is already embedded within the network, and therefore an additional swelling step is not required, guaranteeing a precise control over the amount of water embedded inside, enabling determining a correlation between properties and water content. Furthermore, water, and phosphate buffer solution as its derivative, combined with nontoxic monomers, favors cell encapsulation and proliferation, which is useful for potential biomedical applications. Visible-light sources can be employed with these systems to print resins already containing cells in the liquid state, resulting in a more homogeneous distribution of the encapsulated cells within the printed object.

It is also possible to control the mechanical properties, such as the softness of a loosely cross-linked network by varying the water content, which allows the diffusion of small molecules inside the system. In particular, water enables the use of ions inside the hydrogels that can provide several different properties, from functional characteristics, such as conductivity, to the ion-mediated self-healing mechanism. [259] Water is also a very easily removable solvent, which could be extracted from the network either by heating or, more preferably, by freeze-drying, an approach that leaves the network unmodified, enabling one to study its morphology.

However, the use of water comes with several drawbacks, among which the main one is its fast evaporation, which causes a drastic change in the hydrogel properties, which requires the implementation of retention techniques, either by modifying the system or by storing the samples in a humid environment. [260] The polar nature of water strongly limits the compatible chemical species and induces extensive solvation of hydrophilic species and functional groups, especially hydroxyl groups due to their affinity, which competes with the formation of hydrogen bonds. The use of water also largely limits the useful

temperature range for their application, and to expand the useful window, anti-freezing or anti-drying mechanisms based on the addition of salts, organic solvents (organohydrogels) and ionic liquids (ionogels) are required. [261,262]

4.2.3 Structural Complexity

We wanted to exploit the full potential given by the specific 3D printing technique. Vat photopolymerization enables the fabrication of elements on several different dimensional scales combined together, enabling a high level of detail and precision in soft materials or swollen networks. The use of a 3D printing processing enables to introduce self-healing potentiality within the bulk of the object. SH water-based systems have been initially developed as planar systems or bulk hydrogels, which reproduce the shape of their containers when they are thermally polymerized. [15,140]

Soft hydrogels can deform under their weight especially when excessively swollen, and this may be limiting for shape retention after printing, but it is an advantage when deformable and foldable systems are required. Another drawback is the need to design self-supporting architectures because supports cannot be removed without damaging the final objects, unlike in extrusion printing where it is possible to easily print two different materials at the same time.

4.2.4 Non-heating triggered self-healing

Heating is the most common approach to activate SH because it enables the system to be brought above its glass transition temperature, activating free chain movements. [88] This kind of trigger can also be used to activate SH in hydrogels, but it requires the use of samples inserted in sealed bags and immersed in hot water, which would be incompatible with complex structures printed via vat photopolymerization. [263] The presence of water hinders the use of heat as a trigger without any water evaporation prevention approach, and therefore, healing mechanisms capable of restoring properties at room temperature are the most suitable for use with printed complex hydrogels. [264]

Physical, chemical, or biological stimuli-mediated self-healing could also be explored, such as pH, electromagnetic fields, ions or glucose addition or enzyme-activated. [5] Stimuli responsiveness is highly controllable and tunable, but every trigger has its own limitation, since light is limited by the penetration depth of the selected wavelength, pH and ion responsive systems are strongly dependent on the concentration gradient of the species within the system, and the use of

electromagnetic fields require the presence of additives capable of interacting with the stimuli, such as metallic nanoparticles or graphene oxide capable of localized conversion of electromagnetic radiation into heat, which could interfere with the light absorption required for an effective printing process.

4.3 Innovation and perspectives of the work

The main innovation of this PhD research lies in the use of vat photopolymerization to precisely shape hydrogels with self-healing properties. SH hydrogels fabricated via direct writing or extrusion-based printing technologies are well established in the literature, because of the compatibility of the intrinsic characteristics of these technologies with the properties of these materials, such as the very loose or absent chemical cross-linking and shear-thinning behavior. [265] This work aims to overcome the inherent incompatibility between several apparently antagonistic attributes to demonstrate the feasibility of merging the VP printing process with autonomous restoration by exploiting different strategies.

Soft systems must be designed accurately to allow mechanical strength, printability, and repairability, which is not trivial, since an interdependent and well-balanced relationship is fundamental for a successful fabrication and for achieving suitable self-healing. SH is also beneficial because it helps reduce the impact of errors and defects created after fabrication and reduces the mechanical anisotropy by increasing layer adhesion. VP printing enables precise spatio-temporal control over material position, allowing to fine-tune the local properties, especially where there is a higher probability of failure. This is particularly relevant in geometrically intricate structures, which are complicated to repair by external intervention after a damage, usually requiring a complete replacement of the object to restore functionality.

Materials able to autonomously reestablish the connection in the structure interrupted by the damage are fundamental for the evolution of additive manufacturing, particularly vat photopolymerization. A further expansion of the potential applications of 3D-shaped hydrogels could arise from the use of low-cost commercial 3D printers and commercially available components in water-based resins. The complexity related to stringent reaction conditions and complex synthesis and purification procedures for SH materials hinders mass production and economic practicability, together with the difficulties related to shape soft materials. The processing and systems proposed here offer a general and versatile approach that could potentially enable fast adaptation to larger scales or for

specific applications, pushing the hydrogels beyond their conventional roles and use.

We envision that there is still a large margin for progress and improvement in the field, which will expand the potential application of hydrogels to both structural and functional purposes, also given the growing global attention to resource consumption reduction and performance optimization. The proposed approaches pave the way for future applications in diverse fields beyond biomedicine, ranging from soft robotics and wearable sensors to energy storage and harvesting. [186,266–268]

Additional considerations can be made to extend the useful lifetime of printed parts by introducing self-healing properties, given the intrinsic limitations associated with irreversible crosslinking in thermosetting materials. [269] The life cycle of a printed component does not end at end-of-life; therefore, healability, recyclability, and degradability by design are key concepts to meet the recent demand to increase the sustainability of AM technologies by further reducing waste, already minimal, and producing less hazardous residuals, which can be reused or easily disposed. [270,271] The transition towards polymerization mechanisms completely based on dynamic chemistries that could intrinsically provide printability and repairability would address some of the environmental issues arising from unprocessed thermosets, which could also greatly benefit from the development of monomers and active species from renewable sources. [272–274]

As a relevant step further, self-healing could also be combined with another smart property relying on similar dynamic interactions and chemistries, such as shape-memory ability for a completely autonomous restoration. The component would be capable of recovering the original shape while restoring its initial properties after the application of a specific controlled stimulus. [275,276] The synergy between programmable materials and on-purpose design for a predictable response results in 4D printing, which enables the fabrication of dynamic adjustable architectures to best exploit the characteristics of smart materials. [277,278]

4.4 Critical aspects of the research

4.4.1 Hydrogel printing via vat photopolymerization

Hydrogels are a class of hydrophilic polymer networks that can hold considerable amounts of water, 10 to 100 times their original weight or volume, without dissolving or collapsing, and retain the characteristics of solids. [279] These jelly-like materials have broadly tunable physical and chemical properties ranging from soft and weak to hard and tough, allowing control over degradability, processability, gelation mechanisms, as well as functional properties. [280] This versatility and adaptability make them suitable for mimicking complex natural tissue structures, drawing tremendous attention in the biomedical field. [281] 3D printing via vat photopolymerization merges two processes since it gives a shape to the hydrogel while synthesizing it. The versatility provided by hydrogels via chemical functionalization, together with a synergistic design of the shape, function, or physicochemical variation in response to a stimulus, offer a large potential for 4D printing applications. [282] Hydrogels are capable of environmental stimuli-responsiveness, which results in a reversible macroscopic change that may be used to build dynamic 3D-printed architectures, also called smart 4D materials.

Hydrogels can be easily prepared using aqueous chemistries and photocrosslinking under relatively mild conditions starting from either natural or synthetic molecules as building blocks. Hydrophilic monomers exhibit more versatile adaptivity and easily controlled properties thanks to their well-defined chemical structure and can be properly selected and modified. [283] Chemically modified natural biomolecules are commonly used to manufacture biocompatible hydrogels with suitable mechanical properties and can be combined with synthetic species to combine biocompatibility and tunable physical properties. [197] Conventional hydrogels usually possess relatively poor mechanical properties and are prone to failure, which makes it difficult the shaping into geometrically complex structures. Soft and loosely cross-linked networks may not be able to withstand their own weight and may collapse outside a watery environment. Furthermore, their soft yet brittle nature hinders their fabrication by means of conventional subtractive manufacturing techniques, limiting their potential applications and development. [284] Additive manufacturing of hydrogels, in particular light-based techniques, enables the construction of intricate and self-standing structures with functional and structural applications, ranging from scaffolds and organ-like structures for tissue engineering to soft robotics and

bioresorbable electronics. [285] Hydrogels in lithography-based printing are most commonly fabricated as water-swollen polymer networks rather than being printed dry and then swollen after printing to better control their final shape and avoid distortions. [187] AM enables the hydrogel to be synthesized at the focal plane and forming it three-dimensionally at the same time, starting from a liquid precursor using water as a non-toxic, green, and cheap solvent. [286]

However, the main problem with aqueous formulations, unlike classical organic compositions, is that only limited commercially available photoinitiators show adequate water solubility and reaction efficiency. [287] Conventional PIs have been designed with hydrophobic moieties for nonpolar environments, since they were mainly used directly in photocurable resins. This makes the PIs poorly water soluble and unable to be homogeneously dispersed within the resin, thus not resulting in clear precursor solutions, an issue that causes light scattering and uncontrolled polymerization. This problem has prompted the development of water-soluble PIs, especially for biomedical applications (Fig. 4.1). [288] Irgacure 2959 is the most common water-soluble PI, but it has no absorption in the visible range and its initiation rate is not high. The water-soluble analogues of acetylphosphine oxides show a very high molar extinction coefficient to light at 365 nm and show absorption also in the visible light range (405 nm), making them more efficient at lower concentrations than Irgacure 2959 and also rapid gelation with longer wavelengths. [197] These water-soluble PIs have been prepared by salt formation, such as LAP, functionalization with a water-soluble non-ionic polymer, such as PEG-BAPO, or by encapsulation within a surfactant shell, such as water-dispersible TPO nanoparticles. [287,289,290] Recently, particular attention has been dedicated to the development of novel photoinitiating systems based on natural organic compounds with excellent visible light absorption, such as Eosin Y, curcumin, riboflavin, and coumarin, but also organometallic compounds, such as RuII combined with a thermal co-initiator such as a persulfate. [288,291–293]

4.4.2 Combination of printability and healability

Printability is defined as the ability of a material to be three-dimensionally shaped and result in an outcome with specific properties desirable for a given application when subjected to a certain set of printing conditions. [294] Therefore, the properties of the material have an impact on various parameters of the printing process, sometimes limiting the correct fabrication. Maintaining the proper biological, functional, or mechanical properties while meeting the manufacturing

requirements is a challenge and requires the design of polymers with a tailored structure, architecture, and functionality. [295]

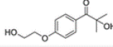
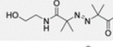
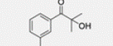
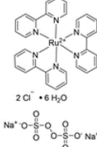
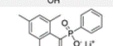
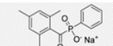
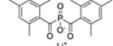
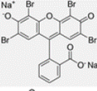
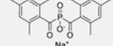
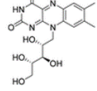
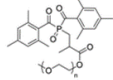
PI	Chemical Structure	Water solubility (g/L)	λ_{max} (nm)	ϵ_{max} ($M^{-1} cm^{-1}$)	PI	Chemical Structure	Water solubility (g/L)	λ_{max} (nm)	ϵ_{max} ($M^{-1} cm^{-1}$)
I2959		5	328 365	296 5	VA-086		45	375	30
API-180		74	329	97	Ru(bpy) ₃ /SPS		10	450	14600
LAP		47	365 380 405	218 191 30					
Na-TPO		29	380	250					
BAPO-OLi		54	383	197	Eosin Y		1	515 516	69800 86500
BAPO-ONa		60	383	256	Riboflavin		0.06-1.2	374 449	10300 12100
PEG-BAPO		1.38	390	450					

Figure 4.1 Water-soluble photoinitiators. Chemical structures and maximum absorption wavelength of the water-soluble photoinitiators most commonly used in light-activated additive manufacturing techniques. Adapted with permission from [160]

The integration of SH into materials for 3D printing is a more straightforward approach because it usually does not comprise a modification of the matrix material but the addition of an external healing agent, following an extrinsic SH mechanism. [3] Properly shaping intrinsic SH systems in complex 3D shapes could be difficult, especially for soft materials or hydrogels, unless it is performed through additive manufacturing. [296] Intrinsic systems are well suited as inks for 3D printing thanks to their dynamic nature and the absence of additional elements within the structure, such as capsules or vesicles.

Another convenient and common strategy to gather repairability and printability in intrinsic systems is the development of interpenetrated network (IPN) materials, which represents an intermediate approach among the two ways presented before. This solution combines one or more rigid and robust frames made of generally irreversible chemical bonds, generated during 3D fabrication, with at least one much weaker network based on mostly reversible bonds, imparting SH capability. [297] IPNs can display customized features while maintaining the characteristics of both constituents simultaneously and matching the requirements for fabrication with different AM techniques. [280,298]

The network adaptability and integrity must be carefully balanced to enable polymer chain mobility for a sufficient timescale of healing and gelation, while still providing appropriate stability to the structure without affecting printing

fidelity. Reversible linkages contribute to the overall crosslinking density, providing additional support, but the interactions among the moieties should be labile enough to undergo significant breakage upon stress and enable reformation under favorable conditions without impacting the efficiency of restoration of the properties. [299] Self-healing must be independent from the fabrication process, to be preserved and compatible with the target properties for the final application. [300]

The formulation must be specifically adapted to be compatible with the fabrication process, especially in terms of viscosity and solidification mechanism, in accordance with the dynamic and labile nature of the interacting functional groups. [265] Monomers and long macromolecules can be tailored in terms of relative ratio and distribution of reactive groups to match the desired properties together with traditional parameters such as molecular weight, polymer concentration, and cross-linking density.

In hydrogels, the presence of water provides high mobility of the chains by increasing the molecular distance, which increases the recovery efficiency but reduces the mechanical strength, directly related to the cross-linking density, inversely proportional to the self-healing ability. [30] In contrast, good mechanical properties are achieved by increasing the number or strengthening the crosslinks, but this has a detrimental effect on effective restoration. [301] 3D printing of SH hydrogels has more stringent prerequisites than conventional fabrication of hydrogels via additive manufacturing because a balanced compromise must be achieved among competing elements such as water content, cross-linking density, and effectiveness of chain interactions. [302] A loose cross-linking would entail a soft hydrogel, beneficial to chain migration but resulting in structures with poor shape fidelity, while the polymer content would favor self-healing if low, but hinder it if excessively low, or support shape retention and abating the restoration capability at the same time when high. [303] The simultaneous need for these opposite requirements leads to the definition of a fabrication window determined by the range of material properties suitable for efficient self-healing and accurate printability. [299]

For extrusion printing, the ink can already be polymerized or pre-cross-linked and in the final configuration, while for VP a liquid resin comprising multifunctional building blocks must be used. These reacting species are highly versatile and can be functionalized with functional groups that are able to form dynamic bonds that can be either a pendant group or integrated into the backbone

after polymerization. [304] Interacting motifs tend to establish reversible dynamic bonds in both the liquid and solid phase before and after printing. [155,198] Viscosity in VP is not as crucial as in extrusion printing, but it is still fundamental. Similarly, for extrusion printing, the viscosity of the ink is determined by the molecular weight and concentration of all elements as well as the presence of solvents and plasticizers, but in this case the viscosity must be sufficiently low to process the formulation with sufficient precision and rapid solid-liquid separation during printing. [187] A low resin viscosity at processing temperature is beneficial because it can easily flow around the build platform to form new layers upon further exposures by recoating and self-leveling, thus reducing construction times, and it also facilitates the removal of unreacted excess resin from the negative features in the construct before post-curing. [198]

The curing speed after exposure to light is the most important parameter for a successful VP printing, and interactions in the liquid phase can reduce the mobility of reacting radicals, affecting the reaction rate speed and thus the printing efficiency and the final shape fidelity. [305] SH moieties must not interfere with radical polymerization, but at the same time the polymerization must not affect the SH properties, with the two sets of bonds that should be orthogonal between them to coexist efficiently. Unlike extrusion printing, VP fabrication relies on generally irreversible reactions that form strong covalent bonds, producing a dense and rigid chemically cross-linked network, allowing for the simultaneous accurate tuning of the macrostructure and mesostructure. [159,284] After damage, densely cross-linked networks, related to the number of functionalities in the oligomers, would result in short chains, which would not be able to generate sufficiently strong bonds across the rejoin interface. [162,165] A solution to overcome these issues are hybrid networks, which encompass both reversible and non-reversible crosslinks, either in the same or independent networks. Those are designed to have self-healing properties by the coexistence of sacrificial labile bonds within a chemical structural network that provides mechanical properties, reinforced by the reversible bonds. [306] Self-healing properties can help retain the final shape by reinforcing the adhesion among layers, already ensured by chemical bonds among them obtained by increasing curing depth within an already printed layer, tuning the extent of light penetration in the ink. Reversible bonds are also beneficial in soft materials, such as hydrogels. Self-supporting structures with intricate architecture require high mechanical robustness, given by a dense chemical network, which causes a loss in potential self-healing ability, evident only in systems with low cross-link density, which may collapse when loaded or simply under their own weight. [307] The

presence of the solvent allows proper free motion of the chains across the surfaces, which could otherwise be activated by heating.

4.4.3 Definition of a self-healing procedure

Self-healing is not achieved in a unique way, since the procedure is strongly dependent on the healing mechanism selected and the associated stimuli required to trigger it. To describe the restoration of conventional self-healing hydrogels, it is fundamental to establish the time scale of healing, which can last from a few seconds to days. [263,308,309] This belongs to the dynamics of macromolecular rearrangements and the kinetics of reversible linkages. [21] Sometimes in literature healing results are presented in the discussion, but the restoration procedure is not described in detail in the Methods section. [310,311] To give a comprehensive overview and describe how the healing procedure and parameters have been selected it is useful to report the influence of different composition and time in contact on the healing efficiency, and more in general describe the effects of the variation of all the relevant variables that could affect restoration. [312,313] Another important element of the procedure that must be reported is the number of samples used to define the healing efficiency for statistical purposes, to determine the precision and variability of the reported result. [83,311,313] Among the pieces of information that are not usually provided, the most commonly missing are those related to external indirect aspects, such as sample preparation and storage conditions, which could have a significant impact on systems that require several hours to achieve sufficient restoration. [252,314]

There are systems capable of autonomously self-heal in air under ambient conditions at room temperature, especially those characterized by anti-drying properties. [82,262] Generally, given the large amount of water embedded and its tendency to easily evaporate even under ambient conditions, conventional hydrogels after being cut are rejoined into a sealed container, such as a poly (ethylene) bag. [86,315,316] Alternatively, the gel samples can be coated with a thin layer of silicon oil to prevent the evaporation. [83] More commonly, samples are kept in a container with moisture or controlled humidity to counterbalance evaporation. [26,79,317] It is interesting to note that humidity is not always beneficial, but in some cases it could have a detrimental effect on the healing efficiency. [80] Sometimes humidity could not be sufficient and therefore a small amount of water, usually few drops, is placed on the fracture surfaces to prevent water loss and at the same time to promote chain interdiffusion. [318,319] Self-healing could also require to be performed underwater or in a hot water bath.

[320,321] Underwater self-healing could also be used to demonstrate the ability of the system to self-heal even in harsh conditions, which could also be very low temperatures. [322,323] Healing in a medium with different characteristics from simple deionized water, such as acidic or basic conditions, seawater, or buffer solutions, is required for systems that rely on various pH values to restore bonds and interactions. [14,26] A particular case is represented by systems relying on ion-mediated mechanism, which can either already contain the ions within the network or the broken hydrogel pieces can be immersed in an ion-rich solution to promote the adhesion of the interfaces. [255,259]

Another information that is not frequently reported is the presence of self-adhesion between cut pieces to keep the samples together, with the fusion process occurring immediately after the rejoining. [15] The application of an external force is an important aspect to be taken into consideration because there are systems that do not need any force to be brought into contact, while others require to be pressed together to be merged. [14,324] To guarantee contact and compliance among surfaces, some systems need to be placed in a mold or a narrow container, in particular when the cut pieces have shapes such as quarter of cylinders. [26,86,325] A common approach is to combine pressure and confinement, with the pieces merged within a plastic syringe by slight pressing the piston plunger to keep it at room temperature or immersed in a hot water bath for a prescribed time. [140,326,327] To better contain water evaporation and at the same time prevent water swelling, the plastic syringes can also be sealed in polyethylene bags, and then immersed into water baths. [141,312] This approach excludes any practical application, because the hydrogel is healable under strict and non-operational conditions and only with specific simple shapes compatible with the syringe.

4.4.4 Assessment of self-healing efficiency

In analogy to the large variety of possible restoration approaches, there are several different procedures to assess self-healing efficiency, sometimes not comparable. The self-healing phenomenon is mostly proven by macroscopic visual demonstrations, which is a common and simple test. Two freshly cut pieces of a specimen are placed in contact for a specific period, after which restoration of the contact interface is observed. [14] In some cases, the efficient repair can be easily shown using different dyes dispersed in the polymeric matrix, which can diffuse when in contact. Diffusion of the dyes reveals the mobility of the cross-linking network and therefore gives an indirect indication of the magnitude of interaction.

[15] Testing the ability of the material to support its own weight after healing without breaking is another common test. [311] To have more detailed information, the topography of the restored interface can be evaluated by optical microscopy, while its morphology at a micro/nanoscale can be characterized by scanning electron microscopy (SEM) or atomic force microscopy (AFM). [322] Qualitative considerations can be accompanied by quantitative evaluations to determine the effectiveness in recovering the initial mechanical or functional properties. [328] Healing efficiency can be expressed by calculating the ratio (or percentage) between the value of a specific, measurable property of the virgin specimen and the same property measured after restoration. [329]

Since the trigger for self-healing is mechanical damage, recovery of mechanical properties is the most common assessment performed, but the same general approach can be used to determine recovery in several properties, such as electrical or thermal conductivity, or optical transparency. [140,330,331] Among the different techniques used to determine the bulk healing efficiency in mechanical properties, uniaxial tensile strength and compression strength tests are the most widely employed, from which useful parameters such as Young's modulus, stress and elongation at break, and fracture energy can be obtained and compared. [332] These tests are performed on an intact and rejoin sample, the results of which are compared to determine the efficiency and can be repeated on the same samples various times to determine the ability of the specimen to recover after damage/healing cycles. [14] Another common experimental method is bending resistance tests to assess healing capacity by comparing the plane strain fracture toughness (K_{IC}) or the strain energy release rate (G_{IC}) of the material before and after recovery. [333]

Mechanically weak materials, such as hydrogels, can have the ability to withstand their weight but may not have the structural stability to withstand clamping for uniaxial tensile testing. [20] Therefore, their healing efficiencies can be determined using cyclic compression testing, where hysteresis indicates the decreased number of cross-links and thus reduced structure recovery over many deformation cycles, each one followed by a recovery period. [119] Another frequent characterization for SH hydrogels is a step-strain measurement with oscillatory rheology, subjecting the hydrogel to a variable strain periodically alternating high and low strain for damage recovery cycles at constant oscillation frequency to determine the recovery rate of the viscoelastic properties. [300]

Comparison among results from different self-healing systems is often difficult due to inconsistency in healing efficiencies calculated on different parameters arising from different characterization techniques (Fig. 4.2). Furthermore, the outcomes of the characterizations, and thus of the resulting healing efficiency, strongly depend on the testing parameters, such as sample dimension and geometry, temperature of analysis, as well as the undamaged material properties, the extent of the damaged volume, the time elapsed between breakage and rejoin and the time required for repair to occur, and proper alignment of the joint surfaces.

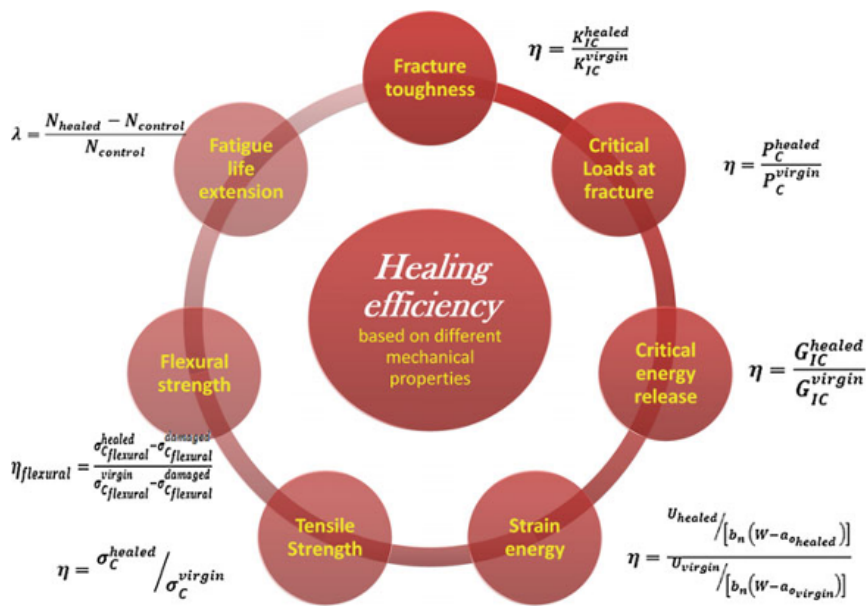


Figure 4.2 Healing efficiency assessment. Physical parameters and formulas used to determine the performance in mechanical properties restoration. Reproduced with permission [331]

Chapter 5

Hydrogen bonds-based self-healing system

This section is based on the original research article titled "3D-printed self-healing hydrogels via Digital Light Processing". This article was published in Nature Communications in 2021, DOI: 10.1038/s41467-021-22802-z.

5.1 Introduction

As introduced in the previous chapter, meeting antithetical requirements for both vat photopolymerization and self-healing is challenging and could explain the absences in the literature of systems bearing both properties simultaneously. To address this challenge, we exploited a healing agent to provide autonomous repairability combined with an independent covalent network fabricated during the printing process. This approach allows to preserve the two contributions separately, but at the same time enables a homogeneous system. For self-healing mechanisms, we exploited electrostatic interactions, constituted between a large extent of functional groups in the healing agent. Among the possible choices, the most employed are hydroxyl groups, which are capable of establishing hydrogen bonding, a strong non-covalent interaction. [75] Poly (vinyl alcohol) (PVA) is a semicrystalline synthetic polymer very rich in pendant hydroxyl groups, which provide a hydrophilic nature that results in excellent water solubility, good mechanical properties, and optical transparency of the water-based solutions and of thin films. [334] PVA is odorless, tasteless, and it is known for its low toxicity and biodegradability that enable a wide range of uses, from food packaging, thanks to its film-forming capability and barrier properties to oxygen and carbon dioxide, to food and cosmetics products, as well as for pharmaceutical and biomedical applications. [335] The monomer, vinyl alcohol, does not exist in a stable form rearranging to its tautomer, acetaldehyde. Therefore, PVA is prepared from the hydrolysis of poly (vinyl acetate) (PVAc); this reaction never reaches completion, always resulting in a copolymer of PVA and PVAc. [336] The degree

of hydrolysis (DH), which defines the percentage of hydroxyl groups present along the backbone, the molecular weight and the polydispersity index determine the physiochemical characteristics of PVA, first of all from the temperature at which it is soluble in water. [337] A high DH, and therefore a lower ratio of residual acetate groups, leads to a large extent of hydrogen bonding, with increased stereoregularity and degree of crystallinity, resulting in a higher temperature required to be dissolved in water, since water molecules have to break down the crystallites and intercalate the polymer chains. Water itself behaves as a plasticizer for PVA, which is usually very brittle, and plasticization is generally required to give PVA the properties for many of its applications. [338] The final properties strongly depend on the water content, which can modify the polymer matrix, increasing free volume and enabling chain mobility.

PVA is a well-known material to fabricate efficient self-healing hydrogels because of chain interdiffusion and the presence of numerous hydroxyl groups that can form extensive hydrogen bonding. Zhang et al. proposed a hydrogel made of PVA alone showing the ability to self-repair at room temperature without the need for any stimulus or healing agent. [82] This hydrogel was prepared using the freezing/thawing method to form crystallites acting as nodes within a physically cross-linked network, necessary to hold the three-dimensional structure together while partially restricting the motion of the residual amorphous phase. PVA can be combined with a chemically cross-linked network to fabricate a fully interpenetrated network (IPN) with the aim of imparting additional functionalities, such as shape memory properties. [86] The IPN can also be established with a covalent network formed by monomers capable of both copolymerize via thermal polymerization and establish labile noncovalent bonds, such as acrylamide (Aam) and acrylic acid (AAc), to achieve a double interacting network with a dual physically cross-linking. [83] Carboxylic acids in AAc are also capable of providing metal ion complexation, resulting in a triple cross-linked system based on chemical, physical, and ionic bonds that could provide both structural properties, such as higher strength and toughness, but also functional characteristics, such as motion upon external electrical field application. [310]

Acrylic Acid also possess a fast polymerization kinetic, which makes it a suitable monomer for vat photopolymerization applications. Larush and co-workers combined AAc with a bifunctional crosslinker such as poly (ethylene glycol) diacrylate (PEGDA) to fabricate drug-loaded systems with special designs for unique drug-release characteristics, which cannot be obtained by conventional pharmaceutical manufacturing methods. [339] A similar system, placed in an

electrolyte solution, such as phosphate buffered saline (PBS) exhibits bending deformation when an electric field is applied due to the concentration gradient of mobile cations in the solution. [340] The carboxylic acids on AAc and poly (AAc) can be exploited to achieve ion mediated self-weldability, also in the absence of the multifunctional cross-linker. [255,341]

To achieve the objectives we set, we started from the composition of water-based printing resin proposed by Larush and coworkers and we added in the system PVA with a specific molecular weight and hydrolysis degree to induce self-healing capability deriving from the hydrogen bonding established between PVA chains across the interface of the cut surfaces, as suggested by Zhang et al. The idea was to include PVA chains within a chemically crosslinked network to achieve a semi-interpenetrated chemical-physical network and favor better diffusion across the rejoined interface exploiting the large volume of water embedded within the hydrogel, to promote interactions not only at the interface but on a deeper extent. The interpenetrated network (IPN) (interpenetrated network) design is a convenient strategy to gather 3D shaping (printability) and self-healing properties, since it allows to integrate a rigid and robust frame (chemical bonds, generally non-reversible) with a much weaker one (physical bonds, mostly reversible). [260] The results here reported were achieved by printing with a commercial DLP printer with a water-based formulation composed of only commercially available compounds, including the photoinitiator which has been initially developed by Prof. Magdassi's group. [290] The final goal was to offer a general and easily adaptable approach to introduce self-healing into complex self-standing 3D printed structures using dispersive forces at room temperature without any stimuli to avoid water evaporation without affecting chain mobility.

5.2 Methods

Materials

Poly (vinyl alcohol) (PVA) (MW 89,000-98,000 Da, 99+% hydrolyzed); Acrylic Acid (AAc), Water-soluble TPO based nanoparticle photoinitiator (containing ionic surfactant), methyl red sodium salt (MR), and brilliant green (BG) were purchased from Sigma Aldrich (USA). Poly (ethylene glycol diacrylate) (PEGDA-SR610) was purchased from Sartomer-Arkema (France). All chemicals were used as received without further purification. The deionized (DI) water used here was purified with a Milli-Q system (Millipore, USA).

3D ink preparation and 3D printing

In a typical procedure, various amounts of PVA powder were added in deionized water (16 mL) placed in a container immersed in iced water (4°C) under magnetic stirring at 150 rpm for 15 minutes. The temperature was then gradually raised to room temperature (RT), keeping the mixture stirring constantly at 150 rpm for 30 minutes to avoid insoluble aggregates. Subsequently, the container was transferred to an oil bath at ~90°C, maintaining the magnetic stirring at 100 rpm for 1 hour. At the end of this process, the PVA was successfully dissolved in water and the solution appeared homogeneous. Then, the solution was slowly cooled down at RT. Afterward, SR 610 (50 mg), AAc (5 g), dye (1.5 mg), and photoinitiator (75 mg) were added to the solution at RT, and the whole formulation was thoroughly mixed with a centrifugal mixer (THINKY Mixer AR-100 and AR-250) for 5 minutes at 2000 rpm. For naming the samples, the relative ratio between PVA and AAc in the different samples (e.g., PVA %wt / AAc %wt = 0.8 is sample PVA_0.8) was used.

STL models were 3D printed using a DLP printer (Asiga Pico 2HD). The DLP printing system operates with a 385 nm LED light source. The printing process was carried out with a layer thickness of 200 µm layer thickness, an approach and separation velocity of 0.2 mm/min, a slider velocity of 1 mm/min, and a wait time of 3 s after each step. The light intensity was set at 21 mW/cm² with a burn-in irradiation time of 8 s for two layers and a normal exposure time of 5 s for the remaining layers. The entire printing process occurred under a water aerosol flux between 10 and 30 ml/h generated by a TaoTronics TT-AH002 humidifier. After printing, the samples were cleaned using compressed air to remove the unpolymerized resin, and for some structures that have residual resin, it was manually removed with a cloth wetted with ethanol. The objects were then postcured after the unreacted resin was removed to complete the polymerization and to strengthen the printed objects. The post-curing was carried out in a UV chamber with a medium pressure mercury lamp (Asiga Flash or RobotFactory UV oven) for 2 minutes. The printed samples were stored in a sealed environment with a high moisture content to prevent excessive water evaporation. The resolution was estimated by digitalizing the photographs of 3D objects designed specifically for this purpose. This CAD file was printed to determine which was the finest feature that could be printed.

Formulation characterization

Fourier Transform Infrared Spectroscopy (FT-IR) tests were conducted on Nicolet iS FTIR 50 Spectrometer (Thermo Fisher, Germany) using Attenuated Total Reflection (ATR) mode with a Smart iTX module collecting 32 scans from 400 to 4000 cm^{-1} . Rheological measurements of formulations with increasing PVA concentrations were performed using a rheometer (Anton Paar Physica MCR 302) in a 25 mm diameter parallel plate mode. The gap between the two plates was set at 0.2 mm and the formulation was kept at a constant temperature of 25 ° C. Amplitude sweep tests were performed at a constant frequency of 10 rad/s over a strain ramp ranging from 0.01% to 1000%. The viscosity of the inks was tested in a rotation shear ramp test ranging from 0.01 1/s to 1000 1/s over two minutes. Real-time photo-rheology tests were performed with a setup comprising a quartz lower plate and under a constant shear frequency of 10 rad/s and a constant strain amplitude of 1% in the linear viscoelastic region. The light source used was a Hamamatsu LC8 lamp, equipped with an 8 mm light guide, with a bulb emitting UV light with an intensity on the quartz window between 23 and 25 mW/cm^2 (measured with a UV radiometer EIT Power Puck II). The light was turned on after 60 s to stabilize the system. Simultaneous changes in the moduli of viscoelastic material during polymerization were measured as a function of exposure time.

Self-healing assessment

Self-healing experiments were conducted by cutting the samples, printed in the shape of dog bones, into two equal pieces with a sharp blade to separate the parts. The cut faces were then brought in contact with each other and gently pressed together and held in contact by hand for a few seconds to ensure uniform surface contact without any other external force. The rejoined samples were left to heal at room temperature for various allotted times, from 1 to 12 hours, stored inside closed and sealed vessels with saturated moisture to decrease water evaporation. The mending efficiency was quantified, subjecting both pristine and rejoined samples to uniaxial tensile tests. Mechanical properties were measured using Universal Testing Machine (Instron 3345 or MTS QTest/10, both equipped with a 10 N load cell) testing printed dog-bone samples. The dumbbell-shaped specimens were inspired by a standard sample (ASTM D1708–18) with a length of 40 mm, a gauge length of 22 mm, a width of 15 mm, a gauge width of 5 mm, and a thickness of 3 mm. The test was carried out at room temperature with a cross head speed of 50 mm/min and a sample length between the jaws of 12 ± 1 mm, recording the load and elongation at the peak of the curve. The nominal

stress was calculated as the force over the initial cross-section area of the sample, while the strain was calculated as the percent of the ratio of the final length at break over the initial sample length between jaws. A minimum of five samples were tested for each batch and the results were averaged for reproducibility. The samples were held between knurled clamps or clamps covered with antislip strips to secure the slippery hydrogels. Bulk UV irradiation of the formulation was performed, pouring the formulation into a dumbbell-shaped silicon mold, and placing it under a medium pressure mercury lamp for 2 minutes (Asiga Flash). Both sets of samples were tested under identical conditions.

5.3 Discussion

The system was designed as a sequential semi-IPN since the precursors of the chemical covalent network are added to a solution containing a linear polymer that is trapped in the crosslinked matrix after polymerization (Fig. 5.1a). [297] The photocurable ink was prepared by mixing an aqueous solution of Poly (vinyl alcohol) (PVA) with acrylic acid (AAc), Poly (ethylene glycol) diacrylate (PEGDA) and a new water compatible photoinitiator based on diphenyl (2,4,6-trimethylbenzoyl) phosphine oxide (TPO) (Fig. 5.1b). The formation of the semi-IPN occurs as follows: the physical network is mixed with the precursors of the chemical network, which is formed during light irradiation. The result is a hydrogel composed of PVA chains that are homogeneously distributed and incorporated within a cross-linked acrylic matrix. This IPN allows the system to recover: once the covalent bonds are broken, the damage can be overcome by restoring the reversible physical cross-linking amid the cut interfaces. Furthermore, as will be shown, the self-repair occurs without external stimuli or adhesives, and it is only due to internal forces because the printed material itself is already rich in functional groups able to form hydrogen bonds and contains a large proportion of water, providing PVA mobility to migrate across the ruptured interface. [73] The key for effective self-healing is to have an appropriate balance between high concentration of free hydroxyl groups on PVA chains on the cut surfaces prior to contact and sufficient PVA chain mobility in the hydrogel. The secondary forces established should be strong enough to be effective despite the significant amount of water in the gel, and there is an additional contribution to the self-healing ability of the carboxylic groups of the acrylic acid that can form multiple hydrogen bonds with the abundant hydroxyl groups along the PVA chains. [342]

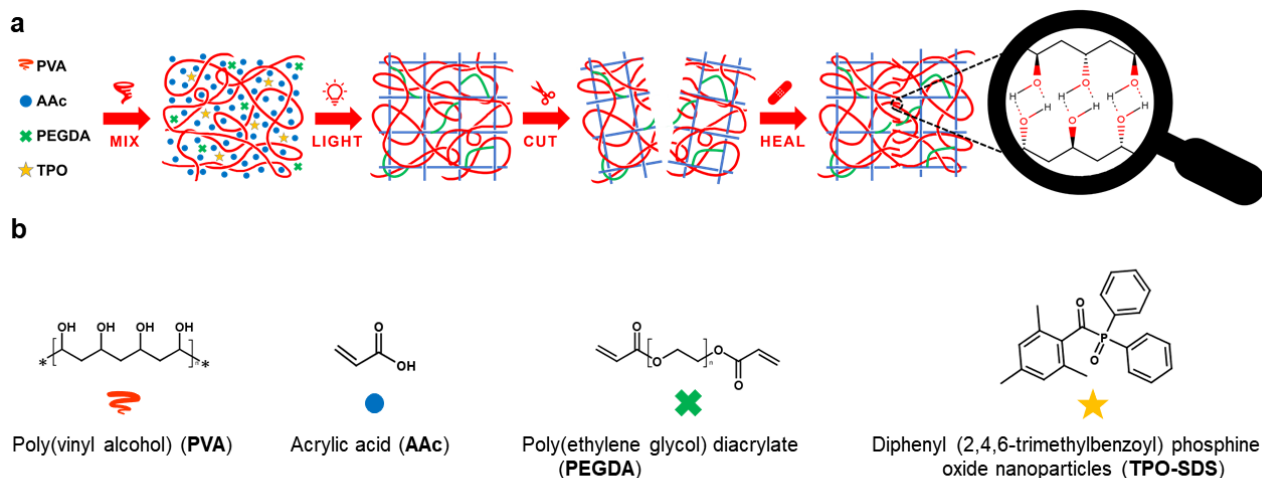


Figure 5.1 Formulation composition and network formation. a) Schematic representation of the semi-interpenetrated network (semi-IPN) and healing process. c) Chemical structure of the healing agent, monomer, cross-linker, and initiator in the photocurable resin.

Preliminary experiments were performed to determine the optimal Mw and concentration of the PVA to match DLP printability and efficient self-healing (Fig. 5.2a), after which the MW of 89-98KDa was selected. The lower MW did not show adequate self-healing even at a high weight percentage, 30% in water, the highest achievable that allowed a suitable viscosity for DLP. Similarly, higher MWs did not show acceptable efficiency, resulting from excessive viscosity even at low concentrations. The assumption for the configuration of the system to be a semi-IPN, combining homogeneously constituents of a different nature and not covalently bound together, is impossible to prove with direct evidence in the wet hydrogel state. However, homogeneity is indirectly confirmed by ATR-IR spectra collected at different points of dried samples (Fig.5.2b), in which typical peaks of both PVA and AAc are present simultaneously, as presented in Table 5.1. This result, together with the transparency of the formulations and the final samples, allows concluding that there are no separate phases and so the two networks can be considered homogeneously mixed.

Once the most appropriate PVA was defined and the homogeneity of the formulation was proven, we conducted feasibility studies to evaluate the effect of relative PVA concentrations on AAC to control the extent of secondary forces and define the printability window with various formulations, which composition is presented in Table 5.2.

It was found that the viscosity of the resulting solutions drastically increases with increasing PVA concentration (Fig. 5.2c), and the solutions could not be effectively printed above the PVA / AAc ratio of 0.8 (wt/wt). Viscosity is a very important limiting parameter for vat 3D printing, and its effects had to be addressed during the process. The rheological behavior of the inks was strongly related to the amount of PVA, with an increase in both the storage (G') and loss (G'') shear moduli with an increase in the polymer percentage. Similarly, viscosity at room temperature increased moderately when PVA was added. PVA_0.8 formulation (the number indicates the weight ratio between PVA and AAc) showed a sharp increase in viscosity, determining an upper limit in the maximum content of PVA attainable due to limitations in the mixing step. To overcome the issue and to guarantee well-mixed solutions, we employed a planetary mixer, which is commonly used to homogenize viscous paints, and we designed and fabricated a compatible adapter to host 40 ml glass vials inside (Fig. 5.2d).

Photorheology experiments were also conducted to assess the effects of PVA concentration on the photopolymerization kinetics of the various formulations (Fig. 5.2e). Because selected water-soluble acrylates, AAc and PEGDA, have been widely exploited for vat photopolymerization to fabricate high-resolution objects because they provide rapid photoinduced radical photopolymerization reaction even in large amounts of water, we wanted to explore potential adverse effects of the presence of PVA. It was found that the polymerization process occurred in less than 10 seconds (well within the acceptable range for high-resolution DLP printing) without significant differences in the reaction onset or rate, indicating that the presence of PVA does not hinder the reactivity of the acrylate species. As expected, differences in the initial G' storage shear modulus values and different final plateau values were observed for the different PVA concentrations, in agreement with the previous rheological measurements. Furthermore, the considerable amount of water present in all the formulations prevents the use of most of the commercial photoinitiators because of the low solubility in water of most available photoinitiators for the wavelength used in VP printing. Therefore, the application of water-compatible photoinitiator nanoparticles was crucial to achieve rapid printing using a commercial printer. We explored the effect of the concentration of PI on the polymerization kinetic, and it resulted that the effect was negligible (Fig. 5.2f). Since the self-healing performance should increase with the increase of PVA content, hence the apparent cross-linking density, we mainly focused our attention on the composition containing the highest PVA concentration, in a weight ratio of 0.8 related to AAc.

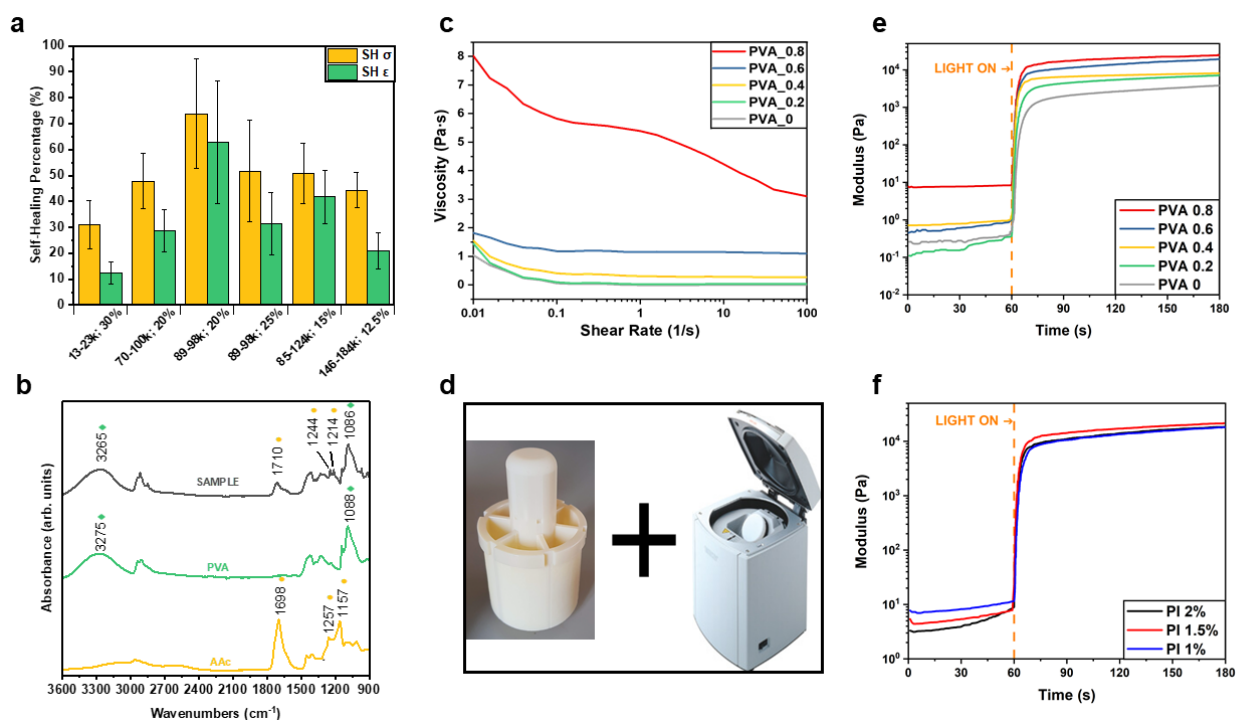


Figure 5.2 Preliminary investigation. a) Healing efficiencies estimated from tensile strength at break ($SH\sigma$) and elongation at break ($SH\epsilon$) for formulations containing PVA with different Mw at the highest concentration suitable for printing. b) ATR-FTIR spectra of Acrylic Acid (AAc), Poly(vinyl alcohol) (PVA) and of a dried sample. c) Viscosities of formulations with increasing PVA contents under continuous shear rate sweep. d) adapter and Thinky planetary mixer used for mixing the formulations. e-f) Real-time photorheology of formulations e) with different PVA/AAc ratios and f) of the PVA_0.8 formulation with different photoinitiator concentrations.

Table 5.1: Characteristic peaks identification in the FTIR spectra reported in Fig. 5.2b

Peak Assignment	PVA	AAc	SAMPLE
PVA OH stretching	3275 cm^{-1}	—	3265 cm^{-1}
AAc C=O stretching	—	1698 cm^{-1}	1710 cm^{-1}
AAc C-OH stretching	—	1257 cm^{-1}	1244 cm^{-1}
AAc C-OH bending	—	1157 cm^{-1}	1214 cm^{-1}
PVA OH bending	1088 cm^{-1}	—	1086 cm^{-1}

In the printing compositions, we used only one concentration of the chemical cross-linker at a molar ratio of 1:1000 to acrylic acid, which was the lowest concentration of cross-linker that enabled a successful printing. The selected PEGDA 700 guaranteed a good compromise between water solubility, reaction kinetics, mesh size, and mechanical strength of the final object. A higher concentration of PEGDA (and then higher cross-linking density) still enabled printing 3D objects but affected the SH properties. The apparent values for cross-

linking, including physical and chemical bonds, were estimated from the elastic shear modulus on the plateau of the formulations, using the following equation:

$$\nu_e = \frac{G'_p N_A}{RT}$$

Where ν_e is the density of network cross-linking, G'_p is the shear storage modulus in the frequency-independent plateau region, R is the universal gas constant, T is the temperature, and N_A is the Avogadro number. [343] For PVA-free formulations, the density was found to be $4.6 \times 10^{23} \text{ m}^{-3}$, and for the highest PVA concentration, it was $4.0 \times 10^{24} \text{ m}^{-3}$. Table 5.3 shows the calculated values for the various PVA ratios.

Table 5.2: Formulations composition in weight

BATCH	AAc	PVA	DIW	PEGDA	PI	DYE
<i>PVA 0</i>	23.67%	0%	75.73%	0.24%	0.36%	0.007%
<i>PVA 0.2</i>	22.60%	4.52%	72.31%	0.23%	0.34%	0.007%
<i>PVA 0.4</i>	21.62%	8.65%	69.18%	0.22%	0.32%	0.006%
<i>PVA 0.6</i>	20.72%	12.43%	66.32%	0.21%	0.31%	0.006%
<i>PVA 0.8</i>	19.90%	15.92%	63.68%	0.20%	0.30%	0.006%

After the preliminary studies proving the applicability of the proposed formulation as resin for VP, we had to address the issue of the thickening of the formulation during printing, which had to be overcome to achieve high structural quality in the printed objects (Fig. 5.3a). The main crucial challenge was to avoid evaporation of water, boosted by the exothermic polymerization reaction. This causes the thickening of the printable ink associated with the gradual increase in PVA concentration at the interface and interferes with the layer separation/approach step. At last, the high photoreactivity of the monomer led to the thickening of the ink and eventually uncontrolled polymerization, with loss of printing precision.

Table 5.3: Apparent cross-linking density for each formulation

<i>PVA 0.2</i>	1.0×10^{24}
<i>PVA 0.4</i>	1.5×10^{24}
<i>PVA 0.6</i>	2.6×10^{24}
<i>PVA 0.8</i>	4.0×10^{24}

The addition of a dye helps to reduce the thickening of the resin by reducing the light actually absorbed by the PI and therefore the amount of AAc activated by the radical initiation, but an increase in the ink viscosity is still present, which results in a tendency to delaminate the layers immersed in a thick formulation because of an increase in the adhesion forces (Fig. 5.3b). To counterbalance the effects of viscosity, we had to operate on some printing parameters. We increased

the layer thickness, resulting in a decreased z-resolution, to avoid failure of the printing process caused by delamination of thin layers. The motion of the building platform was also set to be very slow to avoid the incorporation of air bubbles in the ink, which can lead to detachment of the printed object and interlayer delamination, and to allow enough time for the resin to flow and fill the gap for printing the following layer given the high viscosity of the ink. The evaporation of water causes a surface solidification of the ink as a result of a change in the solubility of PVA in the formulation. This solid film hinders the printed object from reaching the bottom of the vat and immersing in the liquid resin, impeding the completion of the printing, and depleting the useful formulation (Fig. 5.3c). We overcome this problem by carefully flushing a water aerosol over the printing area during printing, as shown in the schematic representation of the DLP printer in our modified setup in Fig. 5.3d. Without drastically modifying the printer, we introduced an auxiliary system on top of the vat composed of a lid to confine the aerosol within the printing area connected to a tube carrying the aerosol generated by a household humidifier (Fig. 5.3e). Many of the components, such as the lid, the tube fittings, and the components necessary to modify the humidifier, were designed and 3D printed for the purpose and used in combination with a custom-made smaller platform with a bottom glass plate to enhance the adhesion of the objects at the onset of the printing process. We also introduced a double exhaust system, composed of an aspiration system and a portable hood to remove the excess aerosol to avoid its condensation and a detrimental dilution of the resin with a consequent change in properties, as well as to preserve the electronics of the equipment (Fig. 5.3f).

After the problem of ink viscosity was addressed, we explored also the effects of the addition of organic water-soluble dyes, aiming to improve the printing resolution to achieve good shape fidelity. The dye helps control the extent of reaction and photoinitiation kinetics, increasing the resolution along the Z-axis by both limiting the light penetration depth and confining the light at the x-y plane only in the area supposed to be irradiated. To better demonstrate the improvement ascribable to the dye, cuboid samples (25 x 10 x 5 mm) were printed with formulations containing two different dyes, methyl red and brilliant green, and then compared to a sample printed without adding a dye (Fig. 5.4a). The sample printed without dye shows extensive polymerization and its shape is undefined, while the addition of a dye results in good shape fidelity with sharp edges and flat surfaces.

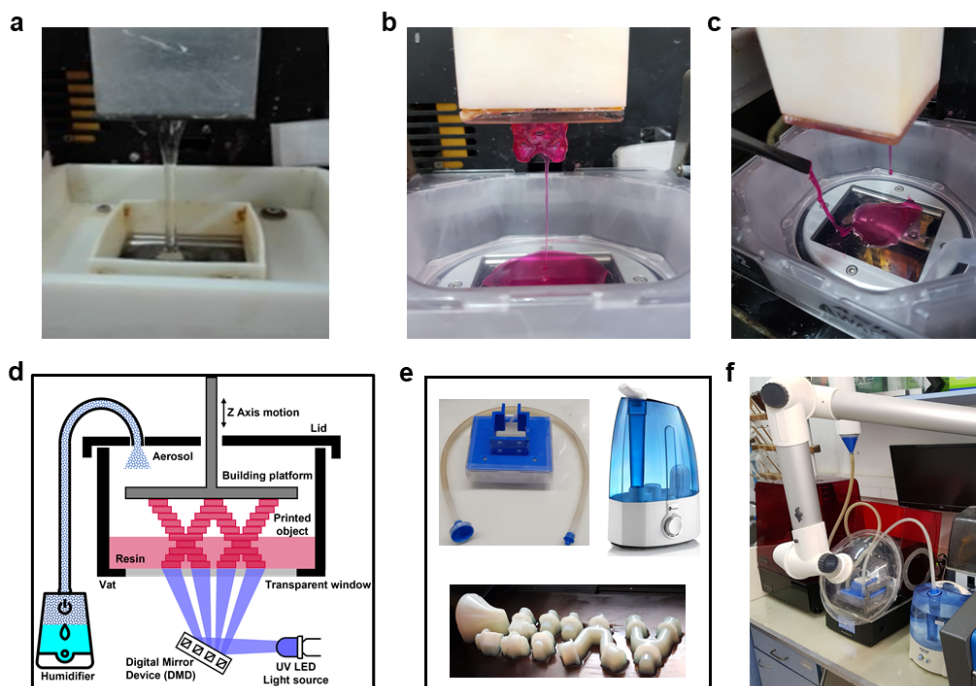


Figure 5.3 Printer Modification. a) Formulation thickening during printing. b) Effect of the dye on the thickening of the formulation. c) Superficial drying of the resin. d) Schematic illustration of the Digital Light Processing (DLP) printing modified apparatus used. e) Components and f) assembled aerosol-reflux printing apparatus.

Samples printed with different dyes achieved similar conversion after post-curing, as shown by the superimposable peaks in the highlighted area of the FTIR-ATR spectra normalized with respect to the peak centered at 1088 cm^{-1} in Fig. 5.4b, where the despite the different absorption spectrum of the two dyes (reported in the inset). It is fundamental to have the same conversion, because the process is performed just to gelation to minimize the irradiation and thus reduce the printing. A post-curing step after the unreacted resin is removed is usually required to complete the polymerization and strengthen the printed object. The resolution, in terms of the finest feature that could be printed as a function of PVA, and dye concentration was estimated by the digitalization of the photographs of a benchmark object printed starting from a CAD file designed specifically for this purpose (Fig. 5.4c). As shown by the resulting benchmarks (Fig. 5.4d), a low dye concentration provided detailed features at every concentration, but an increasing PVA concentration determined an accumulation of excessively reacting material between the reference walls. A higher dye concentration progressively suppressed the finest features, but this effect was partially balanced by an increase in the PVA concentration, resulting that the intermediate dye concentration tested provided a good compromise between the

minimal feature dimension and shape fidelity. Given the considerations above, the smallest feature we achieved is around 1 mm. Unfortunately, the resolution obtained is well above 37 μm , the nominal maximum resolution declared for the commercial DLP printer used, mostly because of the very high concentration of PVA and the large amount of water that limit 3D printing of small features. Although the dimensional accuracy of these printed samples is in good agreement with previous 3D printed SH hydrogels via deposition-based printing, the presented system enables better precision, CAD fidelity, shape fixity, and edge sharpness. [130,300] Given the previous considerations, all the printing and self-healing tests were carried out on objects printed with the PVA_0.8 formulation which contains the highest amount of PVA suitable for processing.

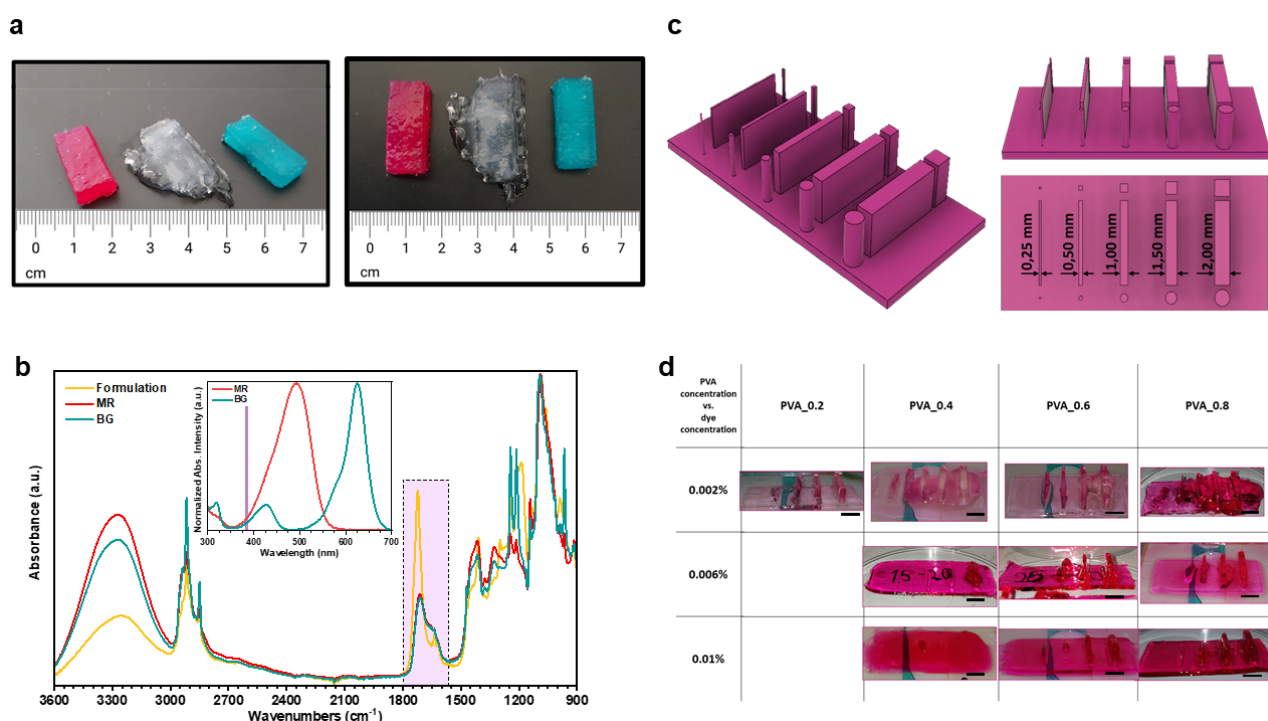


Figure 5.4 Effect of the dye on the printing process. a) Cuboid-shaped samples (25 mm x 10 mm x 5 mm) printed with formulations containing two different dyes, methyl red (left) and brilliant green (right), compared to a sample printed without adding a dye (center). b) ATR-FTIR spectra of the dry PVA_0.8 formulation without the dye before curing (yellow) and of dried samples printed with the two different dyes, methyl red (MR) and brilliant green (BG). In the inset: UV-Vis absorption spectra of dyes compared with the printer light source emission wavelength. c-d) CAD file of the benchmark used to determine the finest printable feature and comparison of the effects of the PVA concentration versus the dye concentration on printed benchmarks (scale bar 5 mm).

We were able to fabricate 3D printed structures with a good CAD fidelity, as shown in Fig. 5.5, despite the very high amount of water (64 % by weight of the

total amount) and the high viscosity. We were able to print the same structures with both dyes, confirming the previous assumption that the different dyes did not visibly affect the printing process and the effective cross-linking. The printed objects are characterized by flat surfaces, straight elements, and clean and sharp edges (Fig. 5.5a), and elements usually difficult to achieve in hydrogel printing, such as overhanging features and through-holes, could be printed with this composition without any support. Another example of complex unsupported structure, such as an object with rotational symmetry and independent self-standing segments, with smooth rounded surfaces and a central pillar, is shown in Fig. 5.5b. The resin showed a particular affinity for the printed objects, and large amounts of residues are detrimental to precision because they polymerize on the surfaces during the postcuring step. Manual cleaning could be problematic for very complex architectures, so the cleaning method was based on first blowing compressed air onto the sample, removing most of the residual resin. For some structures, we needed to remove some remaining residues, and this was done manually using ethanol-soaked cloths. It should be noted that such cleaning processes are typical for a variety of printing technologies.

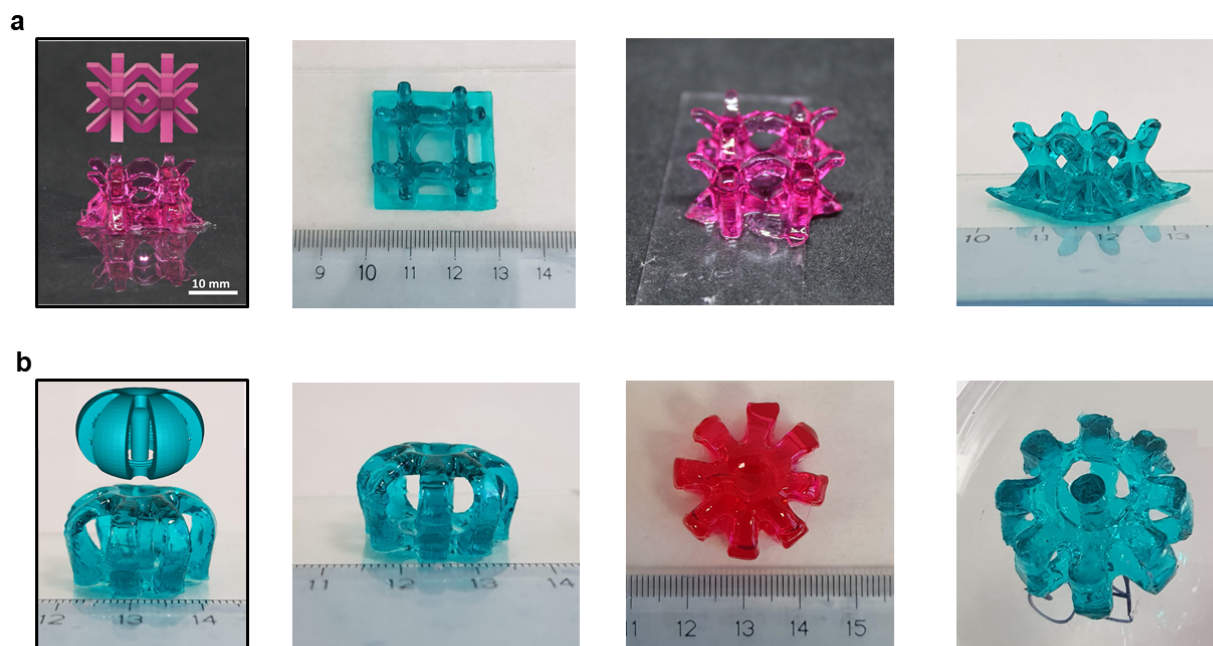


Figure 5.5 3D printing of complex geometries. Various view of 3D samples fabricated with the different dyes. a) Body-centered cubic lattice-like structure b) Axisymmetric structure with central pillar.

Dyes not only have a functional purpose, enabling a more precise printing, but also enable a better visualization of the SH as well, since two samples printed

with different colors, red and green, could be cut and rejoined with mixed colors. Several 3D printed objects having different shapes were split into two pieces, and then the two halves were rapidly placed in contact first to have a qualitative demonstration of the SH properties. The structures were indeed macroscopically repaired, and the self-healing can be attributed to the efficient adhesion at the rejoined surface, which is due to the possible formation of hydrogen bonds across the interface both by carboxylic and mostly hydroxyl groups. The adhesion occurred instantly upon rejoining, and the mended hydrogel could immediately hold its weight and support the bending deformation without breaking apart (Fig. 5.6a). After 2 hours, the healed sample could withstand moderately large stretching deformation before failure (Fig. 5.6b). The restoration of complex architectures with overhanging features was successfully achieved and a purple color is observed at the interface after some time in contact (Fig. 5.6c).

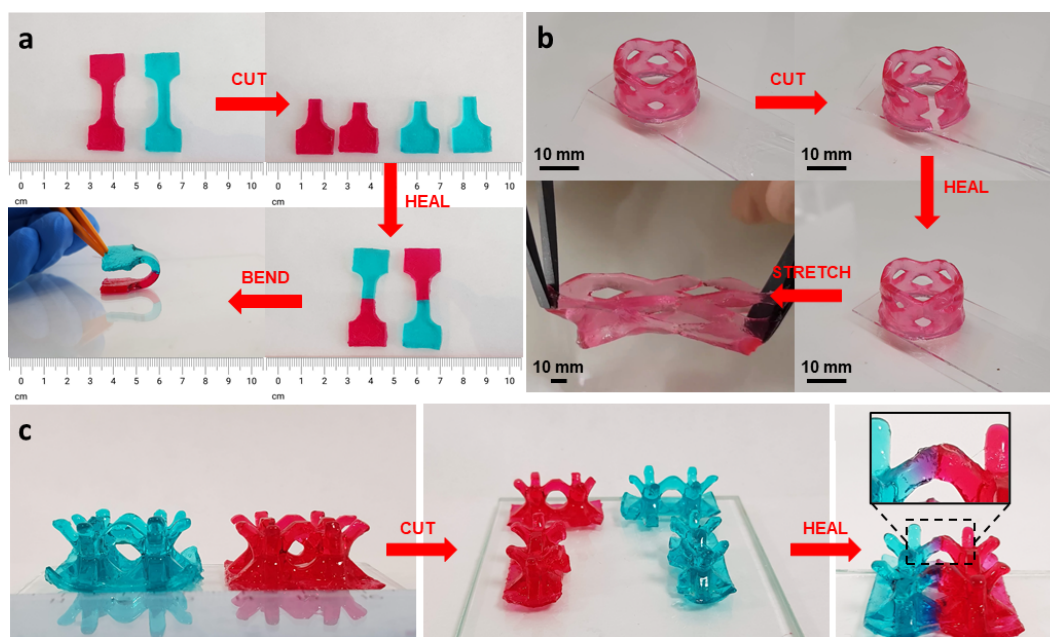


Figure 5.6 Self-healing of samples with complex geometries. a) Tensile test specimens that could withstand a bending deformation immediately upon rejoining. b) Holed cylindrical structure, once reconnected and healed for 2 h it could endure a large stretching deformation. c) Body-centered cubic lattice-like structures cut and rejoined. Diffusion at the interface after 12 h in contact is clearly visible (inset) thanks the gradient of the dye.

The color resulted from diffusion beyond the interface plan and mixing of the red and green dyes (Fig. 5.7a) as shown in a qualitative test performed on Cuboid-shaped samples (25 mm x 10 mm x 5 mm) printed with formulations containing the two different dyes and without the dye (removing the over-cured parts

afterward). The colored samples were cut in half and two differently colored halves were attached to the undyed sample, from where the two ends were cut to expose fresh surfaces. The two dyes have different diffusivity in the hydrogel, and therefore the purple color appears to be mainly on one side of the interface in the inset of Fig. 5.6c. Methyl red migrates more rapidly than brilliant green in the central part. The two molecules show different diffusivity in the hydrogel, probably due to their different hindrance, nature, and affinity with the matrix, so they need a different time to diffuse along the same length. After 24 hours, methyl red shows visible diffusion in the central part, while brilliant green does not. After 15 days, the diffusion gradients are in contact, with a purple color similar to samples shown in the manuscript. The prolongation of the diffusion path helps to show the differences in the diffusion kinetic of the two dyes (Fig. 5.7b). It can be concluded that the diffusion of methyl red is faster and tends to hinder the diffusion of brilliant green. This is only a qualitative demonstration of the dye diffusion through the healed surface that can be ascribed to dye mobility within the network but gives no information on the actual diffusion of the PVA chains. A quantification of this diffusion (for instance, by means of UV-Vis spectroscopy) would result in only a relative evaluation. Note that quantifying the diffusion by following the dye movement would require a chemical linking of each dye to the polymer, which would also affect the properties of the polymers. Therefore, it will not provide quantitative information on the diffusion of the PVA and PAA molecules in the system.

However, as previously stated, PVA-based systems have been thoroughly studied in the literature, and the SH mechanism is commonly accepted as resulting from both interdiffusion and hydrogen bonding, but to the best of our knowledge, it is still a hypothesis that should be proven in the future while overcoming the problem of distinguishing such bonds in systems containing very high-water concentrations. [86] The strong similarity between hydrogen bonding among PVA chains and H bonds in water in FT-IR (broad peak around 3200 cm^{-1}) (Fig. 5.7c) makes it impossible to quantitatively analyze the diffusion of polymer chains or the formation of interchain interactions by hydrogen bonding across the ruptured surfaces. In fact, the bands of hydroxyl groups are hidden by the dominant bands of water (65 wt% water in the hydrogel) so no useful information could be extracted. As already reported in the literature, it has not been possible to reveal direct support for the H bonds by the PVA while in water, also because it is almost impossible to distinguish the interactions across the interfaces from those established in the bulk. [82] However, some straightforward yet rudimentary evidence of H bond formation can be deduced from a contact angle test performed

on cut surfaces (Fig. 5.7d). Freshly cut surfaces are hydrophilic, as a deposited water droplet spread over, but if the same surface is left to dry for some time, there is a decrease in the hydrophilicity. This behavior can be explained by the presence of many unassociated groups on the fracture surface, and this explains the immediate adhesion of freshly cut and rejoined samples, because many available moieties are ‘eager’ to interact. This availability of hydroxylic groups at the interface is progressively lost with time because of water evaporation and hydrophobic rearrangement of the exposed surface. An additional experiment carried out on showed that the SH on freshly cut surfaces is indeed more efficient than simple adhesion forces (Fig. 5.7e). As-printed samples stored in a sealed vessel to minimize water evaporation and to ensure clean surfaces without contamination were cut and rejoined on a freshly cut surface and on an external surface, showing that adhesion of cut surfaces is more efficient than on other parts in sustaining gentle pulling.

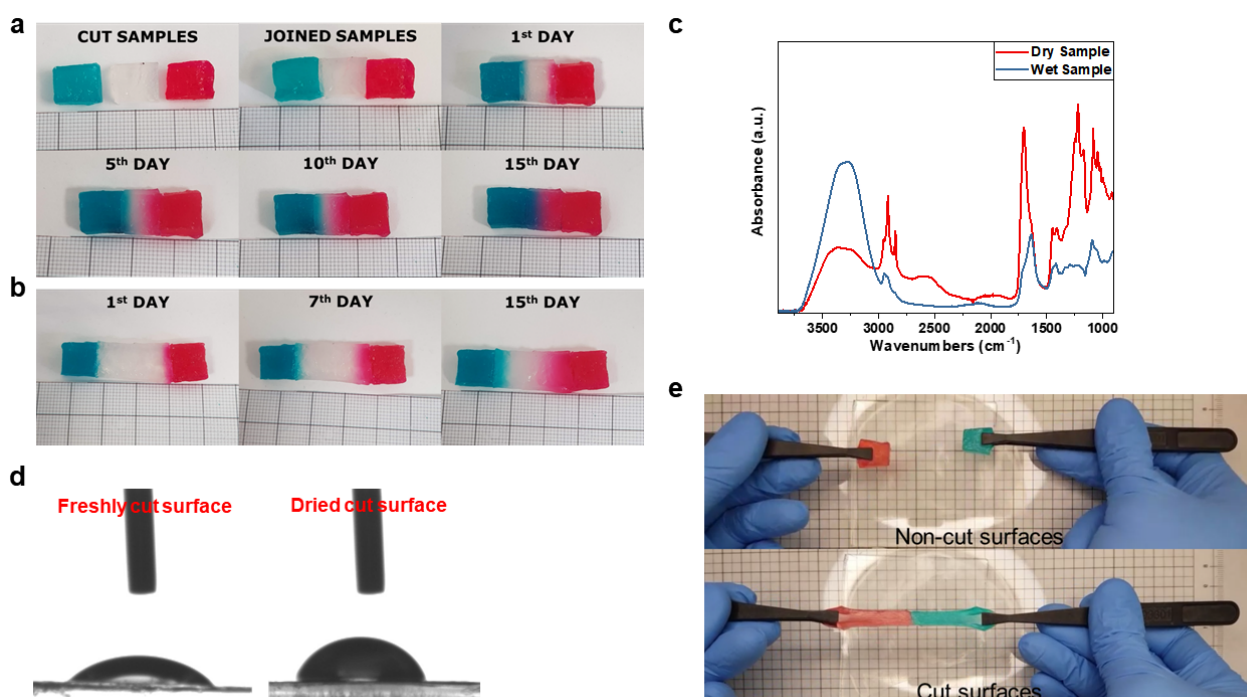


Figure 5.7 Healing mechanism investigation. a-b) Diffusion experiments of different dyes in a similar matrix. a) Similarly-sized cuboid to show the mixing of the dyes b) Cuboids with longer non-colored central part to show differences in the diffusion speed. c) ATR-IR spectra comparison of an as-printed wet sample and a dried sample. d) Contact angle image of a freshly cut surface and a dried cut surface and e) comparison of the behavior of freshly cut and non-cut surfaces when manually stretched.

Tensile tests were performed at different restoration times to obtain a quantitative evaluation of SH with time (Fig. 5.8a). The system already yields a

considerable recovery within the first two hours, and the recovery increases slightly with time, reaching a plateau in the achievable restoration after 12 hours of contact (Fig. 5.8b). Once the restoration time was fixed, we compared the tensile strength and elongation at the break of self-healed objects with those of pristine uncut objects. Healing efficiency was calculated from the ratio of tensile strength at break ($SH\sigma$) and elongation at break ($SH\varepsilon$) of the rejoined objects to the values of pristine objects. Printed dumbbell-shaped samples showed an average recovery of 72% in tensile after healing for 12 hours, in good agreement with the results reported for neat PVA-based non-3D printed hydrogels, in which the addition of a chemically cross-linked network had detrimental effects on self-healing. [82,83,86,310] It is interesting to note that the SH of the printed objects was better than those that were prepared by casting in a dumbbell-shaped mold and UV-irradiated in bulk for 2 minutes, which regained only around 50% of the initial strength (Fig. 5.8c). This difference may be explained by a more homogeneous cross-linking density due to the layer-by-layer fabrication compared to that in bulk photopolymerization, which is strongly affected by the light penetration depth. The data variance can be related to the manual operation to carry out the self-healing procedure and testing. There is no commonly shared standard for both self-healing procedure and testing, and many studies are reporting on procedures for evaluating self-healing that are not totally comparable. However, the general trend is visible with the highest performance achieved after 10-12 hours in contact. Unlike typical simple shapes in SH studies, we could not provide an exact alignment of the rejoined surfaces because of the small dimensions during the manual attachment; thus, we performed the tests on multiple specimens to reduce the experimental uncertainty. Moreover, the swollen nature of the hydrogel caused deformation upon compression while clamping the samples in the tensile test machine, with a possible misalignment among the clamps. Lastly, the experimental variation may also be attributed to the irregular and gradual rupture of the healed samples that failed at the contact interface after elongation. Pristine samples separated abruptly after reaching the ultimate tensile strength (Fig. 5.8d). In contrast, the healed samples did not split at once, but gradually detached along the cut region (Fig. 5.8e). This feature imparts an additional safety mechanism to repaired samples, because it avoids sudden detachment of less robust mended interfaces. It can be argued that the self-healing mechanism is similar to the behavior of pressure-sensitive adhesives (PSA) between two separate surfaces. A common measure of this effect is the Dahlquist criterion, which requires that the elastic shear modulus G' should be $< 0.1\text{MPa}$. [344] Our material showed rheological properties below the Dahlquist criterion;

therefore, the mechanism of self-healing can also be influenced by the surface self-adhesiveness at the interface. However, this aspect does not exclude the fact that the material is self-healing, as macroscopic self-repairing can be defined as the recovery of the initial mechanical properties. Furthermore, the time required to achieve sufficient self-healing can be explained by the necessity of chains to diffuse across the surface and to maximize the strength by extending the surface of interaction to a volume of interaction. [21] In contrast, if the cut surfaces are kept apart, PVA chains on the same surface would rearrange to minimize surface energy. Therefore, there will be fewer free hydroxyl groups available to form H-bonds across the interface when the two surfaces are brought together.

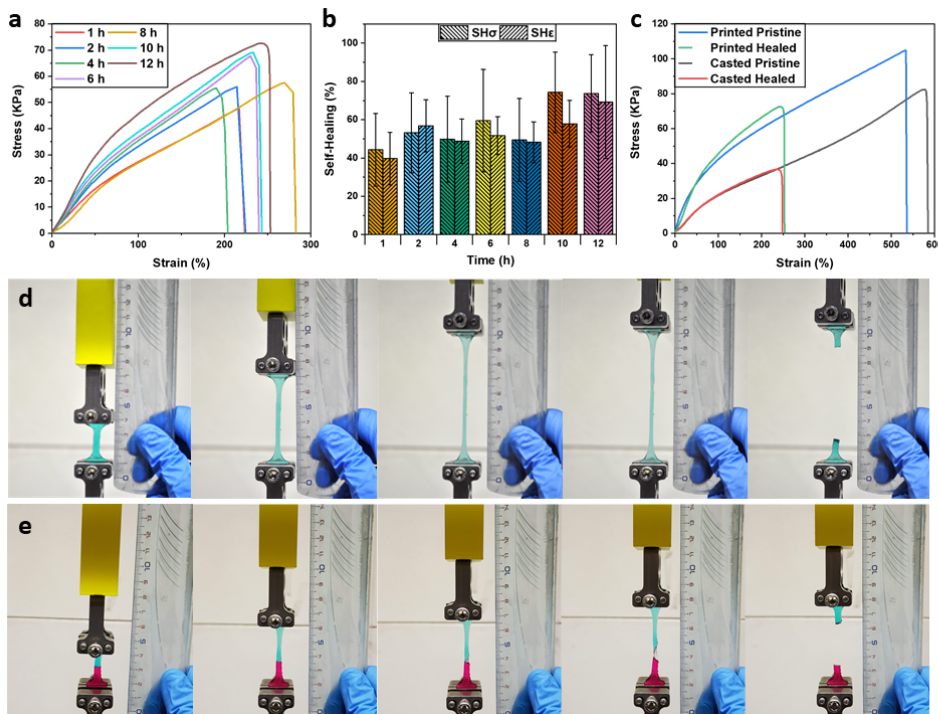


Figure 5.8 Self-healing efficiency assessment. a) Stress–strain curves from Uniaxial tensile test on self-healed PVA_0.8 specimens for increasing healing time and b) comparison of the healing efficiencies estimated from tensile strength at break ($SH\sigma$) and elongation at break ($SH\epsilon$). Error bars represent standard deviation, $n = 5$ independent replicates. c) Stress–strain curves of printed pristine and healed samples compared with the same curves obtained from casted pristine, and healed samples. d-e) Elongation and rupture behavior during the test of d) pristine sample and e) 12 h healed sample.

The presence of available moieties at the interface enables multiple cyclic repairs of the samples, which is a peculiar property of intrinsic self-healing systems. The samples were kept in a sealed closed vessel with a humid environment to reduce water evaporation and maintain controlled conditions after

printing during the entire healing process. This solution was crucial to preserve SH properties, as also proven by control experiments on 3D printed dumbbell-shaped specimens tested in tensile tests, keeping the reconnected in a sealed environment with and without controlled humidity. The objects healed in a humid environment show an average value of about 65% with certain repeatability that falls in the error range (Fig. 5.9a). A second set of experiments was performed, keeping the samples in a sealed container without controlled humidity, evidencing a lower recovery efficiency every cycle, while the first healing process resulted as efficient as the humidly stored samples (Fig. 5.9b). This behavior can be explained by the loss of water during setting up, handling, and testing the sample to measure self-healing (Fig. 5.9c). These results confirm that it is crucial to maintain a constant water concentration in the hydrogel to preserve the SH properties over time.

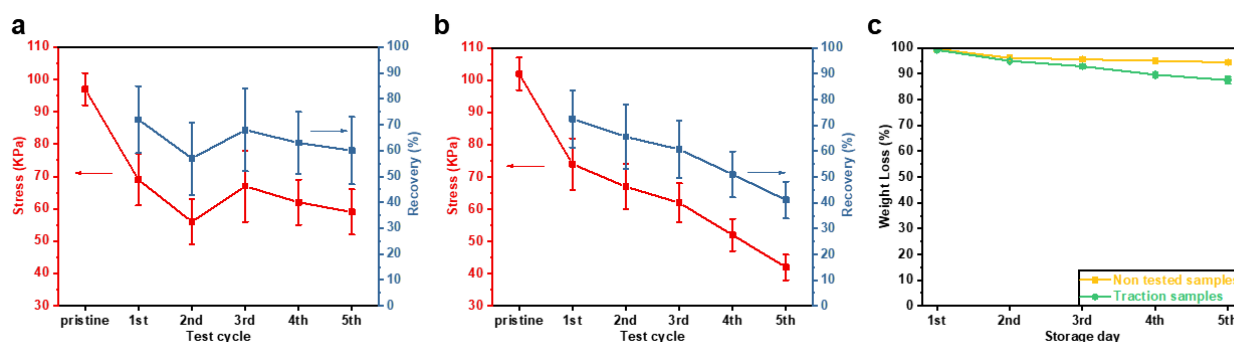


Figure 5.9 Repetitive restoration. Tensile strength and recovery percentage of samples after five separation-healing cycles, on samples a) stored in humid sealed environment or b) with no controlled humidity for 24 hours while healing for every cycle. c) Comparison of weight loss during several days between samples only stored in closed and sealed vials and samples subjected to manipulation for tensile testing.

5.4 Conclusions and perspectives

In summary, our goal was to demonstrate the feasibility of 3D printing of hydrogels with self-healing properties via vat photopolymerization. The processing of commercially available materials via a widely available apparatus to fabricate 3D printed hydrogels could enable fast adaptation of the proposed approach. We overcome the inherent incompatibility between vat photopolymerization and self-repairing properties (i.e., high cross-linking density vs. large chain mobility) using a photocurable formulation that generates a physical-chemical double network.

The system was designed as a semi-IPN, comprises commercial materials only, and is based on combining a covalent network of acrylic acid and poly

(ethylene glycol) diacrylate with a physical network of uncross-linked Poly (vinyl alcohol). We performed preliminary studies to determine the optimal MW and hydrolysis degree and to evaluate the effect of the PVA on the viscosity and photoreactivity of the formulation. The solidification of the PVA resulted in the fact that it is detrimental to the printing process, because of the change in the solubility of the PVA caused by water evaporation. Therefore, we modified the commercially available 3D DLP printer used to overcome the issue of the superficial drying of the high viscosity resin by performing the printing process under a water aerosol flux, thus maintaining a constant humidity above the vat. We studied in more depth the effect of the dye concentration on the photopolymerization because the dye helped reduce the exothermicity of the reaction. We also explored the effect of the two dyes on the precision of objects and conversion, as well as the combined effect of dye concentration and PVA concentration on the resolution of the objects and the finest feature achievable. The proposed approach enabled reaching a complexity of self-supporting architectures, especially in terms of overhanging and hollow features, with sharp edges, which are not achievable with conventional extrusion-based printing processes, enabling better precision, CAD fidelity, shape fixity, and edge sharpness. The smallest achievable feature is around 1 mm, well above 37 μm , the nominal maximum resolution declared for the printer used, but the dimensional accuracy of these printed samples is in good agreement with previous self-healing hydrogels 3D printed via deposition-based printing. The self-healing of complex samples produced with the formulation with the highest amount of PVA suitable for printing occurred rapidly at room temperature, without requiring any external stimuli. Immediately after joining the two cut halves, they were instantly able to withstand bending deformation. Efficient self-recovery was accomplished only at the highest printable concentration of PVA, given the viscosity limitations, indicating that there must be a trade-off for collect printability and self-repair. An insufficient amount of PVA in the hydrogel prevents the possibility of holding its weight after being cut and brought into contact, so the objects could not withstand the tensile test and failed immediately regardless of the healing time. Furthermore, if the PVA amount is too low, the chains would be surrounded by an excessive volume of water molecules, exceedingly weakening the adhesion force between the two halves in contact. The hydrogen bonding mechanism is commonly accepted, but to the best of our knowledge, it is still a hypothesis that should be proven in the future, overcoming the problem of distinguishing such bonds in systems containing a very high water concentration. The dumbbell-shaped samples recovered 72% of their initial tensile strength, which can be considered

good given the literature; the PVA introduced introduces an additional safety mechanism to the repaired samples because abrupt ruptures are avoided. The samples also showed repeatable partial restoration when stored in a humid environment. It should be noted that, in our study, we had to face not only the problem of restoration but also the limitation arising from the fabrication of complex shapes. We demonstrated that 3D-shaped self-healing hydrogels with very complex architectures can be fabricated through precise control over the printing composition by a low-cost commercial 3D printer and commercially available materials.

The complexity related to stringent reaction conditions and complex synthesis and purification procedures for self-healing materials hinders mass production and economic practicability and, together with the difficulties related to the shaping, the potential applications are restricted. The use of commercial species could provide high versatility to the system, but the presence of PVA largely limits the compatible monomers, which should be liquid monomers with low viscosity given the high viscosity of the starting PVA water solution, cause the PVA precipitation and guarantee sufficiently high reactivity. These requirements rule out Hydroxy ethyl methacrylate (HEMA) because it causes PVA precipitation, Poly (ethylene glycol) methacrylate (PEGMA) is too viscous, Methacrylic acid (MAAc) and Dimethyl amino ethyl methacrylate (DMAEMA) because characterized by low reactivity, while Acrylamide (AAm) was excluded given its intrinsic safety issues. A possible action could be the use of PVA plasticizers to reduce viscosity and increase the mobility of polymer chains, thus potentially improving the self-healing efficiency of PEG, as well as urea, citric acid, and other small molecules. Another interesting approach could be the use of conductive salts, such as LiCl, to evaluate a potential application as a sensor. Another interesting approach could be the introduction in the system of bidimensional materials, such as nanocellulose, graphene oxide, exploiting hydroxyl groups for enhancing interactions and maybe varying the relative concentrations in the formulation to counterbalance the high viscosity.

Chapter 6

Cold-triggered self-healing system

6.1 Introduction

As observed in the previous chapter, chains mobility is crucial to pursue self-healing, since it was observed that effective mending can be achieved only with the correct level hydration and it was demonstrated that self-healing is achieved thorough interdiffusion, as shown by dye experiment. Effective diffusion of chains across a fracture interface can be easily achieved by an increase in temperature, which is well acknowledged as an effective method to repair objects, as shown in Chapter 4.

From these considerations, we wanted to investigate an inverse strategy, employing a decrease in temperature and cooling to activate the self-healing mechanism and also to favor water retention within the hydrogel. To that end, we investigated the use of thermoreversible polymers as healing agents incorporated within a covalent network made from commercial monomers; in analogy with the study in the previous chapter, polymer solutions showing an inverse gelation behavior present a lower critical solution temperature (LCST) below which the polymer is miscible in the solvent, usually water, while above which a phase separation occurs. In particular, thermoresponsive triblock copolymers can aggregate in a controlled and tunable manner into micelles capable of extensive interactions until they form fully physical and self-supporting hydrogels. [345,346] Colly and colleagues proposed a self-healing system based on a thermoreversible hydrogel formed by entangled Pluronic micelles. [347] Pluronic, also called Poloxamer or Lutrol, is the commercial name for poly (ethylene oxide)-poly (propylene oxide)-poly (ethylene oxide) ($\text{PEO}_m\text{-PPO}_n\text{-PEO}_m$) symmetric triblock copolymers, used in a variety of applications including emulsions, paints and coatings, controlled drug delivery, and nanoparticle synthesis. [348] These copolymers are amphiphilic thanks to the presence of both water-soluble PEO blocks and water-insoluble PPO blocks, and their behavior and properties can be controlled by varying the composition and overall molecular

weight. According to these conditions, Pluronic can show different consistencies at room temperature, from solid to paste or liquid. (Fig. 7.1a). [349] Different ratios of PEO to PPO determine the solubility of the polymer in water and the sol-gel transition temperature of the aqueous solution, which shows a lower critical solution temperature (LCST). [350] This behavior is also described as reverse thermal gelation (RTG): at low concentrations and temperatures below LCST, the PEO-PPO-PEO molecules are solvated and separated, and the solution has a low viscosity. Upon an increase in concentration or solution temperature, the solution undergoes a dramatic change in viscosity because the block copolymers associate into micelles, which are the entropically favored structures (Fig. 7.1b). The increase in Brownian motion upon warming breaks the hydrogen bonds in the water solvation shell around the PPO segments, with a decrease in the solubility. This resulted in a collapse of PPO segments into a hydrophobic core surrounded by a shell of highly hydrated PEO blocks, with the micelles able to self-assemble into diverse topologies to form a solid-like gel network. [351] The minimum concentration where micelles form is known as critical micelle concentration (CMC), while the temperature at which micellization occurs at constant concentration is called critical micelle temperature (CMT). [352] The temperature is an easier parameter for controlling the structure, and the gelation process is reversible by lowering the temperature below the LCST to liquefy the gel, again obtaining the initial polymer solution, which makes it reusable.

The most widely used symmetric block copolymer is Pluronic F127, or Poloxamer 407, which has a structure $(EO)_{99}-(PO)_{65}-(EO)_{99}$ and a molecular weight of 12,500. [353] At room temperature, it is in the form of white solid flakes that are soluble in cold water (5°C), and aqueous solutions require a minimum concentration of 15% wt. / vol to show the sol-gel transition and form a semi-solid gel around body temperature and pH, and therefore in the physiological range, which makes it suitable for biomedical applications, also because of its inherent biocompatibility. [354] F127 micelles pack into a face-centered cubic structure, and their aggregation can be influenced by the presence of additives, such as solvents and small oligomers. In particular, gelation is greatly influenced by the addition of poly (ethylene glycol), which increases the transition temperature because it enhances the stability of the liquid phase because it intercalates the hydrophilic segments, disturbing micelle entanglements. [355] The gel melting capacity of PEO increases with increasing concentration and molecular weight, until gelation is completely suppressed, while, on the other hand, the addition of poly(propylene glycol) increases the gel stability region, lowering the transition temperature.

Colly and colleagues exploited this plasticizer effect of the PEG as a softening agent to tune the Pluronic-based hydrogel properties to enable better self-healing by using it as a reusable support bath for free-form reversible embedding of suspended hydrogel (FRESH) printing, with the structures built by embedding the printed material within a suspended hydrogel working as a temporary support. [347] Pluronic has also been used as a sacrificial fugitive ink to create internal tracks or cavities, which could then be easily removed from the pattern by washing with cold water. [356,357] Pluronic has been used largely as a 3D printing ink due to its good printability and due to its shear-thinning behavior, which makes it particularly suitable for extrusion-based printing. [354] Due to its inverse thermogelling properties, a pluronic solution behaves as a liquid fluid at low temperatures capable of generating self-assembled soft gels by raising the temperature to room temperature. [358] Pluronic versatility enables control of its thermoreversible properties, and it can also be modified by reacting the terminal hydroxyl chain ends to include photo-cross-linkable groups to obtain more stable and hard gels by combining physical and chemical cross-linking. [359,360] Diacrylate-modified F127 (F127-DA) was used for the printing of free-standing patterned microvascular networks using unmodified F127 as sacrificial component removed after stabilization by UV crosslinking. [361–363] Pluronic aqueous solutions have been proven to be suitable as resin for vat photopolymerization by functionalizing the chain ends with 2-isocyanatoethyl methacrylate (IEMA) to form the cross-linkable F127 dimethacrylate (FdMA) macro-monomer. [363] Acrylic acid was added to act as the pH sensitive monomer to copolymerize with F127 dimethacrylate, generating 3D printed architectures capable of changing their size and geometry accordingly with dual environmental asymmetrical responsiveness to temperature and pH.

To achieve the goal of developing a formulation composed of commercial species to fabricate 3D printed hydrogels healable at low temperature, we started from the solution proposed by Colly and colleagues to exploit the self-healing induced by the entanglement of Pluronic micelles, and we replaced the plasticizer with methacrylated PEG (Fig. 6.1c). The idea was to trap the micelles within a chemically cross-linked network to achieve an interpenetrated chemical-physical network, with pendant PEG chains that can act at the same time as a structural network and plasticizer. This system is composed only of commercial monomers and polymers except for the photoinitiator, since we used PEG-BAPO, which is not commercially available [287] instead of the previously used TPO-SDS, to always have the same chemical specie as the plasticizer and to avoid unwanted effects from the presence of sodium dodecyl sulfate (SDS), which has a plasticizer

effect on micellization as well. [364] The final goal was to achieve self-healing by cooling below RT instead of heating up, to avoid water evaporation without affecting chain mobility.

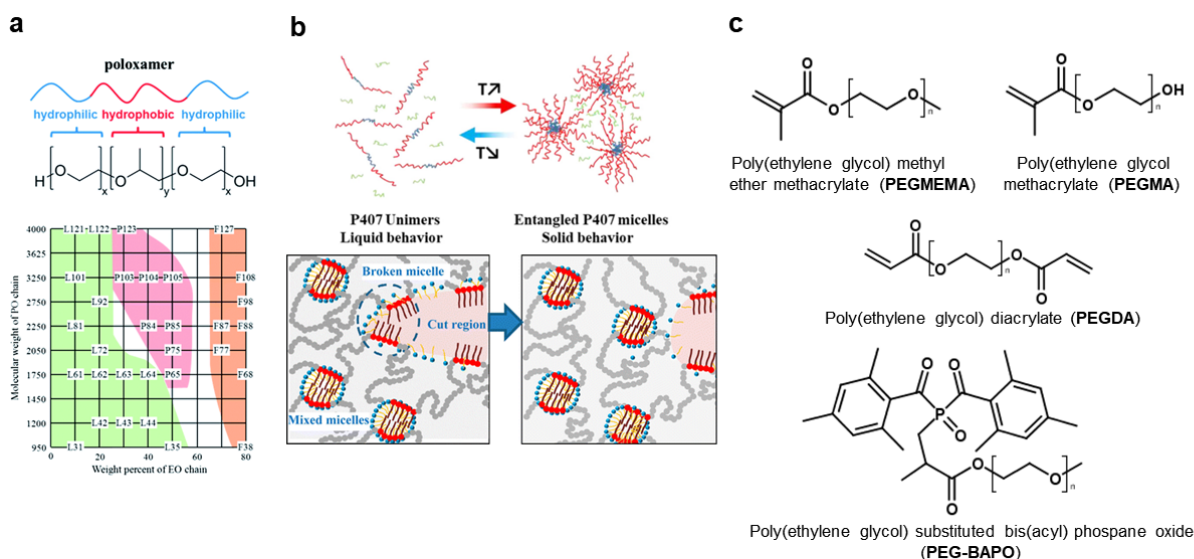


Figure 6.1 Temperature sensitive system design. a) Molecular structure of a Pluronic® triblock copolymer and the Pluronic® grid. b) Schematic illustration of the thermoreversible property of the Pluronic hydrogel with plasticizer forming the micellar hydrogel and representation of the proposed self-healing mechanism. c) Chemical structure of the monomers, cross-linker and photoinitiator present in the photocurable resin. Reproduced with permission from [346,347,349]

6.2 Methods

Materials

Pluronic F127, Poly (ethylene glycol) (PEG) (Mn 400), Poly (ethylene glycol) methacrylate (PEGMA) (Mn 500), Poly (ethylene glycol) methyl ether methacrylate (PEGMEMMA) (Mn 300, 500, 950), Poly (ethylene glycol) diacrylate (Mn 700), Brilliant green dye were purchased by Sigma Aldrich. All chemicals were used as received without further purification. The PEG-BAPO photoinitiator was kindly provided by Prof. Hansjorg Grützmacher from ETH Zürich.

Characterizations

The rheological measurements of the formulations were performed using a Physica MCR 302 rheometer (Anton Parr Italia, Rivoli, Italy) in a 25 mm diameter parallel plate mode with the gap between the two plates set at 0.2 mm. Amplitude sweep tests were performed at a constant frequency of 10 rad/s on a strain ramp ranging from 0.01% to 1000% and the formulation was kept at a

constant temperature of 5 °C or 25°C. The viscosity of the inks was tested in a rotation shear ramp test ranging from 0.01 1/s to 1000 1/s over two minutes. Real-time photorheology tests were carried out with a setup consisting of a glass lower plate at a constant shear frequency of 10 rad/s and a constant strain amplitude of 1% in the linear viscoelastic region at a constant temperature of 5 °C. The light source used was a Hamamatsu LC8 lamp, equipped with an 8 mm light guide with a bulb that emits visible light with an intensity on the glass window of around 30 mW/cm², measured with a Hamamatsu power meter C6080-04. The light was turned on after 300 s to stabilize the system. Concomitant changes in the moduli of viscoelastic materials during polymerization were measured as a function of exposure time. Temperature sweep tests were performed with a set-up comprising a glass lower plate and at a constant shear frequency of 10 rad/s and a constant strain amplitude of 0.1% in the linear viscoelastic region. After a 300-s stabilization of the temperature without strain applied, the temperature changed in the range of 5 °C - 35 °C - 5 °C with a constant 1°C/min linear rate, with a 1 min wait before starting the descent.

3D Printing and Printer Modification

In a typical procedure, 4.5 g of Pluronic F-127 were added to deionized (DI) water (15 mL) (30 w/v%) placed in a container immersed in iced water (4°C) under magnetic stirring at 150 rpm until complete dissolution when the solution was clear with no residues visible. The addition was carried out slowly to avoid the formation of lumps or insoluble aggregates. Then, various concentrations by weight/volume % (20-25-30-35-40 w/v%) of PEG or monomers solution containing PEGDA and PEG-BAPO at a 1 %wt. concentration and BG at 0.02 %wt. concentration were added under constant magnetic stirring until the solution became homogeneous. The prepared formulations were stored in a refrigerator at 5 °C in the dark.

STL models were 3D printed using a DLP printer (Asiga Pico 2HD). The DLP printing system operates with a 405-nm LED light source. The printing process was carried out with a layer thickness of 100 µm layer thickness, and an approach and separation velocity of 1 mm/min, a slider velocity of 1 mm/min, and a waiting time of 3 s after each step. The light intensity was set at XX mW/cm² with a burn-in irradiation time of 25 s for two layers and a normal exposure time of 15 s for the remaining layers. The entire printer was kept at a constant temperature of 6 °C throughout the printing process by introducing it into a refrigerator. After printing, the samples were cleaned using compressed air to remove the unpolymerized resin, and for some structures that have residual resin, it was manually removed with a cloth wetted with ethanol. The objects were then

post-cured after the unreacted resin was removed to complete the polymerization and strengthen the printed objects. The post-curing was performed in a UV chamber with a medium pressure mercury lamp (Asiga Flash or RobotFactory UV oven) for 2 minutes. The printed samples were stored in a sealed environment with a high moisture content to prevent excessive water evaporation.

Air cooling and temperature control

Cooling tests at the bottom of the printing vat were carried out using a vortex tube connected to compressed air at 2.5 bar and two tubes that directed the air flow to the bottom of the vat. The cooling of the resin was measured using a probe thermometer (ThermoPro TP16S) and thermal imaging was obtained with a thermocamera (FLIR E5, with a thermal sensibility of 0.1 ° C and an IR resolution of 10,800 pixels) set to register the temperature at different time intervals.

6.3 Discussion

At the start of the investigation, we evaluated the effect of the various monomers on the thermal gelation of the Pluronic solution before curing through temperature ramps at constant shear rates (Fig. 6.2a). We compared the plasticizing effect induced by PEG 400 with those caused by similar chemical species, all based on methacrylated PEG but with different chain ends, hydroxyl or methyl groups. Another relevant difference in the monomers selected is their molecular weight: there is a linear relationship between the concentration of plasticizer at which a Pluronic solution shows no gelation and the reciprocal of the PEG molecular weight, and therefore differences are expected. [365] A neat F127 30 w/v% solution was used as reference and its thermal response shows a dramatic increase in elastic shear modulus indicating gel formation at 21°C, which is the critical micellization temperature (CMT), with the onset of thermogelling determined by the percolation point of micelles. The addition of PEG 400 induced a decrease in CMT with an increase in its concentration, with anticipation of micellization. This can be explained by a decrease in the solubility of the PPO core in water at low temperatures because the solvation of the hydrophilic additive is more thermodynamically favored, with an earlier phase separation. [366] PEG is a small homopolymer that would create over-concentrated zones where water molecules hydrate more PEG than F127, therefore, less water molecules are then available for the hydration of the copolymer, leading to an increase in its apparent concentration and, by extension, a decrease of CMT. All PEGMEMA monomers have the opposite effect on gelation, improving the solubility of F127 in water

and, therefore, shifting the CMT towards higher temperatures. The molecular weight of the monomers has an important effect on the stabilization because longer hydrophilic chains determine a more efficient shielding effect at the same concentration, as expected. The PEGMA 500 monomer shows interesting behavior, because at low concentrations the predominant effect is comparable to the one induced by PEG, with a gelation temperature change towards low temperature. An increasing concentration of PEGMA causes a sequential delay in the CMT toward higher temperatures, in analogy with the PEGMEMA monomers, but without completely suppressing gelation in the range of interest at the higher concentration investigated. It must be inferred that the different effects on the solubility of F127 between monomers and neat PEG can be explained by the presence of the methacrylate group, which has a hydrophobic tendency, allowing these species to act as compatibilizing agents that interact with the hydrophobic core and stabilize it, also interfering with the packing of Pluronic micelles in the superlattices. [367] Furthermore, PEGMA 500 and PEGMEMA 500 were expected to show an analogous behavior given the similar structure and molecular weight, but the different chain ends strongly influence the effect on F127 micellization.

Once the thermal behavior of the uncured solutions was fully analyzed, photorheology tests were carried out, showing that the different terminal groups also have an effect on the polymerization kinetics (Fig. 6.2b). An increasing concentration and a higher molecular weight determine a higher reactivity in PEGMEMA monomers, and PEGMA showed a fast reaction kinetics and high final moduli even at low concentrations, with a behavior between PEGMEMA 950 and PEGMEMA 500. After irradiation, a temperature sweep test was performed on the same gel, to investigate the influence of the presence of the covalent network on Pluronic micellization compared to neat F127 and PEG (Fig. 6.2c). At the lowest concentration, all of the systems showed an increase in the curve, indicating gelation by the copolymer. The CMT was shifted toward lower temperatures, denoting anticipation in the micellization, even earlier than that of PEG. The main difference is in the final modulus achieved by the system, because while all PEGMEMA monomers resulted in a lower modulus than the neat F127 solution, also dependent on molecular weight, PEGMA 500 provided a higher modulus than the reference solution without additives. With increasing concentration, only PEGMEMA 300 did not suppress gelation and showed the same behavior as PEG 400 by shifting the CMT toward lower temperatures, but also lowered the final elastic shear modulus. PEGMA 500, on the other hand, showed a tendency to increase the final modulus with increasing concentration,

and we can conclude that only in this system the covalent network has a combined effect with the micelle lattices in providing mechanical strength.

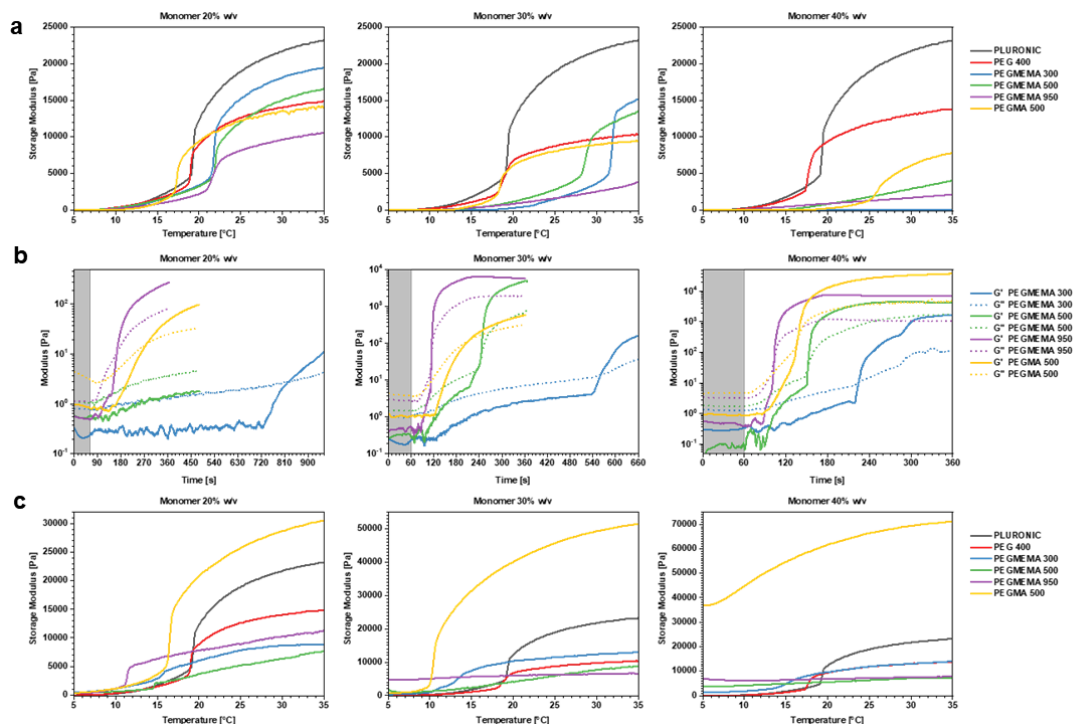


Figure 6.2 Plasticizer selection. Comparison of the effect of the different monomers at various concentrations on the a) thermal gelation of Pluronic before curing, b) on the photopolymerization kinetic of the resin, and on the c) thermal gelation of the Pluronic after curing and covalent network formation.

To provide a more comprehensive view, we tested several concentrations of each monomer to have a better visualization of the trends in their behavior. It can be seen that an increasing molecular weight of the PEGMEMA monomer determined a lower final shear modulus in the formulations before curing, as well as an increasing concentration, which also determined a shift in the CMT toward higher temperatures (Fig. 6.3a). PEGMA 500 showed a plasticization effect on the gel by decreasing the storage modulus, and this can be ascribed to the interference of the hydrophilic chain with the packing of Pluronic micelles into the superlattices. [367] As reported before, PEGMA also determines a complex effect on the CMT, which is first anticipated at low percentages, with a predominance of the hydrophilic part, and then delayed with increasing amounts of monomer due to the predominance of the hydrophobic methacrylated head. The monomer concentration also has an effect on its kinetics of polymerization, inducing the reaction to occur earlier and at a faster rate (Fig. 6.3b). PEGMA showed an interesting concentration-dependent behavior, with a change in kinetics above 30

%w/v, going from a steady slope to a two-section curve with a sudden vertical increase after a change in the slope of the curve, similar to the photopolymerization curves obtained by PEGMEMA, which can probably be attributed to some alignment effect above a certain threshold. The effect of the covalent networks fabricated by curing the different monomers is clearly visible in Fig. 6.3c, where it can be seen how PEGMEMA 300 was the only monomer of its class to not suppress gelation after curing, but the final modulus is lower than neat Pluronic. The PEGMEMA 500 and PEGMEMA 950 systems did not show any sigmoids for gelation, and their curve starts already from a storage modulus higher than zero, proving that there is some kind of stabilization of the copolymer that is not able to collapse and form the micelles. On the other hand, increasing concentrations of PEGMA resulted in an increase in the final modulus and a shift of the CMT toward lower temperatures until they went below 5°C; nevertheless, a change in the curve could still be seen, proving that the packing of the Pluronic continues to occur. The resulting shear modulus is a combination between the modulus provided by the F127 superlattice and the modulus of the covalent network, the contribution of which becoming larger with increasing monomer concentration.

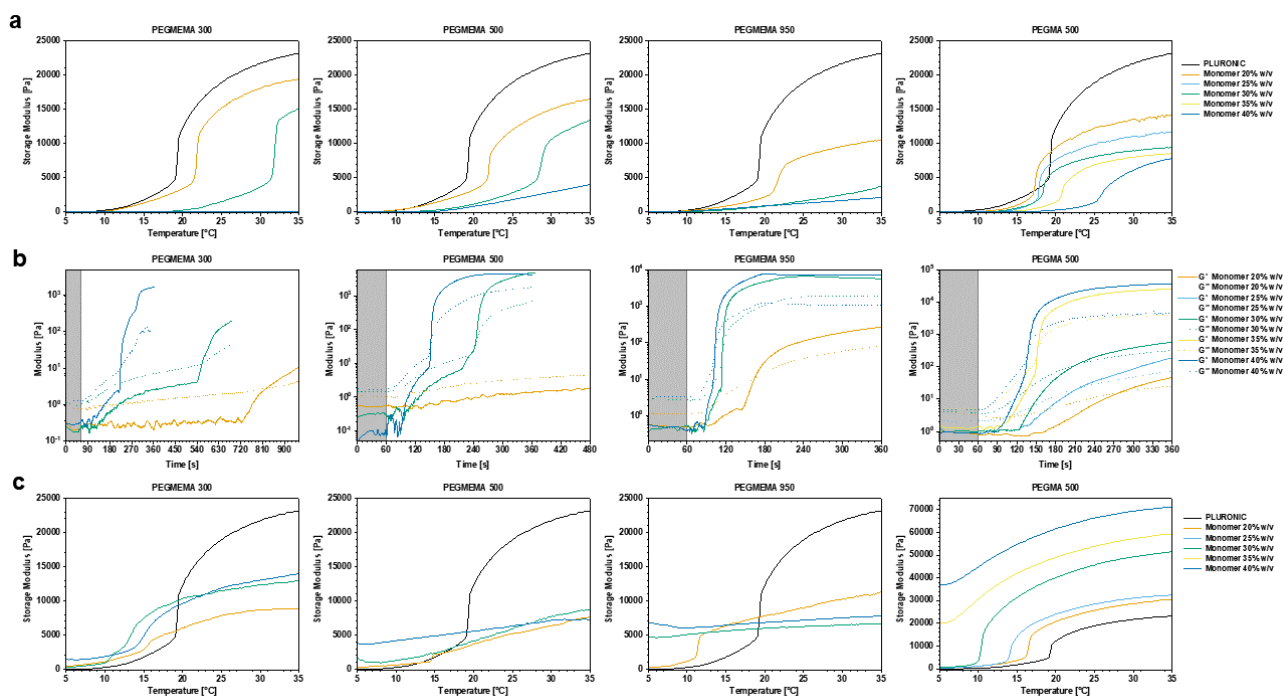


Figure 6.3 Concentration effect. Comparison of the effect of an increasing concentration for each monomer on the a) thermal gelation of Pluronic before curing, b) on the photopolymerization kinetics of the resin, and on the c) thermal gelation of the Pluronic after covalent network formation.

Given all the previous considerations, none of the PEGMEMA monomers seems suitable for the application, since PEGMEMA 950 is the only one that provides a kinetic compatible with vat photopolymerization printing, but suppresses gelation, while PEGMEMA 300 shows a behavior similar to that of PEG 400 after curing but its reaction kinetic is too slow and unsteady and the final modulus is too low even at the highest concentration. Therefore, we investigated in more detail the characteristics of the systems containing PEGMA 500, which is the most suitable monomer since it showed more consistent behavior and regular curves, a fast kinetic, and a combined effect with Pluronic micellization.

The rheological behavior was evaluated using an oscillatory shear test at two different temperatures before and after curing, comparing formulations containing PEG 400 and PEGMA and using a neat Pluronic solution as reference to study the dynamic response of the gels (Fig. 6.4). Before curing, at 5 ° C both systems showed a similar trend (Fig. 6.4a-b), with a gradual increase in the loss modulus with higher concentrations within a similar range, slightly lower for PEGMA. The test repeated at 25 ° C resulted in an elastic modulus with a similar trend but in the opposite direction, with lower moduli than neat Pluronic, which form a higher number of physical cross-links, and a regular decrease for increasing PEG concentration (Fig. 6.4d). PEGMA shows a larger gap between the curves for the lowest concentration and the reference and lower variability among the various curves, proving a limited effect on the rheology of the thermal gel, mainly due to the gelation of the copolymer, which is constant in each formulation (Fig. 6.4e). After curing, at 5 ° C there is no contribution of the gelled F127 and the curves are evenly distributed with a different shape from the thermal gel because they arise from a covalently cross-linked network, whose response strongly depends on the concentration, which determines a drastic increasing trend in the modulus (Fig. 6.4c). The linear elastic modulus is related to the number of cross-linking points that form the network, since the small amplitude oscillatory shear deformation provides the mechanical response of the gels in the viscoelastic region. [368] When the temperature is increased to 25 ° C after curing, the difference before and after curing is less prominent because the covalent network gives a limited contribution to the elastic shear modulus compared to the physical network generated by the Pluronic (Fig. 6.4f). There is a combined effect between the covalent network and thermal gel; due to the previous increasing trend with the shift toward higher storage moduli there is the addition of the convergence of the curves as seen in the amplitude sweep tests carried out at 25 ° C before curing.

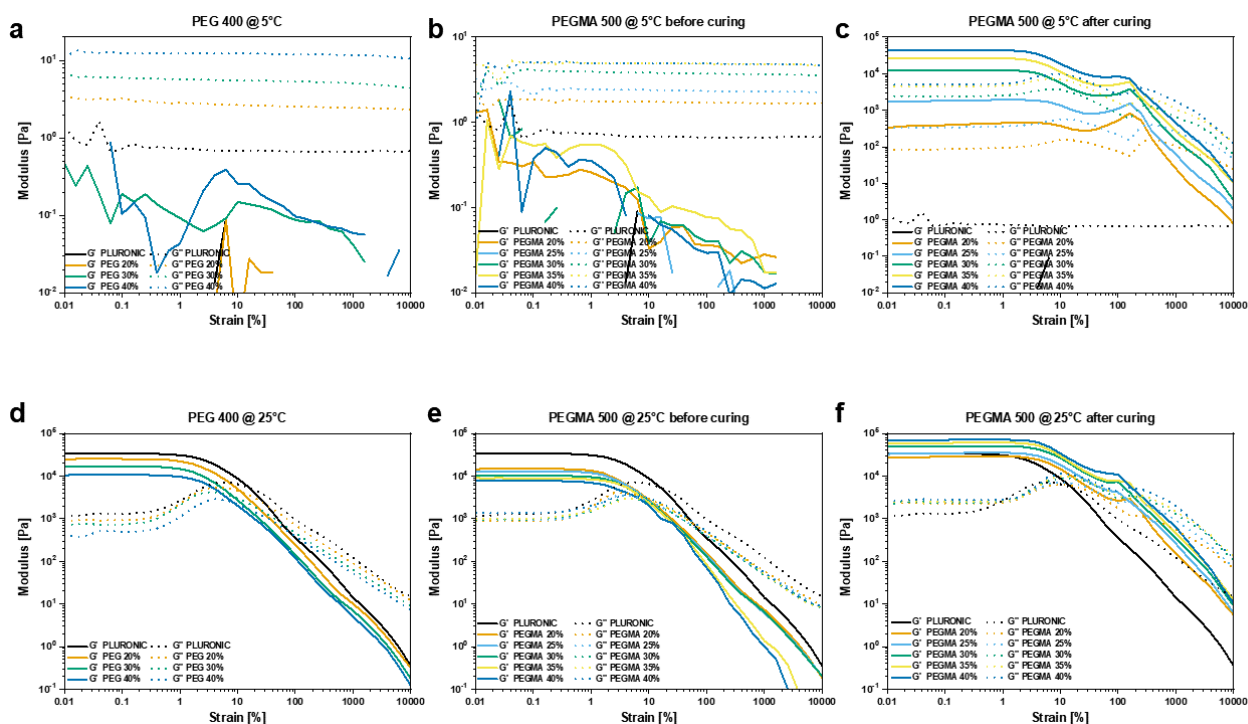


Figure 6.4 Rheological behavior. Amplitude sweep tests results performed at 5°C using as plasticizer a) PEG 400 and b) PEGMA 500 before curing and c) PEGMA 500 after curing. Amplitude sweep tests results performed at 25°C using as plasticizer d) PEG 400 and e) PEGMA 500 before curing and f) PEGMA 500 after curing.

We also investigated the effect of the small PEG-based species and the covalent network on the thermo-reversibility of the gels (Fig. 6.5a-c). All the profiles describing the temperature-dependent elastic shear modulus show a hysteresis between the cooling and the heating cycles, because of slower kinetics at the gel phase, with the bottom curve resulting from increasing the temperature, whereas the upper curve is the one obtained by lowering the temperature. The sol-to-gel temperature is always higher than the gel-to-sol temperature because an under-cooling is required to completely break down the micelle structure and to promote the solvation of the hydrophobic cores. [368] Nevertheless, the results show that the addition of PEG and PEGMA, even at the highest concentration, does not significantly alter the thermoreversible nature of the gels. Before curing, an increasing concentration of plasticizer determines a decrease in the final storage modulus of the hydrogel and a shift in the gelation temperature and on the hysteresis curve in general (Fig. 6.5a-b), which, however, depends on the nature of the plasticizer, as previously observed. The formation of the covalent network after curing does not affect the thermo-reversibility (Fig. 6.5c), and the gelation of F127 does not significantly alter the microstructure of the PEGMA/PEGDA

network since any drop in the shear modulus was not measured during cooling, i.e. breakage of covalent bonds. [368] It is likely to be inferred that micelle formation occurs within the mesh of the covalent network, and this confinement could reduce the critical micelle concentration, which combined with the hydrophilic pendant groups that do not have any more a hydrophobic head because they are involved in the formation of the network and therefore behave similarly to low Mw PEG, causes a decrease in gelation temperature by favoring micelle dehydration due to an increase in its apparent concentration. [367] The systems above 30 %w/v did not show any CMT and therefore no sigmoid curve, but started already from an initial storage modulus higher than zero, and it is noticeable how the final shear modulus values of all samples do not return to the starting level at low temperature, unlike thermal gels obtained before curing. The gaussian shape of the curves over time (Fig. 6.5d-f) suggests that the micellization follows the same mechanism for gelation and dissolution before and after curing, with no relevant influence given by the covalent network. The formulations already starting above the threshold require additional under-cooling to rapidly return to their initial conditions independently of the initial concentration of the monomer (Fig. 6.5f), and even keeping the formulation at 5 ° C for a long time did not restore the modulus, and it must be inferred as shear thickening–shear thinning behavior and not a micellization. [368]

Before printing, we eventually explored the influence of the concentration of PEGDA on the thermal reversibility and final mechanical properties of the hydrogel. An increasing cross-linker concentration resulted in a reaction kinetic that was faster than could be expected, with anticipation in the induction time and an increase in the slope of the curve (Fig. 6.6a-c). There is a relevant difference between the kinetics of formulations with 1 and 5 phr, while there is not much difference between 5 and 10 phr. Interestingly, the final moduli achieved during thermal sweep are comparable between formulations at the same monomer concentration but with a 1 phr and 5 phr cross-linker, while the use of a 10 phr cross-linker determined an increase in the final modulus (Fig. 6.6d-f). The increasing cross-linker concentration at the same monomer concentration also induced a shift of gelation toward lower temperatures until complete suppression, while 1 phr PEGDA formulations showed micellization even at 30% w/v monomer concentration. Therefore, we selected a concentration of 1 phr for the cross-linker because it effectively enables the gelation after the reaction without suppressing it also at low concentrations of monomer. We did not test any concentration below 1phr because the system already shows a low final modulus

even at room temperature; a lower concentration would have not guaranteed sufficient stiffness and resistance for self-supporting structures after printing.

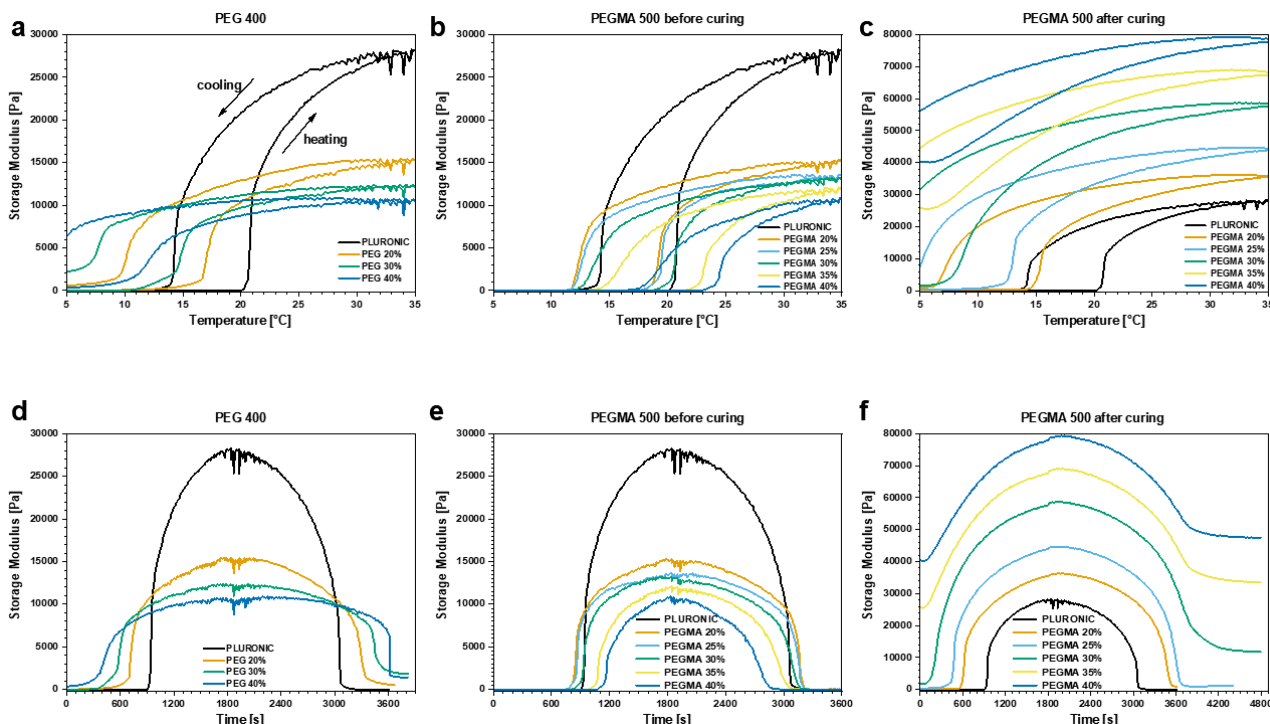


Figure 6.5 Thermal hysteresis. Reversible gelation tests results performed using as plasticizer a) PEG 400 and b) PEGMA 500 before curing and c) PEGMA 500 after curing. Storage shear modulus evolution over time during the reversible gelation tests results performed using as plasticizer d) PEG 400 and e) PEGMA 500 before curing and f) PEGMA 500 after curing.

Given all the considerations above, the formulation selected for printing was PLURONC 30% w/v, PEGMA 500 30% w/v, PEGDA 700 1 phr, and PEG-BAPO 1 phr. Given the LCST of the pluronic-based water solution, the ink had to be stored in a cold environment to avoid any physical gelation. Printing had also to be performed while the system was cooled to preserve the fluidity of the resin during the whole process. For example, Cohn and Dutta used a custom-made monomer bath with a cooling system embedded to maintain the ink solution at 6 °C during the printing process. [363] We wanted to explore a more versatile and less demanding system both in terms of effort and space; therefore, we tried to use air cooling (Fig. 6.7a). Taking advantage of the characteristics of the printer, which has a hole beneath the vat corresponding to the optical window, we used a Vortex tube, exploiting the Ranque-Hillsch effect, to cool the air, [369] which was then directed towards the bottom of the vat to cool the resin from the bottom over an area corresponding to the irradiated area (Fig. 6.7b). Due to the aforementioned

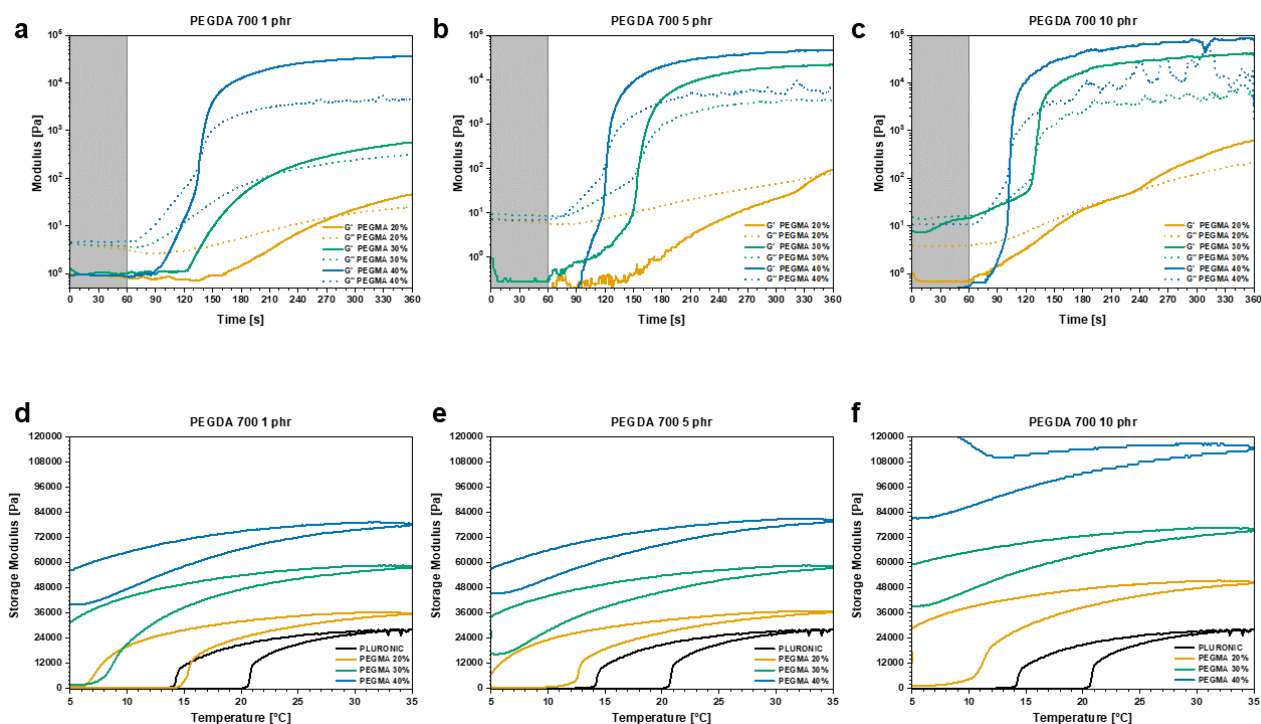


Figure 6.6 Cross-linker effect. Comparison of the effect of an increasing concentration of crosslinker (1-5-10phr) at different concentrations of monomer a-c) on the photopolymerization kinetics d-f) on the Pluronic reversible gelation

effect, compressed air at 2.5 bar could be lowered between 15 and 20 ° C below the input temperature. This required some changes in the printing process, such as stopping the motion of the slider, to even stop the bottom of the resin beneath the printed object before irradiating a layer. The absence of a slider is common in other commercial printers and requires a large volume and low viscosity of the resins that make them able to completely fill the below gap, compatible with our formulations. We tested the effective cooling of the bottom window using a thermal camera (Fig. 6.8a). We proved that the bottom of the vat, and therefore the resin, could be cooled down at a temperature well below the CMT of the uncured formulations, and therefore it was theoretically possible to perform a printing process with this configuration. Additionally, we proved the effect of the dye on the physical gelation of the system, which thus not only has a positive effect on the printing itself by simply confining the light along the vertical axis (Fig. 6.8b). The presence of the dye allowed thermal gelation to be avoided, as can be seen from the images. The yellow part is resin, which is only physically gellified, while the white part is a chemically gellified part. On the right, it can be clearly seen where the reaction took place, compared with where the formulation

remained unreacted, evenly spread, and distributed at the bottom of the vat, as shown by the sharp difference in the color, as can also be seen in the pictures below, where the difference in behavior of the resin inside the vat can be seen. Unfortunately, this solution caused some hardware-related problems.

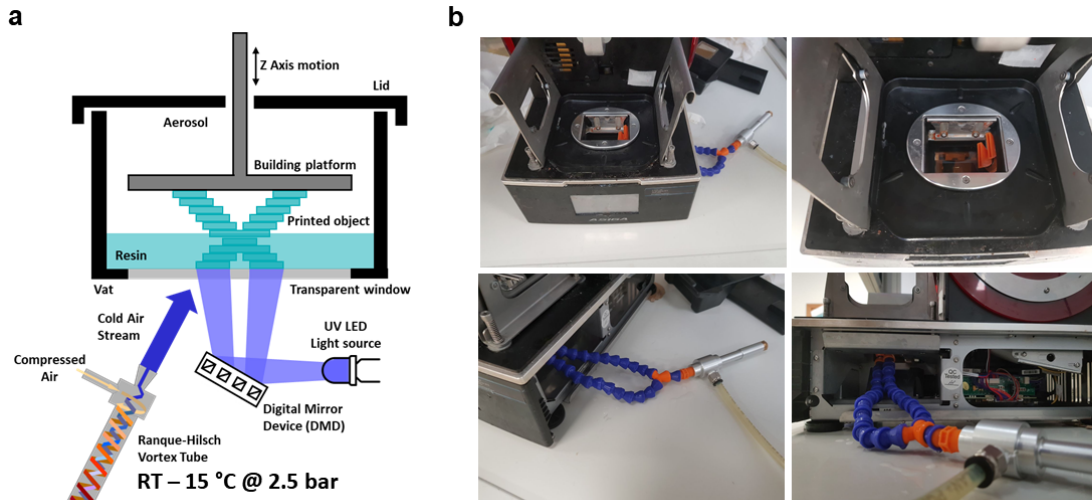


Figure 6.7 Printer Modification. a) Schematic illustration of the Digital Light Processing (DLP) printing apparatus used modified with the cooling vortex tube below. b) Real configuration of the printing system with the vat cooled by compressed air.

The compressed cooled air caused condensation of air humidity in the optical group (Fig. 6.9a), and this could be detrimental to the electronic components of the printer, affecting the useful lifetime of the instrument. The same issue arises from the cooling along the tube used to direct the air toward the bottom of the vat (Fig. 6.9b), and this dripping water could cause damage to the instrument. Furthermore, this configuration enabled cooling only at the center of the FEP window even by using large diffusers (Fig. 6.9c), leaving a gradient in the temperature, with the consequence of a possible early thermal gelation of the resin, hindering the correct printing because of the unavailability of liquid resin. The lack of homogeneous cooling caused an uneven resin distribution after irradiation, causing an incomplete or uneven distribution. To cope with this limitation, we did not use the vat completely full, but we used a small pool of material located between the window and the platform to use low volumes of resin (Fig. 6.9d), refilling the area while printing and when necessary. Cooling the printing platform was vital as well, because while the bottom of the vat was cooled, the platform was at room temperature and when encountering the resin, it caused rapid thermal gelation of the resin (Fig. 6.9e), hindering correct printing as

well. The issues arising from this solution, combined with the slow kinetics, led us to change the approach to achieve an effective printing process.

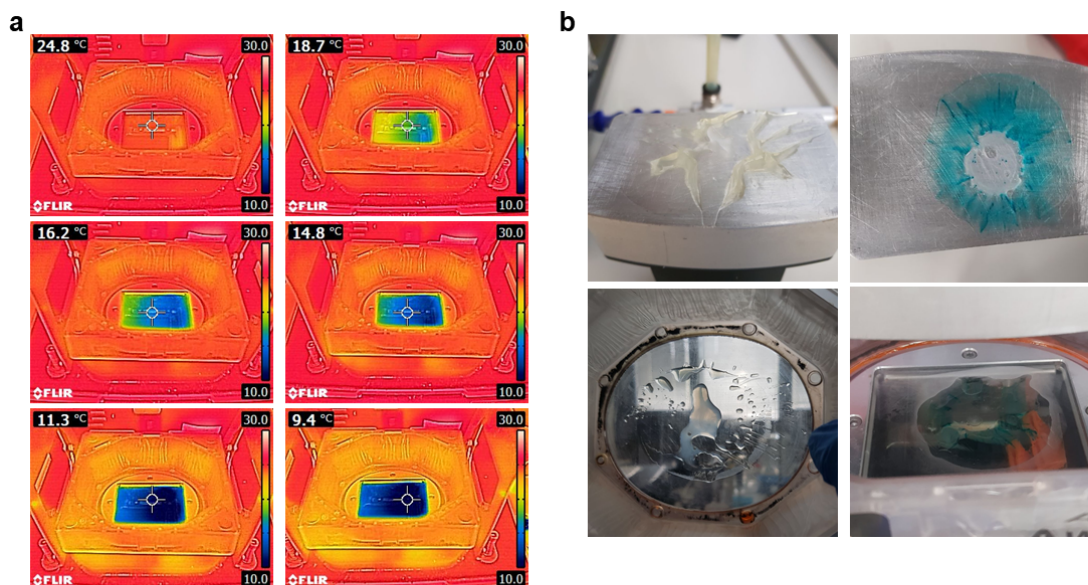


Figure 6.8 Vortex tube-cooling efficiency. a) Thermal camera images of the vat of the printer at various temperature during cooling. b) Formulation thermal gelation during printing without the dye (above) and after the addition of the dye (below).

We solved all the issues mentioned above by performing the printing process inside a refrigerator set at 6 ° C, taking advantage of the small dimensions of the printer to place it inside (Fig. 6.10a). The printing was started only after letting the system sit for 10 minutes with the door closed to reach an even temperature, and as can be seen, the formulation remained liquid after an entire printing process with very few residues were found in the residual resin in the bottom vat (Fig. 6.10b) and almost no thermally gelled residues are present around the printed object and on the platform (Fig. 6.10c). We also used a building platform with a glass bottom to have a more even surface to facilitate the adhesion of the printed object onto it and facilitate the object removal, since the printed objects were characterized by a very high softness that made their removal from the platform and handling. We encountered the same problems as with the previously described system based on uncrosslinked PVA that involved the removal of a large amount of residual resin present on the surface of the objects at the end of the process that needed to be removed by hand. We could print self-standing 3D structures with a low size ratio during a very slow printing process due to the long irradiation required. An irregular tetrahedron (Fig. 6.10d) showed sharp edges but irregular flat surfaces, even on vertical walls. The resolution of full bulky

structures was acceptable, whereas in the presence of holes, the xy resolution resulted in satisfactory resolution, while the vertical resolution was insufficient. (Fig. 6.10e) The sample broke during handling due to its intrinsic softness, which did not cause excessive distortions in shape but did not allow the achievement of overhanging features, which were also hindered by the low strength of the hydrogel in bearing its weight, resulting in a failure of the upper layers caused by delamination and limiting the tallest achievable objects to around 4 mm. We also tested the printing of a holed cube (Fig. 6.10f) that showed visible features along the horizontal plane with insufficient resolution, no vertical holes, and clogged horizontal holes, likely ascribable to an incorrect flow of the resin during platform motion. We hypothesize that further studies on the printing parameters and the concentration of dye and PI could enable printing overhanging features and vertical holes.

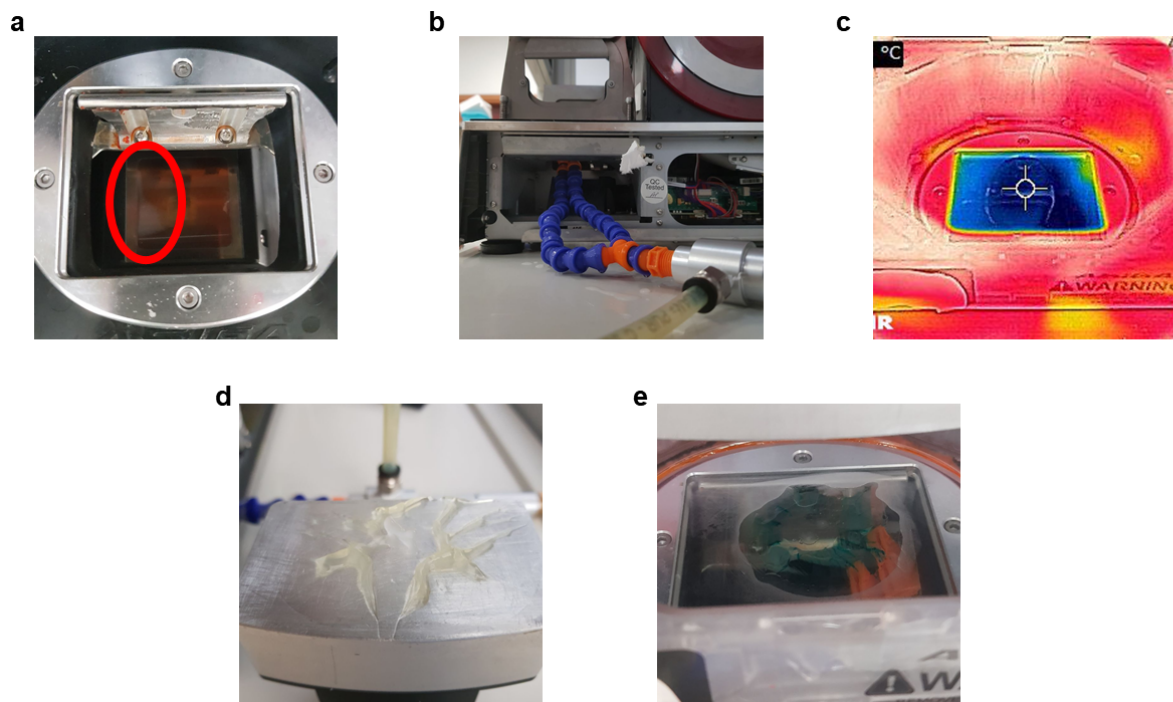


Figure 6.9 Vortex tube-cooling issues. Moisture condensation a) in the optical group of the printer and b) along the flexible tubes. c) Limited cooling only at the transparent window. d) Thermal gelation of uncured resin on the building platform. e) Uncured resin thickening and hindered flow in the vat.

Eventually, we tried to define a self-healing procedure for printed samples, but despite the various methods tested, no SH was detected, even though a Pluronic-based thermal gel was proven to self-heal at room temperature in a

confined container, which was crucial in helping the restoration of the crevices. [347] We tried several approaches, like cutting the sample at RT or at low temperature and rejoining them either at RT or at low temperature, performing a cycling in temperature with cooling-heating cycle or viceversa, by blowing cold air directly at the surfaces to promote the disruption of the micelle before rejoining, or applying pressure on the samples at RT or low temperature to exploit the gel softness for surfaces compliance, with all the related problems caused by the transition to the sol state of the Pluronic, but every tryout was unsuccessful.

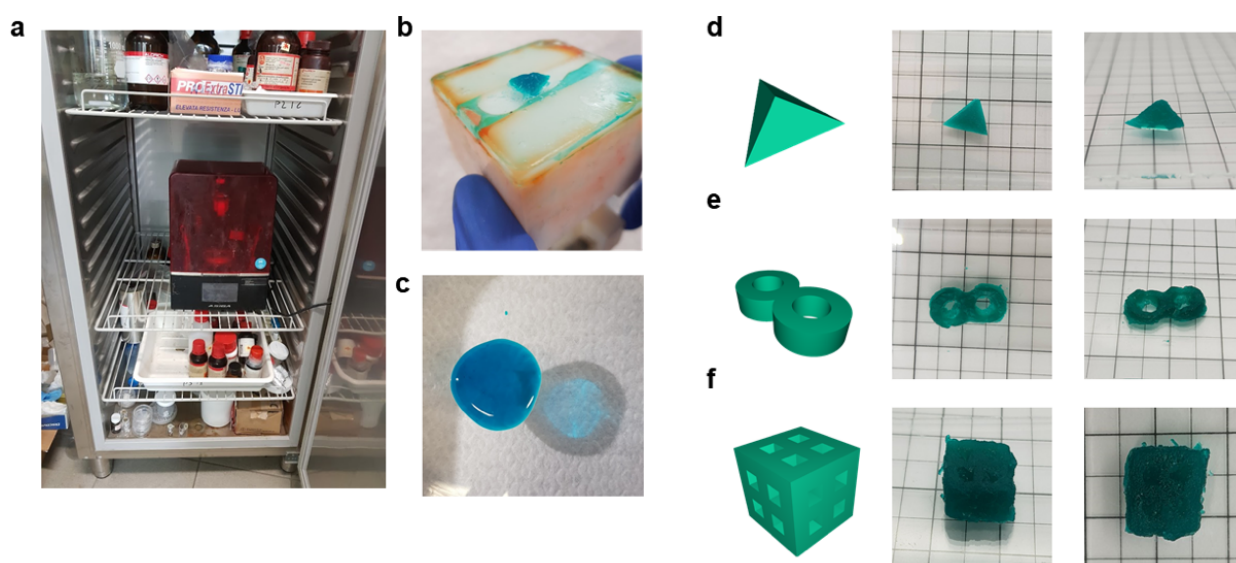


Figure 6.10 Printing process in a cool environment. a) Real configuration of the printing system located in the refrigerator. Absence of thermal gelation of both b) on the building platform and c) in the vat. d-f) CAD files and resulting printed samples of a d) tetrahedron, e) “eight” figure, f) holed cube (scale 10 mm)

6.4 Conclusions and perspectives

In summary, our goal was to demonstrate the feasibility of using an interpenetrated system based on a covalent network containing an amphiphilic triblock copolymer capable of forming electrostatically interacting micelles to achieve cold-activated self-healing in DLP printed hydrogels.

In particular, we wanted to exploit the plasticization effect of hydrophilic chains in methacrylated PEG-derivatives to influence the interaction between branches in the hydrophilic corona of the micelles formed by Pluronic F127. Initially, we explored the effect of several potential monomers on the thermal

reversibility of a Pluronic solution at constant concentration before and after the formation of the covalent network and compared their effect with unmodified PEG with a similar low molecular weight. It resulted that while PEG induces a shift toward lower CMTs, PEGMEMA monomers induced a shift in the opposite direction, while PEGMA has a more complex effect, initially shifting the formulation behavior toward low CMT, and then with increasing concentrations, the gelation temperature of the system increased. Furthermore, PEGMA was the only chemical specie that provided a reaction kinetic compatible with vat photopolymerization and did not suppress the micellization, increasing the overall elastic modulus of the system and decreasing the CMT with an increase in the monomer concentration. We then independently explored the effects of the thermal gelation and covalent network by amplitude sweep testing, demonstrating that both contribute to the final properties of the system, especially thermal reversibility, for which the system shows a regular hysteresis in modulus for a heating cooling cycle at a regular rate. We also showed that the system requires an undercooling to restore the initial conditions, and that even a cooling for a long time did not bring the modulus to the starting point. Before printing, we evaluated the effect of the cross-linker concentration on the polymerization kinetics, final mechanical properties of the hydrogel, and thermal reversibility of the polymer, proving that increasing the concentration in the cross-linker suppressed the effective micellization in the range of interest above a threshold concentration. Given the LCST of the formulation, it was necessary to keep the resin below the CMT during the entire printing process; therefore, we explored the feasibility of a cooling procedure by blowing cold air onto the bottom of the vat. Despite the effective cooling of the resin at a useful temperature, we encountered various issues; therefore, we moved onto a different approach, performing the printing in a cold environment. We were able to print simple shapes with sharp edges, but a limited size ratio, and poor resolution, especially along the vertical axis, because of the poor mechanical strength of the hydrogel and limitation ascribable to undesired thermal gelation. Unfortunately, we were unable to define an effective procedure to evaluate potential self-healing efficiency despite the various possibilities and the various methods explored.

A suitable solution to mitigate low mechanical strength and limited size ratio could be the use of Poly(ethylene Glycol) dimethacrylate (PEGDMA) as crosslinker, which is more similar to the PEGMA monomer and more rigid thanks to the additional methyl group. Alternatively, a water-soluble monomer could be added in a small quantity, such as Hydroxyethyl methacrylate (HEMA), which could stiffen the network. [370] To improve the poor resolution, a change in the

dye, such as tartrazine, could be explored, to evaluate if the problem is related to overheating or poor light confinement, which could also be prevented by introducing a radical scavenger, such as ascorbic acid, to avoid unwanted polymerization outside the designated areas. Another approach could be the combination of the refrigerated printing with the aerosol system presented in chapter 5, which could help reduce the thickening of the resin and the adhesion on the surface of the printed objects.

This work focused more on investigating macroscopic behavior and practical applications than molecular detail and mechanism definition, but an investigation focused on micelle formation, shape, and interactions by means of several different techniques, such as DSC, SAXS, and turbidity tests, could help the definition of an effective SH procedure. [371,372] Potential adjustments of the composition of the system could be evaluated in terms of SH effectiveness, such as the introduction of monomers known to give a thermoreversible effect, such as NIPAM or DMAEMA to tune the gelation temperature, but that could have negative effects on the polymerization kinetic given the lower reactivity of these monomers. [350,373] Another interesting approach could be the use of modified Pluronic, such as the methacrylated one, which has already been proven to be an effective oligomer in vat photopolymerization, and its combination with an unmodified one, maybe using different molecular weights to exploit different properties. Another potential could be the use of reverse Pluronic, a BAB-type triblock copolymer with a hydrophilic core, proven to bridge across ABA Pluronic micelles and whose methacrylated version has already been proven as oligomer for vat photopolymerization. [360,374] The versatility of the system would also enable testing other thermally-induced properties which were out of the scope of the initial assessment of the system and were planned for further studies, such as cold-triggered shape memory.

Chapter 7

Light-mediated self-healing system

1.1 Introduction

In the previous chapter 5 we used the dyes to improve the printing resolution, for a visual discrimination of the rejoined pieces and to prove the actual interdiffusion across the mended interface. In the work reported in this chapter, the aim was to use a custom dye as the main healing agent. Furthermore, while in the previous work we used unmodified PVA as a healing agent, here the PVA is modified to be used as an oligomer for the fabrication of the covalent network, but it is not directly responsible for the healing, despite being indirectly involved.

As a further development of the investigation of the 3D printable hydrogel, we wanted to explore the possibility to introduce a second level of control to trigger self-repair of structures. In particular, our attention was taken by light because it is spatially and temporally controllable, so it perfectly fits with self-healing requirements. Accardo and Kalow proposed a hydrogel with photocontrolled dynamic covalent bonds established between PEG tetramers bearing either a boronic acid or a diol. Those are used to form a boronic ester that could be activated by altering the configuration of the azobenzene adjacent to the boronic acid, which acts as an externally controlled photoswitch. [375] In this work, two different wavelengths of irradiation were used to obtain reversible mechanical changes, with controlled softening and stiffening of the resulting hydrogel; furthermore, the use of this azo dye provides light-induced self-healing, due to the strength and directionality of dynamic covalent bonds, which undergo reversible exchange by hydrolysis and esterification. The tuning of the azo group with visible light was used to influence the kinetics or equilibria for the interconversion between boronic acids and boronic esters. Azobenzene derivatives are considered archetypical molecular switches because their properties can be readily tuned and incorporated into host materials without compromising their reactivity by using different functional groups for cross-linking or photoexcitation. [376] Azo compounds undergo reversible isomerization between

two forms, a metastable E or cis isomer and a Z or trans isomer, typically more stable. The characteristics of this molecular switch are a fast response (picoseconds), absence of side reactions other than the isomerization, stability to photobleaching, and repeatable cycling with low fatigue over time (Fig. 7.1a). [377] The two different isomers have two distinct levels of energy, so the isomerization occurs in response to two different wavelengths of light (i.e., two energies), with trans-to-cis isomerization induced by UV light irradiation and cis-to-trans isomerization induced by visible light irradiation. Alternatively, isomerization can also be controlled by heating. [378] The geometric isomerization between the two energy states determines differences in absorption spectra and in the steric hindrance of the molecules. In fact, isomerization causes a shortening of the end-to-end distance by 3.5 Å. This is related to the fact that the planar trans form switches to the non-planar and more compact cis-azobenzene form, where the two phenyl rings are twisted dihedral angle of 60 ° relative to the C-N=N-C plane, occupying a larger volume than the Z isomer. [379] This geometric change also increases the dipole moment, from zero in the trans form to 3.1 D in the cis form. [380,381] This dipole variation has an even greater difference in push-pull-type azopolymers, which are functionalized with electron-donating and electron-withdrawing substituents. In these azoderivatives, the absorption band of the trans isomer completely overlaps with the absorption band of the cis isomer, and therefore irradiating the push-pull-type azopolymer using visible light induces trans-to-cis and cis-to-trans isomerization simultaneously. It is difficult to obtain a cis-rich state for push-pull-type azopolymers due to the spectral overlap and short half-life of the cis isomer due to its metastability. Due to the chemical modification of the azobenzene group, they can be harnessed and engineered, to obtain macroscopical mechanical and shape effects thanks to macromotions. [377] Azo-containing photoresponsive materials are thus designed to take advantage of the differences between the trans- and cis states. The introduction of azobenzene into macromolecular architectures and polymer matrices facilitates its processability and application. In the study proposed by Accardo and Kalow, the azobenzene dye was further modified with a functional group (boronic acid) capable of establishing ester bonds with a diol only when the azo is in the cis form, enabling locking of the configuration. (Fig. 7.1b). [375]

As reported in Chapter 1, phenylboronic acid (PBA) derivatives have higher stability than aliphatic derivatives, due to the charge conjugation effect of the benzene ring, which provides hydrolytic stability higher than that of the aliphatic counterpart. The phenylboronic group has often been employed as a pendant group used for its glucose responsiveness, but also for its pH-triggered shape

memory properties and for its self-healing ability at room temperature under ambient conditions. The latter was demonstrated to occur at basic, neutral, or acidic pHs, depending on the binding group and the surrounding species. [304,382–384]

The selection of polyols as cross-linking agents is fundamental in determining the hydrolysis equilibrium and the efficiency of the boronate ester formation; multi-hydroxyl polymers such as poly (vinyl alcohol) (PVA) have been demonstrated to be the most suited to yield polymer networks with phenylboronic ester linkages with autonomous self-healing without external intervention. [27] PVA is a polyol system very sensitive to inorganic borides, especially boric acid, and aromatic boronic acids, the latter less efficient at reacting due to their steric hindrance that hinders effective interaction with hydroxyl groups. Like the majority of polymeric macromolecules, PVA chains are normally entangled and arranged into random coils; therefore, PVA must be properly dissolved and hydrated to allow access to diol pendant groups. [385,386] PBA has already been used as a pendant group in an interpenetrated network with PVA to spontaneously form hydrogels in aqueous medium upon mixing, showing self-healing and shape memory ability upon pH activation. [387,388] PVA is a versatile polymer that can be used for various applications both as is and after chemical modification of its pendant hydroxyl groups with a variety of functional groups, such as photopolymerizable (meth)acrylates. [337] Modified PVA has been used to achieve high-fidelity vat photopolymerization printing of hydrogels via commercial 3d printers by using water-based formulations relying on a free radical mechanism that involves methacrylation or thiol-ene chemistry. [235,335,389]

To achieve the objectives of developing a water-based resin for vat photopolymerization composed of molecules synthesized with simple chemistry and, we prepared methacrylated PVA and a methacrylated dye bearing a boronic acid pendant group (Fig 7.1c) to endow printability and enable its embedding within the matrix. The idea was to achieve a covalently cross-linked PVA network with pendant azoboronate groups that can act at the same time as dyes for light confinement during vat photopolymerization and as photoswitchable cross-linkers for light-activated self-healing. [58] The final goal was to achieve self-healing by photocontrolled activation of labile covalent chemistries to enable localized restoration of complex features, even in areas not directly accessible, or to reconnect fine elements difficult to rejoin by hand.

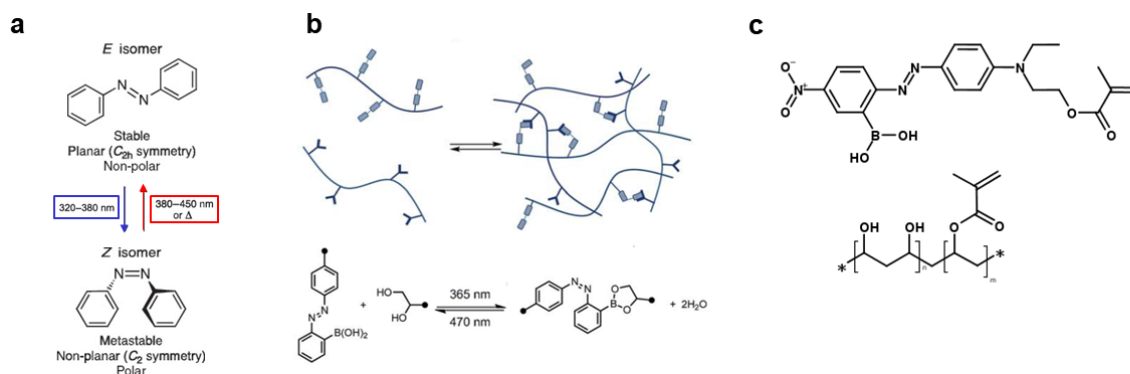


Figure 7.1 Light-triggered system design. a) Photoisomerization mechanism of a generic azobenzene group. b) Schematic illustration of the dynamic covalent bond formation and representation of the proposed self-healing mechanism based on boronate-ester bonds. c) Chemical structure of the reactive dye and oligomer present in the photocurable resin. Adapted and reproduced with permission from [126,375]

This project was developed in collaboration with Matteo Gastaldi from the Chemistry department of the Università di Torino, a Ph.D. student under the supervision of Prof. Guido Viscardi and Prof. Claudia Barolo, who kindly provided the modified dye used in the following experiments.

1.2 Methods

Materials

Poly(vinyl alcohol) (PVA) with molecular weight range of 13000–23000, 88% and 98% hydrolysis, dimethyl sulfoxide (DMSO), Toluene, Acetone, Propylene Carbonate (PC), Glycidyl methacrylate (GMA), 4-(Dimethylamino)pyridine (DMAP), Water-soluble TPO based nanoparticle photoinitiator, 2-Hydroxy-4'-(2-hydroxyethoxy)-2-methylpropiophenone (I2959), Tris(2,2'-bipyridyl)dichlororuthenium(II) hexahydrate (Ru), Ammonium persulfate (APS), Disperse Red 1 (DR1), Disperse Red 1 Methacrylate (DR1-MA), Phenyl diboronic acid (PDBA) were purchased by Sigma Aldrich. All chemicals were used as received without further purification. The PEG-BAPO photoinitiator was kindly provided by Prof. Hansjorg Grutzmacher. 2-(Ethyl(4-((4-nitrophenyl)diazanyl)phenylboronic acid)amino)ethyl methacrylate (APAM) was kindly provided by Matteo Gastaldi.

PVA methacrylation

The methacrylation of PVA was performed following the procedure described by Zhou et al. [390] 10 g of PVA were dissolved in 200 ml of dimethylsulfoxide (DMSO) at 60 °C. DMAP was added to the solution in a 1.0 mol% relative ratio

to the hydroxyl group of PVA until the solution became clear. The GMA was then added dropwise under vigorous stirring and the reaction mixture was left to react with constant stirring for 6 h at 60 ° C. The solution was poured into 500 ml of toluene to stop the reaction, extract PVA from DMSO by precipitation, and remove unreacted GMA and the catalyst. The liquid was then removed, and the deposited material was further precipitated in acetone for additional cleaning and concentration. The solvent was removed by rotary evaporation and the resulting yellow powder was collected, dried under vacuum, and then stored in a refrigerator at 5° C in the dark. DMSO ⁶D NMR spectra were collected with a Bruker AV 400 NMR instrument to demonstrate the methacrylation of PVA.

Characterization

UV-VIS Spectroscopy was performed on 0.1 mM dye solutions in acetonitrile with a BioTek™ Synergy™ HTX Multi-Mode Microplate Reader (Fisher Scientific Italia, Rodano, Italy). The selected range was from 300 nm to 700 nm with a 1 nm scanning step. Real-time photo-rheology tests were performed using a Physica MCR 302 rheometer (Anton Parr Italia, Rivoli, Italy) in a 25 mm diameter parallel plate mode with a set-up comprising a quartz lower plate and a gap between the two plates set to 0.2 mm. The tests were carried out at a constant shear frequency of 10 rad/s and a constant strain amplitude of 1% in the linear viscoelastic region at a constant temperature of 25 ° C. The light source used was a Hamamatsu LC8 lamp, equipped with an 8 mm light guide, either with a bulb emitting visible light with an intensity on the quartz window around 30 mW/cm², measured with a Hamamatsu power meter C6080-04, or with a bulb emitting UV light with an intensity on the quartz window between 23 and 25 mW/cm² measured with a UV radiometer EIT Power Puck II. The light was turned on after 60 s to stabilize the system. Concomitant changes in the moduli of viscoelastic materials during polymerization were measured as a function of exposure time. Compression tests were performed with a Physica MCR 302 rheometer (Anton Parr Italia, Rivoli, Italy) in parallel plate mode with a set-up comprising an 8 mm diameter aluminum upper plate and a knurled bottom plate. The test was performed by slowly putting in contact with the upper plate on the upper surface of printed cylinders of 8 mm diameter and 3 mm thickness. The test was then carried out with a normal force of 5N and a constant downward velocity of 10 μm/s until complete failure of the sample. A minimum of five samples for each batch were tested, and the results were averaged for reproducibility. Swelling tests in DMSO were carried out on printed cylinders of 8 mm diameter and 3 mm thickness. The samples were printed and then dried to remove all the water and then immersed in the same volume of DMSO, 1 ml. At various times, the samples

were taken out from the solvent, blotted, and weighed. A minimum of five samples for each batch were tested, and the results were averaged for reproducibility.

Resin Preparation and 3D Printing Procedure

In a typical procedure, 1 g of PVA-MA flakes was added to 10 ml of deionized water under magnetic stirring at 300 rpm at room temperature until the solution became clear and appeared homogeneous with no residues visible. Subsequently, 100 mg of photoinitiator and 1 ml of a 10 mg / ml dye solution in an organic solvent were added to the solution, maintaining magnetic stirring at 300 rpm until the solution became homogeneous.

The STL models were 3D printed using a DLP printer (Asiga Pico 2HD or Asiga MAX). The Asiga Pico 2HD operates with a 405-nm LED light source and the printing process was performed with a 50 μm layer thickness, an approach and separation velocity of 1 mm/min, a slider velocity of 1 mm/min, and no wait time after each step. The light intensity was set at 40 mW/cm² with a burn-in irradiation time of 35 s for four layers and a normal exposure time of 30 s for the remaining layers. The Asiga Max operates with a 385 nm LED light source and the printing process was performed with a 50 μm layer thickness, an approach and separation velocity of 1 mm/min, and no wait time after each step. The light intensity was set at 45 mW/cm² with a burn-in irradiation time of 6 s for four layers and a normal exposure time of 5 s for the remaining layers. After printing, the samples were cleaned using compressed air to remove the unpolymerized resin, and for some structures that have residual resin, it was manually removed with cleanroom paper to not leave paper residues on the samples. The objects were then post-cured after the unreacted resin was removed to complete the polymerization and to strengthen the printed objects. Post-curing was performed in a UV chamber with a medium-pressure mercury lamp (Asiga Flash or RobotFactory UV oven) for 2 minutes. The printed samples were stored in a sealed container to prevent excessive water evaporation.

1.3 Discussion

The system is based on two poly(vinyl alcohol) (PVA) polymers with the same molecular weight but different hydrolysis degrees (DH) to study the effect of the presence of different concentrations of vinyl groups on methacrylation and the effect of two different ratios between the hydroxyl and non-hydroxyl groups on solubility, reactivity, and interaction with boronic acid of the PVA-MA. PVA was selected with a low molecular weight because it was proven to be an effective

reactive species for vat photopolymerization because it acts as a macromer without increasing the viscosity of the formulation. [235] Furthermore, there is higher mobility compared to a PVA with the same percentage of functionalization, and this would enable a higher degree of conversion. We initially tried to perform PVA functionalization using water as a medium to facilitate solvent removal. Two different procedures were followed, one using methacrylic anhydride and another using glycidyl methacrylate, both of which required adjustment of pH prior to the addition of the functionalizing agent. [235,391] Unfortunately, we were unable to obtain any reaction following these two water-based pathways, while the methacrylation carried out using DMSO as a solvent and catalyst (Fig. 7.2a) resulted in an effective outcome. PVA-MA from PVA 88% DH appeared to be a pale yellow powder with large flakes, while PVA-MA from PVA 98% DH appeared to be a white powder with smaller flakes (Fig. 7.2b). An indirect proof of an actual modification was given by the solubility of PVA-MA after the reaction, because while pristine PVA requires heating to be effectively dissolved in water, both PVA-MA 88% DH and 98% DH were rapidly soluble in water at room temperature under stirring with no heating required. NMR spectra confirmed the effective functionalization of the polymers, with an average methacrylation degree of 5% for PVA-MA 88% DH and an average methacrylation degree of 17% for PVA-MA 98% DH, calculated from the ratio of the relative integrations of the vinyl protons peak at 5.6 ppm with respect to the methyl protons peak of at 2.0 ppm (Fig. 7.2c). These results confirmed the rapid and comparable dissolution of the two different powders, which could be explained by the similar percentage of residual groups, around 82%, which do not interact as extensively as prior functionalization, with the methacrylate groups acting as spacers, facilitating the intercalation of water molecules. Interestingly, the higher number of reactive pendant groups on PVA-MA 98% DH did not determine a higher reactivity compared to PVA-MA 88% DH (Fig. 7.2d).

The difference in behavior is further confirmed by the difference in kinetics after the addition of the methacrylated boronated azobenzene derivative dye, which suggests an effect of the residual acetate groups on the PVA that lowers the degree of hydrogen bonding, reduces stereoregularity, and decreases the degree of crystallinity intercalating the methacrylated groups. [334] The azo phenylboronic acid methacrylate (APAM) dye used in this system was designed to have a structure similar to commercial methacrylate disperse red 1 with boronic acid in ortho position on benzene bearing the nitric group in order to activate it by removing the steric hindrance when the dye switches from the stable trans position to the metastable cis position after light irradiation. The synthesis of the

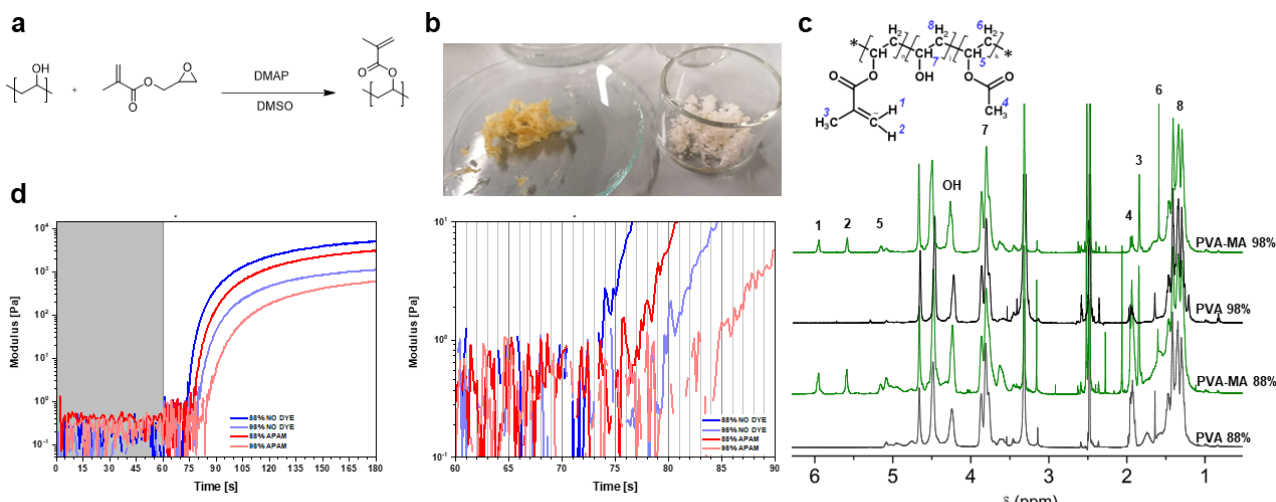


Figure 7.2 Poly(vinyl alcohol) methacrylation. a) Methacrylation reaction for PVA. b) Methacrylated PVA powder after drying, 88% hydrolysis degree (left) and 98% hydrolysis degree (right), and c) resulting NMR spectra. d) Preliminary photorheology tests to assess the effect of the dye on the photopolymerization kinetics.

functional dye is out of the scope of this thesis, but a brief description is provided here. A dispersed red 1 derivative was synthesized with a halogen in the ortho position, which enabled further functionalization through borylation using boric acid pinacol ester, which acted as a temporary protective capping agent during methacrylation of the only available hydroxyl group via acryloyl chloride, after which it was removed (Fig. 7.3a). We compared the behavior of the synthesized APAM dye with its commercial analogues (Fig. 7.3b): Disperse Red 1 (DR1) to study simple absorption without any interaction between the network and the dye; Disperse Red 1 methacrylate (DR1-MA) to use a dye with a similar absorption spectrum that is incorporated within the network, but does not interact with it; 1,4-phenyldiboronic acid (PDBA) to study the behavior of a small molecule capable of acting as a cross-linking agent via dynamic covalent bonds. We recorded the UV-Vis absorption spectra in acetonitrile of the three dyes, all of which are push-pull azodye and therefore have the cis and trans absorption bands overlapped due to resonance, but the absorption spectra for DR1 and APAM are both centered on 480 nm, while the DR1-MA has the absorption band centered around 470 nm (Fig. 7.3.c). The presence of boronic acid does not affect the absorption spectrum; it moves it back towards the absorption spectrum of the unmodified Disperse Red 1, balancing the effect of the presence of the methacrylated group. Despite the push-pull nature of the synthesized dyes, it is possible to assume that an irradiation of a light with a wavelength around 430-440nm (blue light) would favor the formation of a majority of Cis (Z) isomers and therefore enable the

formation of the ester bond, which would also stabilize the dye and prevent the continuous switching, while a green light, with a wavelength 520-530 nm (green light) would cause the disruption of the ester bond by promoting the trans (E) isomer.

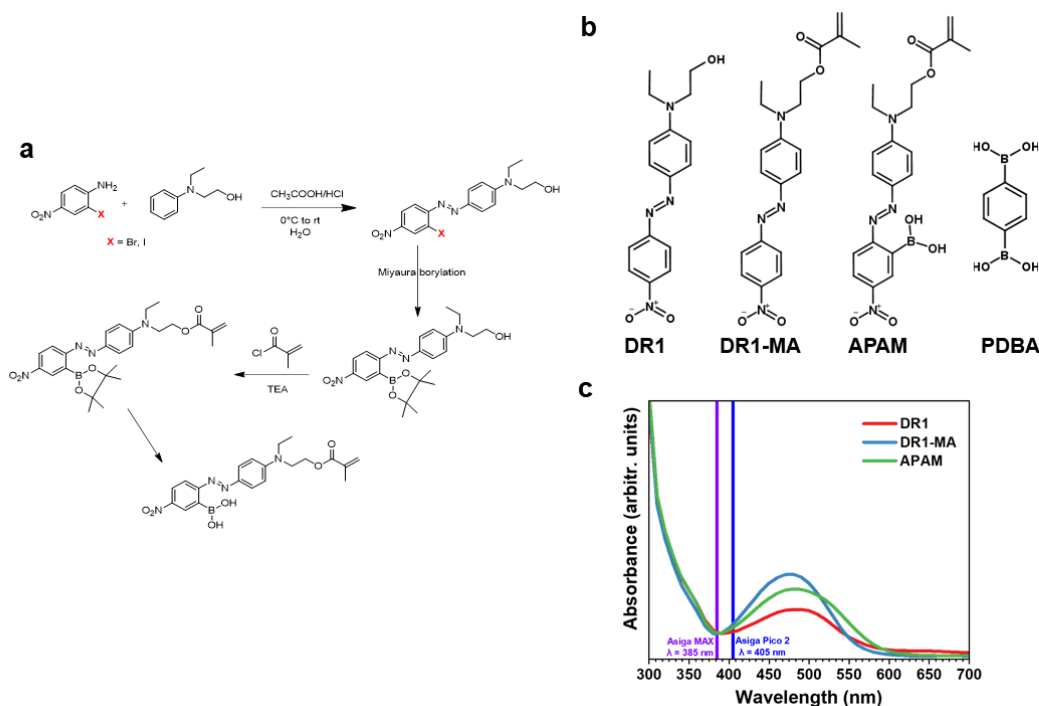


Figure 7.3 Functional dye synthesis and comparison. a) Reaction path for the synthesis of the azobenzene phenylboronic acid methacrylate (APAM) dye and b) comparison of the structure with the other commercial dyes and additives used. c) UV-Vis absorption spectra of the various dyes compared with the printers light source emission wavelength.

The dyes under evaluation are all non water-soluble, so an organic solvent compatible with water was required to dissolve the dyes in the aqueous formulations without causing precipitation of PVA-MA, and this immediately ruled out common solvents such as acetone and ethanol, well-known nonsolvents for PVA. The dyes proved to be highly soluble in organic solvents, so we performed solubility tests of PVA in various water-organic solvent binary mixtures, and the only two suitable candidates capable of dissolving both the dye and PVA-MA and compatible with water were DMSO and PC. In any tested formulation, we used a dye/monomer weigh ratio of 1%, an average dye/PVA repeating unit monomer molar ratio of 0.125% and an average dye, dihydroxyl molar ratio of 0.31%, and all dyes were previously dissolved in organic solvent

and then added to the aqueous formulation. We performed photorheology testing for each dye various combinations between one of the two solvents and one of the two different PVA-MA, either 88% DH or 98% DH, using water-soluble TPO nanoparticles as photoinitiator, to evaluate the effects of the solvents on the kinetics and potential combined effects with the dye and the degree of hydrolysis (Fig. 7.4). We also tested the combinations of solvent/polyvinyl alcohol with different hydrolysis degrees with no dye and the simple PVA-MA aqueous solution as a reference. It can be seen, as shown before, that PVA-MA 88% DH has a kinetics faster than PVA-MA 98% DH, even though the number of methacrylated groups is lower; this behavior is confirmed independently of the solvent and dye used. The combination between PC and PVA-MA 88% DH is the one that provides the fastest kinetic independently of the dye used, followed by PVA-MA 88% DH DMSO, then PVA-MA 98% DH PC and eventually PVA-MA 98% DH DMSO, with a prominent variability in the curves for the formulations containing DR1, which only has a competitive effect with the absorption of the photoinitiator and did not contribute to the formation of the network, unlike methacrylated dyes or PDBA. Therefore, the results show that DMSO induces reduced kinetics, and the final modulus achieved by the hydrogel is lower than that achieved in the systems with PC. This effect adds up to the absorption effect induced by the dye, which reduces the kinetics of photopolymerization as well.

When comparing the effect of various dyes on the same combination of organic solvent and hydrolysis degree, it was noted that the presence of DMSO does not suppress the reactivity of the system compared to those without the organic solvent, although it is a well-known radical scavenger (Fig. 7.5). This can be attributed to the better compatibilization and aggregation of the hydrophilic segments into aggregates that favor an effective reactivity. This effect is even more visible with PC, whose presence anticipates the reaction kinetics, especially for PVA-MA 98% DH, because it likely favors the separation between hydroxyl groups and methacrylates. The presence of APAM has an additional slowing effect, likely due to its additional cross-linking effect combined with its light absorption that slows down the reaction by decreasing the effective absorption of the photoinitiator. As expected, PBDA behaves as an additional crosslinker to PVA without absorbing incident light, just like boric acid, producing a stiffer crosslinked network, as proven by the anticipation of the G curve, that reaches the plateau earlier than the samples containing the dyes. DMSO reduces the kinetics and the final modulus achieved by the hydrogel compared to the systems with PC, and this trend can be seen independently from the dye used, which already induced a decrease in the photopolymerization kinetics. Given all the previous

considerations, PC seems to be the solvent most suitable, since it shows a positive impact on kinetics. Unfortunately, the dyes in solutions with PC showed the tendency to precipitate if stored for some time. Therefore, DMSO was used as an organic solvent to dissolve the dye and guarantee its stability in the aqueous formulation.

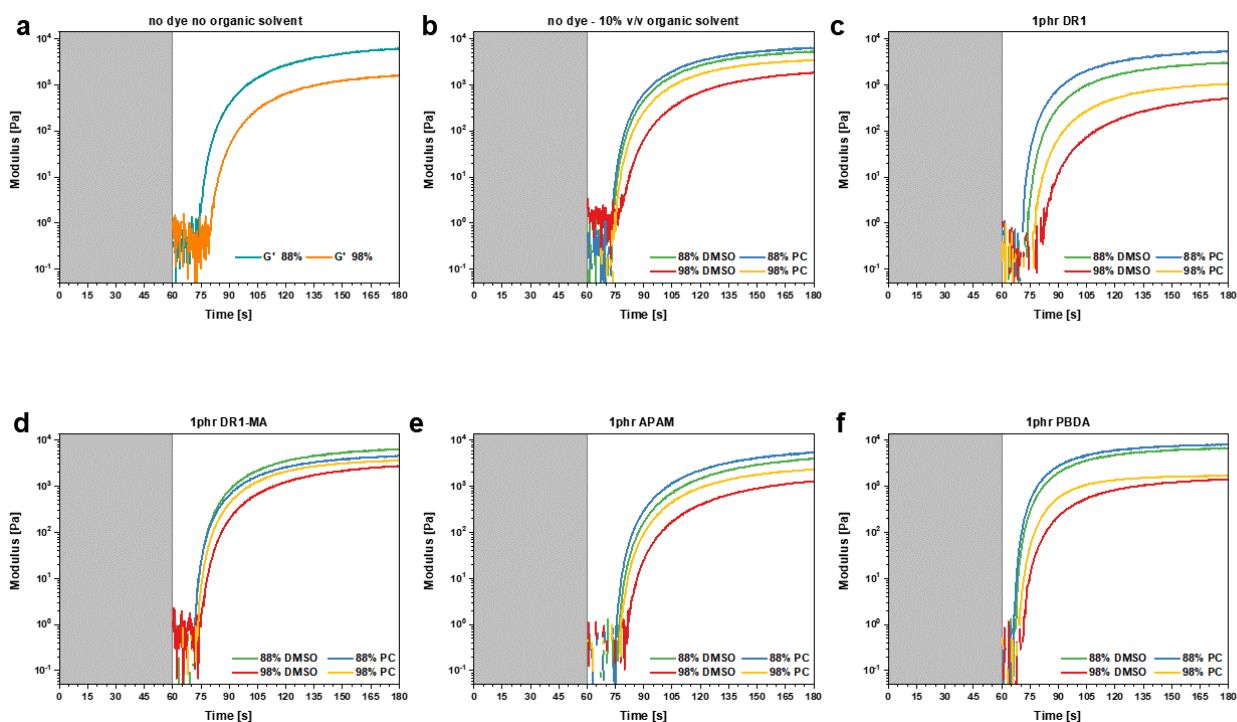


Figure 7.4 Hydrolysis degree and organic solvent comparison. Photorheology tests carried out to evaluate the effect of hydrolysis degree and organic solvent depending on the dye used: a) no dye and no organic solvent, b) no dye, c) Disperse Red 1 (DR1), d) Disperse Red 1 methacrylate (DR1-MA), e) Azobenzene phenylboronic acid methacrylate (APAM), f) 1,4 - Phenyl diboronic acid (PBDA).

To further explore the effect of the dyes in the formulation, we performed tests on printed samples to evaluate the variation of the mechanical properties, because of the formation of the boronate ester bonds. For these tests, cylindrical specimens were 3D printed and tested. Unfortunately, it was not possible to accurately print cylinders with the PBDA-containing formulation, due to uncontrolled polymerization, even trying to use DR1 as a dye. Therefore, the tests were carried out only on samples printed with the azoderivative dyes and without any dye.

The compression tests (Fig. 7.6b) showed a large variability of the results, not matching the results of the photorheology tests in terms of the final shear elastic

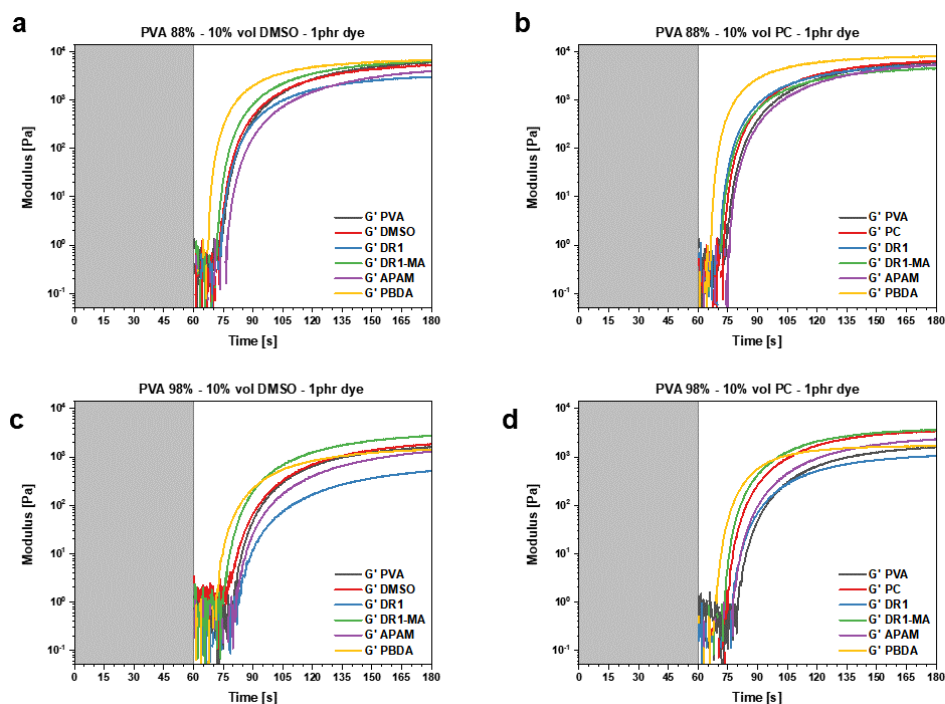


Figure 7.5 Dye effect on the polymerization kinetic. Photorheology tests carried out to evaluate the effect of hydrolysis degree and organic solvent depending on the hydrolysis degree and the organic solvent used a) 88% DH and DMSO, b) 88% DH and PC, c) 98% DH and DMSO, d) 98% DH and PC.

modulus. This can be due to the less controlled testing environment, since it was not possible to confine the cylinders during compression, which could have led to incorrect alignment of the samples with the upper plate. The samples printed without dye showed the lowest resistance, and PVA-MA 88% DH exhibited a higher compression resistance than the samples printed with PVA-MA 98% DH, with the formulations containing methacrylated dyes characterized by a slightly higher maximum compression stress before failure, regrettably no relevant differences between DR1-MA and APAM were revealed. Instead, swelling tests in DMSO of dried printed samples (Fig. 7.5c) showed differences among formulations: samples containing APAM present slightly reduced swelling compared to samples containing the other dyes that are not embedded within the network, even if within the error range. The samples without dye showed the largest swelling. This can be related to the additional limited cross-linking effect introduced by the APAM in the cis isomer, which was likely to be predominantly isomerized in the cis form by the light at 405nm of the printer. The two PVA-MA exhibited comparable swelling despite the results obtained in the compression tests, backing the hypothesis that the differences in the functionalization starting

material influence the final mechanical properties and the reaction kinetic, while the presence of the APAM dye has a partial effect on the overall network crosslinking, limited by the very low concentration of the dye.

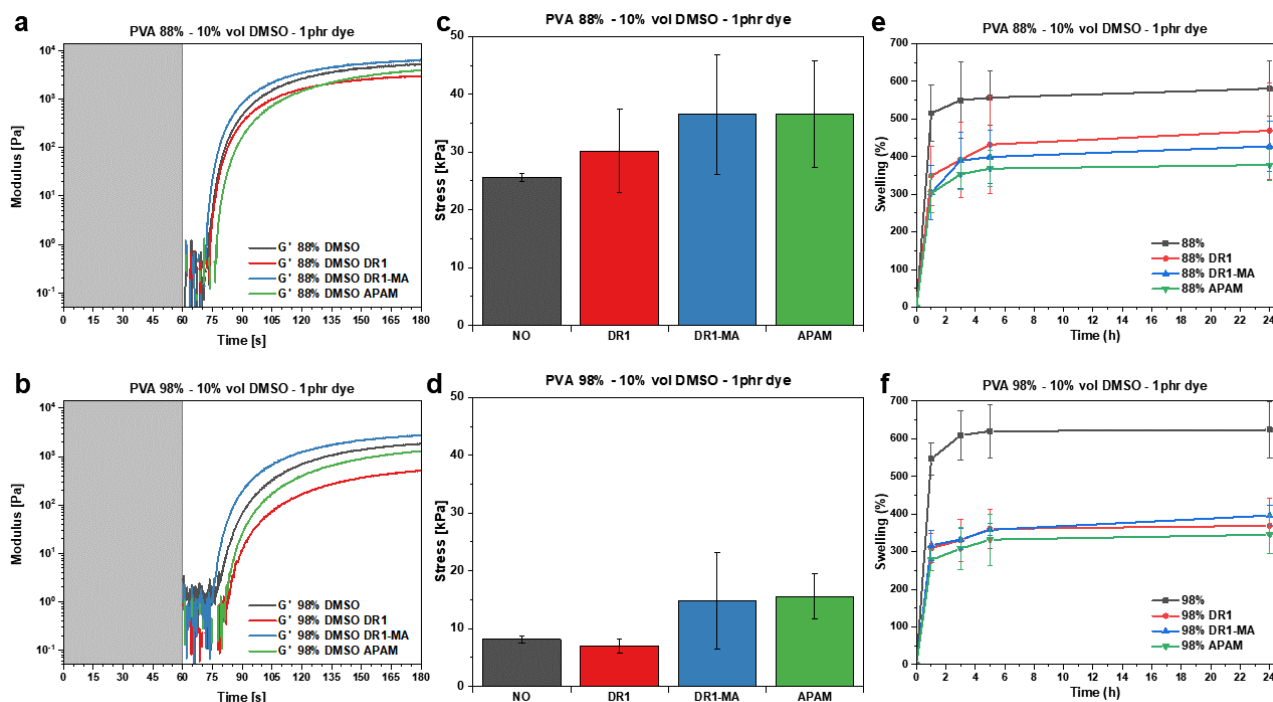


Figure 7.6 Dye effect on various properties. Comparison of the effects of the absence or presence of various dyes on a-b) Photorheology tests for reaction kinetics, c-d) compression tests for mechanical properties, e-f) swelling tests in MDSO for crosslinking density.

Before printing complex structures, we tested different photoinitiators with both visible and UV light sources, to assess their efficiency and versatility with the two light sources (Fig. 7.7a and b). These tests were carried out because we wanted to assess the behavior of the formulation in response to two different wavelengths given the availability of two DLP printers with 365 nm and 405 nm light sources. The longer wavelength would induce as little as possible E to Z isomerization, and therefore the samples would have limited additional crosslinking and would enable the effective activation of the dye. The photorheology showed that Ru/SPS system, already proven to be effective in DLP printing of PVA-MA, is particularly efficient with visible light (Fig. 7.7a), given its absorption peak at 532 nm, but not sufficiently efficient with UV light, showing also a tendency to precipitate during storage. I2959 was particularly efficient with UV light irradiation, but does not show absorption in the visible light range (Fig.

7.7b). PEG-BAPO showed for both visible and UV light sources, but it is not a commercial photoinitiator, and therefore we decided to use the TPO water-soluble nanoparticles, which showed suitable reactivity in tests with both light sources and both PVA-MA with different hydrolysis degrees. Given all the considerations mentioned above, for complex 3D printing we decided to use DMSO as the organic solvent and PVA-MA obtained from PVA 88% as the main components for the printing resins, in which the dye used was APAM and the photoinitiator was TPO in the form of water-soluble nanoparticles. We performed some printing tests of a benchmark cad file using both printers and we found that the object printed with the Asiga Pico 2 equipped with the 405 nm light source showed well controllable polymerization along the xy plane using the highest light intensity available, to shorten as much as possible the layer irradiation time (Fig. 7.7c). On the other hand, the same benchmark printed with the Asiga MAX, equipped with the 385 nm light source, showed uncontrolled polymerization when using a high light intensity and short irradiation time, while reducing the light intensity and keeping a constant light dose by prolonging the irradiation time produced an incomplete object (fig. 7.7d). We also tried to change the light dose, but no relevant differences were observed. This issue could be related to the combination between the low reactivity of the macromers and the incompatibility of the absorption spectra of the dye with the wavelength of the UV light source, and therefore we decided to print the following samples with the Asiga Pico 2.

We have been able to print simple shapes with flat surfaces and sharp edges with good resolution along the xy plane (Fig. 7.8a). The smallest feature we could print was a wall of around 1 mm thick with a limited size ratio (Fig.7.8b). The printed vertical walls were very sharp and precise, but we encountered problems in achieving an object taller than 3 mm, and this could be attributed to the low resistance of the hydrogel to bearing its weight, which resulted in a failure of the upper layers caused by delamination. We were also able to fabricate vertical holes (Fig. 7.8c) but there was some undesired polymerization in the initial layers, not visible in other samples because of the use of a full base. At the moment, we were unable to achieve overhanging features, possibly because of the limitation in strength hypothesized earlier, even though a similar formulation with an analogue macromer had been proven to be able to bear overhanging elements, and therefore, further study in the printing parameters is necessary. [235]

Eventually, we tried to define a self-healing procedure for printed samples, but despite the various methods tested, no SH was detected, even though a boronate ester hydrogel was proven to self-heal under light irradiation. [375] In

the system used for inspiration, the ester bond was the only linkage responsible for the formation of the network, and therefore its formation was clearly visible. Our system comprised an irreversible covalent network that contributed for the larger part to the mechanical properties, while the additional crosslinking effect ascribable to the dye was limited because of its concentration, which was the maximum allowed to achieve effective printing, but it was still too low to have a clear and relevant effect. We tried several approaches, like irradiating the cut interface with a fiber optics UV light centered at 365 nm and a broad range white (Hamamatsu LC8) to induce the isomerization, even though the dye is a push-pull dye, while keeping the rejoined pieces confined in a mold, or we tried to heat up the samples in a closed sealed container to prevent water evaporation and thermally induce the E-Z transition, but every tryout was unsuccessful.

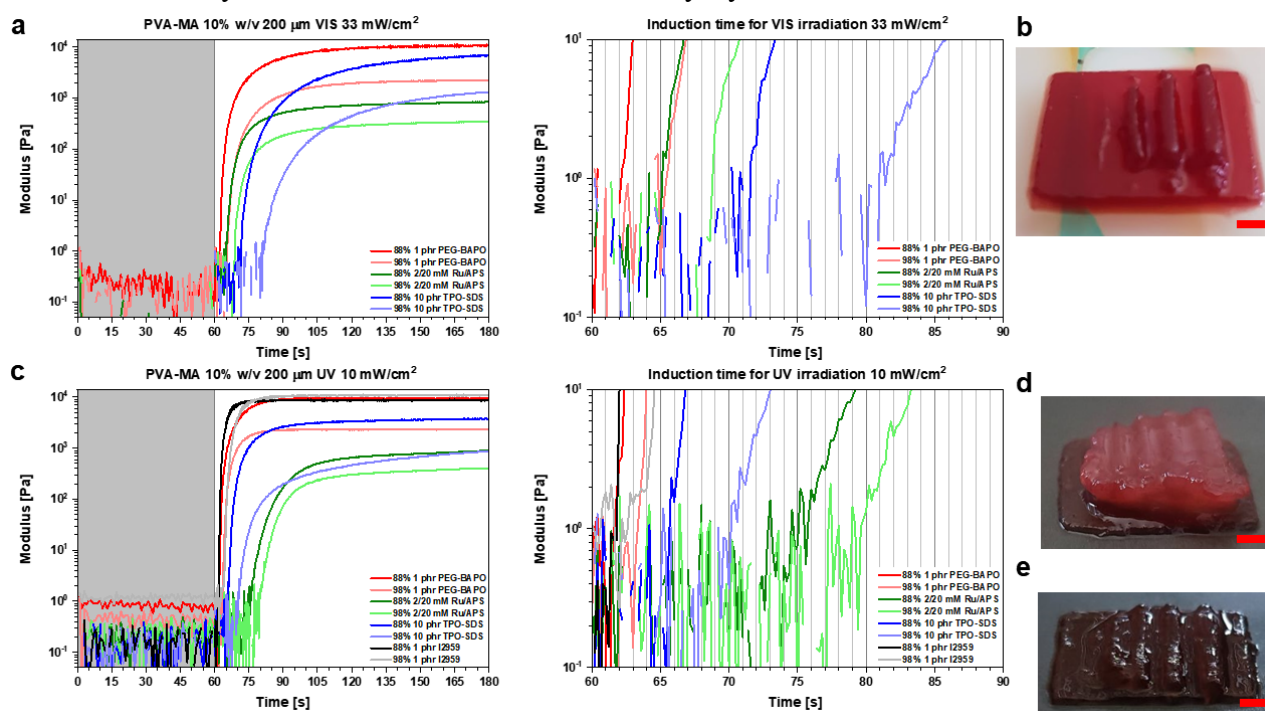


Figure 7.7 Preliminary tests for 3D printing. a) Visible-light photorheology tests carried out on the PVA 88% DMSO APAM 1phr formulation to evaluate the effect of various photoinitiators and b) resulting 3D printed benchmark (printed at 40 mW/cm², Irradiation time 25s). c) UV-light photorheology tests carried out on the PVA 88% DMSO APAM 1phr formulation to evaluate the effect of various photoinitiators and d-e) resulting 3D printed benchmarks (d printed at 45 mW/cm², Irradiation time 5s; e printed at 20 mW/cm², Irradiation time 12s). (Scale bar 20 mm)

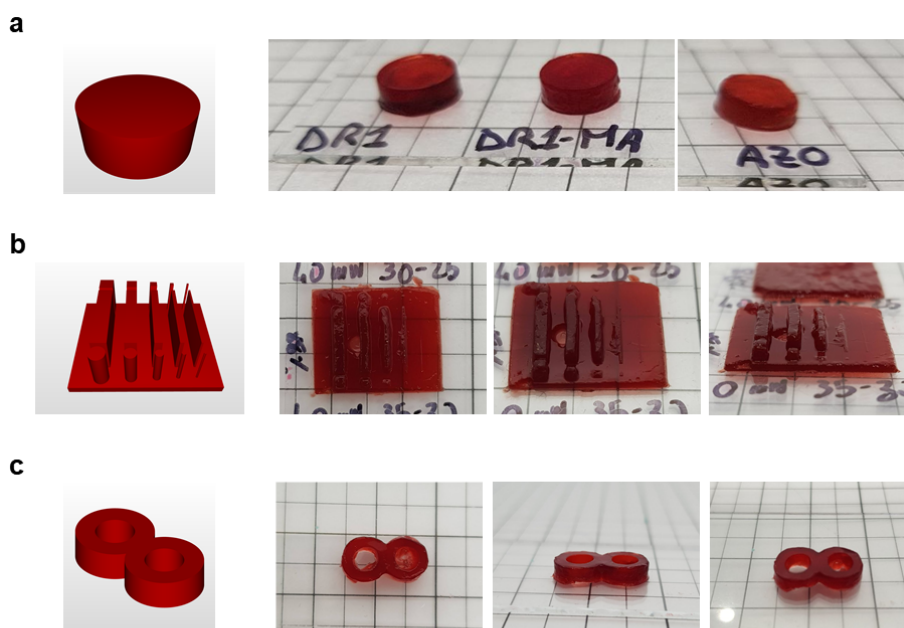


Figure 7.8 3D printing of simple geometries. CAD files and resulting printed samples of a) full cylinder, b) benchmark c) “eight” figure. (scale 10 mm)

1.4 Conclusions and perspectives

In summary, our goal was to demonstrate the feasibility of using a light-activated dynamic covalent chemistry to achieve self-healing in DLP printed hydrogels.

We functionalized PVA with two different degrees of hydrolyzation and tested the effect of this difference on the polymerization kinetics and final mechanical properties of the hydrogel. The result was that a higher concentration of residual acetate groups favors the reaction kinetics and provides higher mechanical properties, despite the lower degree of methacrylation obtained due to a lower availability in reactive hydroxyl groups. Afterwards, we tested the effect of a methacrylated azobenzene dye functionalized with a boronic acid to be used as a photoswitchable crosslinker on the polymerization kinetic of PVA-MA and the final mechanical properties of the hydrogel and compared it to similar commercial dyes with the same absorption spectra but not capable of establishing additional crosslinking within the network. We demonstrated that the boronated dye does not affect the polymerization kinetics excessively and, at the same time, has some positive, yet limited, effect on the final mechanical properties of the hydrogel in terms of compression strength and swelling. The boronate-ester bond is highly effective when there are no irreversible covalent bonds competing with the dynamic covalent bonds established between the boronic acid and the diol, given the difference in the binding energy. [392] Furthermore, a low

concentration of the dye has a limited or negligible effect on the overall mechanical properties, but a higher concentration would have troubled or hindered an effective printing. We were able to print simple shapes with sharp edges, but a limited size ratio because of the poor mechanical strength of the hydrogel, limited by the low cross-linking and the large amount of solvent embedded. Unfortunately, we have not yet been able to define an effective procedure to assess the potential self-healing efficiency. This was due to unforeseen circumstances, to which the crisis in the supply chain caused by the pandemic contributed, which prevented us from being able to receive in time by the supplier the specific LED light sources with the narrow light wavelength range emission required to induce a controlled isomerization of the photoswitchable molecule. We tried to use broad-range white light to test potential self-healing, but the push-pull nature of the dye likely prevented a controlled trans-cis isomerization because the system did not reveal any interaction. This could also be attributed to some other aspects of the system, such as the restricted mobility of the azobenzene owing to the short chain, which could have suffered from the steric hindrance of the connected polymer backbone.

A potential modification to the system could be the introduction of a longer hydrophilic chain, such as a PEG, [287] for better motion and enhanced water solubility, which are currently lacking. The versatility of the system would enable testing other light-induced properties which were out of the scope of the initial assessment of the system and were planned for further studies, such as light-triggered shape memory, to be potentially combined with light-induced self-healing if proven, as well as photostiffening or light-induced motion. [393]

General conclusions

In summary, the goal of this thesis work was to demonstrate the feasibility of 3D printing of hydrogels with self-healing properties via vat photopolymerization. The processing here proposed could potentially enable fast adaptation to larger scales or for specific applications since we employed a widely available DLP apparatus and the proposed water-based resins are composed of commercially available materials. During the investigation here carried out, we overcame the inherent incompatibility between vat photopolymerization and self-repairing properties by merging the characteristics of the VP printing process with self-healing properties by exploiting different strategies.

The first system investigated relies on an interpenetrated network (IPN) design. This is a convenient strategy to gather 3D shaping (printability) and autonomous restoration, since it allows to integrate a rigid and robust frame (chemical bonds, generally non-reversible) with a much weaker one (physical bonds, mostly reversible). Such approach is applicable to a large variety of stable/labile bonds combinations and results in a homogeneous system that preserves the two contributions separately. A semi-IPN is presented in the first work based on a covalent network of acrylic acid and poly (ethylene glycol) diacrylate containing uncross-linked Poly (vinyl alcohol), used as healing agent by exploiting its capability of establishing hydrogen bonding. The main issue with the system was the surface drying of the resin caused by water evaporation that interfered with the printing process. To overcome this issue, we modified the printer to maintain a constant humidity by fluxing aerosol in the vat. The resolution and the finest feature achievable in the printed objects were strongly dependent on dye concentration and PVA concentration, but we were able to precisely print self-supporting and geometrically complex architectures, with overhanging and hollow features. Efficient self-healing of printed samples occurred rapidly at room temperature without requiring any external stimuli, resulting in a 72% recovery of their initial tensile strength, with repeatable partial restoration when stored in a humid environment.

The possibility to exploit a decrease in temperature to trigger self-healing was explored in the second study presented, in which the healing mechanism was based on entangled Pluronic micelles capable of establishing electrostatic

interactions. The amphiphilic triblock copolymer was embedded in a covalent network made of methacrylated PEG-derivatives that could have a plasticization effect by intercalating the hydrophilic corona of the micelles. Among the tested monomers, poly (ethylene glycol) methacrylate (PEGMA) was the only one which did not suppress the Pluronic reversible micellization but decreased the gelation temperature and introduced an additional contribution to the final elastic modulus of the system. Furthermore, PEGMA has a polymerization kinetics compatible with vat photopolymerization, but the resin had to be kept below its gelation temperature to stay in the sol phase. To this end, the printing had to be performed in a cold environment, resulting in the fabrication of objects with simple geometries and poor mechanical properties.

Another commonly used stimulus is light, which was explored in the third and last part of the experimental section as trigger for light-activated self-healing based on dynamic covalent chemistry. We used a methacrylated azobenzene-derivative dye bearing a boronic acid functional group as photoswitchable crosslinker aimed to establish an ester bond with diols on the methacrylated PVA constituting the covalent network. The hydrolyzation degree of the PVA had a strong influence on the final properties of the system, with higher concentration of residual acetate groups favors the reaction kinetics and provides higher mechanical properties, despite the lower degree of methacrylation. The customized dye showed modest positive effects on the final mechanical properties of the hydrogels, mainly limited by the low concentrations admitted for an effective printing. Samples with sharp edges but simple shapes and limited size ratio were fabricated, hampered by the poor mechanical strength due to the low crosslinking density.

Unfortunately, it was not possible to define an effective self-healing procedure for the last two studies, despite the examples of applications of the selected mechanisms in self-healing hydrogels. Our approach to the investigation was to provide printability to systems known to perform self-healing, but two possible routes can be followed to accomplish the goal: testing first healability and then printability or evaluating the 3D printing followed by the self-healing assessment. The first route addresses the more stringent condition, but initially relies on qualitative tests such as visual confirmation, since rheological measurements does not accurately describe the actual macroscopic healing behavior of solid bulk components. This was the approach used in the first study presented, which required long time to be completed. For the following studies, we followed the second direction, that provides more quantitative data but

depends on the assumption of the “potential” self-healing ability of the system. To back the assumption, we performed SH tests in parallel to printability by producing the samples in molds, but both systems had constraints for this kind of procedure. Thermal gelation and limited light penetration hindered the fabrication of samples sufficiently thick for handling and therefore perform cut and rejoining tests to assess self-healing. As a conclusion, in the following tables, a final general comparison among the three proposed systems and with two relevant examples from literature reporting DLP-printed self-healing hydrogels is presented. The assessment presents the healing systems and the efficiency in restoration, as well as the composition of the printable resin and the geometrical characteristics of the printed objects. It must be noted that Ref. [252] has been published after our first publication and cites our work among the references, while the system Ref. [255] is not autonomous but requires immersion in a Fe^{3+} salt-rich solution prior restoration. To the best of the author’s knowledge, at the moment of the drafting of this thesis, there are no other comparable systems, and the state-of-the-art works reported in chapter 3 do not employ hydrogels or water-based resins. As can be deduced by the results, the combination between hydrogels, printability and healability in one system requires to reach a compromise between the performance of the single characteristics. Each property acts as a variable and at the same time as a constraint with opposite and sometime contradictory requirements, compelling to reach a challenging balance.

WORK	HEALING MECHANISM	HEALING AGENT	TRIGGER	HEALING CONDITIONS
Chapter 6	Hydrogen bonding	PVA 89-98k	None	Room Temperature, sealed vessel
Chapter 7	Micelles entanglement	Pluronic F-127	Temperature	Cold Temperature
Chapter 8	Boronate-ester complexation	DR1-MA Boronic acid	Light	Room Temperature, monochromatic light
Ref. [252]	Metal-ligand coordination	AAc, Zn ²⁺ ions	None	Room Temperature
Ref. [255]	Metal-ligand coordination	PAAc, Fe ³⁺ ions	Ionic insertion	Immersion in the salt solution
WORK	HEALING EFFICIENCY	HEALING TIME	HEALING ASSESSMENT	CYCLIC RESTORATION
Chapter 6	72%	12h	Uniaxial tensile test	Yes, 5 cycles
Chapter 7	—	—	—	—
Chapter 8	—	—	—	—
Ref. [252]	81-91%	24h	Uniaxial tensile test	Unknown
Ref. [255]	85%	1h	Three-point flexural test	Unknown
WORK	MONOMER(S)	PHOTOINITIATOR	PHOTOABSORBER(S)	PRINTING CONDITIONS
Chapter 6	AAc, PEGDA 700	TPO-SDS	Methyl Red, Brilliant Green	Aerosol flux
Chapter 7	PEGMA 500, PEGDA 700	PEG-BAPO	Brilliant Green	Printer @ 5°C
Chapter 8	PVA-MA 13-23k	TPO-SDS	DR1-MA Boronic acid	Ambient conditions
Ref. [252]	AAc, NVP	TPO	None	Unknown
Ref. [255]	PEGDA 700	Irgacure 2959	None	Formulation added for each layer
WORK	ASPECT RATIO	DIMENSIONAL COMPLEXITY	HOLLOWNESS / THROUGH-HOLES	OVERHANGS / UNDERCUTS
Chapter 6	medium (width ≈ height)	3D	Yes / Yes	Yes / Yes
Chapter 7	low (width > height)	2D	No / No	No / No
Chapter 8	low (width > height)	2.5D	No / No	No / No
Ref. [252]	high (height > width)	3D	No / Yes	Yes / Yes
Ref. [255]	medium (width ≈ height)	2.5D	No / No	No / No

Figure 8.1 Results summary. Comparison of the results achieved in the works presented in the thesis in terms of healability and printability compared with relevant results in the literature.

Appendix

A1 List of abbreviations

3DP	Three-dimensional printing
AAc	Acrylic Acid
AAm	Acrylamide
ACMO	N-acryloylmorpholine
AFM	Atomic force microscopy
AM	Additive Manufacturing
APAM	2-(Ethyl(4-((4-nitrophenyl)diazenyl)phenylboronic acid)amino)ethyl methacrylate
APS	Ammonium Persulphate
ASTM	American Society for Testing and Materials
ATR	Attenuated Total Reflection
Az	Azobenzene
BAPO	Bis(2,4,6-trimethylbenzoyl)phenylphosphine oxide
BA	Butyl acrylate
BERs	Bond exchange reactions
BG	Brilliant Green
BMA	Benzyl methacrylate
BP	Benzophenone
CAD	Computer-aided Design
CAM	Computer Aided Manufacturing
Cas	Calixarenes
CBs	Cucurbiturils
CDs	Cyclodextrins
CLIP	Continuous liquid interface production

CMC	Critical Micelle Concentration
CMC	Carboxymethylcellulose
CMT	Critical Micelle Temperature
CNT	Carbon Nanotubes
CQ	Camphorquinone
DA	Diels-Alder
DAT	2,6-Diamino triazine
DBTDL	Ditin butyl dilaurate
DCC	Dynamic Covalent Chemistry
DGDA	1,3-Diglycerolate diacrylate
DH	Degree of hydrolysis
DLP	Digital Light Processing
DMAP	4-(Dimethylamino)pyridine
DMD	Digital micromirroring device
DMSO	Dimethylsulphoxide
DPEA	N,N'-diisopropylethylenediamine
DR1	Disperse Red 1
DR1-MA	Disperse Red 1 methacrylate
EDTA	Ethylenediamine tetraacetic acid
Fc	Ferrocene
FdMA	Pluronic F127 dimethacrylate
FRESH	Freeform reversible embedding of suspended hydrogel
FT-IR	Fourier Transform Infrared Spectroscopy
G'	Storage shear modulus
G''	Loss shear modulus
GMA	Glycidyl methacrylate
GO	Graphene oxide
IBO	Isobornyl acrylate
IEMA	2-Isocyanatoethyl acrylate
IPDI	Isophorone diisocyanate

IPN	Interpenetrated Network
Irgacure 1173	2-Hydroxy-2-methyl-1-phenyl-propan-1-one
Irgacure 2959	2-Hydroxy-4'-(2-hydroxyethoxy)-2-methylpropiophenone
Irgacure 651	2,2-Dimethoxy-2-phenylacetophenone
ITX	Isopropyltioanthone
LAP	Lithium phenyl-2,4,6-trimethylbenzoylphosphinate
LCST	Lower critical solution temperature
MMA	Methyl acrylate
MMDS	Mercaptopropyl)methylsiloxane-dimethylsiloxane
MR	Methyl Red
MS	Mercaptosiloxane
NVP	1-Vinyl-2-pyrrolidinone
PAAc	Poly (acrylic acid)
PBA	Phenylboronic acid
PBS	Phosphate buffered saline
PC	Propylene carbonate
PCL	Poly (caprolactone)
PCLDMA	Poly (caprolactone) dimethacrylate
PDBA	Phenyl diboronic acid
PDMS	Poly (dimethyl siloxane)
PEA	2-Phenoxyethyl acrylate
PEG	Poly (ethylene glycol)
PEGDA	Poly (ethylene glycol) diacrylate
PEGMA	Poly (ethylene glycol) methacrylate
PEGMA	Poly (ethylene glycol) dimethacrylate
PEGMEMA	Poly (ethylene glycol) methyl ether methacrylate
PEO	Poly (ethylene oxide)
Ph	Phenolphthalein
PI	Photoinitiator
PMMA	Poly (methyl methacrylate)

PMP	Poly-4-methylpentene
PPO	Poly (propylene oxide)
PS	Poly (styrene)
PTMEG	Polytetramethylene ether glycol
PU	Poly (urethane)
PVA	Poly (vinyl alcohol)
PVAc	Poly (vinyl acetate)
PVA-MA	Poly (vinyl alcohol) methacrylate
rDA	Retro Diels-Alder
RT	Room Temperature
RTG	Reverse thermal gelation
SA	Suberic acid
SDS	Sodium dodecyl sulphate
SEM	Scanning electron microscopy
SH	Self-Healing
SHE	Self-healing elastomer
SLA	Stereolithography
SMASH	Shape memory assisted self-healing
STL	Standard Triangle Language
THFA	Tetrahydrofurfuryl acrylate
Tg	Glass Transition Temperature
TPO	Diphenyl(2,4,6-trimethylbenzoyl)phosphine oxide
TTMP	Trimethylolpropane tri(3-mercaptopropionate)
UMA	Urethane monoacrylate
UPy	Ureidopyrimidinone
UPyMA	2-Ureido-4[1H]-pyrimidinone methacrylate
UV-Vis	Ultraviolet - Visible Light
VP	Vat Photopolymerization
VS	Vinylsiloxane
ZDMA	Zinc dimethacrylate

A2 List of figures

Figure 1.1 Self-healing materials and classification. a) Comparison of a visual restoration experiment between a non-self-healing material and a self-healing material. c) Schematic illustration of the self-healing materials classes. Adapted and reproduced with permission from [18,70]2

Figure 1.2 Intrinsic self-healing mechanisms. Illustration of some different non-covalent interactions (left) and dynamic covalent bonds (right) employed in self-healing materials to achieve restoration. Reproduced with permission from [25].....4

Figure 1.3 Dynamic covalent chemistries. General and dynamic reversible covalent reaction pathways. Adapted with permission from [27]5

Figure 1.4 Non-covalent interactions. Examples of strategies for the synthesis of noncovalently crosslinked hydrogels with self-healing capability. Adapted with permission from <https://doi.org/10.1002/admi.201800118>..... 11

Figure 2.1 Vat photopolymerization technologies comparison. a) Planar resolution comparison between SLA and DLP. b) Different configurations of platform movement along the z axis and relative position between light source and vat. Adapted and reproduced with permission from [160,171]25

Figure 2.2 Classification of light-based 3D printing modalities. a) Primary configuration involving dot-by-dot or line-by-line deposition. b) Secondary configuration involving planar 2D patterning. c) Tertiary configuration involving volumetric 3D patterning. d) Schematic representation of the three main vat photopolymerization technologies. Reproduced with permission from [160,165]29

Figure 2.3 Photopolymerization mechanisms. Photopolymerization mechanisms. Schematic representation of a) chain-growth and b) example of reactions for various classes of reactive species. Schematic representation of c) step-growth polymerization mechanisms and d) example of reactions for various classes of reactive species. Reproduced with permission from [160]32

Figure 2.4 Photoinitiators absorption. Chemical structures and maximum absorption wavelength of some photoinitiators employed in 3D photopolymerization. Some of these PI have multiple absorption peaks.34

Figure 2.5 Dyes absorptions. UV-Vis absorption spectra of organic dyes and biocompatible photoabsorbers commonly used in vat photopolymerization. Adapted with permission from [166,238].....36

Figure 3.1 Additive manufacturing of self-healing elastomers. a) Molecular design of the self-healing elastomer based on dynamic disulfide bonds among thiol-disulfide oligomer formed by thiol-ene reaction. b) Various manufactured 3D samples: logo of the University of Southern California, a circular cone, a pyramid lattice unit, a cup, and an octet truss lattice. c) Self-healing of a shoe pad-shaped sample. (scale bars 4mm). Adapted with permission from [241].....39

Figure 3.2 Transformable lattice structure with shape-memory-assisted healing. a) Schematics of the system, with key monomers, the chemical formula of the urethane-acrylate oligomer with disulfide-bonds incorporated. b) Manual-contact-assisted healing process of an octet lattice structure capable of sustaining a static weight after rupture under a three-point-bending load (scale bars 4mm) Adapted with permission from [242].....40

Figure 3.3 Self-healing Polyurethane-based Elastomers. a) Composition of the resin and schematic representation of the polyurethane elastomer with disulfide bonds in the network after UV irradiation. b) Various manufactured 3D samples: Letters, a honeycomb structure, a circular cone, a hollow cube, and a Maya Pyramid (scale bar 10 mm). c) Self-healing experiment of the honeycomb structure with bending deformation after healing. Adapted with permission from [243].....41

Figure 3.4 Reprocessable repairable thermosets system. a) Chemical composition of the photopolymer solution and b) resulting permanent (blue) and reversible (red) covalent bonds. c) 3D printed Kelvin foam (scale bar 1mm). d) 3D printed rabbit undergone to preparation and reprinting process for restoration. e) Uniaxial tensile test samples before and after testing and f) resulting stress-strain curves. Adapted with permission from [244]42

Figure 3.5 Thiol–acrylate vitrimers. a) Composition of the resin used for the preparation of covalent adaptable thiol–acrylate photopolymers. b) Uniaxial tensile test samples before and after testing and c) resulting stress-strain curves. d) 3D printed test structure with a length of 2.6 cm. e) Thermally triggered healing of a flower-shaped 3D printed specimen. Adapted with permission from [246].....43

Figure 3.6 Photosynthesis-assisted Self-healing. a) Schematic of the healing mechanism based on the formation of additional cross-links between free isocyanate (NCO) side groups and photosynthesis-produced glucose around the fracture surface. b) Healing process of a 3D printed propeller and practical demonstration of the correct operability. Adapted with permission from [247] ...44

Figure 3.10 Biomimetic, Adhesive, and Self-healing Elastomers. a) Composition and schematic illustration of the copolymer elastomer formation. b) CAD file and printed gecko undergoing c) cutting and healing cycle. Adapted with permission from [251]	48
Figure 3.11 Fully physically cross-linked double network. a) Composition of the resin and schematic representation of the hydrogen bonds and metal-ligand bonds formation. b) Various manufactured wearable flexible sensors. c) Self-healing process and stretching of a dumbbell-shaped sample. Adapted with permission from [252]	49
Figure 3.12 Dually-cured recyclable elastomer. a) Composition of the resin and schematic representation of photo-thermal dual-curing and interactions. b) Self-healing process of a 3d printed component. c) Stress–strain curves of repeatedly self-healed 3D printed samples. Adapted with permission from [253]	50
Figure 3.13 Temperature-dependent rigidity. a) Temperature-dependent behavior. b) Dynamic polymer networks cross-linked by reversible ionic bonding and hydrogen bonding. Self-healing demonstration of various manufactured samples: c) soft octopus and d) rigid bridge. Adapted with permission from [254]	51
Figure 3.14 Self-adhesive hydrogels. a) Chemical composition and schematic illustration of the ionically crosslinked system. b) Comparison among different samples under 3-points bending test and resulting load-displacement curves. c) Self-adhesion of a manufactured salamander tail. Adapted with permission from [255]	52
Figure 3.15 Self-healing and shape memory double system. a) Chemical composition and b) schematic representation of the double network. c) Self-healing process of a manufactured stent. d) Self-healing and application demonstration of a manufactured gripper. Adapted with permission from [256]	53
Figure 4.1 Water-soluble photoinitiators. Chemical structures and maximum absorption wavelength of the water-soluble photoinitiators most commonly used in light-activated additive manufacturing techniques. Adapted with permission from [160]	64
Figure 4.2 Healing efficiency assessment. Physical parameters and formulas used to determine the performance in mechanical properties restoration. Reproduced with permission [315].....	70

Figure 5.1 Formulation composition and network formation. a) Schematic representation of the semi-interpenetrated network (semi-IPN) and healing process. c) Chemical structure of the healing agent, monomer, cross-linker, and initiator in the photocurable resin.77

Figure 5.2 Preliminary investigation. a) Healing efficiencies estimated from tensile strength at break ($SH\sigma$) and elongation at break ($SH\epsilon$) for formulations containing PVA with different Mw at the highest concentration suitable for printing. b) ATR-FTIR spectra of Acrylic Acid (AAc), Poly (vinyl alcohol) (PVA) and of a dried sample. c) Viscosities of formulations with increasing PVA contents under continuous shear rate sweep. d) adapter and Thinky planetary mixer used for mixing the formulations. e-f) Real-time photorheology of formulations e) with different PVA/AAc ratios and f) of the PVA_0.8 formulation with different photoinitiator concentrations.79

Figure 5.3 Printer Modification. a) Formulation thickening during printing. b) Effect of the dye on the thickening of the formulation. c) Superficial drying of the resin. d) Schematic illustration of the Digital Light Processing (DLP) printing modified apparatus used. e) Components and f) assembled aerosol-reflux printing apparatus.82

Figure 5.4 Effect of the dye on the printing process. a) Cuboid-shaped samples (25 mm x 10 mm x 5 mm) printed with formulations containing two different dyes, methyl red (left) and brilliant green (right), compared to a sample printed without adding a dye (center). b) ATR-FTIR spectra of the dry PVA_0.8 formulation without the dye before curing (yellow) and of dried samples printed with the two different dyes, methyl red (MR) and brilliant green (BG). In the inset: UV-Vis absorption spectra of dyes compared with the printer light source emission wavelength. c-d) CAD file of the benchmark used to determine the finest feature possible to print and table comparing the effects of the concentration of the PVA versus the concentration of the dye on printed benchmarks (scale bar 5 mm).71

Figure 5.5 3D printing of complex geometries. Various view of 3D samples fabricated with the different dyes. a) Body-centered cubic lattice-like structure b) Axisymmetric structure with central pillar.84

Figure 5.6 Self-healing of samples with complex geometries. a) Tensile test specimens that could withstand a bending deformation immediately upon rejoining. b) Holed cylindrical structure, once reconnected and healed for 2 h it could endure a large stretching deformation. c) Body-centered cubic lattice-like

structures cut and rejoined. Diffusion at the interface after 12 h i contact is clearly visible (inset) because of the gradient of the dye..... 85

Figure 5.7 Healing mechanism investigation. a-b) Diffusion experiments of different dyes in a similar matrix. a) Similarly-sized cuboid to show the mixing of the dyes b) Cuboids with longer non-colored central part to show differences in the diffusion speed. c) ATR-IR spectra comparison of an as-printed wet sample and a dried sample. d) Contact angle image of a freshly cut surface and a dried cut surface and e) comparison of the behavior of freshly cut and non-cut surfaces when manually stretched. 87

Figure 5.8 Self-healing efficiency assessment. a) Stress–strain curves from Uniaxial tensile test on self-healed PVA_0.8 specimens for increasing healing time and b) comparison of the healing efficiencies estimated from tensile strength at break ($SH\sigma$) and elongation at break ($SH\varepsilon$). Error bars represent standard deviation, $n = 5$ independent replicates. c) Stress–strain curves of printed pristine and healed samples compared with the same curves obtained from cast pristine, and healed samples. d-e) Elongation and rupture behavior during the test of d) pristine sample and e) 12 h healed sample. 89

Figure 5.9 Repetitive restoration. Tensile strength and recovery percentage of samples after five separation-healing cycles, on samples a) stored in humid sealed environment or b) with no controlled humidity for 24 hours while healing for every cycle. c) Comparison of weight loss during several days between samples only stored in closed and sealed vials and samples subjected to manipulation for tensile testing..... 90

Figure 6.1 Temperature sensitive system design. a) Molecular structure of a Pluronic® triblock copolymer and the Pluronic® grid. b) Schematic illustration of the thermoreversible property of the Pluronic hydrogel with plasticizer forming the micellar hydrogel and representation of the proposed self-healing mechanism. c) Chemical structure of the monomers, cross-linker and photoinitiator present in the photocurable resin. Reproduced with permission from [330,331,333] 96

Figure 6.2 Plasticizer selection. Comparison of the effect of the different monomers at various concentrations on the a) thermal gelation of Pluronic before curing, b) on the photopolymerization kinetic of the resin, and on the c) thermal gelation of the Pluronic after curing and covalent network formation. 100

Figure 6.3 Concentration effect. Comparison of the effect of an increasing concentration for each monomer on the a) thermal gelation of Pluronic before

curing, b) on the photopolymerization kinetics of the resin, and on the c) thermal gelation of the Pluronic after covalent network formation. 101

Figure 6.4 Rheological behavior. Amplitude sweep tests results performed at 5°C using as plasticizer a) PEG 400 and b) PEGMA 500 before curing and c) PEMGA 500 after curing. Amplitude sweep tests results performed at 25°C using as plasticizer d) PEG 400 and e) PEGMA 500 before curing and f) PEMGA 500 after curing. 103

Figure 6.5 Thermal hysteresis. Reversible gelation tests results performed using as plasticizer a) PEG 400 and b) PEGMA 500 before curing and c) PEMGA 500 after curing. Storage shear modulus evolution over time during the reversible gelation tests results performed using as plasticizer d) PEG 400 and e) PEGMA 500 before curing and f) PEMGA 500 after curing. 105

Figure 6.6 Cross-linker effect. Comparison of the effect of an increasing concentration of crosslinker (1-5- 10phr) at different concentrations of monomer a-c) on the photopolymerization kinetics d-f) on the Pluronic reversible gelation 106

Figure 6.7 Printer Modification. a) Schematic illustration of the Digital Light Processing (DLP) printing apparatus used modified with the cooling vortex tube below. b) Real configuration of the printing system with the vat cooled by compressed air. 107

Figure 6.8 Vortex tube-cooling efficiency. a) Thermal camera images of the vat of the printer at various temperature during cooling. b) Formulation thermal gelation during printing without the dye (above) and after the addition of the dye (below). 108

Figure 6.9 Vortex tube-cooling issues. Moisture condensation a) in the optical group of the printer and b) along the flexible tubes. c) Limited cooling only at the transparent window. d) Thermal gelation of uncured resin on the building platform. e) Uncured resin thickening and hindered flow in the vat. 109

Figure 6.10 Printing process in a cool environment. a) Real configuration of the printing system located in the refrigerator. Absence of thermal gelation of both b) on the building platform and c) in the vat. d-f) CAD files and resulting printed samples of a d) tetrahedron, e) “eight” figure, f) holed cube (scale 10 mm) 110

Figure 7.1 Light-triggered system design. a) Photoisomerization mechanism of a generic azobenzene group. b) Schematic illustration of the dynamic covalent

bond formation and representation of the proposed self-healing mechanism based on boronate-ester bonds. c) Chemical structure of the reactive dye and oligomer present in the photocurable resin. Adapted and reproduced with permission from [125,358]..... 116

Figure 7.2 Poly(vinyl alcohol) methacrylation. a) Methacrylation reaction for PVA. b) Methacrylated PVA powder after drying, 88% hydrolysis degree (left) and 98% hydrolysis degree (right), and c) resulting NMR spectra. d) Preliminary photorheology tests to assess the effect of the dye on the photopolymerization kinetics..... 120

Figure 7.3 Functional dye synthesis and comparison. a) Reaction path for the synthesis of the azobenzene phenylboronic acid methacrylate (APAM) dye and b) comparison of the structure with the other commercial dyes and additives used. c) UV-Vis absorption spectra of the various dyes compared with the printers light source emission wavelength. 121

Figure 7.4 Hydrolysis degree and organic solvent comparison. Photorheology tests carried out to evaluate the effect of hydrolysis degree and organic solvent depending on the dye used: a) no dye and no organic solvent, b) no dye, c) Disperse Red 1 (DR1), d) Disperse Red 1 methacrylate (DR1-MA), e) Azobenzene phenylboronic acid methacrylate (APAM), f) 1,4 - Phenyl diboronic acid (PBDA). 123

Figure 7.5 Dye effect on the polymerization kinetic. Photorheology tests carried out to evaluate the effect of hydrolysis degree and organic solvent depending on the hydrolysis degree and the organic solvent used a) 88% DH and DMSO, b) 88% DH and PC, c) 98% DH and DMSO, d) 98% DH and PC. 124

Figure 7.6 Dye effect on various properties. Comparison of the effects of the absence or presence of various dyes on a-b) Photorheology tests for reaction kinetics, c-d) compression tests for mechanical properties, e-f) swelling tests in MDSO for crosslinking density. 125

Figure 7.7 Preliminary tests for 3D printing. a) Visible-light photorheology tests carried out on the PVA 88% DMSO APAM 1phr formulation to evaluate the effect of various photoinitiators and b) resulting 3D printed benchmark (printed at 40 mW/cm², Irradiation time 25s). c) UV-light photorheology tests carried out on the PVA 88% DMSO APAM 1phr formulation to evaluate the effect of various photoinitiators and d-e) resulting 3D printed benchmarks (d printed at 45 mW/cm², Irradiation time 5s; e printed at 20 mW/cm², Irradiation time 12s). (Scale bar 20 mm)..... 127

Figure 7.8 3D printing of simple geometries. CAD files and resulting printed samples of a a) full cylinder, b) benchmark c) “eight” figure. (scale 10 mm)..... 128

References

- [1] Murphy EB, Wudl F. The world of smart healable materials. *Progress in Polymer Science* (Oxford) 2010;35:223–51. <https://doi.org/10.1016/j.progpolymsci.2009.10.006>.
- [2] Qamar IPS, Sottos NR, Trask RS. Grand challenges in the design and manufacture of vascular self-healing. *Multifunctional Materials* 2019;3:013001. <https://doi.org/10.1088/2399-7532/ab69e2>.
- [3] Utrera-Barrios S, Verdejo R, López-Manchado MA, Hernández Santana M. Evolution of self-healing elastomers, from extrinsic to combined intrinsic mechanisms: A review. *Materials Horizons* 2020;7:2882–902. <https://doi.org/10.1039/d0mh00535e>.
- [4] Yang Y, Urban MW. Self-healing polymeric materials. *Chemical Society Reviews* 2013;42:7446–67. <https://doi.org/10.1039/c3cs60109a>.
- [5] Amaral AJR, Pasparakis G. Stimuli responsive self-healing polymers: Gels, elastomers and membranes. *Polymer Chemistry* 2017;8:6464–84. <https://doi.org/10.1039/c7py01386h>.
- [6] Campanella A, Döhler D, Binder WH. Self-Healing in Supramolecular Polymers. *Macromolecular Rapid Communications* 2018;39:1700739. <https://doi.org/10.1002/marc.201700739>.
- [7] Shafranek RT, Millik SC, Smith PT, Lee CU, Boydston AJ, Nelson A. Stimuli-responsive materials in additive manufacturing. *Progress in Polymer Science* 2019;93:36–67. <https://doi.org/10.1016/j.progpolymsci.2019.03.002>.
- [8] Boydston AJ, Cao B, Nelson A, Ono RJ, Saha A, Schwartz JJ, et al. Additive manufacturing with stimuli-responsive materials. *Journal of Materials Chemistry A* 2018;6:20621–45. <https://doi.org/10.1039/C8TA07716A>.
- [9] Billiet S, Hillewaere XKD, Teixeira RFA, du Prez FE. Chemistry of crosslinking processes for self-healing polymers. *Macromolecular Rapid*

Communications 2013;34:290–309.
<https://doi.org/10.1002/marc.201200689>.

- [10] Almutairi MD, Aria AI, Thakur VK, Khan MA. Self-healing mechanisms for 3D-printed polymeric structures: From lab to reality. *Polymers (Basel)* 2020;12:1–27. <https://doi.org/10.3390/polym12071534>.
- [11] Zhong N, Post W. Self-repair of structural and functional composites with intrinsically self-healing polymer matrices: A review. *Composites Part A: Applied Science and Manufacturing* 2015;69:226–39. <https://doi.org/10.1016/j.compositesa.2014.11.028>.
- [12] Huynh TP, Sonar P, Haick H. Advanced Materials for Use in Soft Self-Healing Devices. *Advanced Materials* 2017;29. <https://doi.org/10.1002/adma.201604973>.
- [13] Herbst F, Döhler D, Michael P, Binder WH. Self-healing polymers via supramolecular forces. *Macromolecular Rapid Communications* 2013;34:203–20. <https://doi.org/10.1002/marc.201200675>.
- [14] Phadke A, Zhang C, Arman B, Hsu CC, Mashelkar RA, Lele AK, et al. Rapid self-healing hydrogels. *Proc Natl Acad Sci U S A* 2012;109:4383–8. <https://doi.org/10.1073/pnas.1201122109>.
- [15] Bai T, Liu S, Sun F, Sinclair A, Zhang L, Shao Q, et al. Zwitterionic fusion in hydrogels and spontaneous and time-independent self-healing under physiological conditions. *Biomaterials* 2014;35:3926–33. <https://doi.org/10.1016/j.biomaterials.2014.01.077>.
- [16] Wang Z, Scheres L, Xia H, Zuillhof H. Developments and Challenges in Self-Healing Antifouling Materials. *Advanced Functional Materials* 2020;30. <https://doi.org/10.1002/adfm.201908098>.
- [17] Wang S, Urban MW. Self-healing polymers. *Nature Reviews Materials* 2020;5:562–83. <https://doi.org/10.1038/s41578-020-0202-4>.
- [18] Dahlke J, Zechel S, Hager MD, Schubert US. How to Design a Self-Healing Polymer: General Concepts of Dynamic Covalent Bonds and Their Application for Intrinsic Healable Materials. *Advanced Materials Interfaces* 2018;5:1800051. <https://doi.org/10.1002/admi.201800051>.

- [19] Urdl K, Kandelbauer A, Kern W, Müller U, Thebault M, Zikulnig-Rusch E. Self-healing of densely crosslinked thermoset polymers—a critical review. *Progress in Organic Coatings* 2017;104:232–49. <https://doi.org/10.1016/j.porgcoat.2016.11.010>.
- [20] Taylor DL, in het Panhuis M. Self-Healing Hydrogels. *Advanced Materials* 2016;28:9060–93. <https://doi.org/10.1002/adma.201601613>.
- [21] Gyarmati B, Szilágyi B^Á, Szilágyi A. Reversible interactions in self-healing and shape memory hydrogels. *European Polymer Journal* 2017;93:642–69. <https://doi.org/10.1016/j.eurpolymj.2017.05.020>.
- [22] Talebian S, Mehrali M, Taebnia N, Pennisi CP, Kadumudi FB, Foroughi J, et al. Self-Healing Hydrogels: The Next Paradigm Shift in Tissue Engineering? *Advanced Science* 2019;6:1801664. <https://doi.org/10.1002/advs.201801664>.
- [23] McBride MK, Worrell BT, Brown T, Cox LM, Sowan N, Wang C, et al. Enabling applications of covalent adaptable networks. *Annual Review of Chemical and Biomolecular Engineering* 2019;10:175–98. <https://doi.org/10.1146/annurev-chembioeng-060718-030217>.
- [24] Wang H, Wang H, Wang Z, Tang L, Zeng G, Xu P, et al. Covalent organic framework photocatalysts: Structures and applications. *Chemical Society Reviews* 2020;49:4135–65. <https://doi.org/10.1039/d0cs00278j>.
- [25] Jiang Z, Bhaskaran A, Aitken HM, Shackleford ICG, Connal LA. Using Synergistic Multiple Dynamic Bonds to Construct Polymers with Engineered Properties. *Macromolecular Rapid Communications* 2019;40:1–10. <https://doi.org/10.1002/marc.201900038>.
- [26] Deng G, Li F, Yu H, Liu F, Liu C, Sun W, et al. Dynamic hydrogels with an environmental adaptive self-healing ability and dual responsive Sol-Gel transitions. *ACS Macro Letters* 2012;1:275–9. <https://doi.org/10.1021/mz200195n>.
- [27] Zhang ZP, Rong MZ, Zhang MQ. Polymer engineering based on reversible covalent chemistry: A promising innovative pathway towards new materials and new functionalities. *Progress in Polymer Science* 2018;80:39–93. <https://doi.org/10.1016/j.progpolymsci.2018.03.002>.

- [28] Xu J, Liu Y, Hsu S hui. Hydrogels based on schiff base linkages for biomedical applications. *Molecules* 2019;24:3005. <https://doi.org/10.3390/molecules24163005>.
- [29] Wei Z, Yang JH, Zhou J, Xu F, Zrínyi M, Dussault PH, et al. Self-healing gels based on constitutional dynamic chemistry and their potential applications. *Chemical Society Reviews* 2014;43:8114–31. <https://doi.org/10.1039/c4cs00219a>.
- [30] Wang H, Heilshorn SC. Adaptable Hydrogel Networks with Reversible Linkages for Tissue Engineering. *Advanced Materials* 2015;27:3717–36. <https://doi.org/10.1002/adma.201501558>.
- [31] Kuhl N, Abend M, Bode S, Schubert US, Hager MD. Oxime crosslinked polymer networks: Is every reversible covalent bond suitable to create self-healing polymers? *Journal of Applied Polymer Science* 2016;133. <https://doi.org/10.1002/app.44168>.
- [32] Grover GN, Lam J, Nguyen TH, Segura T, Maynard HD. Biocompatible hydrogels by oxime click chemistry. *Biomacromolecules* 2012;13:3013–7. <https://doi.org/10.1021/bm301346e>.
- [33] Dirksen A, Yegneswaran S, Dawson PE. Bisaryl hydrazones as exchangeable biocompatible linkers. *Angewandte Chemie - International Edition* 2010;49:2023–7. <https://doi.org/10.1002/anie.200906756>.
- [34] Tu Y, Chen N, Li C, Liu H, Zhu R, Chen S, et al. Advances in injectable self-healing biomedical hydrogels. *Acta Biomaterialia* 2019;90:1–20. <https://doi.org/10.1016/j.actbio.2019.03.057>.
- [35] McKinnon DD, Domaille DW, Cha JN, Anseth KS. Bis-aliphatic hydrazone-linked hydrogels form most rapidly at physiological pH: Identifying the origin of hydrogel properties with small molecule kinetic studies. *Chemistry of Materials* 2014;26:2382–7. <https://doi.org/10.1021/cm5007789>.
- [36] Ying H, Zhang Y, Cheng J. Dynamic urea bond for the design of reversible and self-healing polymers. *Nature Communications* 2014;5:3218. <https://doi.org/10.1038/ncomms4218>.

- [37] Zheng N, Xu Y, Zhao Q, Xie T. Dynamic Covalent Polymer Networks: A Molecular Platform for Designing Functions beyond Chemical Recycling and Self-Healing. *Chemical Reviews* 2021;121:1716–45. <https://doi.org/10.1021/acs.chemrev.0c00938>.
- [38] Zhang Y, Ying H, Hart KR, Wu Y, Hsu AJ, Coppola AM, et al. Malleable and Recyclable Poly(urea-urethane) Thermosets bearing Hindered Urea Bonds. *Advanced Materials* 2016;28:7646–51. <https://doi.org/10.1002/adma.201601242>.
- [39] Yan J, Springsteen G, Deeter S, Wang B. The relationship among pK_a, pH, and binding constants in the interactions between boronic acids and diols - It is not as simple as it appears. *Tetrahedron* 2004;60:11205–9. <https://doi.org/10.1016/j.tet.2004.08.051>.
- [40] Cromwell OR, Chung J, Guan Z. Malleable and Self-Healing Covalent Polymer Networks through Tunable Dynamic Boronic Ester Bonds. *J Am Chem Soc* 2015;137:6492–5. <https://doi.org/10.1021/jacs.5b03551>.
- [41] Wang B, Jeon YS, Park HS, Kim JH. Self-healable mussel-mimetic nanocomposite hydrogel based on catechol-containing polyaspartamide and graphene oxide. *Materials Science and Engineering C* 2016;69:160–70. <https://doi.org/10.1016/j.msec.2016.06.065>.
- [42] Dong Y, Wang W, Veisheh O, Appel EA, Xue K, Webber MJ, et al. Injectable and Glucose-Responsive Hydrogels Based on Boronic Acid-Glucose Complexation. *Langmuir* 2016;32:8743–7. <https://doi.org/10.1021/acs.langmuir.5b04755>.
- [43] Fernandes PA, Ramos MJ. Theoretical Insights into the Mechanism for Thiol/Disulfide Exchange. *Chemistry - A European Journal* 2004;10:257–66. <https://doi.org/10.1002/chem.200305343>.
- [44] Pepels M, Filot I, Klumperman B, Goossens H. Self-healing systems based on disulfide-thiol exchange reactions. *Polymer Chemistry* 2013;4:4955–65. <https://doi.org/10.1039/c3py00087g>.
- [45] Canadell J, Goossens H, Klumperman B. Self-healing materials based on disulfide links. *Macromolecules* 2011;44:2536–41. <https://doi.org/10.1021/ma2001492>.

- [46] Bermejo-Velasco D, Azémar A, Oommen OP, Hilborn J, Varghese OP. Modulating Thiol p K a Promotes Disulfide Formation at Physiological pH: An Elegant Strategy to Design Disulfide Cross-Linked Hyaluronic Acid Hydrogels. *Biomacromolecules* 2019;20:1412–20. <https://doi.org/10.1021/acs.biomac.8b01830>.
- [47] Qin H, Zhang T, Li HN, Cong HP, Antonietti M, Yu SH. Dynamic Au-Thiolate Interaction Induced Rapid Self-Healing Nanocomposite Hydrogels with Remarkable Mechanical Behaviors. *Chem* 2017;3:691–705. <https://doi.org/10.1016/j.chempr.2017.07.017>.
- [48] Nair DP, Cramer NB, Scott TF, Bowman CN, Shandas R. Photopolymerized thiol-ene systems as shape memory polymers. *Polymer (Guildf)* 2010;51:4383–9. <https://doi.org/10.1016/j.polymer.2010.07.027>.
- [49] Nandivada H, Jiang X, Lahann J. Click Chemistry: Versatility and Control in the Hands of Materials Scientists. *Advanced Materials* 2007;19:2197–208. <https://doi.org/10.1002/adma.200602739>.
- [50] Otto S, Engberts JBFN. Diels-Alder reactions in water. *Pure and Applied Chemistry* 2000;72:1365–72. <https://doi.org/10.1351/pac200072071365>.
- [51] Scheltjens G, Diaz MM, Brancart J, van Assche G, van Mele B. A self-healing polymer network based on reversible covalent bonding. *Reactive and Functional Polymers* 2013;73:413–20. <https://doi.org/10.1016/j.reactfunctpolym.2012.06.017>.
- [52] Liu Y-L, Chuo T-W. Self-healing polymers based on thermally reversible Diels–Alder chemistry. *Polymer Chemistry* 2013;4:2194. <https://doi.org/10.1039/c2py20957h>.
- [53] Roy N, Bruchmann B, Lehn JM. DYNAMERS: Dynamic polymers as self-healing materials. *Chemical Society Reviews* 2015;44:3786–807. <https://doi.org/10.1039/c5cs00194c>.
- [54] Wei Z, Yang JH, Du XJ, Xu F, Zrinyi M, Osada Y, et al. Dextran-Based Self-Healing Hydrogels Formed by Reversible Diels-Alder Reaction under Physiological Conditions. *Macromolecular Rapid Communications* 2013;34:1464–70. <https://doi.org/10.1002/marc.201300494>.

- [55] Koehler KC, Alge DL, Anseth KS, Bowman CN. A Diels–Alder modulated approach to control and sustain the release of dexamethasone and induce osteogenic differentiation of human mesenchymal stem cells. *Biomaterials* 2013;34:4150–8. <https://doi.org/10.1016/j.biomaterials.2013.02.020>.
- [56] Kirchhof S, Brandl FP, Hammer N, Goepferich AM. Investigation of the Diels–Alder reaction as a cross-linking mechanism for degradable poly(ethylene glycol) based hydrogels. *Journal of Materials Chemistry B* 2013;1:4855. <https://doi.org/10.1039/c3tb20831a>.
- [57] Cardenas-Daw C, Kroeger A, Schaertl W, Froimowicz P, Landfester K. Reversible Photocycloadditions, a Powerful Tool for Tailoring (Nano)Materials. *Macromolecular Chemistry and Physics* 2012;213:144–56. <https://doi.org/10.1002/macp.201100399>.
- [58] Habault D, Zhang H, Zhao Y. Light-triggered self-healing and shape-memory polymers. *Chemical Society Reviews* 2013;42:7244–56. <https://doi.org/10.1039/c3cs35489j>.
- [59] Ling J, Rong MZ, Zhang MQ. Photo-stimulated self-healing polyurethane containing dihydroxyl coumarin derivatives. *Polymer (Guildf)* 2012;53:2691–8. <https://doi.org/10.1016/j.polymer.2012.04.016>.
- [60] Jin Y, Yu C, Denman RJ, Zhang W. Recent advances in dynamic covalent chemistry. *Chemical Society Reviews* 2013;42:6634–54. <https://doi.org/10.1039/c3cs60044k>.
- [61] Zou W, Dong J, Luo Y, Zhao Q, Xie T. Dynamic Covalent Polymer Networks: from Old Chemistry to Modern Day Innovations. *Advanced Materials* 2017;29:1606100. <https://doi.org/10.1002/adma.201606100>.
- [62] Montarnal D, Capelot M, Tournilhac F, Leibler L. Silica-Like Malleable Materials from Permanent Organic Networks. *Science (1979)* 2011;334:965–8. <https://doi.org/10.1126/science.1212648>.
- [63] van Zee NJ, Nicolaÿ R. Vitrimers: Permanently crosslinked polymers with dynamic network topology. *Progress in Polymer Science* 2020;104:101233. <https://doi.org/10.1016/j.progpolymsci.2020.101233>.

- [64] Zhu M, Liu J, Gan L, Long M. Research progress in bio-based self-healing materials. *European Polymer Journal* 2020;129:109651. <https://doi.org/10.1016/j.eurpolymj.2020.109651>.
- [65] Denissen W, Winne JM, du Prez FE. Vitrimers: permanent organic networks with glass-like fluidity. *Chemical Science* 2016;7:30–8. <https://doi.org/10.1039/C5SC02223A>.
- [66] Yang Y, Urban MW. Self-Healing of Polymers via Supramolecular Chemistry. *Advanced Materials Interfaces* 2018;5:1800384. <https://doi.org/10.1002/admi.201800384>.
- [67] Seiffert S, Sprakel J. Physical chemistry of supramolecular polymer networks. *Chem Soc Rev* 2012;41:909–30. <https://doi.org/10.1039/C1CS15191F>.
- [68] de Espinosa LM, Fiore GL, Weder C, Johan Foster E, Simon YC. Healable supramolecular polymer solids. *Progress in Polymer Science* 2015;49–50:60–78. <https://doi.org/10.1016/j.progpolymsci.2015.04.003>.
- [69] Diba M, Spaans S, Ning K, Ippel BD, Yang F, Loomans B, et al. Self-Healing Biomaterials: From Molecular Concepts to Clinical Applications. *Advanced Materials Interfaces* 2018;5:1–21. <https://doi.org/10.1002/admi.201800118>.
- [70] Bekas DG, Tsirka K, Baltzis D, Paipetis AS. Self-healing materials: A review of advances in materials, evaluation, characterization and monitoring techniques. *Composites Part B: Engineering* 2016;87:92–119. <https://doi.org/10.1016/j.compositesb.2015.09.057>.
- [71] Blaiszik BJ, Kramer SLB, Olugebefola SC, Moore JS, Sottos NR, White SR. Self-healing polymers and composites. *Annual Review of Materials Research* 2010;40:179–211. <https://doi.org/10.1146/annurev-matsci-070909-104532>.
- [72] Rodriguez ED, Luo X, Mather PT. Linear/network poly(ϵ -caprolactone) blends exhibiting shape memory assisted self-healing (SMASH). *ACS Applied Materials and Interfaces* 2011;3:152–61. <https://doi.org/10.1021/am101012c>.

- [73] Chen K, Feng Y, Zhang Y, Yu L, Hao X, Shao F, et al. Entanglement-Driven Adhesion, Self-Healing, and High Stretchability of Double-Network PEG-Based Hydrogels. *ACS Applied Materials and Interfaces* 2019;11:36458–68. <https://doi.org/10.1021/acsami.9b14348>.
- [74] Huang X, Nakagawa S, Houjou H, Yoshie N. Insights into the Role of Hydrogen Bonds on the Mechanical Properties of Polymer Networks. *Macromolecules* 2021;54:4070–80. <https://doi.org/10.1021/acs.macromol.1c00120>.
- [75] Steiner T. The Hydrogen Bond in the Solid State. *Angewandte Chemie International Edition* 2002;41:48–76. [https://doi.org/10.1002/1521-3773\(20020104\)41:1<48::AID-ANIE48>3.0.CO;2-U](https://doi.org/10.1002/1521-3773(20020104)41:1<48::AID-ANIE48>3.0.CO;2-U).
- [76] Desiraju GR. Hydrogen bridges in crystal engineering: Interactions without borders. *Accounts of Chemical Research* 2002;35:565–73. <https://doi.org/10.1021/ar010054t>.
- [77] Appel EA, del Barrio J, Loh XJ, Scherman OA. Supramolecular polymeric hydrogels. *Chemical Society Reviews* 2012;41:6195. <https://doi.org/10.1039/c2cs35264h>.
- [78] Lin Y, Li G. An intermolecular quadruple hydrogen-bonding strategy to fabricate self-healing and highly deformable polyurethane hydrogels. *Journal of Materials Chemistry B* 2014;2:6878–85. <https://doi.org/10.1039/c4tb00862f>.
- [79] Cui J, del Campo A. Multivalent H-bonds for self-healing hydrogels. *Chemical Communications* 2012;48:9302–4. <https://doi.org/10.1039/c2cc34701f>.
- [80] Jeon I, Cui J, Illeperuma WRK, Aizenberg J, Vlassak JJ. Extremely Stretchable and Fast Self-Healing Hydrogels. *Advanced Materials* 2016;28:4678–83. <https://doi.org/10.1002/adma.201600480>.
- [81] Guo M, Pitet LM, Wyss HM, Vos M, Dankers PYW, Meijer EW. Tough stimuli-responsive supramolecular hydrogels with hydrogen-bonding network junctions. *J Am Chem Soc* 2014;136:6969–77. <https://doi.org/10.1021/ja500205v>.

- [82] Zhang H, Xia H, Zhao Y. Poly(vinyl alcohol) hydrogel can autonomously self-heal. *ACS Macro Letters* 2012;1:1233–6. <https://doi.org/10.1021/mz300451r>.
- [83] Gong Z, Zhang G, Zeng X, Li J, Li G, Huang W, et al. High-Strength, Tough, Fatigue Resistant, and Self-Healing Hydrogel Based on Dual Physically Cross-Linked Network. *ACS Applied Materials and Interfaces* 2016;8:24030–7. <https://doi.org/10.1021/acsami.6b05627>.
- [84] Yan Y, Xu S, Liu H, Cui X, Shao J, Yao P, et al. A multi-functional reversible hydrogel adhesive. *Colloids and Surfaces A: Physicochemical and Engineering Aspects* 2020;593:124622. <https://doi.org/10.1016/j.colsurfa.2020.124622>.
- [85] Li G, Yan Q, Xia H, Zhao Y. Therapeutic-Ultrasound-Triggered Shape Memory of a Melamine-Enhanced Poly(vinyl alcohol) Physical Hydrogel. *ACS Applied Materials and Interfaces* 2015;7:12067–73. <https://doi.org/10.1021/acsami.5b02234>.
- [86] Li G, Zhang H, Fortin D, Xia H, Zhao Y. Poly(vinyl alcohol)-Poly(ethylene glycol) Double-Network Hydrogel: A General Approach to Shape Memory and Self-Healing Functionalities. *Langmuir* 2015;31:11709–16. <https://doi.org/10.1021/acs.langmuir.5b03474>.
- [87] Lin X, Grinstaff MW. Ionic supramolecular assemblies. *Israel Journal of Chemistry* 2013;53:498–510. <https://doi.org/10.1002/ijch.201300034>.
- [88] Yang Y, Ding X, Urban MW. Chemical and physical aspects of self-healing materials. *Progress in Polymer Science* 2015;49–50:34–59. <https://doi.org/10.1016/j.progpolymsci.2015.06.001>.
- [89] Kalista SJ, Ward TC. Thermal characteristics of the self-healing response in poly(ethylene-co-methacrylic acid) copolymers. *Journal of the Royal Society Interface* 2007;4:405–11. <https://doi.org/10.1098/rsif.2006.0169>.
- [90] Kalista SJ, Pflug JR, Varley RJ. Effect of ionic content on ballistic self-healing in EMAA copolymers and ionomers. *Polymer Chemistry* 2013;4:4910–26. <https://doi.org/10.1039/c3py00095h>.
- [91] Abu-Thabit NY, Hamdy AS. Stimuli-responsive Polyelectrolyte Multilayers for fabrication of self-healing coatings – A review. *Surface and*

Coatings Technology 2016;303:406–24.
<https://doi.org/10.1016/j.surfcoat.2015.11.020>.

- [92] Reisch A, Roger E, Phoeung T, Antheaume C, Orthlieb C, Boulmedais F, et al. On the benefits of rubbing salt in the cut: Self-healing of saloplastic PAA/PAH compact polyelectrolyte complexes. *Advanced Materials* 2014;26:2547–51. <https://doi.org/10.1002/adma.201304991>.
- [93] Sun TL, Kurokawa T, Kuroda S, Ihsan A bin, Akasaki T, Sato K, et al. Physical hydrogels composed of polyampholytes demonstrate high toughness and viscoelasticity. *Nature Materials* 2013;12:932–7. <https://doi.org/10.1038/nmat3713>.
- [94] Fang X, Sun J. One-Step Synthesis of Healable Weak-Polyelectrolyte-Based Hydrogels with High Mechanical Strength, Toughness, and Excellent Self-Recovery. *ACS Macro Letters* 2019:500–5. <https://doi.org/10.1021/acsmacrolett.9b00189>.
- [95] Lowe AB, McCormick CL. Synthesis and solution properties of zwitterionic polymers. *Chemical Reviews* 2002;102:4177–89. <https://doi.org/10.1021/cr020371t>.
- [96] Laschewsky A. Structures and synthesis of zwitterionic polymers. *Polymers (Basel)* 2014;6:1544–601. <https://doi.org/10.3390/polym6051544>.
- [97] Otto S, Engberts JBFN. Hydrophobic interactions and chemical reactivity. *Organic and Biomolecular Chemistry* 2003;1:2809–20. <https://doi.org/10.1039/b305672d>.
- [98] An SY, Arunbabu D, Noh SM, Song YK, Oh JK. Recent strategies to develop self-healable crosslinked polymeric networks. *Chemical Communications* 2015;51:13058–70. <https://doi.org/10.1039/c5cc04531b>.
- [99] Khusnutdinova JR, Milstein D. Metal-Ligand Cooperation. *Angewandte Chemie - International Edition* 2015;54:12236–73. <https://doi.org/10.1002/anie.201503873>.
- [100] Shi L, Carstensen H, Hölzl K, Lunzer M, Li H, Hilborn J, et al. Dynamic Coordination Chemistry Enables Free Directional Printing of Biopolymer

- Hydrogel. *Chemistry of Materials* 2017;29:5816–23. <https://doi.org/10.1021/acs.chemmater.7b00128>.
- [101] McConnell AJ, Wood CS, Neelakandan PP, Nitschke JR. Stimuli-Responsive Metal-Ligand Assemblies. *Chemical Reviews* 2015;115:7729–93. <https://doi.org/10.1021/cr500632f>.
- [102] Li Q, Liu C, Wen J, Wu Y, Shan Y, Liao J. The design, mechanism and biomedical application of self-healing hydrogels. *Chinese Chemical Letters* 2017;28:1857–74. <https://doi.org/10.1016/j.cclet.2017.05.007>.
- [103] Shi L, Ding P, Wang Y, Zhang Y, Ossipov D, Hilborn J. Self-Healing Polymeric Hydrogel Formed by Metal–Ligand Coordination Assembly: Design, Fabrication, and Biomedical Applications. *Macromolecular Rapid Communications* 2019;40:1800837. <https://doi.org/10.1002/marc.201800837>.
- [104] Harrington MJ, Masic A, Holten-Andersen N, Waite JH, Fratzl P. Iron-clad fibers: A metal-based biological strategy for hard flexible coatings. *Science* (1979) 2010;328:216–20. <https://doi.org/10.1126/science.1181044>.
- [105] Yavvari PS, Srivastava A. Robust, self-healing hydrogels synthesised from catechol rich polymers. *Journal of Materials Chemistry B* 2015;3:899–910. <https://doi.org/10.1039/c4tb01307g>.
- [106] Wei Z, He J, Liang T, Oh H, Athas J, Tong Z, et al. Autonomous self-healing of poly(acrylic acid) hydrogels induced by the migration of ferric ions. *Polymer Chemistry* 2013;4:4601–5. <https://doi.org/10.1039/c3py00692a>.
- [107] Zheng Q, Zhao L, Wang J, Wang S, Liu Y, Liu X. High-strength and high-toughness sodium alginate/polyacrylamide double physically crosslinked network hydrogel with superior self-healing and self-recovery properties prepared by a one-pot method. *Colloids and Surfaces A: Physicochemical and Engineering Aspects* 2020;589:124402. <https://doi.org/10.1016/j.colsurfa.2019.124402>.
- [108] Jiang H, Duan L, Ren X, Gao G. Hydrophobic association hydrogels with excellent mechanical and self-healing properties. *European Polymer Journal* 2019;112:660–9. <https://doi.org/10.1016/j.eurpolymj.2018.10.031>.

- [109] Tuncaboylu DC, Sahin M, Argun A, Oppermann W, Okay O. Dynamics and large strain behavior of self-healing hydrogels with and without surfactants. *Macromolecules* 2012;45:1991–2000. <https://doi.org/10.1021/ma202672y>.
- [110] Okay O. Semicrystalline physical hydrogels with shape-memory and self-healing properties. *Journal of Materials Chemistry B* 2019;7:1581–96. <https://doi.org/10.1039/c8tb02767f>.
- [111] Tuncaboylu DC, Argun A, Sahin M, Sari M, Okay O. Structure optimization of self-healing hydrogels formed via hydrophobic interactions. *Polymer (Guildf)* 2012;53:5513–22. <https://doi.org/10.1016/j.polymer.2012.10.015>.
- [112] Jin J, Cai L, Jia YG, Liu S, Chen Y, Ren L. Progress in self-healing hydrogels assembled by host-guest interactions: Preparation and biomedical applications. *Journal of Materials Chemistry B* 2019;7:1637–51. <https://doi.org/10.1039/c8tb02547a>.
- [113] Li J, Harada A, Kamachi M. Sol–Gel Transition during Inclusion Complex Formation between α -Cyclodextrin and High Molecular Weight Poly(ethylene glycol)s in Aqueous Solution. *Polymer Journal* 1994;26:1019–26. <https://doi.org/10.1295/polymj.26.1019>.
- [114] Harada A, Okada M, Li J, Kamachi M. Preparation and Characterization of Inclusion Complexes of Poly(propylene glycol) with Cyclodextrins. *Macromolecules* 1995;28:8406–11. <https://doi.org/10.1021/ma00128a060>.
- [115] Harada A, Kawaguchi Y, Nishiyama T, Kamachi M. Complex formation of poly(ϵ -caprolactone) with cyclodextrin. *Macromolecular Rapid Communications* 1997;18:535–9. <https://doi.org/10.1002/marc.1997.030180701>.
- [116] Liu DE, Chen Q, Long YB, Ma J, Gao H. A thermo-responsive polyurethane organogel for norfloxacin delivery. *Polymer Chemistry* 2018;9:228–35. <https://doi.org/10.1039/c7py01803g>.
- [117] Liu KL, Zhang Z, Li J. Supramolecular hydrogels based on cyclodextrin-polymer polypseudorotaxanes: Materials design and hydrogel properties. *Soft Matter* 2011;7:11290–7. <https://doi.org/10.1039/c1sm06340e>.

- [118] Schmidt BVKJ, Barner-Kowollik C. Dynamic Macromolecular Material Design—The Versatility of Cyclodextrin-Based Host–Guest Chemistry. *Angewandte Chemie - International Edition* 2017;56:8350–69. <https://doi.org/10.1002/anie.201612150>.
- [119] Strandman S, Zhu XX. Self-Healing Supramolecular Hydrogels Based on Reversible Physical Interactions. *Gels* 2016;2:16. <https://doi.org/10.3390/gels2020016>.
- [120] Rodell CB, MacArthur JW, Dorsey SM, Wade RJ, Wang LL, Woo YJ, et al. Shear-thinning supramolecular hydrogels with secondary autonomous covalent crosslinking to modulate viscoelastic properties in vivo. *Advanced Functional Materials* 2015;25:636–44. <https://doi.org/10.1002/adfm.201403550>.
- [121] Schneider HJ, Yatsimirsky AK. Selectivity in supramolecular host–guest complexes. *Chemical Society Reviews* 2008;37:263–77. <https://doi.org/10.1039/b612543n>.
- [122] Nakahata M, Takashima Y, Harada A. Highly Flexible, Tough, and Self-Healing Supramolecular Polymeric Materials Using Host-Guest Interaction. *Macromolecular Rapid Communications* 2016;37:86–92. <https://doi.org/10.1002/marc.201500473>.
- [123] Yang X, Yu H, Wang L, Tong R, Akram M, Chen Y, et al. Self-healing polymer materials constructed by macrocycle-based host-guest interactions. *Soft Matter* 2015;11:1242–52. <https://doi.org/10.1039/c4sm02372b>.
- [124] Yu G, Jie K, Huang F. Supramolecular Amphiphiles Based on Host-Guest Molecular Recognition Motifs. *Chemical Reviews* 2015;115:7240–303. <https://doi.org/10.1021/cr5005315>.
- [125] Wang Z, Ren Y, Zhu Y, Hao L, Chen Y, An G, et al. A Rapidly Self-Healing Host–Guest Supramolecular Hydrogel with High Mechanical Strength and Excellent Biocompatibility. *Angewandte Chemie - International Edition* 2018;57:9008–12. <https://doi.org/10.1002/anie.201804400>.
- [126] Xiong C, Zhang L, Xie M, Sun R. Photoregulating of Stretchability and Toughness of a Self-Healable Polymer Hydrogel. *Macromolecular Rapid*

<https://doi.org/10.1002/marc.201800018>.

- [127] Hetzer M, Fleischmann C, Schmidt BVKJ, Barner-Kowollik C, Ritter H. Visual recognition of supramolecular graft polymer formation via phenolphthalein-cyclodextrin association. *Polymer (Guildf)* 2013;54:5141–7. <https://doi.org/10.1016/j.polymer.2013.07.031>.
- [128] Nakahata M, Takashima Y, Yamaguchi H, Harada A. Redox-responsive self-healing materials formed from host–guest polymers. *Nature Communications* 2011;2:511. <https://doi.org/10.1038/ncomms1521>.
- [129] Cai L, Liu S, Guo J, Jia YG. Polypeptide-based self-healing hydrogels: Design and biomedical applications. *Acta Biomaterialia* 2020;113:84–100. <https://doi.org/10.1016/j.actbio.2020.07.001>.
- [130] Uman S, Dhand A, Burdick JA. Recent advances in shear-thinning and self-healing hydrogels for biomedical applications. *Journal of Applied Polymer Science* 2020;137:48668. <https://doi.org/10.1002/app.48668>.
- [131] Fichman G, Gazit E. Self-assembly of short peptides to form hydrogels: Design of building blocks, physical properties and technological applications. *Acta Biomaterialia* 2014;10:1671–82. <https://doi.org/10.1016/j.actbio.2013.08.013>.
- [132] Nowak AP, Breedveld V, Pakstis L, Ozbas B, Pine DJ, Deming TJ. Rapidly recovering hydrogel scaffolds from self-assembling diblock copolypeptide amphiphiles. *Nature* 2002;417:424–8. <https://doi.org/10.1038/417424a>.
- [133] Ikeda M, Tanida T, Yoshii T, Kurotani K, Onogi S, Urayama K, et al. Installing logic-gate responses to a variety of biological substances in supramolecular hydrogel-enzyme hybrids. *Nature Chemistry* 2014;6:511–8. <https://doi.org/10.1038/nchem.1937>.
- [134] Golinska MD, Włodarczyk-Biegun MK, Werten MWT, Stuart MAC, de Wolf FA, de Vries R. Dilute self-healing hydrogels of silk-collagen-like block copolypeptides at neutral pH. *Biomacromolecules* 2014;15:699–706. <https://doi.org/10.1021/bm401682n>.
- [135] Clarke DE, Pashuck ET, Bertazzo S, Weaver JVM, Stevens MM. Self-Healing, Self-Assembled β -Sheet Peptide-Poly(γ -glutamic acid) Hybrid

- Hydrogels. *J Am Chem Soc* 2017;139:7250–5. <https://doi.org/10.1021/jacs.7b00528>.
- [136] Gaharwar AK, Peppas NA, Khademhosseini A. Nanocomposite hydrogels for biomedical applications. *Biotechnology and Bioengineering* 2014;111:441–53. <https://doi.org/10.1002/bit.25160>.
- [137] Kostina NY, Sharifi S, de Los Santos Pereira A, Michálek J, Grijpma DW, Rodriguez-Emmenegger C. Novel antifouling self-healing poly(carboxybetaine methacrylamide-co-HEMA) nanocomposite hydrogels with superior mechanical properties. *Journal of Materials Chemistry B* 2013;1:5644–50. <https://doi.org/10.1039/c3tb20704h>.
- [138] Thakur VK, Kessler MR. Self-healing polymer nanocomposite materials: A review. *Polymer (Guildf)* 2015;69:369–83. <https://doi.org/10.1016/j.polymer.2015.04.086>.
- [139] Sun JY, Zhao X, Illeperuma WRK, Chaudhuri O, Oh KH, Mooney DJ, et al. Highly stretchable and tough hydrogels. *Nature* 2012;489:133–6. <https://doi.org/10.1038/nature11409>.
- [140] Haraguchi K, Uyama K, Tanimoto H. Self-healing in nanocomposite hydrogels. *Macromolecular Rapid Communications* 2011;32:1253–8. <https://doi.org/10.1002/marc.201100248>.
- [141] Gao G, Du G, Sun Y, Fu J. Self-healable, tough, and ultrastretchable nanocomposite hydrogels based on reversible polyacrylamide/montmorillonite adsorption. *ACS Applied Materials and Interfaces* 2015;7:5029–37. <https://doi.org/10.1021/acsami.5b00704>.
- [142] Huang W, Qi C, Gao Y. Injectable Self-Healable Nanocomposite Hydrogels with Mussel-Inspired Adhesive Properties for 3D Printing Ink. *ACS Applied Nano Materials* 2019;2:5000–8. <https://doi.org/10.1021/acsanm.9b00936>.
- [143] Kim JW, Park H, Lee G, Jeong YR, Hong SY, Keum K, et al. Paper-Like, Thin, Foldable, and Self-Healable Electronics Based on PVA/CNC Nanocomposite Film. *Advanced Functional Materials* 2019;29:1–14. <https://doi.org/10.1002/adfm.201905968>.

- [144] Thangavel G, Tan MWM, Lee PS. Advances in self-healing supramolecular soft materials and nanocomposites. *Nano Convergence* 2019;6. <https://doi.org/10.1186/s40580-019-0199-9>.
- [145] Sanka RVSP, Krishnakumar B, Leterrier Y, Pandey S, Rana S, Michaud V. Soft self-healing nanocomposites. *Frontiers in Materials* 2019;6:1–20. <https://doi.org/10.3389/fmats.2019.00137>.
- [146] Jones N. Science in three dimensions: The print revolution. *Nature* 2012;487:22–3. <https://doi.org/10.1038/487022a>.
- [147] Bhatia A, Sehgal AK. Additive manufacturing materials, methods and applications: A review. *Materials Today: Proceedings* 2021. <https://doi.org/10.1016/j.matpr.2021.04.379>.
- [148] Oropallo W, Piegl LA. Ten challenges in 3D printing. *Engineering with Computers* 2016;32:135–48. <https://doi.org/10.1007/s00366-015-0407-0>.
- [149] Berman B. 3-D printing: The new industrial revolution. *Business Horizons* 2012;55:155–62. <https://doi.org/10.1016/j.bushor.2011.11.003>.
- [150] Gao W, Zhang Y, Ramanujan D, Ramani K, Chen Y, Williams CB, et al. The status, challenges, and future of additive manufacturing in engineering. *CAD Computer Aided Design* 2015;69:65–89. <https://doi.org/10.1016/j.cad.2015.04.001>.
- [151] Sanchez-Rexach E, Johnston TG, Jehanno C, Sardon H, Nelson A. Sustainable Materials and Chemical Processes for Additive Manufacturing. *Chemistry of Materials* 2020;32:7105–19. <https://doi.org/10.1021/acs.chemmater.0c02008>.
- [152] Ligon SC, Liska R, Stampfl J, Gurr M, Mülhaupt R. Polymers for 3D Printing and Customized Additive Manufacturing. *Chemical Reviews* 2017;117:10212–90. <https://doi.org/10.1021/acs.chemrev.7b00074>.
- [153] Tibbits S. 4D Printing: Multi-Material Shape Change. *Architectural Design* 2014;84:116–21. <https://doi.org/10.1002/ad.1710>.
- [154] Vaneker T, Bernard A, Moroni G, Gibson I, Zhang Y. Design for additive manufacturing: Framework and methodology. *CIRP Annals* 2020;69:578–99. <https://doi.org/10.1016/j.cirp.2020.05.006>.

- [155] Tan LJ, Zhu W, Zhou K. Recent Progress on Polymer Materials for Additive Manufacturing. *Advanced Functional Materials* 2020;30:1–54. <https://doi.org/10.1002/adfm.202003062>.
- [156] Guzzi EA, Tibbitt MW. Additive Manufacturing of Precision Biomaterials. *Advanced Materials* 2020;32:1901994. <https://doi.org/10.1002/adma.201901994>.
- [157] Jung K, Corrigan N, Ciftci M, Xu J, Seo SE, Hawker CJ, et al. Designing with Light: Advanced 2D, 3D, and 4D Materials. *Advanced Materials* 2020;32:1–21. <https://doi.org/10.1002/adma.201903850>.
- [158] Alghamdi SS, John S, Choudhury NR, Dutta NK. Additive manufacturing of polymer materials: Progress, promise and challenges. *Polymers (Basel)* 2021;13:1–39. <https://doi.org/10.3390/polym13050753>.
- [159] Appuhamillage GA, Chartrain N, Meenakshisundaram V, Feller KD, Williams CB, Long TE. 110th Anniversary: Vat Photopolymerization-Based Additive Manufacturing: Current Trends and Future Directions in Materials Design. *Industrial and Engineering Chemistry Research* 2019;58:15109–18. <https://doi.org/10.1021/acs.iecr.9b02679>.
- [160] Lee M, Rizzo R, Surman F, Zenobi-Wong M. Guiding Lights: Tissue Bioprinting Using Photoactivated Materials. *Chemical Reviews* 2020;120:10950–1027. <https://doi.org/10.1021/acs.chemrev.0c00077>.
- [161] Samadian H, Maleki H, Allahyari Z, Jaymand M. Natural polymers-based light-induced hydrogels: Promising biomaterials for biomedical applications. *Coordination Chemistry Reviews* 2020;420:213432. <https://doi.org/10.1016/j.ccr.2020.213432>.
- [162] Bagheri A, Jin J. Photopolymerization in 3D Printing. *ACS Applied Polymer Materials* 2019;1:593–611. <https://doi.org/10.1021/acsapm.8b00165>.
- [163] Cooperstein I, Sachyani-Keneth E, Shukrun-Farrell E, Rosental T, Wang X, Kamyshny A, et al. Hybrid Materials for Functional 3D Printing. *Advanced Materials Interfaces* 2018;5:1–15. <https://doi.org/10.1002/admi.201800996>.
- [164] Kuang X, Wu J, Chen K, Zhao Z, Ding Z, Hu F, et al. Grayscale digital light processing 3D printing for highly functionally graded materials.

Science Advances 2019;5:eaav5790.
<https://doi.org/10.1126/sciadv.aav5790>.

- [165] Yu C, Schimelman J, Wang P, Miller KL, Ma X, You S, et al. Photopolymerizable Biomaterials and Light-Based 3D Printing Strategies for Biomedical Applications. *Chemical Reviews* 2020;120:10695–743. <https://doi.org/10.1021/acs.chemrev.9b00810>.
- [166] Grigoryan B, Paulsen SJ, Corbett DC, Sazer DW, Fortin CL, Zaita AJ, et al. Multivascular networks and functional intravascular topologies within biocompatible hydrogels. *Science* (1979) 2019;364:458–64. <https://doi.org/10.1126/science.aav9750>.
- [167] Xu X, Awad A, Robles-Martinez P, Gaisford S, Goyanes A, Basit AW. Vat photopolymerization 3D printing for advanced drug delivery and medical device applications. *Journal of Controlled Release* 2021;329:743–57. <https://doi.org/10.1016/j.jconrel.2020.10.008>.
- [168] Miri AK, Khalilpour A, Cecen B, Maharjan S, Shin SR, Khademhosseini A. Multiscale bioprinting of vascularized models. *Biomaterials* 2019;198:204–16. <https://doi.org/10.1016/j.biomaterials.2018.08.006>.
- [169] Lee JM, Ng WL, Yeong WY. Resolution and shape in bioprinting: Strategizing towards complex tissue and organ printing. *Applied Physics Reviews* 2019;6. <https://doi.org/10.1063/1.5053909>.
- [170] Zhang J, Xiao P. 3D printing of photopolymers. *Polymer Chemistry* 2018;9:1530–40. <https://doi.org/10.1039/c8py00157j>.
- [171] Pagac M, Hajnys J, Ma QP, Jancar L, Jansa J, Stefek P, et al. A review of vat photopolymerization technology: Materials, applications, challenges, and future trends of 3d printing. *Polymers (Basel)* 2021;13:1–20. <https://doi.org/10.3390/polym13040598>.
- [172] Zhang F, Zhu L, Li Z, Wang S, Shi J, Tang W, et al. The recent development of vat photopolymerization: a review. *Additive Manufacturing* 2021:102423. <https://doi.org/10.1016/j.addma.2021.102423>.
- [173] Touri M, Kabirian F, Saadati M, Ramakrishna S, Mozafari M. *Additive Manufacturing of Biomaterials – The Evolution of Rapid Prototyping*.

- [174] Herzberger J, Sirrine JM, Williams CB, Long TE. Polymer Design for 3D Printing Elastomers: Recent Advances in Structure, Properties, and Printing. *Progress in Polymer Science* 2019;97:101144. <https://doi.org/10.1016/j.progpolymsci.2019.101144>.
- [175] Wu J, Zhao Z, Hamel CM, Mu X, Kuang X, Guo Z, et al. Evolution of material properties during free radical photopolymerization. *Journal of the Mechanics and Physics of Solids* 2018;112:25–49. <https://doi.org/10.1016/j.jmps.2017.11.018>.
- [176] Husár B, Ligon SC, Wutzel H, Hoffmann H, Liska R. The formulator's guide to anti-oxygen inhibition additives. *Progress in Organic Coatings* 2014;77:1789–98. <https://doi.org/10.1016/J.PORGCOAT.2014.06.005>.
- [177] Taormina G, Sciancalepore C, Messori M, Bondioli F. 3D printing processes for photocurable polymeric materials: technologies, materials, and future trends. *Journal of Applied Biomaterials and Functional Materials* 2018;16:151–60. <https://doi.org/10.1177/2280800018764770>.
- [178] Ng WL, Lee JM, Zhou M, Chen YW, Lee KXA, Yeong WY, et al. Vat polymerization-based bioprinting - process, materials, applications and regulatory challenges. *Biofabrication* 2020;12. <https://doi.org/10.1088/1758-5090/ab6034>.
- [179] Naik DL, Kiran R. On anisotropy, strain rate and size effects in vat photopolymerization based specimens. *Additive Manufacturing* 2018;23:181–96. <https://doi.org/10.1016/J.ADDMA.2018.08.021>.
- [180] Nadgorny M, Ameli A. Functional Polymers and Nanocomposites for 3D Printing of Smart Structures and Devices. *ACS Applied Materials and Interfaces* 2018;10:17489–507. <https://doi.org/10.1021/acsami.8b01786>.
- [181] Sampson KL, Deore B, Go A, Nayak MA, Orth A, Gallerneault M, et al. Multimaterial Vat Polymerization Additive Manufacturing. *ACS Applied Polymer Materials* 2021. <https://doi.org/10.1021/acsapm.1c00262>.

- [182] Maines EM, Porwal MK, Ellison CJ, Reineke TM. Sustainable advances in SLA/DLP 3D printing materials and processes. *Green Chemistry* 2021;23:6863–97. <https://doi.org/10.1039/D1GC01489G>.
- [183] Kelly BE, Bhattacharya I, Heidari H, Shusteff M, Spadaccini CM, Taylor HK. Volumetric additive manufacturing via tomographic reconstruction. *Science* (1979) 2019;363:1075–9. <https://doi.org/10.1126/science.aau7114>.
- [184] Melchels FPW, Feijen J, Grijpma DW. A review on stereolithography and its applications in biomedical engineering. *Biomaterials* 2010;31:6121–30. <https://doi.org/10.1016/j.biomaterials.2010.04.050>.
- [185] Msallem B, Sharma N, Cao S, Halbeisen FS, Zeilhofer H-F, Thieringer FM. Evaluation of the Dimensional Accuracy of 3D-Printed Anatomical Mandibular Models Using FFF, SLA, SLS, MJ, and BJ Printing Technology. *Journal of Clinical Medicine* 2020;9:817. <https://doi.org/10.3390/jcm9030817>.
- [186] Zhao W, Wang Z, Zhang J, Wang X, Xu Y, Ding N, et al. Vat Photopolymerization 3D Printing of Advanced Soft Sensors and Actuators: From Architecture to Function. *Advanced Materials Technologies* 2021;6:2001218. <https://doi.org/10.1002/admt.202001218>.
- [187] Lim KS, Galarraga JH, Cui X, Lindberg GCJ, Burdick JA, Woodfield TBF. Fundamentals and Applications of Photo-Cross-Linking in Bioprinting. *Chemical Reviews* 2020;120:10662–94. <https://doi.org/10.1021/acs.chemrev.9b00812>.
- [188] Tumbleston JR, Shirvanyants D, Ermoshkin N, Januszewicz R, Johnson AR, Kelly D, et al. Continuous liquid interface production of 3D objects. *Science* (1979) 2015;347:1349–52. <https://doi.org/10.1126/science.aaa2397>.
- [189] Ligon-Auer SC, Schwentenwein M, Gorsche C, Stampfl J, Liska R. Toughening of photo-curable polymer networks: A review. *Polymer Chemistry* 2016;7:257–86. <https://doi.org/10.1039/c5py01631b>.
- [190] Layani M, Wang X, Magdassi S. Novel Materials for 3D Printing by Photopolymerization. *Advanced Materials* 2018;30:1706344. <https://doi.org/10.1002/adma.201706344>.

- [191] Crivello J v., Reichmanis E. Photopolymer materials and processes for advanced technologies. *Chemistry of Materials* 2014;26:533–48. <https://doi.org/10.1021/cm402262g>.
- [192] Cowie JMG, Arrighi V. *Polymers: Chemistry and Physics of Modern Materials*, Third Edition 2007. <https://doi.org/10.1201/9781420009873>.
- [193] Odian G. *Principles of Polymerization*. Principles of Polymerization 2004. <https://doi.org/10.1002/047147875X>.
- [194] Asua JM, Beuermann S, Buback M, Castignolles P, Charleux B, Gilbert RG, et al. Critically Evaluated Rate Coefficients for Free-Radical Polymerization, 5,. *Macromolecular Chemistry and Physics* 2004;205:2151–60. <https://doi.org/10.1002/MACP.200400355>.
- [195] Jafferson JM, Chatterjee D. A review on polymeric materials in additive manufacturing. *Materials Today: Proceedings* 2021;46:1349–65. <https://doi.org/10.1016/j.matpr.2021.02.485>.
- [196] Beuermann S, Paquet DA, McMinn JH, Hutchinson RA. Determination of free-radical propagation rate coefficients of butyl, 2-ethylhexyl, and dodecyl acrylates by pulsed-laser polymerization. *Macromolecules* 1996;29:4206–15. <https://doi.org/10.1021/MA960081C/ASSET/IMAGES/LARGE/MA960081CF00013.JPEG>.
- [197] Choi JR, Yong KW, Choi JY, Cowie AC. Recent advances in photocrosslinkable hydrogels for biomedical applications. *Biotechniques* 2019;66:40–53. <https://doi.org/10.2144/btn-2018-0083>.
- [198] Mondschein RJ, Kanitkar A, Williams CB, Verbridge SS, Long TE. Polymer structure-property requirements for stereolithographic 3D printing of soft tissue engineering scaffolds. *Biomaterials* 2017;140:170–88. <https://doi.org/10.1016/j.biomaterials.2017.06.005>.
- [199] Schuster M, Turecek C, Kaiser B, Stampfl J, Liska R, Varga F. Biocompatible Photopolymers I: Photoreactivity and Mechanical Properties of Reactive Diluents. *Journal of Macromolecular Science, Part A* 2007;44:547–57. <https://doi.org/10.1080/10601320701235958>.

- [200] Kim LU, Kim JW, Kim CK. Effects of molecular structure of the resins on the volumetric shrinkage and the mechanical strength of dental restorative composites. *Biomacromolecules* 2006;7:2680–7. <https://doi.org/10.1021/BM060453H/ASSET/IMAGES/LARGE/BM060453HF00007.JPEG>.
- [201] Kannurpatti AR, Anseth JW, Bowman CN. A study of the evolution of mechanical properties and structural heterogeneity of polymer networks formed by photopolymerizations of multifunctional (meth)acrylates. *Polymer (Guildf)* 1998;39:2507–13. [https://doi.org/10.1016/S0032-3861\(97\)00585-5](https://doi.org/10.1016/S0032-3861(97)00585-5).
- [202] Kade MJ, Burke DJ, Hawker CJ. The power of thiol-ene chemistry. *Journal of Polymer Science Part A: Polymer Chemistry* 2010;48:743–50. <https://doi.org/10.1002/POLA.23824>.
- [203] Nair DP, Podgórski M, Chatani S, Gong T, Xi W, Fenoli CR, et al. The Thiol-Michael addition click reaction: A powerful and widely used tool in materials chemistry. *Chemistry of Materials* 2014;26:724–44. <https://doi.org/10.1021/cm402180t>.
- [204] Hoyle CE, Lee TY, Roper T. Thiol–enes: Chemistry of the past with promise for the future. *Journal of Polymer Science Part A: Polymer Chemistry* 2004;42:5301–38. <https://doi.org/10.1002/POLA.20366>.
- [205] Cramer NB, Bowman CN. Kinetics of thiol-ene and thiol-acrylate photopolymerizations with real-time Fourier transform infrared. *Journal of Polymer Science, Part A: Polymer Chemistry* 2001;39:3311–9. <https://doi.org/10.1002/pola.1314>.
- [206] Bertlein S, Brown G, Lim KS, Jungst T, Boeck T, Blunk T, et al. Thiol–Ene Clickable Gelatin: A Platform Bioink for Multiple 3D Biofabrication Technologies. *Advanced Materials* 2017;29:1–6. <https://doi.org/10.1002/adma.201703404>.
- [207] Hoyle CE, Bowman CN. Thiol-ene click chemistry. *Angewandte Chemie - International Edition* 2010;49:1540–73. <https://doi.org/10.1002/anie.200903924>.

- [208] Lowe AB. Thiol-ene “click” reactions and recent applications in polymer and materials synthesis. *Polymer Chemistry* 2010;1:17–36. <https://doi.org/10.1039/B9PY00216B>.
- [209] Rydholm AE, Reddy SK, Anseth KS, Bowman CN. Controlling network structure in degradable thiol-acrylate biomaterials to tune mass loss behavior. *Biomacromolecules* 2006;7:2827–36. <https://doi.org/10.1021/BM0603793/ASSET/IMAGES/LARGE/BM0603793F00013.JPEG>.
- [210] Lu H, Carioscia JA, Stansbury JW, Bowman CN. Investigations of step-growth thiol-ene polymerizations for novel dental restoratives. *Dental Materials* 2005;21:1129–36. <https://doi.org/10.1016/J.DENTAL.2005.04.001>.
- [211] Kloxin JC, Scott FT, Bowman NC. Stress relaxation via addition fragmentation chain transfer in a thiol-ene photopolymerization. *Macromolecules* 2009;42:2551–6. https://doi.org/10.1021/MA802771B/ASSET/IMAGES/LARGE/MA-2008-02771B_0010.JPEG.
- [212] Roppolo I, Frascella F, Gastaldi M, Castellino M, Ciubini B, Barolo C, et al. Thiol-yne chemistry for 3D printing: Exploiting an off-stoichiometric route for selective functionalization of 3D objects. *Polymer Chemistry* 2019;10:5950–8. <https://doi.org/10.1039/c9py00962k>.
- [213] Ifkovits JL, Burdick JA. Review: Photopolymerizable and Degradable Biomaterials for Tissue Engineering Applications. <https://HomeLiebertpubCom/Ten> 2007;13:2369–85. <https://doi.org/10.1089/TEN.2007.0093>.
- [214] Xiao P, Zhang J, Dumur F, Tehfe MA, Morlet-Savary F, Graff B, et al. Visible light sensitive photoinitiating systems: Recent progress in cationic and radical photopolymerization reactions under soft conditions. *Progress in Polymer Science* 2015;41:32–66. <https://doi.org/10.1016/j.progpolymsci.2014.09.001>.
- [215] Fouassier JP, Lalevée J. Photoinitiators for Polymer Synthesis: Scope, Reactivity and Efficiency. 2012. <https://doi.org/10.1002/9783527648245>.

- [216] Jasinski F, Zetterlund PB, Braun AM, Chemtob A. Photopolymerization in dispersed systems. *Progress in Polymer Science* 2018;84:47–88. <https://doi.org/10.1016/J.PROGPOLYMSCI.2018.06.006>.
- [217] Warner J, Soman P, Zhu W, Tom M, Chen S. Design and 3D Printing of Hydrogel Scaffolds with Fractal Geometries. *ACS Biomaterials Science and Engineering* 2016;2:1763–70. https://doi.org/10.1021/ACSBiomaterials.6B00140/ASSET/IMAGES/LARGE/AB-2016-00140Y_0003.JPEG.
- [218] Bryant SJ, Nuttelman CR, Anseth KS. Cytocompatibility of UV and visible light photoinitiating systems on cultured NIH/3T3 fibroblasts in vitro. *Journal of Biomaterials Science, Polymer Edition* 2000;11:439–57. <https://doi.org/10.1163/156856200743805>.
- [219] Lavker R, Kaidbey K. The Spectral Dependence for UVA-Induced Cumulative Damage in Human Skin. *Journal of Investigative Dermatology* 1997;108:17–21. <https://doi.org/10.1111/1523-1747.EP12285613>.
- [220] Fedorovich NE, Oudshoorn MH, van Geemen D, Hennink WE, Alblas J, Dhert WJA. The effect of photopolymerization on stem cells embedded in hydrogels. *Biomaterials* 2009;30:344–53. <https://doi.org/10.1016/j.biomaterials.2008.09.037>.
- [221] Fantino E, Chiappone A, Calignano F, Fontana M, Pirri F, Roppolo I. In Situ Thermal Generation of Silver Nanoparticles in 3D Printed Polymeric Structures. *Materials* 2016;9:589. <https://doi.org/10.3390/ma9070589>.
- [222] Fantino E, Chiappone A, Roppolo I, Manfredi D, Bongiovanni R, Pirri CF, et al. 3D Printing of Conductive Complex Structures with in Situ Generation of Silver Nanoparticles. *Advanced Materials* 2016;28:3712–7. <https://doi.org/10.1002/adma.201505109>.
- [223] Chan V, Zorlutuna P, Jeong JH, Kong H, Bashir R. Three-dimensional photopatterning of hydrogels using stereolithography for long-term cell encapsulation. *Lab on a Chip* 2010;10:2062. <https://doi.org/10.1039/c004285d>.
- [224] Stassi S, Fantino E, Calmo R, Chiappone A, Gillono M, Scaiola D, et al. Polymeric 3D Printed Functional Microcantilevers for Biosensing

- Applications. *ACS Applied Materials and Interfaces* 2017;9:19193–201. <https://doi.org/10.1021/acsami.7b04030>.
- [225] Patel DK, Sakhaei AH, Layani M, Zhang B, Ge Q, Magdassi S. Highly Stretchable and UV Curable Elastomers for Digital Light Processing Based 3D Printing. *Advanced Materials* 2017;29:1606000. <https://doi.org/10.1002/adma.201606000>.
- [226] Shukrun E, Cooperstein I, Magdassi S. 3D-Printed Organic–Ceramic Complex Hybrid Structures with High Silica Content. *Advanced Science* 2018;5:1–7. <https://doi.org/10.1002/advs.201800061>.
- [227] Dietliker K, Hüsler R, Birbaum JL, Ilg S, Villeneuve S, Studer K, et al. Advancements in photoinitiators-Opening up new applications for radiation curing. *Progress in Organic Coatings* 2007;58:146–57. <https://doi.org/10.1016/j.porgcoat.2006.08.021>.
- [228] Lalevée J, Fouassier JP, Graff B, Zhang J, Xiao P. Chapter 6: How to Design Novel Photoinitiators for Blue Light. *RSC Polymer Chemistry Series* 2018;2018-Janua:179–99. <https://doi.org/10.1039/9781788013307-00179>.
- [229] Jauk S, Liska R. Photoinitiators with Functional Groups, 8. *Macromolecular Rapid Communications* 2005;26:1687–92. <https://doi.org/10.1002/MARC.200500507>.
- [230] Fors BP, Hawker CJ, Fors BP, Hawker CJ. Control of a Living Radical Polymerization of Methacrylates by Light. *Angewandte Chemie International Edition* 2012;51:8850–3. <https://doi.org/10.1002/ANIE.201203639>.
- [231] Ohtsuki A, Goto A, Kaji H. Visible-light-induced reversible complexation mediated living radical polymerization of methacrylates with organic catalysts. *Macromolecules* 2013;46:96–102. https://doi.org/10.1021/MA302244J/SUPPL_FILE/MA302244J_SI_001.PDF.
- [232] Lim KS, Schon BS, Mekhileri N v., Brown GCJ, Chia CM, Prabakar S, et al. New Visible-Light Photoinitiating System for Improved Print Fidelity in

Gelatin-Based Bioinks. *ACS Biomaterials Science and Engineering* 2016;2:1752–62. <https://doi.org/10.1021/acsbiomaterials.6b00149>.

- [233] Lim KS, Klotz BJ, Lindberg GCJ, Melchels FPW, Hooper GJ, Malda J, et al. Visible Light Cross-Linking of Gelatin Hydrogels Offers an Enhanced Cell Microenvironment with Improved Light Penetration Depth. *Macromolecular Bioscience* 2019;19:1900098. <https://doi.org/10.1002/mabi.201900098>.
- [234] Gastaldi M, Cardano F, Zanetti M, Viscardi G, Barolo C, Bordiga S, et al. Functional Dyes in Polymeric 3D Printing: Applications and Perspectives. *ACS Materials Letters* 2021;3:1–17. <https://doi.org/10.1021/acsmaterialslett.0c00455>.
- [235] Lim KS, Levato R, Costa PF, Castilho MD, Alcala-Orozco CR, van Dorenmalen KMA, et al. Bio-resin for high resolution lithography-based biofabrication of complex cell-laden constructs. *Biofabrication* 2018;10:034101. <https://doi.org/10.1088/1758-5090/aac00c>.
- [236] Roppolo I, Chiappone A, Angelini A, Stassi S, Frascella F, Pirri CF, et al. 3D printable light-responsive polymers. *Materials Horizons* 2017;4:396–401. <https://doi.org/10.1039/c7mh00072c>.
- [237] Lantean S, Roppolo I, Sangermano M, Pirri C, Chiappone A. Development of New Hybrid Acrylic/Epoxy DLP-3D Printable Materials. *Inventions* 2018;3:29. <https://doi.org/10.3390/inventions3020029>.
- [238] Wu MC, Lin MP, Chen SW, Lee PH, Li JH, Su WF. Surface-enhanced Raman scattering substrate based on a Ag coated monolayer array of SiO₂ spheres for organic dye detection. *RSC Advances* 2014;4:10043–50. <https://doi.org/10.1039/c3ra45255g>.
- [239] Wallin TJ, Pikul JH, Bodkhe S, Peele BN, mac Murray BC, Therriault D, et al. Click chemistry stereolithography for soft robots that self-heal. *Journal of Materials Chemistry B* 2017;5:6249–55. <https://doi.org/10.1039/c7tb01605k>.
- [240] Sanders P, Young AJ, Qin Y, Fancey KS, Reithofer MR, Guillet-Nicolas R, et al. Stereolithographic 3D printing of extrinsically self-healing

- composites. *Scientific Reports* 2019;9:388. <https://doi.org/10.1038/s41598-018-36828-9>.
- [241] Yu K, Xin A, Du H, Li Y, Wang Q. Additive manufacturing of self-healing elastomers. *NPG Asia Materials* 2019;11. <https://doi.org/10.1038/s41427-019-0109-y>.
- [242] Yu K, Du H, Xin A, Lee KH, Feng Z, Masri SF, et al. Healable, memorizable, and transformable lattice structures made of stiff polymers. *NPG Asia Materials* 2020;12:26. <https://doi.org/10.1038/s41427-020-0208-9>.
- [243] Li X, Yu R, He Y, Zhang Y, Yang X, Zhao X, et al. Self-Healing Polyurethane Elastomers Based on a Disulfide Bond by Digital Light Processing 3D Printing. *ACS Macro Letters* 2019;8:1511–6. <https://doi.org/10.1021/acsmacrolett.9b00766>.
- [244] Zhang B, Kowsari K, Serjouei A, Dunn ML, Ge Q. Reprocessable thermosets for sustainable three-dimensional printing. *Nature Communications* 2018;9:1831. <https://doi.org/10.1038/s41467-018-04292-8>.
- [245] Gao H, Sun Y, Wang M, Wang Z, Han G, Jin L, et al. Mechanically Robust and Reprocessable Acrylate Vitrimers with Hydrogen-Bond-Integrated Networks for Photo-3D Printing. *ACS Applied Materials and Interfaces* 2021;13:1581–91. <https://doi.org/10.1021/acsaami.0c19520>.
- [246] Rossegger E, Höller R, Reisinger D, Strasser J, Fleisch M, Griesser T, et al. Digital light processing 3D printing with thiol-Acrylate vitrimers. *Polymer Chemistry* 2021;12:638–44. <https://doi.org/10.1039/d0py01520b>.
- [247] Yu K, Feng Z, Du H, Xin A, Lee KH, Li K, et al. Photosynthesis-assisted remodeling of three-dimensional printed structures. *Proc Natl Acad Sci U S A* 2021;118:1–9. <https://doi.org/10.1073/pnas.2016524118>.
- [248] Fang Z, Song H, Zhang Y, Jin B, Wu J, Zhao Q, et al. Modular 4D Printing via Interfacial Welding of Digital Light-Controllable Dynamic Covalent Polymer Networks. *Matter* 2020;2:1187–97. <https://doi.org/10.1016/j.matt.2020.01.014>.

- [249] Invernizzi M, Turri S, Levi M, Suriano R. 4D printed thermally activated self-healing and shape memory polycaprolactone-based polymers. *European Polymer Journal* 2018;101:169–76. <https://doi.org/10.1016/j.eurpolymj.2018.02.023>.
- [250] Guo B, Ji X, Chen X, Li G, Lu Y, Bai J. A highly stretchable and intrinsically self-healing strain sensor produced by 3D printing. *Virtual and Physical Prototyping* 2020;15:520–31. <https://doi.org/10.1080/17452759.2020.1823570>.
- [251] Chen H, Ge P, Yan Z, Chen M, Dai X, Zhuo H, et al. 3D Printable, Biomimetic Adhesive, and Self-healing Acrylic Elastomers for Customized Attachable Strain Sensor. *Chemical Engineering Journal* 2021;133111. <https://doi.org/10.1016/j.cej.2021.133111>.
- [252] Wu Y, Zeng Y, Chen Y, Li C, Qiu R, Liu W. Photocurable 3D Printing of High Toughness and Self-Healing Hydrogels for Customized Wearable Flexible Sensors. *Advanced Functional Materials* 2021;2107202:2107202. <https://doi.org/10.1002/adfm.202107202>.
- [253] Liu Z, Hong P, Huang Z, Zhang T, Xu R, Chen L, et al. Self-healing, reprocessing and 3D printing of transparent and hydrolysis-resistant silicone elastomers. *Chemical Engineering Journal* 2020;387:124142. <https://doi.org/10.1016/j.cej.2020.124142>.
- [254] Zhu G, Hou Y, Xiang J, Xu J, Zhao N. Digital Light Processing 3D Printing of Healable and Recyclable Polymers with Tailorable Mechanical Properties. *ACS Applied Materials and Interfaces* 2021;13:34954–61. <https://doi.org/10.1021/acsami.1c08872>.
- [255] Valentin TM, Dubois EM, Machnicki CE, Bhaskar D, Cui FR, Wong IY. 3D printed self-adhesive PEGDA-PAA hydrogels as modular components for soft actuators and microfluidics. *Polymer Chemistry* 2019;10:2015–28. <https://doi.org/10.1039/c9py00211a>.
- [256] Zhang B, Zhang W, Zhang Z, Zhang YF, Hingorani H, Liu Z, et al. Self-Healing Four-Dimensional Printing with an Ultraviolet Curable Double-Network Shape Memory Polymer System. *ACS Applied Materials and Interfaces* 2019;11:10328–36. <https://doi.org/10.1021/acsami.9b00359>.

- [257] Ceylan Tuncaboylu D. Photo-crosslinked mechanically strong PCL4-PDMAEM hydrogels. *Reactive and Functional Polymers* 2018;126:44–51. <https://doi.org/10.1016/j.reactfunctpolym.2018.03.001>.
- [258] Han D, Lu Z, Chester SA, Lee H. Micro 3D Printing of a Temperature-Responsive Hydrogel Using Projection Micro-Stereolithography. *Scientific Reports* 2018;8:1963. <https://doi.org/10.1038/s41598-018-20385-2>.
- [259] Park S, Shin BG, Jang S, Chung K. Three-Dimensional Self-Healable Touch Sensing Artificial Skin Device. *ACS Applied Materials and Interfaces* 2020;12:3953–60. <https://doi.org/10.1021/acsami.9b19272>.
- [260] Hong S, Sycks D, Chan HF, Lin S, Lopez GP, Guilak F, et al. 3D Printing of Highly Stretchable and Tough Hydrogels into Complex, Cellularized Structures. *Advanced Materials* 2015;27:4035–40. <https://doi.org/10.1002/adma.201501099>.
- [261] Jian Y, Handschuh-Wang S, Zhang J, Lu W, Zhou X, Chen T. Biomimetic anti-freezing polymeric hydrogels: Keeping soft-wet materials active in cold environments. *Materials Horizons* 2021;8:351–69. <https://doi.org/10.1039/d0mh01029d>.
- [262] Naranjo A, Martín C, López-Díaz A, Martín-Pacheco A, Rodríguez AM, Patiño FJ, et al. Autonomous self-healing hydrogel with anti-drying properties and applications in soft robotics. *Applied Materials Today* 2020;21. <https://doi.org/10.1016/j.apmt.2020.100806>.
- [263] Zhong M, Liu XY, Shi FK, Zhang LQ, Wang XP, Cheetham AG, et al. Self-healable, tough and highly stretchable ionic nanocomposite physical hydrogels. *Soft Matter* 2015;11:4235–41. <https://doi.org/10.1039/c5sm00493d>.
- [264] Gharakhloo M, Karbarz M. Autonomous self-healing hydrogels: Recent development in fabrication strategies. *European Polymer Journal* 2022;165:111004. <https://doi.org/10.1016/j.eurpolymj.2022.111004>.
- [265] Jungst T, Smolan W, Schacht K, Scheibel T, Groll J. Strategies and Molecular Design Criteria for 3D Printable Hydrogels. *Chemical Reviews* 2016;116:1496–539. <https://doi.org/10.1021/acs.chemrev.5b00303>.

- [266] Wallin TJ, Pikul J, Shepherd RF. 3D printing of soft robotic systems. *Nature Reviews Materials* 2018;3:84–100. <https://doi.org/10.1038/s41578-018-0002-2>.
- [267] Chen D, Wang D, Yang Y, Huang Q, Zhu S, Zheng Z. Self-healing materials for next-generation energy harvesting and storage devices. *Advanced Energy Materials* 2017;7:1700890. <https://doi.org/10.1002/aenm.201700890>.
- [268] Waheed S, Cabot JM, Macdonald NP, Lewis T, Guijt RM, Paull B, et al. 3D printed microfluidic devices: Enablers and barriers. *Lab on a Chip* 2016;16:1993–2013. <https://doi.org/10.1039/c6lc00284f>.
- [269] Hayashi M. Implantation of recyclability and healability into cross-linked commercial polymers by applying the vitrimer concept. *Polymers (Basel)* 2020;12. <https://doi.org/10.3390/POLYM12061322>.
- [270] Zhu G, Hou Y, Xu J, Zhao N. Reprintable Polymers for Digital Light Processing 3D Printing. *Advanced Functional Materials* 2021;31:2007173. <https://doi.org/10.1002/adfm.202007173>.
- [271] Puppi D, Chiellini F. Biodegradable Polymers for Biomedical Additive Manufacturing. *Applied Materials Today* 2020;20. <https://doi.org/10.1016/j.apmt.2020.100700>.
- [272] Chen Z, Yang M, Ji M, Kuang X, Qi HJ, Wang T. Recyclable thermosetting polymers for digital light processing 3D printing. *Materials and Design* 2021;197:109189. <https://doi.org/10.1016/j.matdes.2020.109189>.
- [273] Shi Q, Yu K, Kuang X, Mu X, Dunn CK, Dunn ML, et al. Recyclable 3D printing of vitrimer epoxy. *Materials Horizons* 2017;4:598–607. <https://doi.org/10.1039/c7mh00043j>.
- [274] Shahbazi M, Jäger H. Current Status in the Utilization of Biobased Polymers for 3D Printing Process: A Systematic Review of the Materials, Processes, and Challenges. *ACS Applied Bio Materials* 2021;4:325–69. <https://doi.org/10.1021/acsabm.0c01379>.

- [275] Perera MM, Ayres N. Dynamic covalent bonds in self-healing, shape memory, and controllable stiffness hydrogels. *Polymer Chemistry* 2020;11:1410–23. <https://doi.org/10.1039/c9py01694e>.
- [276] Joshi S, Rawat K, C K, Rajamohan V, Mathew AT, Koziol K, et al. 4D printing of materials for the future: Opportunities and challenges. *Applied Materials Today* 2020;18:100490. <https://doi.org/10.1016/j.apmt.2019.100490>.
- [277] González-Henríquez CM, Sarabia-Vallejos MA, Rodríguez-Hernandez J. Polymers for additive manufacturing and 4D-printing: Materials, methodologies, and biomedical applications. *Progress in Polymer Science* 2019;94:57–116. <https://doi.org/10.1016/j.progpolymsci.2019.03.001>.
- [278] Momeni F, M.Mehdi Hassani.N S, Liu X, Ni J. A review of 4D printing. *Materials and Design* 2017;122:42–79. <https://doi.org/10.1016/j.matdes.2017.02.068>.
- [279] Creton C. 50th Anniversary Perspective: Networks and Gels: Soft but Dynamic and Tough. *Macromolecules* 2017;50:8297–316. <https://doi.org/10.1021/acs.macromol.7b01698>.
- [280] Li J, Wu C, Chu PK, Gelinsky M. 3D printing of hydrogels: Rational design strategies and emerging biomedical applications. *Materials Science and Engineering R: Reports* 2020;140:100543. <https://doi.org/10.1016/j.mser.2020.100543>.
- [281] Hoffman AS. Hydrogels for biomedical applications. *Advanced Drug Delivery Reviews* 2012;64:18–23. <https://doi.org/10.1016/j.addr.2012.09.010>.
- [282] Champeau M, Heinze DA, Viana TN, de Souza ER, Chinellato AC, Titotto S. 4D Printing of Hydrogels: A Review. *Advanced Functional Materials* 2020;30:1910606. <https://doi.org/10.1002/adfm.201910606>.
- [283] Peng K, Zheng L, Zhou T, Zhang C, Li H. Light Manipulation for Fabrication of Hydrogels and Their Biological Applications. *Acta Biomaterialia* 2021. <https://doi.org/10.1016/j.actbio.2021.10.003>.

- [284] Yao H, Wang J, Mi S. Photo processing for biomedical hydrogels design and functionality: A review. *Polymers (Basel)* 2017;10:11. <https://doi.org/10.3390/polym10010011>.
- [285] Danek C. Recent Advances and Future Challenges in the Additive Manufacturing of Hydrogels. *Polymers (Basel)* 2022;14:494. <https://doi.org/10.3390/polym14030494>.
- [286] Annabi N, Tamayol A, Uquillas JA, Akbari M, Bertassoni LE, Cha C, et al. 25th anniversary article: Rational design and applications of hydrogels in regenerative medicine. *Advanced Materials* 2014;26:85–124. <https://doi.org/10.1002/adma.201303233>.
- [287] Wang J, Stanic S, Altun AA, Schwentenwein M, Dietliker K, Jin L, et al. A highly efficient waterborne photoinitiator for visible-light-induced three-dimensional printing of hydrogels. *Chemical Communications* 2018;54:920–3. <https://doi.org/10.1039/c7cc09313f>.
- [288] Tomal W, Ortyl J. Water-soluble photoinitiators in biomedical applications. *Polymers (Basel)* 2020;12:1–30. <https://doi.org/10.3390/POLYM12051073>.
- [289] Fairbanks BD, Schwartz MP, Bowman CN, Anseth KS. Photoinitiated polymerization of PEG-diacrylate with lithium phenyl-2,4,6-trimethylbenzoylphosphinate: polymerization rate and cytocompatibility. *Biomaterials* 2009;30:6702–7. <https://doi.org/10.1016/j.biomaterials.2009.08.055>.
- [290] Pawar AA, Saada G, Cooperstein I, Larush L, Jackman JA, Tabaei SR, et al. High-performance 3D printing of hydrogels by water-dispersible photoinitiator nanoparticles. *Science Advances* 2016;2:e1501381–e1501381. <https://doi.org/10.1126/sciadv.1501381>.
- [291] Zhao J, Lalevée J, Lu H, MacQueen R, Kable SH, Schmidt TW, et al. A new role of curcumin: As a multicolor photoinitiator for polymer fabrication under household UV to red LED bulbs. *Polymer Chemistry* 2015;6:5053–61. <https://doi.org/10.1039/c5py00661a>.
- [292] Zhao X, Zhao Y, Li M de, Li Z, Peng H, Xie T, et al. Efficient 3D printing via photooxidation of ketocoumarin based photopolymerization. *Nature*

- Communications 2021;12:1–8. <https://doi.org/10.1038/s41467-021-23170-4>.
- [293] Sakai S, Kamei H, Mori T, Hotta T, Ohi H, Nakahata M, et al. Visible Light-Induced Hydrogelation of an Alginate Derivative and Application to Stereolithographic Bioprinting Using a Visible Light Projector and Acid Red. *Biomacromolecules* 2018;19:672–9. <https://doi.org/10.1021/acs.biomac.7b01827>.
- [294] Gillispie G, Prim P, Copus J, Fisher J, Mikos AG, Yoo JJ, et al. Assessment methodologies for extrusion-based bioink printability. *Biofabrication* 2020;12. <https://doi.org/10.1088/1758-5090/ab6f0d>.
- [295] Pekkanen AM, Mondschein RJ, Williams CB, Long TE. 3D Printing Polymers with Supramolecular Functionality for Biological Applications. *Biomacromolecules* 2017;18:2669–87. <https://doi.org/10.1021/acs.biomac.7b00671>.
- [296] Truby RL, Lewis JA. Printing soft matter in three dimensions. *Nature* 2016;540:371–8. <https://doi.org/10.1038/nature21003>.
- [297] Dragan ES. Design and applications of interpenetrating polymer network hydrogels. A review. *Chemical Engineering Journal* 2014;243:572–90. <https://doi.org/10.1016/j.cej.2014.01.065>.
- [298] Bedell ML, Navara AM, Du Y, Zhang S, Mikos AG. Polymeric Systems for Bioprinting. *Chemical Reviews* 2020;120:10744–92. <https://doi.org/10.1021/acs.chemrev.9b00834>.
- [299] Schwab A, Levato R, D’Este M, Piluso S, Eglin D, Malda J. Printability and Shape Fidelity of Bioinks in 3D Bioprinting. *Chemical Reviews* 2020;120:11028–55. <https://doi.org/10.1021/acs.chemrev.0c00084>.
- [300] Heidarian P, Kouzani AZ, Kaynak A, Paulino M, Nasri-Nasrabadi B. Dynamic Hydrogels and Polymers as Inks for Three-Dimensional Printing. *ACS Biomaterials Science and Engineering* 2019;5:2688–707. <https://doi.org/10.1021/acsbiomaterials.9b00047>.
- [301] Zhao X. Multi-scale multi-mechanism design of tough hydrogels: building dissipation into stretchy networks. *Soft Matter* 2014;10:672–87. <https://doi.org/10.1039/C3SM52272E>.

- [302] Chimene D, Kaunas R, Gaharwar AK. Hydrogel Bioink Reinforcement for Additive Manufacturing: A Focused Review of Emerging Strategies. *Advanced Materials* 2020;32:1902026. <https://doi.org/10.1002/adma.201902026>.
- [303] Levato R, Jungst T, Scheuring RG, Blunk T, Groll J, Malda J. From Shape to Function: The Next Step in Bioprinting. *Advanced Materials* 2020;32:1906423. <https://doi.org/10.1002/adma.201906423>.
- [304] Cash JJ, Kubo T, Bapat AP, Sumerlin BS. Room-temperature self-healing polymers based on dynamic-covalent boronic esters. *Macromolecules* 2015;48:2098–106. <https://doi.org/10.1021/acs.macromol.5b00210>.
- [305] da Silva LRR, Sales WF, Campos F dos AR, de Sousa JAG, Davis R, Singh A, et al. A comprehensive review on additive manufacturing of medical devices. vol. 6. Springer International Publishing; 2021. <https://doi.org/10.1007/s40964-021-00188-0>.
- [306] Peak CW, Wilker JJ, Schmidt G. A review on tough and sticky hydrogels. *Colloid and Polymer Science* 2013;291:2031–47. <https://doi.org/10.1007/s00396-013-3021-y>.
- [307] Tuncaboylu DC, Argun A, Algi MP, Okay O. Autonomic self-healing in covalently crosslinked hydrogels containing hydrophobic domains. *Polymer (Guildf)* 2013;54:6381–8. <https://doi.org/10.1016/j.polymer.2013.09.051>.
- [308] Chen WP, Hao DZ, Hao WJ, Guo XL, Jiang L. Hydrogel with Ultrafast Self-Healing Property Both in Air and Underwater. *ACS Applied Materials and Interfaces* 2018;10:1258–65. <https://doi.org/10.1021/acsami.7b17118>.
- [309] Darabi MA, Khosrozadeh A, Mbeleck R, Liu Y, Chang Q, Jiang J, et al. Skin-Inspired Multifunctional Autonomic-Intrinsic Conductive Self-Healing Hydrogels with Pressure Sensitivity, Stretchability, and 3D Printability. *Advanced Materials* 2017;29:1700533. <https://doi.org/10.1002/adma.201700533>.
- [310] Shin SH, Lee W, Kim SM, Lee M, Koo JM, Hwang SY, et al. Ion-conductive self-healing hydrogels based on an interpenetrating polymer

- network for a multimodal sensor. *Chemical Engineering Journal* 2019;371:452–60. <https://doi.org/10.1016/j.cej.2019.04.077>.
- [311] Macdougall LJ, Pérez-Madrigal MM, Shaw JE, Inam M, Hoyland JA, O'Reilly R, et al. Self-healing, stretchable and robust interpenetrating network hydrogels. *Biomaterials Science* 2018;6:2932–7. <https://doi.org/10.1039/c8bm00872h>.
- [312] Liu S, Li L. Ultrastretchable and Self-Healing Double-Network Hydrogel for 3D Printing and Strain Sensor. *ACS Applied Materials and Interfaces* 2017;9:26429–37. <https://doi.org/10.1021/acsami.7b07445>.
- [313] Liu S, Kang M, Li K, Yao F, Oderinde O, Fu G, et al. Polysaccharide-templated preparation of mechanically-tough, conductive and self-healing hydrogels. *Chemical Engineering Journal* 2018;334:2222–30. <https://doi.org/10.1016/j.cej.2017.11.103>.
- [314] Chen H, Hao B, Ge P, Chen S. Highly stretchable, self-healing, and 3D printing prefabricatable hydrophobic association hydrogels with the assistance of electrostatic interaction. *Polymer Chemistry* 2020;11:4741–8. <https://doi.org/10.1039/d0py00003e>.
- [315] Hong Y, Kim JM, Jung H, Park K, Hong J, Choi SH, et al. Facile Synthesis of Poly(ethylene oxide)-Based Self-Healable Dynamic Triblock Copolymer Hydrogels. *Biomacromolecules* 2020;21:4913–22. <https://doi.org/10.1021/acs.biomac.0c01140>.
- [316] Liu S, Li L. Recoverable and Self-Healing Double Network Hydrogel Based on κ -Carrageenan. *ACS Applied Materials and Interfaces* 2016;8:29749–58. <https://doi.org/10.1021/acsami.6b11363>.
- [317] Long T, Li Y, Fang X, Sun J. Salt-Mediated Polyampholyte Hydrogels with High Mechanical Strength, Excellent Self-Healing Property, and Satisfactory Electrical Conductivity. *Advanced Functional Materials* 2018;28:1–9. <https://doi.org/10.1002/adfm.201804416>.
- [318] Pan C, Liu L, Chen Q, Zhang Q, Guo G. Tough, Stretchable, Compressive Novel Polymer/Graphene Oxide Nanocomposite Hydrogels with Excellent Self-Healing Performance. *ACS Applied Materials and Interfaces* 2017;9:38052–61. <https://doi.org/10.1021/acsami.7b12932>.

- [319] Xu J, Ren X, Gao G. Salt-inactive hydrophobic association hydrogels with fatigue resistant and self-healing properties. *Polymer (Guildf)* 2018;150:194–203. <https://doi.org/10.1016/j.polymer.2018.07.045>.
- [320] Cao Y, Tan YJ, Li S, Lee WW, Guo H, Cai Y, et al. Self-healing electronic skins for aquatic environments. *Nature Electronics* 2019;2:75–82. <https://doi.org/10.1038/s41928-019-0206-5>.
- [321] Wang Y, Huang H, Wu J, Han L, Yang Z, Jiang Z, et al. Ultrafast Self-Healing, Reusable, and Conductive Polysaccharide-Based Hydrogels for Sensitive Ionic Sensors. *ACS Sustainable Chemistry and Engineering* 2020;8:18506–18. <https://doi.org/10.1021/acssuschemeng.0c06258>.
- [322] Xia NN, Xiong XM, Rong MZ, Zhang MQ, Kong F. Self-Healing of Polymer in Acidic Water toward Strength Restoration through the Synergistic Effect of Hydrophilic and Hydrophobic Interactions. *ACS Applied Materials and Interfaces* 2017;9:37300–9. <https://doi.org/10.1021/acscami.7b11230>.
- [323] Wu S-D, Hsu S hui. 4D bioprintable self-healing hydrogel with shape memory and cryopreserving properties. *Biofabrication* 2021;13:045029. <https://doi.org/10.1088/1758-5090/ac2789>.
- [324] Tuncaboylu DC, Sari M, Oppermann W, Okay O. Tough and self-healing hydrogels formed via hydrophobic interactions. *Macromolecules* 2011;44:4997–5005. <https://doi.org/10.1021/ma200579v>.
- [325] Lei Z, Wu P. Zwitterionic Skins with a Wide Scope of Customizable Functionalities. *ACS Nano* 2018;12:12860–8. <https://doi.org/10.1021/acsnano.8b08062>.
- [326] Gulyuz U, Okay O. Self-healing poly(N-isopropylacrylamide) hydrogels. *European Polymer Journal* 2015;72:12–22. <https://doi.org/10.1016/j.eurpolymj.2015.09.002>.
- [327] Wang H, Zhu H, Fu W, Zhang Y, Xu B, Gao F, et al. A High Strength Self-Healable Antibacterial and Anti-Inflammatory Supramolecular Polymer Hydrogel. *Macromolecular Rapid Communications* 2017;38:1600695. <https://doi.org/10.1002/marc.201600695>.

- [328] Hager MD, der Zwaag S, Schubert US. *Self-healing Materials*. vol. 273. Cham: Springer International Publishing; 2016. <https://doi.org/10.1007/978-3-319-32778-5>.
- [329] Michael P, Döhler D, Binder WH. Improving autonomous self healing via combined chemical/physical principles. *Polymer (Guildf)* 2015;69:216–27. <https://doi.org/10.1016/j.polymer.2015.01.041>.
- [330] Parida K, Thangavel G, Cai G, Zhou X, Park S, Xiong J, et al. Extremely stretchable and self-healing conductor based on thermoplastic elastomer for all-three-dimensional printed triboelectric nanogenerator. *Nature Communications* 2019;10:2158. <https://doi.org/10.1038/s41467-019-10061-y>.
- [331] Pati S, Singh BP, Dhakate SR. Self-healing Polymer Composites Based on Graphene and Carbon Nanotubes. In: Ponnamma D, Sadasivuni KK, Cabibihan J-J, Al-Maadeed MA-A, editors. *Smart Polymer Nanocomposites*, Cham: Springer International Publishing; 2017, p. 119–52. https://doi.org/10.1007/978-3-319-50424-7_5.
- [332] Okay O. How to Design Both Mechanically Strong and Self-Healable Hydrogels? *Advances in Polymer Science*, vol. 285, 2020, p. 21–62. https://doi.org/10.1007/12_2019_53.
- [333] Zheng SY, Mao S, Yuan J, Wang S, He X, Zhang X, et al. Molecularly Engineered Zwitterionic Hydrogels with High Toughness and Self-Healing Capacity for Soft Electronics Applications. *Chemistry of Materials* 2021. <https://doi.org/10.1021/acs.chemmater.1c02781>.
- [334] Fong R, Robertson A, Mallon P, Thompson R. The Impact of Plasticizer and Degree of Hydrolysis on Free Volume of Poly(vinyl alcohol) Films. *Polymers (Basel)* 2018;10:1036. <https://doi.org/10.3390/polym10091036>.
- [335] Baudis S, Bomze D, Markovic M, Gruber P, Ovsianikov A, Liska R. Modular material system for the microfabrication of biocompatible hydrogels based on thiol-ene-modified poly(vinyl alcohol). *Journal of Polymer Science, Part A: Polymer Chemistry* 2016;54:2060–70. <https://doi.org/10.1002/pola.28073>.

- [336] Hassan CM, Peppas NA. Structure and applications of poly(vinyl alcohol) hydrogels produced by conventional crosslinking or by freezing/thawing methods. *Advances in Polymer Science*, vol. 153, Berlin, Heidelberg: Springer Berlin Heidelberg; 2000, p. 37–65. https://doi.org/10.1007/3-540-46414-x_2.
- [337] Alves MH, Jensen BEB, Smith AAA, Zelikin AN. Poly(vinyl alcohol) physical hydrogels: New vista on a long serving biomaterial. *Macromolecular Bioscience* 2011;11:1293–313. <https://doi.org/10.1002/mabi.201100145>.
- [338] Karaogul E, Altuntas E, Salan T, Hakki Alma M. The Effects of Novel Additives Used in PVA/Starch Biohybrid Films. *Fillers - Synthesis, Characterization and Industrial Application*, vol. i, IntechOpen; 2019, p. 13. <https://doi.org/10.5772/intechopen.81727>.
- [339] Larush L, Kaner I, Fluksman A, Tamsut A, Pawar AA, Lesnovski P, et al. 3D printing of responsive hydrogels for drug-delivery systems. *Journal of 3D Printing in Medicine* 2017;1:219–29. <https://doi.org/10.2217/3dp-2017-0009>.
- [340] Han D, Farino C, Yang C, Scott T, Browe D, Choi W, et al. Soft Robotic Manipulation and Locomotion with a 3D Printed Electroactive Hydrogel. *ACS Applied Materials and Interfaces* 2018;10:17512–8. <https://doi.org/10.1021/acsami.8b04250>.
- [341] Sun Z, Lu Y, Zhao Q, Wu J. A new stereolithographic 3D printing strategy for hydrogels with a large mechanical tunability and self-weldability. *Additive Manufacturing* 2022;50:102563. <https://doi.org/10.1016/j.addma.2021.102563>.
- [342] Liu T, Jiao C, Peng X, Chen YN, Chen Y, He C, et al. Super-strong and tough poly(vinyl alcohol)/poly(acrylic acid) hydrogels reinforced by hydrogen bonding. *Journal of Materials Chemistry B* 2018;6:8105–14. <https://doi.org/10.1039/c8tb02556h>.
- [343] Noè C, Tonda-Turo C, Chiappone A, Sangermano M, Hakkarainen M. Light processable starch hydrogels. *Polymers (Basel)* 2020;12:1359. <https://doi.org/10.3390/POLYM12061359>.

- [344] Parente ME, Ochoa Andrade A, Ares G, Russo F, Jiménez-Kairuz A. Bioadhesive hydrogels for cosmetic applications. *International Journal of Cosmetic Science* 2015;37:511–8. <https://doi.org/10.1111/ics.12227>.
- [345] Matanović MR, Kristl J, Grabnar PA. Thermoresponsive polymers: Insights into decisive hydrogel characteristics, mechanisms of gelation, and promising biomedical applications. *International Journal of Pharmaceutics* 2014;472:262–75. <https://doi.org/10.1016/j.ijpharm.2014.06.029>.
- [346] Can V, Kochovski Z, Reiter V, Severin N, Siebenbürger M, Kent B, et al. Nanostructural Evolution and Self-Healing Mechanism of Micellar Hydrogels. *Macromolecules* 2016;49:2281–7. <https://doi.org/10.1021/acs.macromol.6b00156>.
- [347] Colly A, Marquette C, Courtial EJ. Poloxamer/Poly(ethylene glycol) Self-Healing Hydrogel for High-Precision Freeform Reversible Embedding of Suspended Hydrogel. *Langmuir* 2021;37:4154–62. <https://doi.org/10.1021/acs.langmuir.1c00018>.
- [348] Kancharla S, Zoyhofski NA, Bufalini L, Chatelais BF, Alexandridis P. Association between nonionic amphiphilic polymer and ionic surfactant in aqueous solutions: Effect of polymer hydrophobicity and micellization. *Polymers (Basel)* 2020;12:1–23. <https://doi.org/10.3390/POLYM12081831>.
- [349] Pitto-Barry A, Barry NPE. Pluronic® block-copolymers in medicine: From chemical and biological versatility to rationalisation and clinical advances. *Polymer Chemistry* 2014;5:3291–7. <https://doi.org/10.1039/c4py00039k>.
- [350] Doberenz F, Zeng K, Willems C, Zhang K, Groth T. Thermoresponsive polymers and their biomedical application in tissue engineering-A review. *Journal of Materials Chemistry B* 2020;8:607–28. <https://doi.org/10.1039/c9tb02052g>.
- [351] Basak R, Bandyopadhyay R. Encapsulation of Hydrophobic Drugs in Pluronic F127 Micelles: Effects of Drug Hydrophobicity, Solution Temperature, and pH. *Langmuir* 2013;29:4350–6. <https://doi.org/10.1021/la304836e>.

- [352] Khimani M, Patel H, Patel V, Parekh P, Vekariya RL. Self-assembly of stimuli-responsive block copolymers in aqueous solutions: an overview. *Polymer Bulletin* 2020;77:5783–810. <https://doi.org/10.1007/s00289-019-03046-w>.
- [353] Mishra J, Swain J, Mishra AK. Molecular Level Understanding of Sodium Dodecyl Sulfate (SDS) Induced Sol-Gel Transition of Pluronic F127 Using Fisetin as a Fluorescent Molecular Probe. *Journal of Physical Chemistry B* 2018;122:181–93. <https://doi.org/10.1021/acs.jpcc.7b10170>.
- [354] Shamma RN, Sayed RH, Madry H, el Sayed NS, Cucchiaroni M. Triblock Copolymer Bioinks in Hydrogel Three-Dimensional Printing for Regenerative Medicine: A Focus on Pluronic F127. *Tissue Engineering Part B: Reviews* 2021:1–39. <https://doi.org/10.1089/ten.teb.2021.0026>.
- [355] Malmsten M, Lindman B. Effects of Homopolymers on the Gel Formation in Aqueous Block Copolymer Solutions. *Macromolecules* 1993;26:1282–6. <https://doi.org/10.1021/ma00058a014>.
- [356] Hansen CJ, Wu W, Toohey KS, Sottos NR, White SR, Lewis JA. Self-healing materials with interpenetrating microvascular networks. *Advanced Materials* 2009;21:4143–7. <https://doi.org/10.1002/adma.200900588>.
- [357] Lee S-Y, Tae G, Kim YH. Thermal gelation and photo-polymerization of di-acrylated Pluronic F 127. *Journal of Biomaterials Science, Polymer Edition* 2007;18:1335–53. <https://doi.org/10.1163/156856207782177855>.
- [358] Paxton N, Smolan W, Böck T, Melchels F, Groll J, Jungst T. Proposal to assess printability of bioinks for extrusion-based bioprinting and evaluation of rheological properties governing bioprintability. *Biofabrication* 2017;9:044107. <https://doi.org/10.1088/1758-5090/aa8dd8>.
- [359] Wong J, Gong AT, Defnet PA, Meabe L, Beauchamp B, Sweet RM, et al. 3D Printing Ionogel Auxetic Frameworks for Stretchable Sensors. *Advanced Materials Technologies* 2019;4:1900452. <https://doi.org/10.1002/admt.201900452>.
- [360] Zhang M, Vora A, Han W, Wojtecki RJ, Maune H, Le ABA, et al. Dual-Responsive Hydrogels for Direct-Write 3D Printing. *Macromolecules* 2015;48:6482–8. <https://doi.org/10.1021/acs.macromol.5b01550>.

- [361] Wu W, Deconinck A, Lewis JA. Omnidirectional printing of 3D microvascular networks. *Advanced Materials* 2011;23:H178–83. <https://doi.org/10.1002/adma.201004625>.
- [362] Müller M, Becher J, Schnabelrauch M, Zenobi-Wong M. Nanostructured Pluronic hydrogels as bioinks for 3D bioprinting. *Biofabrication* 2015;7:35006. <https://doi.org/10.1088/1758-5090/7/3/035006>.
- [363] Dutta S, Cohn D. Temperature and pH responsive 3D printed scaffolds. *Journal of Materials Chemistry B* 2017;5:9514–21. <https://doi.org/10.1039/c7tb02368e>.
- [364] Li Y, Xu R, Bloor DM, Holzwarth JF, Wyn-Jones E. Binding of sodium dodecyl sulfate to the ABA block copolymer pluronic F127 (EO97PO69EO97): An electromotive force, microcalorimetry, and light scattering investigation. *Langmuir* 2000;16:10515–20. <https://doi.org/10.1021/la000899y>.
- [365] Pandit NK, McGowan R. Gelation of Pluronic® F127-Polyethylene Glycol Mixtures: Relationship to PEG Molecular Weight. *Drug Development and Industrial Pharmacy* 1998;24:183–6. <https://doi.org/10.3109/03639049809085605>.
- [366] Pandit NK, McIntyre HJ. Cosolvent Effects on the Gel Formation and Gel Melting Transitions of Pluronic® F127 Gels. *Pharmaceutical Development and Technology* 1997;2:181–4. <https://doi.org/10.3109/10837459709022623>.
- [367] Zhang H, Yu L, Ding J. Roles of Hydrophilic Homopolymers on the Hydrophobic-Association-Induced Physical Gelling of Amphiphilic Block Copolymers in Water. *Macromolecules* 2008;41:6493–9. <https://doi.org/10.1021/ma7026484>.
- [368] Kushan E, Senses E. Thermoresponsive and Injectable Composite Hydrogels of Cellulose Nanocrystals and Pluronic F127. *ACS Applied Bio Materials* 2021;4:3507–17. <https://doi.org/10.1021/acsbm.1c00046>.
- [369] Eiamsa-ard S, Promvong P. Review of Ranque–Hilsch effects in vortex tubes. *Renewable and Sustainable Energy Reviews* 2008;12:1822–42. <https://doi.org/10.1016/j.rser.2007.03.006>.

- [370] Moghadam MN, Pioletti DP. Improving hydrogels' toughness by increasing the dissipative properties of their network. *Journal of the Mechanical Behavior of Biomedical Materials* 2015;41:161–7. <https://doi.org/10.1016/j.jmbbm.2014.10.010>.
- [371] White JM, Calabrese MA. Impact of small molecule and reverse poloxamer addition on the micellization and gelation mechanisms of poloxamer hydrogels. *Colloids and Surfaces A: Physicochemical and Engineering Aspects* 2022;638:128246. <https://doi.org/10.1016/j.colsurfa.2021.128246>.
- [372] de Lima CM, Siqueira SMC, de Amorim AFV, Costa KBS, de Brito DHA, Ribeiro MENP, et al. Effects of polypropylene glycol 400 (PPG400) on the micellization and gelation of pluronic F127. *Macromolecules* 2015;48:7978–82. <https://doi.org/10.1021/acs.macromol.5b01655>.
- [373] Jayaramudu T, Varaprasad K, Sadiku ER, Amalraj J. Temperature-sensitive semi-IPN composite hydrogels for antibacterial applications. *Colloids and Surfaces A: Physicochemical and Engineering Aspects* 2019;572:307–16. <https://doi.org/10.1016/j.colsurfa.2019.04.012>.
- [374] Khan S, Raj N, Rayappan Pavul, George L, Kannangara GSK, Milev A, Varadaraju U v., et al. Surfactant-Mediated and Morphology-Controlled Nanostructured LiFePO₄/Carbon Composite as a Promising Cathode Material for Li-Ion Batteries. *ChemistryOpen* 2020;9:23–31. <https://doi.org/10.1002/open.201900175>.
- [375] Accardo J v., Kalow JA. Reversibly tuning hydrogel stiffness through photocontrolled dynamic covalent crosslinks. *Chemical Science* 2018;9:5987–93. <https://doi.org/10.1039/c8sc02093k>.
- [376] Crespi S, Simeth NA, König B. Heteroaryl azo dyes as molecular photoswitches. *Nature Reviews Chemistry* 2019;3:133–46. <https://doi.org/10.1038/s41570-019-0074-6>.
- [377] Chang VY, Fedele C, Priimagi A, Shishido A, Barrett CJ. Photoreversible Soft Azo Dye Materials: Toward Optical Control of Bio-Interfaces. *Advanced Optical Materials* 2019;7:1–25. <https://doi.org/10.1002/adom.201900091>.

- [378] Mandl GA, Rojas-Gutierrez PA, Capobianco JA. A NIR-responsive azobenzene-based supramolecular hydrogel using upconverting nanoparticles. *Chemical Communications* 2018;54:5847–50. <https://doi.org/10.1039/c8cc03101k>.
- [379] Bushuyev OS, Aizawa M, Shishido A, Barrett CJ. Shape-Shifting Azo Dye Polymers: Towards Sunlight-Driven Molecular Devices. *Macromolecular Rapid Communications* 2018;39:1–14. <https://doi.org/10.1002/marc.201700253>.
- [380] Wang D, Zhao W, Wei Q, Zhao C, Zheng Y. Photoswitchable Azobenzene/Cyclodextrin Host-Guest Complexes: From UV- to Visible/Near-IR-Light-Responsive Systems. *ChemPhotoChem* 2018;2:403–15. <https://doi.org/10.1002/cptc.201700233>.
- [381] Weis P, Wu S. Light-Switchable Azobenzene-Containing Macromolecules: From UV to Near Infrared. *Macromolecular Rapid Communications* 2018;39:1–12. <https://doi.org/10.1002/marc.201700220>.
- [382] He L, Fullenkamp DE, Rivera JG, Messersmith PB. PH responsive self-healing hydrogels formed by boronate-catechol complexation. *Chemical Communications* 2011;47:7497–9. <https://doi.org/10.1039/c1cc11928a>.
- [383] Ma R, Shi L. Phenylboronic acid-based glucose-responsive polymeric nanoparticles: synthesis and applications in drug delivery. *Polym Chem* 2014;5:1503–18. <https://doi.org/10.1039/C3PY01202F>.
- [384] Deng CC, Brooks WLA, Abboud KA, Sumerlin BS. Boronic Acid-Based Hydrogels Undergo Self-Healing at Neutral and Acidic pH. *ACS Macro Letters* 2015;4:220–4. <https://doi.org/10.1021/acsmacrolett.5b00018>.
- [385] Seidi F, Jin Y, Han J, Saeb MR, Akbari A, Hosseini SH, et al. Self-healing Polyol/Borax Hydrogels: Fabrications, Properties and Applications. *Chemical Record* 2020;20:1142–62. <https://doi.org/10.1002/tcr.202000060>.
- [386] Nunes MAP, Gois PMP, Rosa ME, Martins S, Fernandes PCB, Ribeiro MHL. Boronic acids as efficient cross linkers for PVA: synthesis and application of tunable hollow microspheres in biocatalysis. *Tetrahedron* 2016;72:7293–305. <https://doi.org/10.1016/j.tet.2016.02.017>.

- [387] Chantasirichot S, Inoue Y, Ishihara K. Amphiphilic Triblock Phospholipid Copolymers Bearing Phenylboronic Acid Groups for Spontaneous Formation of Hydrogels with Tunable Mechanical Properties. *Macromolecules* 2014;47:3128–35. <https://doi.org/10.1021/ma5006099>.
- [388] Meng H, Zheng J, Wen XF, Cai ZQ, Zhang JW, Chen T. PH- and sugar-induced shape memory hydrogel based on reversible phenylboronic acid-diol ester bonds. *Macromolecular Rapid Communications* 2015;36:533–7. <https://doi.org/10.1002/marc.201400648>.
- [389] Hua M, Wu D, Wu S, Ma Y, Alsaïd Y, He X. 4D Printable Tough and Thermo-responsive Hydrogels. *ACS Applied Materials & Interfaces* 2021;13:12689–97. <https://doi.org/10.1021/acsami.0c17532>.
- [390] Zhou Y, Zhang C, Liang K, Li J, Yang H, Liu X, et al. Photopolymerized water-soluble maleilated chitosan/methacrylated poly (vinyl alcohol) hydrogels as potential tissue engineering scaffolds. *International Journal of Biological Macromolecules* 2018;106:227–33. <https://doi.org/10.1016/j.ijbiomac.2017.08.002>.
- [391] Reis A v., Fajardo AR, Schuquel ITA, Guilherme MR, Vidotti GJ, Rubira AF, et al. Reaction of glycidyl methacrylate at the hydroxyl and carboxylic groups of poly(vinyl alcohol) and poly(acrylic acid): Is this reaction mechanism still unclear? *Journal of Organic Chemistry* 2009;74:3750–7. <https://doi.org/10.1021/jo900033c>.
- [392] Li S, Zuo C, Zhang Y, Wang J, Gan H, Li S, et al. Covalently cross-linked polymer stabilized electrolytes with self-healing performance: Via boronic ester bonds. *Polymer Chemistry* 2020;11:5893–902. <https://doi.org/10.1039/d0py00728e>.
- [393] Xiao YY, Gong XL, Kang Y, Jiang ZC, Zhang S, Li BJ. Light-, pH- and thermal-responsive hydrogels with the triple-shape memory effect. *Chemical Communications* 2016;52:10609–12. <https://doi.org/10.1039/c6cc03587f>.